# AN APPRAISAL OF THE LIGNIN/ACTIVATED CARBON ADSORPTION SYSTEM

# AN APPRAISAL OF THE LIGNIN/ACTIVATED CARBON ADSORPTION SYSTEM

BY

PAUL RANKIN

A THESIS

Submitted to the Faculty of Graduate Studies

In Partial Fulfillment of the Requirements

for the Degree

MASTER OF ENGINEERING

McMaster University

April, 1975

MASTER OF ENGINEERING
(Chemical Engineering)

McMASTER UNIVERSITY
Hamilton, Ontario

TITLE: An Appraisal of The Lignin/Activated Carbon Adsorption System.

AUTHOR: Paul Rankin, B.Sc., (Exeter University, U.K.)

SUPERVISOR: Dr. A. Benedek

NUMBER OF PAGES: xix, I.160, II.179, III.83, A.8

ABSTRACT:

The pore structure of a wide array of activated carbons has been evaluated by nitrogen adsorption and mercury penetration techniques. Carbons were found to exhibit total surface areas and pore volumes in the range 93 - 1500 $m^2/g$ and 0.34 - 1.8 $cm^3/g$ respectively. The Darco carbons contain significant pore structure in all pores up to 1000 Å radius. Columbia carbon contains negligible pore structure in pores of greater than approximately 20 Å radius. Special "A" carbon contains virtually all its limited pore structure in pores of 20 - 200 Å radius.

A kraft lignin, Indulin A.T., has been shown by Ultrafiltration and Gel Filtration techniques to exist in aqueous solution as a variety of different molecular weight fragments, with molecular weights ranging from approximately 4,000 to greater than 300,000. Each fragment is characterised by a unique molecular weight, hydrodynamic radius, characteristic diffusivity, solubility, and color and TOC content. The concentration, and color and TOC content per molecule of each species in solution determines overall solution color and TOC. The change in overall solution color and/or TOC with change in solution pH and solution age has been shown to be associated with an alteration in

the molecular distribution, and hence the relative concentrations, of the various fragments in solution.

Adsorption of lignin from aqueous solution onto activated carbon has been shown to proceed by a selective adsorption mechanism. Here the smallest adsorbable fragments are preferentially adsorbed initially, with progressive preferential adsorption of increasingly larger fragments as either contact time or carbon dosage is increased. Correlations between observed adsorption behaviour and pore structure for various carbons tend to support Chen's hypothesis that each fragment will adsorb preferentially into pores of approximately 3.3 to 6.1 times its hydrodynamic radius. It appears that carbon pore structure in pores of greater than 16 Å radius is primarily responsible for adsorption of color and TOC from aqueous lignin solution. Adsorption of each species appears to occur by an ion exchange or concentration-precipitation mechanism.

Most activated carbons contain sufficient pore structure in pores of greater than 16 Å radius to bring about good color and TOC removals at resonably low carbon dosages. Columbia carbon, however, is incapable of removing the bulk of lignin fragments, and hence the major portion of color and TOC, from solution due to lack of adequate pore structure in pores of greater than 15 Å radius. Similarly, Special "A" cannot effectively adsorb the low molecular weight fragments from solution due to a deficiency of pore structure in pores of less than 16 - 20 Å. Good color and TOC removals are, however, possible

with Special "A", as its limited pore structure is specific to adsorption of the fragments responsible for the bulk of overall solution color and TOC.

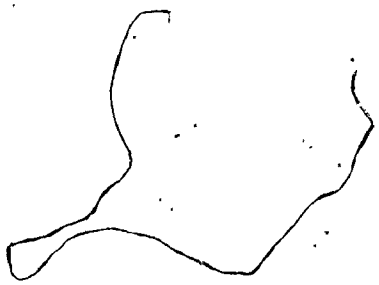

TABLE OF CONTENTS

## ACKNOWLEDGEMENTS

My sincere thanks to Dr. A. Benedek for guidance and supervision in conducting this work; to Dr. R.B. Anderson, Dr. J. Eagan, Mr. A. Nayak and Mrs. A. Robertson for their help in conducting experiments, and to Mrs. J. Costantino and Mrs. D. Ahola for patiently typing this thesis.

## FIGURES

## TABLES

## APPENDICES

# PART I

# BATCH ADSORPTION STUDIES ON THE LIGNIN/ACTIVATED CARBON ADSORPTION SYSTEM

## I.1 INTRODUCTION

### I.1.1 Purpose of Work

Kraft lignin, as it exists in effluents from kraft mill pulping operations, is a pollutant of natural bodies of water. Although contributing negligible $BOD_5$, kraft lignins impart considerable color, TOC and COD to the receiving water. In the future, as government regulations concerning pulp mill effluent discharges tighten, lignin removal may become necessary.

Several studies conducted during the past decade have demonstrated the technological feasibility of activated carbon adsorption as a treatment process for removal of lignin, or more specifically color, from specific, partial and total kraft mill effluents. From these studies, valuable information (to be summarized later) has been obtained regarding the factors to be considered in design and operation of an effective adsorption unit. The mechanisms involved in lignin adsorption onto activated carbon are still, however, generally unclear.

This work is aimed at providing some fundamental

information about the lignin/activated carbon adsorption system. It is of interest to know the manner in which both carbon and lignin solution properties effect subsequent lignin adsorption behaviour. Of prime importance here is the effect of carbon pore structure on lignin adsorption, since an appreciation of this effect will provide important information on carbon selection.

To the writers knowledge, this study represents the first attempt at a fundamental appraisal of the lignin/activated carbon adsorption system in which both the lignin solution and activated carbon adsorbents are first comprehensively investigated in terms of factors which may influence subsequent adsorption behaviour.

I.1.2 Format of Study

The work is divided into three main parts, viz.

Part I Batch Adsorption Studies on the Lignin/Activated Carbon Adsorption System

Part II Activated Carbon Characterisation Studies

Part III Lignin Studies

This has been done for reader convenience, since each part of this study required extensive and relatively independent investigations. Only Part I of this work is considered here. In writing Part I, it is assumed that the reader is already familiar with the activated carbon and lignin solution properties evaluated in Parts II and III.

Solutions of an acid-precipitated pine kraft lignin, Indulin A.T., were used as the lignin solution in this work. This was preferred over the use of an industrial kraft mill effluent since the latter inevitably contains other organic solutes which may interfere with lignin adsorption.

Indulin solution conditions were chosen to duplicate as accurately as possible the conditions of lignin existing in the unbleached decker effluent of a 'typical' kraft mill (Day, 1972), i.e.

| | |
|---|---|
| lignin concentration | 500 mg/l |
| pH | 10 |
| temperature | 35°C |

## I.2 BACKGROUND AND LITERATURE REVIEW

### I.2.1 The Phenomenon of Adsorption

Adsorption is a surface phenomenon, involving interfacial accumulation or concentration of a particular component or components at a surface or interface. When two immiscible phases are contacted, molecules in the vicinity of the surface will have an immediate influence on each other due to inter-molecular attractions; an adsorption potential is thus established between molecules of the two phases. Molecules possessing this adsorption potential tend to assemble at the phase boundary; continuous congregation of molecules eventually leads to establishment of a surface film. This process is termed adsorption.

Adsorption from a one solute, one solvent solution at the liquid surface can be mathematically described by the Gibbs adsorption equation (Gibbs, 1961) for dilute solutions,

$$\Gamma_2^1 = -\frac{C_2}{RT}\left(\frac{d\sigma^{\alpha\beta}}{dC_2}\right)_T \qquad (1.1)$$

where $\Gamma_2^1$ = the surface excess of solute over solvent at the interface

$C_2$ = the concentration of solute in solution

$\sigma^{\alpha\beta}$ = the interfacial surface tension between phases $\alpha$ and $\beta$

T = absolute temperature

R = universal gas constant

From equation (1.1), adsorption of solute can be estimated provided the relationship between $\sigma^{\alpha\beta}$ and $C_2$ is known at a particular temperature. Equation (1.1) also indicates that any solutes capable of reducing $\sigma^{\alpha\beta}$ in solution such as detergents (Weber 1972) will be positively absorbed at the interface, whereas for strong electrolytes the reverse occurs. Both McBain and Humphreys (1962) and Swain (1930) have verified equation (1.1) experimentally.

I.2.2. Adsorption at the Liquid-Solid Interface

In the case of simple liquid-solid adsorption systems, as discussed at length by Kipling (1965) and Chen (1970), the Gibbs adsorption equation cannot be used for prediction of adsorption behaviour. This is because $\sigma^{\alpha\beta}$, which is an interfacial energy term, is not constant over the entire liquid-solid interface. Variations of $\sigma^{\alpha\beta}$ will occur at the interface due to the heterogeneous nature of the solid surface caused by localised surface contamination and roughness. Furthermore, it is

not possible in liquid-solid systems to measure the surface excess $\Gamma_2^1$ directly; only the corresponding surface concentration $n_2^1$ can be evaluated.

For dilute solutions, it can be shown that $n_2^1$ can be related to $\sigma^{\alpha\beta}$ by an equation analogous to equation (1.1), i.e.

$$n_2^1 = - \frac{S\, C_2}{RT} \left( \frac{d\, \sigma^{\alpha\beta}}{d\, C_2} \right)_T \qquad (1.2)$$

where S is the specific surface area of adsorbent available for adsorption. Furthermore, if it is assumed that negligible adsoprtion of solvent occurs in comparison to that of solute, and also that solution volume does not change with adsorption then it can be shown (Kipling, 1965) that the individual adsorption of solute $n_2^s$ is given by

$$n_2^s = \frac{V_o(C_2^o - C_2)}{m} = \frac{x}{m} \qquad (1.3)$$

where $V_o$ = solution volume

$C_2^o$ = the initial concentration of solute in solution

$C_2$ = the equilibrium concentration of solute in solution after contact with amount m of adsorbent.

x = the amount of solute removed from solution after contact with amount m of adsorbate

Combination of equations (1.2) and (1.3) yields

$$\frac{x}{m} = - \frac{S\ C_2}{RT} \left( \frac{d\ \sigma^{\alpha\beta}}{d\ C_2} \right)_T = f(C_2)_T \qquad (1.4)$$

Equation (1.4) is representative of the adsorption of solute onto the surface of a solid adsorbent, in the case of dilute solutions where negligible adsorption of solvent occurs, and is termed the adsorption isotherm for the solute.

I.2.3. Adsorption Isotherm Models

Generally the relation between $\frac{x}{m}$ and $C_2$, which describes the distribution of adsorbed component between surface and bulk solution, is not linear. Several models have been used to describe observed adsoprtion behaviour. These are summarised in Table I.1. The Langmuir model often fits the isotherms obtained for adsorption of solids from solution, namely for adsorption of stearic acid onto carbon black from various solvents (Kipling and Wright, 1962) and phenols from aqueous solution onto activated carbon (Snoeyink, 1968). The Langmuir model cannot be applied to systems in which no limiting adsorption value occurs; however, it has found application even in cases where solvent adsorption is significant. The B.E.T. model

Table I.1 Adsorption Isotherm Models Used in Describing Adsorption Behaviour in Liquid-Solid Systems

| Model | Equation | Linearised Form | Assumption |
|---|---|---|---|
| Langmuir (1918) | $\frac{x}{m} = \frac{Qo\ b\ C^*}{1 + b\ C^*}$ (Qo, b constants) | Plot of $\frac{m}{x}$ versus $\frac{1}{C^*}$ | 1. Limiting adsorption value Qo corresponding to monolayer formation. 2. Homogeneous surface. 3. No lateral interaction between adsorbed molecules. |
| B.E.T. (Brunauer, 1938) | $\frac{x}{m} = \frac{Qo\ B\ C^*}{(C_s - C^*)\left[1+(B-1)(C^*/C_s)\right]}$ (Qo, B, $C_s$ constants) | Plot of $\frac{mC^*}{x(C_s - C^*)}$ versus $C^*$ | 1. Langmuir assumptions 2, 3. 2. Multilayer formation. 3. Heats of adsorption of 2nd, 3rd .... nth layers equal. |
| Freundlich (1926) | $\frac{x}{m} = K\ C^{*1/n}$ (K, n constants) | Plot of $\log \frac{x}{m}$ versus $\log C^*$ | 1. Adsorption sites have exponential distribution of surface energies. 2. Constant b in Langmuir model is a function of x/m. |
| Jowett (1961) | $\frac{x}{m} = A-(A-a)e^{-BC^*}$ (A, a, B constants) | Plot of $\log \frac{x}{m}$ versus $C^*$ | Combination of Langmuir and Freunlich assumptions. |
| Davies and Rideal (1961) | $\frac{x}{m} = \frac{D\ C^*\ e^{w/kT}}{1 + D\ C^* e^{w/kT}}$ (D, k constants) | | 1. Langmuir assumptions. 2. Heat of adsorption w is a function of x/m. |

Note: $C^*$ is analogous to $C_2$ in equation (1.4), being the equilibrium concentration of adsorbable components in solution after contact with an amount m of adsorbent.

can be used where no limiting adsorption value occurs, but as yet has found little application in describing adsorption behaviour in liquid-solid systems. However, it adequately describes the adsorption of benzoic acid from aqueous solution onto non-porous Graphon carbon (Smith, 1953). Conversely, the semi-empirical Freundlich model has found wide applicability in description of observed adsorption behaviour in a variety of liquid-solid systems. Apart from its proven ability in description of simple liquid-solid adsorption systems, it has also been applied successfully in description of adsorption behaviour in multicomponent liquid-solid systems, as in the selective adsorption of a variety of components from domestic and pulp mill effluents onto activated carbon (Weber, 1972: Timpe, 1970 (a), (b): Fuchs 1965: McGlasson, 1967: Bloodgood, 1962). The Jowatt model describes the adsorption of m-cresol from aqueous solution onto coal, whereas the Davis and Rideal model effectively describes adsorption of cetylamine from nuyol onto various metals (Haydon, 1961).

I.2.4. Types of Adsorption

There are three distinct types of adsorption, viz.

a) Physical adsorption

b) Chemisorption

c) Exchange adsorption

Physical adsorption occurs as a result of Van der Waals attraction forces between adsorbate and adsorbent molecules at the surface. Here the adsorbed molecule is not attached to a specific surface site but free to undergo transitional motion at the surface. Since physical adsorption involves low energy attraction forces, heats of adsorption are low, being of the order 2-15 kcal/mol (Chen, 1970). Physical adsorption is easily reversible, and is usually associated with adsorbed multilayers.

Conversely, chemisorption is characterised by chemical reaction between adsorbate and adsorbent molecules at the surface. Here, adsorbed molecules are not free to move but are rigidly attached to specific surface sites by strong localised chemical bonds. Heats of chemisorption are necessarily higher than for physical adsorption, due to formation of high energy chemical bonds, and are of the

order 30-100 kcal/mole, (Adamson, 1967; Graham, 1959). Chemisorption is very rarely reversible, and is usually associated with limiting adsorption behaviour corresponding to monolayer formation.

Exchange adsorption is a form of chemisorption, wherein adsorbate ions are concentrated at a solid surface due to electrostatic attractions to charged surface sites, or alternatively by ion exchange with functional groups already present in the surface film.

Generally in liquid-solid systems it is difficult to distinguish between the various types of adsorption based on values of heats of adsorption (Gregg and Sing, 1967; Hassler, 1962). However, exchange adsorption is most likely to occur in adsorption systems containing solid adsorbents with charged surface sites, such as activated carbon (Weber, 1972).

I.2.5. Rates of Adsorption

The observed overall rate of adsorption of an adsorbate or adsorbates in liquid-solid systems is determined by one or more of several transfer mechanisms. The individual mechanisms at play are

a) Mass transfer of adsorbate from the bulk liquid phase to the adsorbent external surface.

b) Adsorption or reaction of adsorbate at the absorbent external surface.

c) Penetration and diffusion of adsorbate into and along the adsorbent pores

d) Adsorption or reaction of adsorbate on the adsorbent internal pore structure.

Since, when considering porous adsorbents such as activated carbon, the above steps must occur successively for adsorption to take place, they may be considered to offer resistances in series. The step that offers the major resistance is generally considered alone as the rate controlling step in the adsorption process. Kipling (1965), McGlasson (1967) and Weber (1972) have discussed at length experimental procedures that may be used to determine the relative magnitude of the various resistances to transfer steps (a) to (d) above, for liquid-solid systems.

Generally, when dealing with porous adsorbents such as activated carbon in liquid-solid systems, the

overall rate of adsorption is controlled by pore diffusion transport resistance, i.e. the rate of diffusion of adsorbate through the adsorbent pores. The literature evidence for the above statement is summarized in Table I.2.

Weber (1972) has shown in pore diffusion controlled adsorption rate processes, by considering a material balance on an elemental volume of fluid, that the overall rate of adsorption may be represented by the generalised rate equation

$$\frac{dC^*}{dt} = \frac{1}{r}\frac{d}{dr}\left(r\, D_\ell \frac{dC^*}{dr}\right) - \frac{d(x/m)_t}{dt} \qquad (1.5)$$

and $r$ = pore radius
$D_\ell$ = characteristic diffusivity of adsorbate in the r direction
$t$ = contact time
$C$ = the concentration of adsorbate at position r in the pore

Equation (1.5), which is expressed in terms of spherical coordinates, assumes the following

a) Unidirectional pore diffusion in the r direction

b) Isotropic cylindrical pores

c) Spherical adsorbent particles

d) No steric hindrance to adsorption

e) The concentration of adsorbent in the pore

Table I.2. Summary of Liquid-Solid Adsorption Systems Exhibiting Pore Diffusion Controlled Adsorption Rates

| Adsorption System | Reference |
|---|---|
| Phenols from aqueous solution onto activated carbon | Weber and Morris (1963) |
| Aqueous extraction of substances from porous solids | Piret (1951) |
| Alkali metal cations from solution onto phenol-formaldehyde resins | Boyd (1947) |
| Strong inorganic acids from aqueous solution onto activated carbon | Snoeyink (1968) |
| Lignins from aqueous solutions onto activated carbon | Fuchs (1965)<br>McGlasson (1967)<br>Chen (1970)<br>Timpe (1971) |
| Polymers from various solvents onto porous solids | Kipling (1965) |

is proportional to its concentration in the bulk solution at any time t

The limitations of this model are significant. Actual diffusion paths in the radial direction may be greater than the pore radius (Jackson, 1963), the mobility of adsorbate will be reduced as it passes through the pores due to frictional resistance (Faxon, 1922), and molecular screening in a tapered pore may occur with large adsorbates (Grant, 1960).

Provided that the relationship between C* and x/m at time t is linear then equation (1.5) can be readily solved for $D_\ell$, as Edeskuty and Amundson (1952) have done using adsorption rate data of phenol from aqueous solution onto activated carbon. However, the relationship between x/m and C* at any time t is not usually one of direct proportionality, and so solution of equation (1.5) usually involves complex calculations for estimation of $D_\ell$. Crank (1948) has simplified equation (1.5) by stipulating boundary conditions, and has derived a numerical solution based on finite differences, for estimation of $D_\ell$ with the aid of the computer. Weber and Rumer (1965) and Snoeyink (1968)

have calculated values of $D_\ell$ from activated carbon adsorption rate data solving Crank's model by computer. Weber and Rumer used a linear relation between C* and x/m, whereas Snoeyink used a Freundlich relation between C* and x/m.

Crank's model cannot be effectively used to estimate $D_\ell$ in cases where the relationship between C* and x/m at any time t is not linearisable using conventional adsorption models (see Table I.1). Tien (1960) has developed a method for solution of equation (1.5) by relating x/m at any time t to a polynomial expression involving time, i.e.

$$\left.\frac{x}{m}\right|_t = \sum_{i=0}^{m} P_i \, t^i \qquad (1.6)$$

where the various $P_i$ values are determined from experimental rate data. Here using equation (1.5), where $(x/m)_t$ is expressed in terms of a polynomial expression, the characteristic diffusivity can be evaluated by matching observed and calculated adsorption kinetics. Dedrick and Beckman (1967) have indicated that in an infinite bath, solution of equation (1.5) for short contact times and wastewater adsorption systems is given

by

$$\frac{C_o - C^*}{C_o - C_e} = \frac{12}{\pi^{\frac{1}{2}}} \sqrt{\frac{D_\ell t}{D_p^2}} \qquad (1.7)$$

where $C_o$ = initial concentration of adsorbent in bulk solution
$C_e$ = equilibrium concentration of adsorbent in bulk solution
$C^*$ = adsorbent concentration in bulk solution at time t
$D_p$ = adsorbent particle diameter

Thus the intial slope of a plot of $[(C_o - C^*)/(C_o - C_e)]$ versus $t^{\frac{1}{2}}$ can be used in equation (1.7) to estimate $D_\ell$.

The aforementioned discussion has indicated that overall adsorption rates of adsorbates from solution onto porous solids may be expressed terms of a characteristic diffusivity. Other researchers have characterised observed adsorption rate data by the use of empirical models. Such models, listed in Table I.3 enable characterisation of adsorption rate data in terms of a rate constant k, which is related to $D_\ell$.

Table I.3. Models Used in Description of Observed Adsorption Rate Data in Liquid-Solid Systems

| Author | Model | Applicability |
|---|---|---|
| Kawecka (1963) | $\left(\frac{x}{m}\right)_t = \frac{\left(\frac{x}{m}\right)_\infty . t}{k + t}$ | Adsorption rate of p-cresol from solution onto charcoal |
| Fava (1956) | $\frac{-d\phi}{dt} = 2\,k\,\phi \sinh b\phi$ where $\phi = \frac{\left(\frac{x}{m}\right)_\infty - \left(\frac{x}{m}\right)_t}{\left(\frac{x}{m}\right)_\infty}$ | Adsorption of sodium dodecylsulphonate from aqueous solution onto cotton |
| Hobden (1953) | $\frac{\left(\frac{x}{m}\right)_\infty}{\left(\frac{x}{m}\right)_\infty - \left(\frac{x}{m}\right)_t} = e^{kt}$ | Adsorption of polymers from a variety of solvents onto charcoal |
| Snoeyink (1968) | $\left(\frac{x}{m}\right)_t = k\,t^{\frac{1}{2}}$ | Adsorption of phenol from aqueous solution onto activated carbon |

## I.2.6. Factors Influencing Adsorption In Liquid-Solid Systems

### I.2.6. (i) Temperature

System temperature increase generally gives rise to two distinct changes in the adsorption system, namely weakening of adsorbate-adsorbent and adsorbate-adsorbate intermolecular forces in the surface layers, and increase of adsorbate solubility in the solvent. It would thus be expected that system temperature increase would decrease the equilibrium extent of adsorption. This is usually the case, as indicated by Daniel (1951) in adsorption of stearic acid from benzene onto nickel powder, Snoeyink (1968) in adsorption of HCl and NaCl from aqueous solution onto activated carbon, and Benedek and Ho (1973) in adsorption of various components of domestic sewage onto activated carbon. The overall adsorption process is thus usually exothermic.

However, in systems which experience increased solute solubility with temperature, such as aqueous solutions of lead chloride or n-butyl alcohol in water, the solubility effect may override the adsorbent-absorbate effinity effect, resulting in increased

adsorption extent with increase in temperature (Fuchs, 1965). This observation is also experienced in adsorption of some polymers from solution onto porous solids (Kipling, 1965).

Adsorption rate generally increases with increase in adsorption temperature. This is associated with an increase in adsorbate mobility, coupled with a decrease in solvent viscosity. Snoeyink (1968) has confirmed the increase of adsorbate characteristic diffusivity $D_\ell$ with temperature increase for inorganic acids and phenols in their adsorption from aqueous solution onto activated carbon. Hansen (1953) has stated that the effect of temperature on adsorbate diffusivity is of the form

$$D_\ell \cong \frac{KT}{e^{[A + (B/T)]}} \qquad (1.8)$$

where K, A, B are constants for the system.

I.2.6. (ii) Solubility

Generally, increase in solute solubility is associated with an increase in the extent of adsorption of solute. This occurs as a result of changes in the relative magnitudes of solute-solvent and solute-

adsorbent affinities; the less soluble - or more lyophobic - the solute, the greater is its potential to concentrate at the interface and be adsorbed. For adsorption of a 'liquid' solute from a solution of two completely miscible liquids, Eberman(1925) has indicated that the inverse relation between solute solubility and adsorption is of the form

$$\frac{x}{m} = k_1 \left[ \frac{C^* \sigma^{\alpha\beta}}{S_o} \right]^{1/k_2} \qquad (1.9)$$

where $S_o$ is the solute solubility and $k_1$, $k_2$ are constants.

For 'solid' solutes, Lundelius (1920) has shown, in studies on the adsorption of iodine from various organic solvents onto charcoal, that an inverse proportionality exists between solute solubility and extent of adsorption. Lundelius' rule has been confirmed by many researchers for a variety of adsorption systems (Freundlich (1926), McKelvey (1958), Hansen and Craig (1954)), although Weber (1972) points out that many adsorption systems exist in which Lundelius' rule is not obeyed.

I.2.6. (iii) Polarity

The effect of solute polarity on adsorption can generally be estimated from Traubes' rule (1891), which states that a polar solute will prefer the phase that is more polar, with a non-polar solute preferring the more non-polar phase. In this context, the activated carbon surface is essentially non-polar. The observed increased adsorption in a homologous series of organic solutes from aqueous solution onto activated carbon is thus in agreement with Traubes' rule, since an increase in the relative number of non-polar C-H bonds per molecule will give rise to decreased polarity - and solubility - as the homologous series is ascended.

Weber (1972) states that for adsorption of relatively simple solutes from agueous solution onto activated carbon, adsorption is at a minimum for charged species and at a maximum for neutral species. As solutes become more complex, however, the effect of solute polarity becomes less important in comparison to solute molecular size and/or solubility considerations.

It is evident that solute polarity is influenced

by a variety of factors including solution pH and temperature. Phelps (1931) has shown that the occurrence of maximum adsorption of propionic acid from aqueous solution onto activated carbon at pH 3.5-5.5 is associated with minimum solute polarity. Similarly, Fuchs (1965) attributes the maximum adsorption of lime-treated, caustic stage, pulp mill bleach plant effluent at pH 5 to the existance of neutrally charged calco-lignin color bodies in solution at this pH. The low favourability of adsorption of organic pollutants from domestic sewage by activated carbon may also be attributed to decreased solute polarities, although Weber (1972) suggests that this observation may be due to neutralisation of adsorbent surface charges, yielding an increase in the number of available adsorption sites.

I.2.6. (iv) Molecular Size

Generally, for a given class of compounds, increase in solute molecular size - or weight - is associated with increased adsorption. This is especially noticeable for adsorption onto non-porous

solids, where steric hindrance to adsorption is negligible (Kipling, 1965). Here increase in solute molecular size is associated with decreased solubility and polarity, notably in polar solvents such as water, resulting in increased adsorption potential at relatively non-polar surfaces.

For a given class of solutes, the overall rate of adsorption will decrease with increased solute molecular size, notably on porous solids. This effect is associated with decrease of adsorbate mobility with increased molecular size, resulting in a more sluggish movement of adsorbate through the adsorbent pores.

The aforementioned generalisations only hold for molecular size effects in a given class of compounds. As Weber and Morris (1964) have correctly pointed out, large molecules of one particular class of compounds may adsorb more rapidly and less extensively than smaller molecules of another chemical configuration. In addition, steric hindrance effects in adsorption onto porous solids

may prevent adsorption of larger adsorbates, although considerable adsorption of their smaller derivatives may occur.

I.2.6. (v) Molecular Geometry

For simple solutes, provided no steric hindrance to adsorption occurs, the studies of Weber and Morris (1964) on adsorption of sulphonated alkylbenzenes substituted in the 2, 3 and 6 positions onto activated carbon would indicate that molecular geometry has negligible effect on either adsorption rate or capacity. Although Weber and Levy (1959) noted a marked increase in adsorption of solutes onto activated carbon for solutes in the series 2, 6 dimethyl to 2, 6 dibutyl phenol, they attributed this to the decreased solubility of the latter compound over the former in the hydrocarbon solvent, rather than to differences in molecular geometry.

However, Zeichmeister (1950), by demonstrating that the adsorption of hydroxy- and amino-benzoic acid from aqueous solution onto activated carbon is strongly dependent on the substitution position of

hydroxy and amino groups in the benzene ring, suggests that molecular geometry may influence adsorption behaviour.

I.2.6. (vi) Adsorbent Surface Area and Pore Volume

Providing there is no steric hindrance to adsorption, then the extent of adsorption is directly related to the total surface area or pore volume of the adsorbent. As Grant (1960) clearly points out, however, there is generally steric hindrance to adsorption arising from solute molecular size and adsorbent pore size considerations. Here solute molecules having hydrodynamic radii greater than the diameters of some of the adsorbent pore necks will be effectively screened from such pores; a portion of the total surface area and pore volume of the adsorbent will not be available for adsorption. The portion available to adsorption of a given solute is termed the specific surface area and specific pore volume. Specific surface area and specific pore volume available to an adsorbate is dependent on the pore structural characteristics of the adsorbent. In this respect, Kolthoff and Gutmacher (1952) have indicated the

adsorption of GR-S rubber from organic solvents onto various activated carbons is proportional to specific surface area. Similar deductions have been made by Chen (1970) in studies of the adsorption of aqueous solutions of n-butyric acid, sucrose, phenols and lignins onto various activated carbons.

Generally, the specific surface area or specific pore volume available to an adsorbent is difficult to assess. If adsorbate molecular size is sufficiently small, then specific and total surface areas and pore volumes may be assumed to be the same, as Union Carbide (1972) suggests when considering adsorption of odor-causing components from solution onto activated carbon. For larger adsorbates, Chen (1970) suggests that specific surface area may be estimated from evaluation of the adsorbent total surface area by nitrogen adsorption experiments both before and after adsorption. In the Westvaco (1969) study, specific surface areas and pore volumes were determined by evaluating correlation coefficients between observed adsorption capacity and specific surface area in a given range of pore sizes for

several different carbons. However, as both Garten and Weiss (1957) and Kolthoff and Gutmacher (1952) have noted, the 'correllation' approach may break down if there is significant variation in surface nature between the carbons used. In such cases adsorption differences using various carbons may be significantly influenced by carbon surface characteristics, rather than purely by pore structural considerations.

For agueous solutions of 'solid' solutes, Chen (1970) has shown that adsorption of solute from aqueous solution onto activated carbon occurs primarily by a concentration-precipitation mechanism. Here solute molecules are concentrated in an adsorbent pore, to an extent dictated by their initial concentration in solution and pore radius, according to the relationship

$$\frac{2\,\sigma^{\alpha\beta}}{r} = \frac{RT}{V^{o}} \ln\left[\frac{C'}{C_o}\right] \qquad (1.10)$$

where $r$ = pore radius
$V^{o}$ = molar volume of solute
$C'$ = solute concentration in pore of radius $r$
$C_o$ = solute concentration in bulk solution

Chen states that phase separation, precipitation

and hence adsorption will occur in only those pores having the ability to concentrate solute to a point that exceeds its solubility limit in the solvent. He has shown that, for dilute solutions of 'solid' adsorbates such as phenol and lignin, the specific pore volume available for adsorption corresponds to that contained in pores having

$$3.3 \leq \frac{d}{D} \leq 6.1 \qquad (1.11)$$

where d, D are the pore and solute molecular diameters respectively. For $\frac{d}{D} > 6.1$, adsorption will not occur as the solute solubility is not exceeded, whereas for $\frac{d}{D} < 3.3$, steric exclusion and tortuosity effects will prevent pore penetration of adsorbate. Chen has found the specific pore volume for adsorption of a variety of solutes from aqueous solution onto activated carbon to be in the pore size ranges shown below

| | |
|---|---|
| Butyric Acid | 21 - 40 Å |
| Phenol | 20 - 36 Å |
| Sucrose | 27 - 49 Å |
| Lignin | 37 - 70 Å |

The Westvaco study reported the specific pore volume contained in pores of approximately 14 - 40 Å as being primarily responsible for adsorption of TOC-contributing solutes from municipal effluent by activated carbon.

Adsorbent pore structural characteristics can also influence adsorption overall adsorption rates. Weber (1972) has pointed out that in cases where adsorption of solute is limited by steric hindrance effects, effective adsorption will only occur on the external surface of the adsorbent; adsorption will thus be relatively fast. In the case where there is little or no steric hindrance, overall adsorption rate may be much slower due to pore diffusion resistance, although adsorption capacity will be higher. The Westvaco study has confirmed Weber's statement in adsorption rate studies using various powdered carbons.

I.2.6. (vii) Adsorbent Particle Size

Dedrick and Beckman (1967) have indicated that in liquid-solid adsorption systems using a porous adsorbent, final adsorption capacity is

independent of adsorbent particle size. However, overall adsorption rate is a strong function of adsorbent particle size in pore diffusion controlled adsorption processes, being proportional to the reciprocal of some power of the adsorbent particle diameter (Weber, 1972). Recently Timpe (1972) has stated that the overall adsorption rate of lignin components from various total and partial pulp mill effluents onto activated carbon is proportional to the reciprocal of the adsorbent average particle diameter raised to the second power. These observations are consistent with the fact that reduction in adsorbent particle size is associated with a decrease in average pore length; the time required for adsorbate to pass through the pores and reach 'internal' adsorption sites is thus shortened.

I.2.6. (viii) Adsorbent Surface Nature

Although in comparison to silica, glass and quartz, the activated carbon surface is non-polar, it does nonetheless contain many chemical constituents in its surface layer. Such surface

functional groups, as may be present as fixed entities in the carbon surface lattice, or as substances already adsorbed on the carbon surface, may influence adsorptive behaviour in liquid-solid systems. Such surface characteristics are dictated primarily by carbon base material, activation method, and subsequent history. A detailed discussion of the nature of surface functional groups and their relation to carbon pH has been considered elsewhere (see Part II, Section II.7). Suffice it to say here that the nature of the carbon surface can influence the extent of adsorption of adsorbates, notably where exchange adsorption is the predominant adsorption mechanism. In this respect Snoeyink (1968) has shown that the surface characteristics of a carbon containing basic surface functional groups can be altered in the presence of an electrolyte, NaCl, with corresponding influence on its adsorption of acid from solution.

I.2.7. Adsorption In Multicomponent Liquid-Solid Systems

Although adsorption from multisolute liquid-

solid systems generally follows the principles pertainable to simple systems as outlined earlier, there are also some differences in adsorption behaviour of solutes present in a multisolute solution, as extensively discussed by Kipling (1965).

Studies of solutions containing two solutes have shown that the presence of the second solute can either reduce, increase or unchange the extent of adsorption of the first solute compared to its adsorption from a corresponding simple solution. Mutual inhibition of adsorption capacity can also occur. Table I.4 summarises some of the literature information available in this regard. Both Kipling (1965) and Weber and Morris (1964) suggest that the occurrence of reduced individual solute adsorption capacity in multisolute systems containing 'similar' solutes is a result of competitive adsorption of solutes to an extent dicated by the relative sizes, adsorptive affinities and concentrations of the individual solutes in solution. It is also apparent that, when dealing with porous

Table I.4 Adsorption from Solutions Containing More Than One Solute

| Reference | Solutes | Solvent | Adsorbent | Author's Comments |
|---|---|---|---|---|
| Michaelis and Roma (1908) | acetone/acetic acid | Water | Carbon | Adsorption of acetone reduced by presence of acetic acid. |
| Jäger and Erdös (1956) | phenol/p-cresol | Water | Flue dust | Mutual inhibition of adsorption of both solutes. |
| Jäger and Erdös (1959) | phenol/3,4 dimethylphenol | Water | Act. carbon | Dimethylphenol adsorbed to greater extent due to its lower solubility. |
| Dintenfass (1958) | phenol/stearic acid | Ether | Titania | No phenol adsorption due to preferential adsorption of stearic acid on polar adsorbents. |
| Angelescu and Cismaru (1935) | aromatic amines/ aliphatic acids | Water | Act. carbon | Solute interactions give rise to negligible adsorption, even though each solute is adsorbed significantly from simple solution. |

adsorbents, the nature of the adsorbent pore structure can also dictate the extent of solute competition for internal adsorption sites. Here for example, if one solute is smaller in size than the others, it may be effectively adsorbed in some of the smaller adsorbent pores without competition from other solutes.

Some theory has been developed for application to bi-solute systems containing two 'similar' solutes A and B. Butler and Ockrent (1930) have shown that, in cases where competition for all available adsorption sites occurs, and where the individual solutes in simple solution exhibit Langmuir adsorption behaviour, the extents of adsorption $\left(\frac{x}{m}\right)_A$, $\left(\frac{x}{m}\right)_B$ of the solutes from mixed solution are given by

$$\left(\frac{x}{m}\right)_A = \frac{Q_{oA}\, b_A\, C_A^*}{1 + b_A C_A^* + b_B C_B^*} \qquad (1.12)$$

and

$$\left(\frac{x}{m}\right)_B = \frac{Q_{oB}\, b_B\, C_B^*}{1 + b_A C_A^* + b_B C_B^*} \qquad (1.13)$$

Recently Jain and Snoeyink (1973) have adjusted Butler and Ockrent's model to satisfactorily predict adsorption from bisolute solution in the case where a portion of

adsorption of solute A occurs without competition.

Here $$\left(\frac{x}{m}\right)_A = \frac{(Q_{oA}-Q_{oB})\, b_A C_A^*}{1 + b_A C_A^*} + \frac{Q_{oB}\, b_A\, C_A^*}{1 + b_A C_A^* + b_B C_B^*} \qquad (1.14)$$

and

$$\left(\frac{x}{m}\right)_B = \frac{Q_{oB}\, b_A C_A^*}{1 + b_A C_A^* + b_B C_B^*} \qquad (1.15)$$

Equations (1.12) and (1.13) can be used in description of the adsorption of p-nitrophenol and p-bromophenol from mixed aqueous solution, whereas equations (1.14) and (1.15) are more applicable in describing adsorption behaviour of p-nitrophenol and an anionic benzene-sulphonate from mixed solution onto activated carbon.

In the case of multisolute solutions containing 'dissimilar' solutes, the relative solubilities and solute interactions, rather than relative sizes and concentrations of solutes, appear to be the significant factors in determination of individual solute adsorption from mixed solutions. The Freundlich model has successfully been used in description of single solute adsorption behaviour from mixed solutions of 'similar' and 'dissimilar' solutes. (Benedek and Ho (1973), Fuchs (1965), McGlasson (1967), Timpe (1971)).

## I.2.8. Adsorption of Polymer Solutes

Generally adsorption of polymeric solutes from solution onto a solid adsorbent follows the same principles discussed earlier for both simple and mixed solute adsorption. In addition, certain peculiarities unique to polymer adsorption must be considered. These arise primarily from the nature of polymer solutions. Firstly, polymer molecules by their very nature contain a large number of chemical functional groups, each of which may be potentially adsorbed at a surface. Secondly, polymers often exist in solution as cross-linked entities, the degree of cross-linking being proportional to solubility. The existance of very large highly cross-linked species in solution can complicate the adsorption picture as 'adhesion' rather than 'adsorption' may become a significant attachement mechanism (Kipling, 1965). Thirdly, polymers are usually polydisperse in solution, existing as a family of various molecular size and weight constituents. In this respect, adsorption of polymeric solutes may be considered similar to multicomponent adsorption in the special case that all solutes are derived from the same

basic monomeric unit. Finally, since the molecular configuration of a polymeric solute molecule can be anywhere from linear to spherical depending on polymer and solution conditions, adsorption may be influenced significantly by solute configuration.

The overall adsorption rates of polymeric solutes are usually very slow, as indicated in Table I.5. This observation can be explained in terms of the very slow diffusion rates of large polymeric solutes through the adsorbent pores. However, since slow overall rates of polymer adsorption have also been evidenced on non-porous adsorbents (Peterson and Kwei, 1961), other mechanisms are certainly at play. Because of the excessively long contact times required to attain equilibrium polymer adsorption, many authors prefer to use 'apparent equilibrium' conditions in describing polymer adsorption (Kipling, 1965).

Studies on the temperature dependence of polymer adsorption have indicated that adsorption can either decrease (Gilliland and Guthoff, 1960) or increase (Koral, 1958) with temperature rise. The

Table I.5 Overall Rates of Adsorption of Polymeric Solutes

| Reference | Polymer | Solvent | Adsorbent | Author's Comments |
|---|---|---|---|---|
| Kolthoff and Kahn (1950) | GR-S rubber | Benzene | Graphon | Adsorption continues after 48 hours. |
| Kabeya (1971) | Kraft Lignin | Alkali | Activated carbon | Adsorption continues after 48 hours. |
| Chen (1970) | Lignin | Alkali and acid | Activated carbon | Adsorption continues after 20 days. |

latter observation has been attributed to a displacement of adsorbed solvent molecules by polymer molecules (Eirich, 1957).

Provided there is no significant steric hindrance to adsorption, then the extent of adsorption of polymeric solutes usually increases with increase in polymer molecular weight. This is due to the decrease of polymer solubility with molecular weight increase. Sometimes, however, polymer adsorption is found to be independent of polymer molecular weight (Kolthoff and Kahn, 1950). Kipling (1965) suggests that the influence of molecular weight on adsorption capacity in 'unrestricted' adsorption probably depends on

a) the solvent used ('good' versus 'poor' solvent)

b) the closeness of adsorption temperature T to the initial miscibility temperature of the polymer solution.

Here the dependence of adsorption on polymer molecular weight would be more pronounced in 'poor' solvents where T is close to $\Theta$, as in such cases the effect of

polymer molecular weight on polymer solubility is very marked.

Steric hindrance to adsorption is, however, often very evident when dealing with polymer solutions, since usually very large solute molecules are present. The magnitude of the steric hindrance effect is dependent on both polymer molecular size and adsorbent pore size distributions. If steric hindrance is significant, then the reverse observation, i.e. increase in adsorption capacity with decrease in molecular weight, can occur (Huppenthal, 1963). In such cases increasingly larger polymeric solutes are excluded from progressively larger amounts of the adsorbent pore structure, even though the adsorption potential increases with molecular weight due to solubility considerations. At the extreme, with very large solutes and very small adsorbent pores, no appreciable polymer adsorption occurs, in spite of a very high adsorption potential (Kisilev, 1963). Literature information on the effect of polymer molecular weight on adsorption is summarised in Table I.6.

Table I.6 Effect of Polymer Molecular Weight on Adsorption

| Reference | Polymer | Solvent | Adsorbent | Author's Comments |
|---|---|---|---|---|
| Kolthoff and Kahn (1951) | GR-S rubber | Benzene | Graphon | Adsorption virtually independent of polymer molecular weight in the 32,000 - 230,000 range. |
| Amborski (1950) | GR-S rubber | Aromatic Solvents | Carbon Black | Adsorption increases with molecular weight |
| Treiber (1953) | Polystyrene | Cyclohexane | Charcoal | Polystyrene adsorption greater than toluene adsorption at similar concentration. |
| Claesson and Claesson (1945) | Polyvinyl-acetate | Benzene | Charcoal | Adsorption increases with molecular weight |
| Koral (1958) | Polyvinyl-acetate | Benzene | Iron or Tin Powder | Adsorption increases with molecular weight |
| Perkel and Ullman (1961) | Polydimethyl-siloxane | Benzene | Iron or glass | Adsorption increases with molecular weight |
| Gilliland and Guthoff (1960) | Polyisobutene | Benzene | Carbon Black | Preferential adsorption of high molecular weight polymer fractions up to $10^6$ MW. Above $10^6$ MW, adsorption independent of molecular weight. |
| Frisch (1959) | Polystyrene | Toluene | Carbon Black | Lower molecular weight fractions initially preferentially adsorbed, but subsequently displaced by higher molecular weight fractions. |
| Kisilev (1963) | Polydimethyl-siloxane | Hexane | Molecular Sieve 13x | No adsorption of polymer onto internal pore structure, even though monomer is significantly adsorbed. |
| Huppenthal (1963) | Polymeth-acrylic acid | Aqueous Alcohol | Activated carbon | Adsorption decreases with molecular weight, according to $\left(\frac{x}{m}\right)_p = A(MW)_p^{-\beta}$, A,$\beta$ constants |

Several models have been used in description of observed polymer adsorption behaviour. A summary of the more common models is shown in Table I.7. Since polymer adsorption from monodisperse polymer solutions usually tends towards a limiting value (Kipling, 1965), description by the Langmuir model seems appropriate (see Table I.1). However, in most cases the Langmuir model will predict lower initial adsorption values, and a higher limiting adsorption value, than those derived experimentally. Furthermore, the limiting adsorption value has been shown to be associated with an adsorbed layer of several molecular thicknesses (Patat, 1961; Amborski, 1950). In order to account for the discrepancy, Jenkel and Rumbach (1951) proposed the 'anchor segment' theory of polymer adsorption, suggesting that only certain functional groups of the adsorbed macrosolute are attached to adsorption sites, with the remainder of the macromolecule streaming out into the solvent phase, as shown in Fig. I.1. At the extreme, where an extensive number of functional groups are adsorbed, 'total

Fig. I.1 Surface Attachment of Adsorbed Polymer Molecules

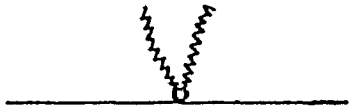

Anchor Segment Adsorption
$\nu = 1$

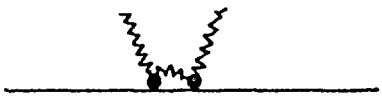

Anchor Segment Adsorption
$\nu = 2$

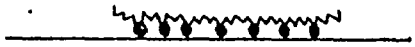

Total Deposition Adsorption
$\nu$ = large

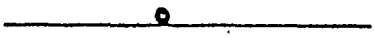

Simple Solute Adsorption
$\nu = 1$

deposition' or 'layer' adsorption of the macromolecule occurs. The polymer adsorption isotherm models based on this theory and indicated in Table I.7 incorporate a term $\nu$, the average number of adsorbed functional groups per polymer molecule, where increase in $\nu$ represents a trend to 'layer' adsorption. In adsorption of simple solutes, $\nu = 1$ and the equations in Table I.1 revert to the simple Langmuir or B.E.T. forms.

In adsorption from polydisperse polymer solutions, both 'anchor segment' and 'layer' adsorption of polymeric solutes certainly occurs, with the latter mechanism predominating in adsorption of low molecular weight species and the former occuring almost exclusively with high molecule weight constituents. In addition, strong interaction between solute and adsorbent will favour 'layer' adsorption, whereas a weaker interaction will favour 'anchor segment ' adsorption. However, adsorption from polydisperse polymer solutions does not usually tend to a limiting value. In such vases either the B.E.T., modified B.E.T. or Freundlich equation has been used

Table I.7 Common Models Used In Describing Polymer Adsorption in Liquid-Solid Systems

| Model | Equation | Assumptions |
|---|---|---|
| Langmuir | $\sigma = \frac{bC^*}{1 + bC^*}$ (b = a constant) | see Table I.1 |
| Simha, Frisch, Eirich (1953) | $\frac{\sigma}{1-\sigma} e^{K_1\sigma} = (K_2 C^*)^{1/2}$ ($K_1$, $K_2$ constants) | 1. Langmuir assumptions.<br>2. 'Anchor Segment' adsorption.<br>3. Gaussian Distribution of polymer strands extending into soln.<br>4. Small interaction between strands in adsorbed layer. |
| Kraus and Dugone (1955) | $\sigma = \frac{(KC^*)^{1/2}}{1 + (KC^*)^{1/2}}$ (K= a constant) | as for S.F.E. model, but no strand interactions. |
| Gilliland and Guthoff (1960) | $\frac{\sigma}{(1-\sigma)^\nu} = \nu KC^*$ (K = a constant) | as for S.F.E. model, but adsorption at critical miscibility temperature. |
| B.E.T. | $\frac{x}{m} = \frac{Q_o B C^*}{(C_s - C^*)\left[1+(B-1)(C^*/C_s)\right]}$ ($Q_o$, B, $C_s$ constants) | see Table I.1 |
| Modified B.E.T. | $\frac{x}{m} = \frac{Q_o t B (C^*)^{1/2}}{\nu\left[(C_s)^{1/2} - (C^*)^{1/2}\right]\left[1+(B-1)(C^*/C_s)^{1/2}\right]}$ | 1. B.E.T. assumptions<br>2. Value of $\nu$ is average of $\nu$ values for each adsorbed layer. |
| Freundlich | $\frac{x}{m} = K C^{*1/n}$ (K, n constants) | see Table I.1 |

Note: C* = equilibrium polymer concentrations , $\sigma = \left[(x/m) / (x/m)_\infty\right]$

to describe adsorption behaviour, (Kipling, 1965), the latter being used extensively in describing adsorption of lignin components from various pulp mill effluents onto activated carbons (see section II.2.9).

The models in Table I.7 all assume negligible solvent adsorption. While this assumption is valid for adsorption of simple solutes, it may not necessarily hold for polymer adsorption. As Kipling (1965) has pointed out, large numbers of solvent molecules may be mechanically or chemically associated with each adsorbed polymer molecule in the surface layer. In such cases, the term $V_o$ in equation (1.3) - see page I.7 - may not be constant during adsorption. Hence the values of polymer adsorption $(x/m)_p$ calculated from equation (1.3) may not be accurately reflective of true polymer adsorption.

Unlike most simple or mixed solute adsorption systems, the polymeric solute molecules can undergo considerable change during the adsorption process, as a result of adsorption conditions. These changes can occur either in bulk solution or in the adsorbed layer. For instance, continuous mechanical degradation of

polymeric solutes to higher or lower molecular weight forms can occur in solution, simply as a result of imposed agitation of the reaction vessel (Sonntag and Jenkel, 1954). Such changes can complicate the adsorption picture, as the adsorbate is presented with solute of continually changing characteristics.

I.2.9 Adsorption of Lignin Onto Activated Carbon

Several researchers have studied the lignin-activated carbon adsorption system. Bloodgood and Sami-el-Naggar (1962) demonstrated in batch experiments using various pulverized activated carbons and a one hour contact time, that virtually complete decolorisation of acid, caustic and combined NSSC pulp mill bleaching effluents could be attained. The adsorption of lignin, as measured by color and TOC, was adequately described by the Freundlich model. In addition, it was also found that lignin adsorption efficiency, as measured by color, increased with decrease in solution pH to approximately 1.7, this observation being attributed to decrease in solubility of the lignin color bodies at lower pH. These researchers also demonstrated that complete decolor-

isation of effluents could be obtained in continuous flow carbon beds at flow rates of 0.5 - 0.8 gal/min-ft$^2$.

Fuchs (1965) studies on the adsorption of lignin, as color, from kraft mill bleachery effluents demonstrated the pore diffusion control of the overall lignin adsorption rate process. In batch experiments using granular carbons and a two hour contact time, adsorption of color was also found to be favoured by low pH and high temperature in the 100°- 200°F and pH 2 - 4 ranges studied. These observations were attributed to decrease in the solubility of lignin color bodies with increase in temperature and decrease of pH. In similar experiments using lime-treated caustic bleachery effluent, Fuchs found that maximum adsorption of color bodies occurs at pH 5, in contrast to the lack of optimum adsorption pH in the case of untreated caustic effluent. He postulated that this is due to the presence of calco-lignin derivatives, which have a different isoelectric pH compared to the untreated color bodies. Fuchs also demonstrated that adsorption isothems based on color removals could be fitted by a Freundlich model, and that complete decolorisation of

all effluents was feasible. Adsorption of color bodies was also found to be significantly irreversible.

McGlasson (1967) characterised the color bodies present in kraft mill bleachery effluents by membrane filtration. He confirmed that the pH effect on lignin adsorption is related to lignin solubility, by showing that in neutral or alkaline pH color bodies exist as sub-colloidal particles or true solutes, but at pHs less than 3 they are present as large gelatinous particlate agglomerates. In activated carbon adsorption studies using IR spectroscopy, McGlasson also showed that complete color removal is associated with removal of all lignin functional groups from solution. Although he found activated carbon adsorption alone is capable of reducing the color of kraft mill effluents to very low concentrations, the most economical use of activated carbon would be as a polishing stage after lime treatment.

Both Thibodeaux (1967) and Smith (1968) have demonstrated the applicability of activated carbon adsorption as a stage in an overall treatment process aimed at yielding a reusable water from pulp mill

effluents. Using granular carbon columns, approximately 70 - 100% removal of color bodies could be achieved at flows of 3.6 - 6 gal/min-ft$^2$.

Timpe (1970 a, b; 1971 a, b) also studied the activated carbon adsorption stage in various combinations of a Lime/Bio-oxidation/activated carbon treatment sequence for purification of pulp mill effluents. Timpe showed that color adsorption isotherms obtained on various mill effluents, using several pulverised carbons and two minutes contact, could be described by the Freundlich model. The variations in the isotherms obtained using different carbons were attributed to differences in carbon pore structure. Unlike the previous researchers, Timpe found the color isotherms exhibited 'dog legs' as shown in Fig. I.2. He suggests that this is due to selective adsorption of certain lignin color bodies from solution; here adsorption of the major portion of lignin color bodies does not occur until the strongly adsorbed color bodies are almost completely removed from solution. Timpe also found that color adsorption was most efficient if the effluent was lime-treated prior to adsorption. In view of Dugal's (1971)

Fig. I.2 Adsorption Isotherms of Color From Pulp Mill Effluents Onto Activated Carbon
(ref. Timpe 1970, Kabeya 1971)

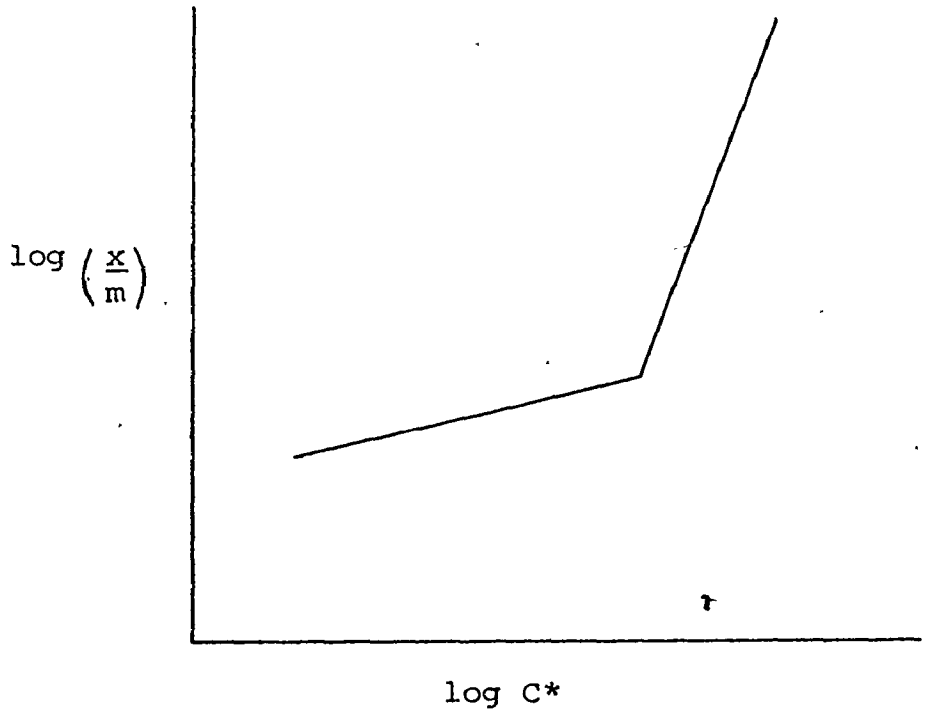

findings, i.e. that lime-treatment of kraft mill bleached decker effluent only removes larger lignin color bodies of greater than 5000 MW, it would appear that the efficiency of color removal by carbon is higher if the color bodies in solution exist as low molecular weight solutes. Timpe also found that color adsorption efficiency increases if the effluent is first bio-oxidised. This is attributed to removal of bio-degradable components present with the lignin color bodies in the effluent, which otherwise may compete with the color bodies for adsorption sites. Timpe also demonstrated the low pH favourability of the color adsorption process.

Kabeya (1971) studied the adsorption of lignin, as color, from kraft mill effluents onto granular activated carbon. Here color adsorption rate was found to be very slow (color adsorption was still continuing after 48 hours contact at 25°C), indicating a pore diffusion controlled process. Kabeya also found the isotherms fitted the Freundlich model, and exhibited the characteristic break or 'dog leg' noted by Timpe. Like Fuchs, Kabeya found

adsorption of lignin color bodies was favoured by lower pH in the 7 - 11 range, and higher temperature in the 50° - 100° F range. He also calculated, via Arrhenius plots, the color adsorption activation energy to be 7.9 kcal/mole, a value which appears to oppose the hypothesis of chemisorption as a significant adsorption mechanism for lignin color bodies.

Chen (1970) studied the adsorption of lignin, as TOC, from a kraft mill bleachery chlorination stage effluent onto various granular activated carbons. The slow adsorption rate of lignin, as TOC, was confirmed; even after 20 days contact at 30°C adsorption was still occurring. Like McGlasson, Chen noted that TOC adsorption rate increased with decrease in carbon particle size, although 'final' adsorption was independent of adsorbent particle size. Chen also suggests that TOC adsorption occurs by a concentration-precipitation mechanism, whereby lignin components 'salt out' and adsorb in the carbon pores to an extent dictated by the initial concentrations of lignin components in bulk solution, and carbon pore structural

characteristics. By relating carbon pore structure in the 37-70 Å pore radii range to observed TOC adsorption isotherms using various carbons, Chen has shown that this pore size range is reasonably reflective of the specific carbon pore structure in which preferential adsorption of TOC-contributing solutes from bleach plant chlorination effluent occurs.

Other researchers have looked at the lignin/activated carbon adsorption system, although their findings are limited. Copeland and Smithson (1971) showed that activated carbon produced from sulphite waste liquor is capable of removing significant amounts of color from paper mill effluents. Berger (1969) has indicated that pre-treatment of coloured mill effluent with an anionic polymer enhances subsequent color and TOC adsorption efficiency on activated carbon.

Unfortunately, the studies of the lignin/activated carbon system summarised here have not been applied to 'simple' lignin solutions but rather have considered pulp mill effluents, which are complex

multisolute solutions containing a variety of lignins in addition to numerous other undefined organic and inorganic solutes. It is thus possible that the deductions regarding lignin adsorption made from these works may not necessarily apply to the adsorption of lignin from 'simple' lignin solutions used in this study. This is because

a) The presence of other non-lignin adsorbates in industrial effluents may influence lignin adsorption behaviour (ref. sections I.2.7 and I.2.8.)

b) The use of color, TOC, COD in quantitising lignin removal from industrial effluents may not be valid since other substances such as tannins, resins, and amines present in such effluents are also known to exert color, COD and TOC (Felicetta and McCarthy, 1963).

## I.3 EXPERIMENTAL

### I.3.1 Carbon Preparation

Prior to its use in adsorption studies, the activated carbon sample was cleaned. Here 300 - 400 g carbon was gently boiled in a 5 litre beaker with distilled deionized water for 3 - 4 hours. After boiling, surface scum and excess water was decanted off and the resultant carbon slurry vacuum filtered on a Watman #2 filter paper, the cake being washed at least twice with distilled water. After filtration, the carbon cake was gently broken up and allowed to dry for 24 hours in a 103°C oven. The dried carbon was stored in a desiccator until required.

### I.3.2 Adsorption Studies

Batch adsorption studies of the lignin/activated carbon system were carried out in 125 ml stoppered flasks contained in a constant temperature water bath shaker.

A 500 mg/l Indulin solution was prepared at desired pH and quantitised in terms of color and TOC content as outlined in Part III. Fifty ml. aliquots

of this solution were then immediately pipetted into 16 Erlenmeyer flasks, which were stoppered and placed in the water bath shaker at desired temperature. The flasks were then agitated at 80 oscillations per minute for half an hour, in order to bring the lignin solution up to temperature.

I.3.2. (i) Kinetic Studies

After initial shaking, the same preweighed amount of dry carbon was added to at least 10 flasks. Here carbon dosages ranged from 0.03 - 0.6 g per flask - corresponding to 0.6 - 12 g carbon/litre solution - depending on the carbon used. Adsorption was then allowed to commence. After each desired contact time, a flask was removed and the contents immediately filtered through a prewashed 0.45 $\mu$ membrane filter. The filtrate was analysed for pH. The following control solutions were also used in the kinetic runs

a) 50 ml buffer solution

b) 50 ml buffer solution and carbon

c) 50 ml lignin solution

These were also filtered and analysed for pH, color and TOC (where appropriate) at the same time as the last 'kinetic' sample.

I.3.2. (ii) Equilibrium Studies

Here, after initial shaking, different pre-weighed amounts of the same dry carbon were added to at least 10 flasks. Carbon dosages ranged from 0.015 - 2 g per flask - corresponding to 3 - 40 g carbon/litre solution - depending on the carbon used. After a suitable 'equilibrium' contact time (as determined from adsorption kinetics with the same carbon), the solutions were filtered and filtrate analysed for pH, color and TOC as before. Control solutions similar to those in kinetic experiments were also used, with control (b) being run with the maximum carbon dosage.

I.3.3. Gel Filtration of Adsorption Residuals

Selected filtered residual solutions from equilibrium and kinetic adsorption studies were subjected to Gel Filtration through a pre-calibrated Sephadex G-100 gel bed, using a 0.1 M NaOH carrier solution. Details of the operation of this Gel Filtration

unit are given in Part III. Residual solutions were stored in a 4 °C incubator in the event that immediate Gel Filtration was not possible.

## I.4 RESULTS AND DISCUSSION

### I.4.1 Kinetic Studies - Rates of Adsorption

The overall adsorption rates of Indulin, measured as color and TOC, from aqueous alkaline solution by different activated carbons are shown in Figs. I.3 to I.6. The Dedrick and Beckman (1967) approach - see Section I.2 - was used to express the data, assuming equilibrium contact times of 15 hours and 4 days when using powdered and granular carbons respectively.

Generally the overall rates of lignin adsorption are observed to be very slow, and are in agreement with other researchers' findings (Fuchs, 1965; McGlasson, 1967; Kabeya, 1971; Chen, 1970) confirming the pore diffusional control of the overall kinetic adsorption process. The faster Indulin adsorption rates achieved with powdered carbons result primarily from carbon particle size considerations. The smaller average particle diameters of the powdered carbons - see Part II, Table II.8 - are associated with smaller pore lengths, enabling more

Fig.I.3 Color Adsorption Kinetics for Granular Carbons

500mg/l Indulin., $C_o$=4200CU, pH=10, 35°C, 10g carbon/l.

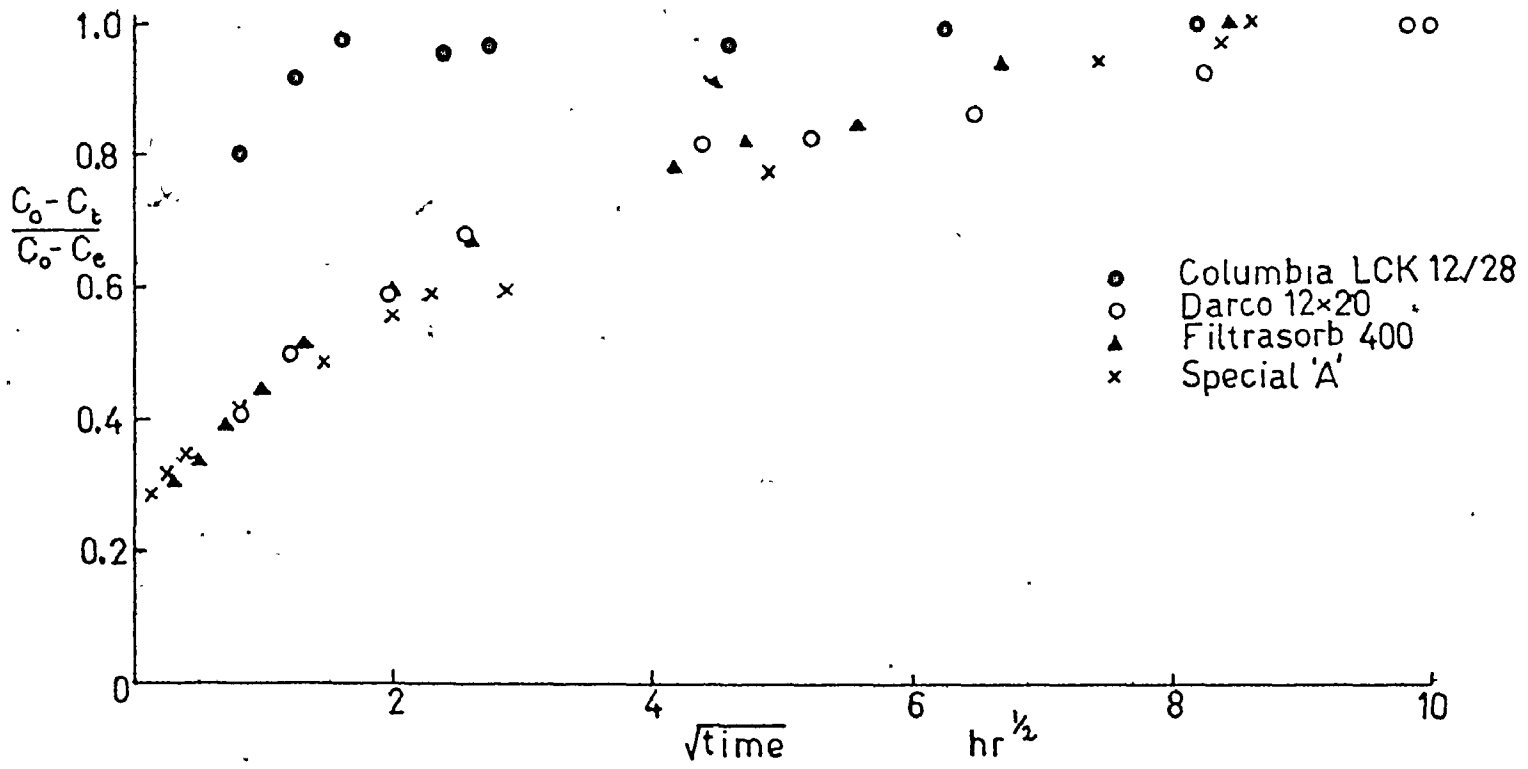

Fig.I.4 TOC Adsorption Kinetics for Granular Carbons

500 mg/l Indulin, $TOC_o$=335 mg/l, pH=10, 35°C, 10g carbon/l.

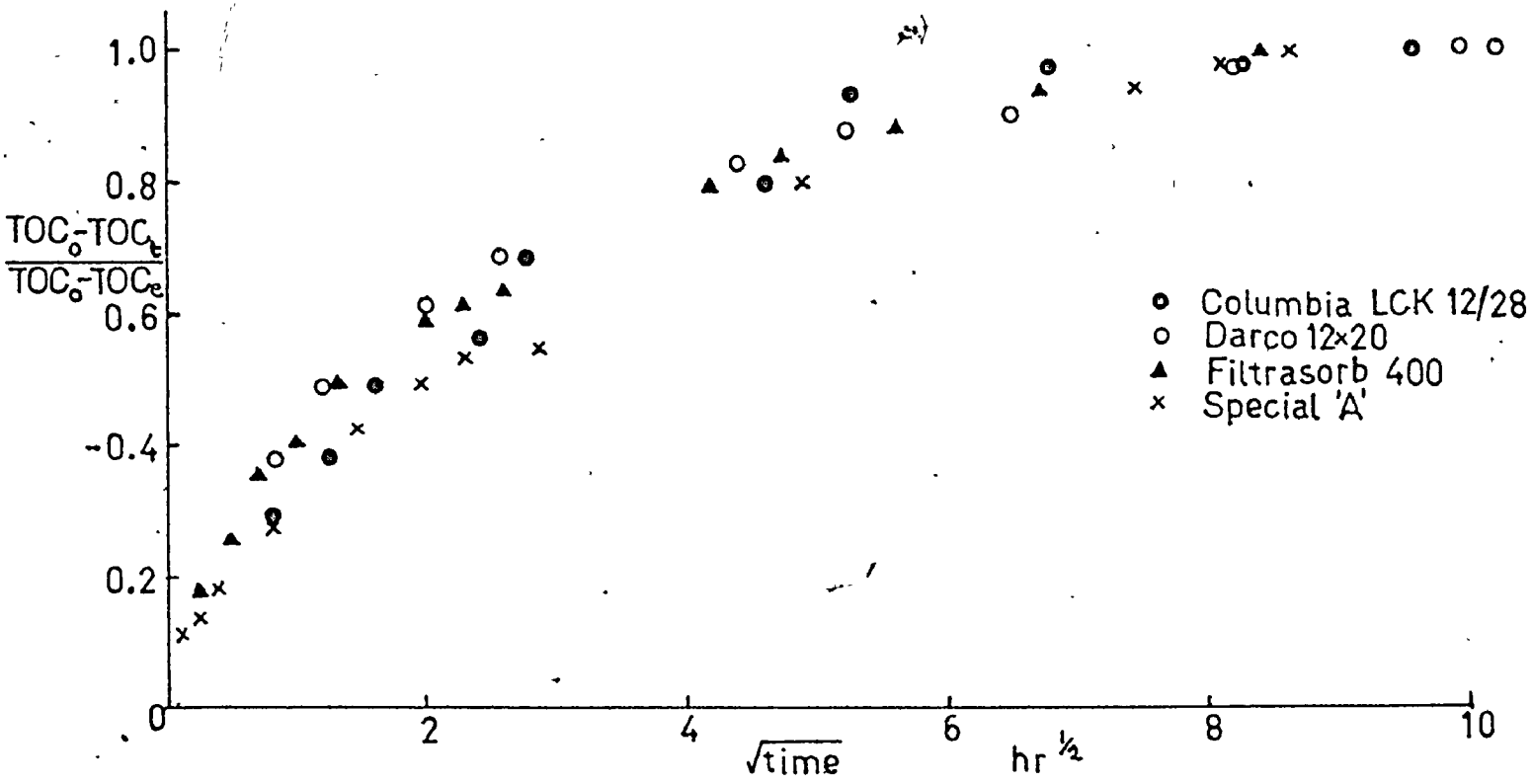

Fig.I.5 Color Adsorption Kinetics for Powdered Carbons

500 mg/l Indulin , $CU_o$=4200 CU , pH=10 , 35°C , 10g carbon/l.

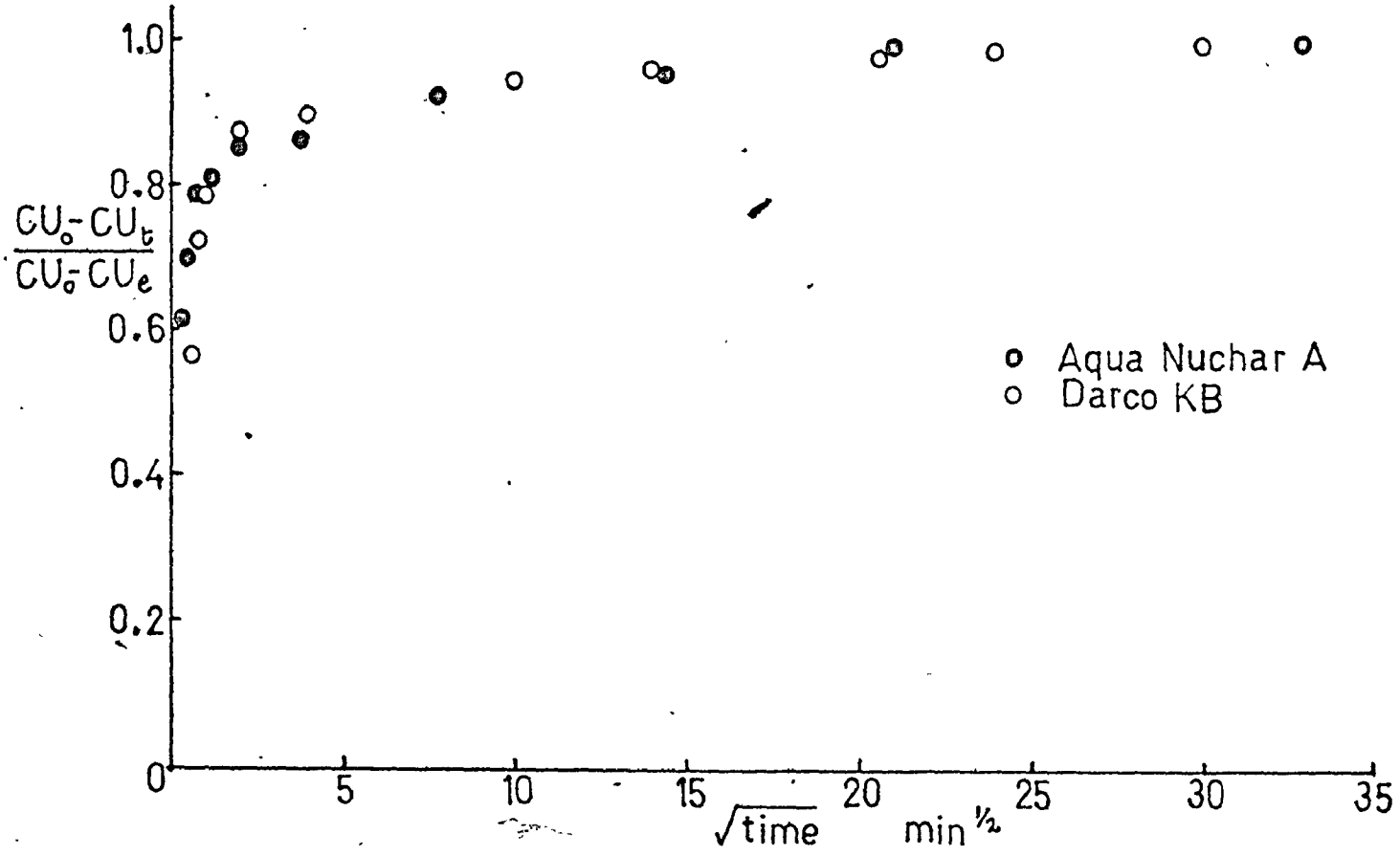

Fig.I.6 TOC Adsorption Kinetics for Powdered Carbons

500 mg/l Indulin, $TOC_o$ = 335 mg/l, pH = 10, 35°C, 10g carbon/l.

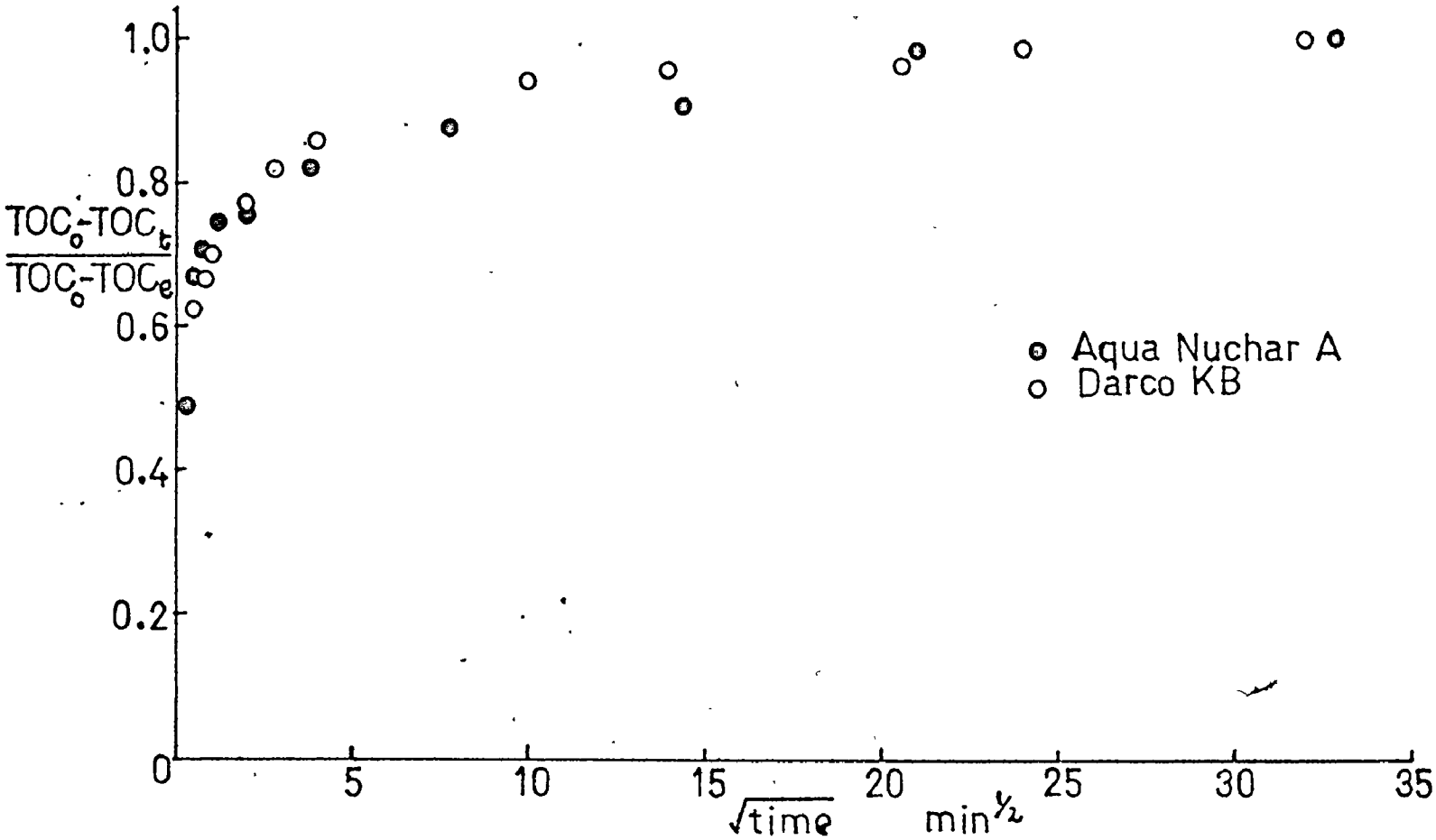

rapid arrival of lignin solutes at pore adsorption sites.

Carbon pore structure also influences lignin adsorption kinetics. Here it can be seen from Fig. I.3 that Columbia LCK 12/28 adsorbs Indulin color at a faster rate than either Darco 12x20 or Filtrasorb 400, even though the average particle sizes of these carbons are similar. As will be shown later, this arises because Columbia is capable of adsorbing only the small molecular weight lignin color bodies, due to lack of sufficient pore structure in the larger pore size range specific to adsorption of larger lignin solutes.

Carbon pore structural effects also serve to explain the 'lower-than-expected' adsorption rate of Indulin onto Special "A". The Indulin adsorption rates using Special "A", Darco 12x20 and Filtrasorb are similar, even though the average particle size of Special "A" granules is approximately half that of the other two carbons. As will again be shown later, this arises from the inability of Special "A" to

adsorb the small lignin solutes, due to a lack of carbon micropore structure appropriate to preferential adsorption of these adsorbates.

Unfortunately the observed adsorption rate data in Figs. I.3 to I.6 is not linearised using the Dedrick and Beckman approach, and so the adsorption kinetics cannot be accurately represented by a unique characteristic diffusivity value $D_l$. This is the result of two main factors, viz.

a) the 'finite bath' nature of adsorption experiments

b) lack of attainment of a true equilibrium adsorption value, even at long contact times.

In a finite bath adsorption system, the Indulin concentration in bulk solution is continually depleted as adsorption proceeds. Hence adsorption will level off with time due to driving force considerations. Likewise, the choice of a practical pseudo-equilibrium adsorption contact time t corresponding to $C_e$ will also cause Figs. I.3 - I.6 to deviate from linearity. How-

ever, by using the aforementioned pseudo-equilibrium contact times for powdered and granular carbons, the latter effect is probably minimal.

The use of other models, as outlined in Section I.2.5, for linearisation of Indulin adsorption rate data proved to be unsatisfactory.

I.4.1 (i) Temperature Effect

The effect of system temperature on the overall rate of adsorption of Indulin from aqueous solution is shown in Figs. I.7 and I.8. Here adsorption rate is seen to increase with system temperature rise, this being more noticeable when considering TOC adsorption kinetics. This observation agrees with the findings Kabeya (1971), and is probably associated with the decrease in solvent viscosity with temperature rise. At higher temperature the lignin solutes will be more mobile in the solvent, and thus take a shorter time to arrive at adsorption sites. This supposition is supported by noting that the viscosities of the water solvent at 20°C and 50°C are 1.000 cp and 0.549 cp respectively, representing approximately 45% drop in

Fig.I.7 Color Adsorption Kinetics at Different Temperatures

500 mg/l Indulin, $CU_o$ = 4200 CU, pH = 10, 4 g/l Darco KB

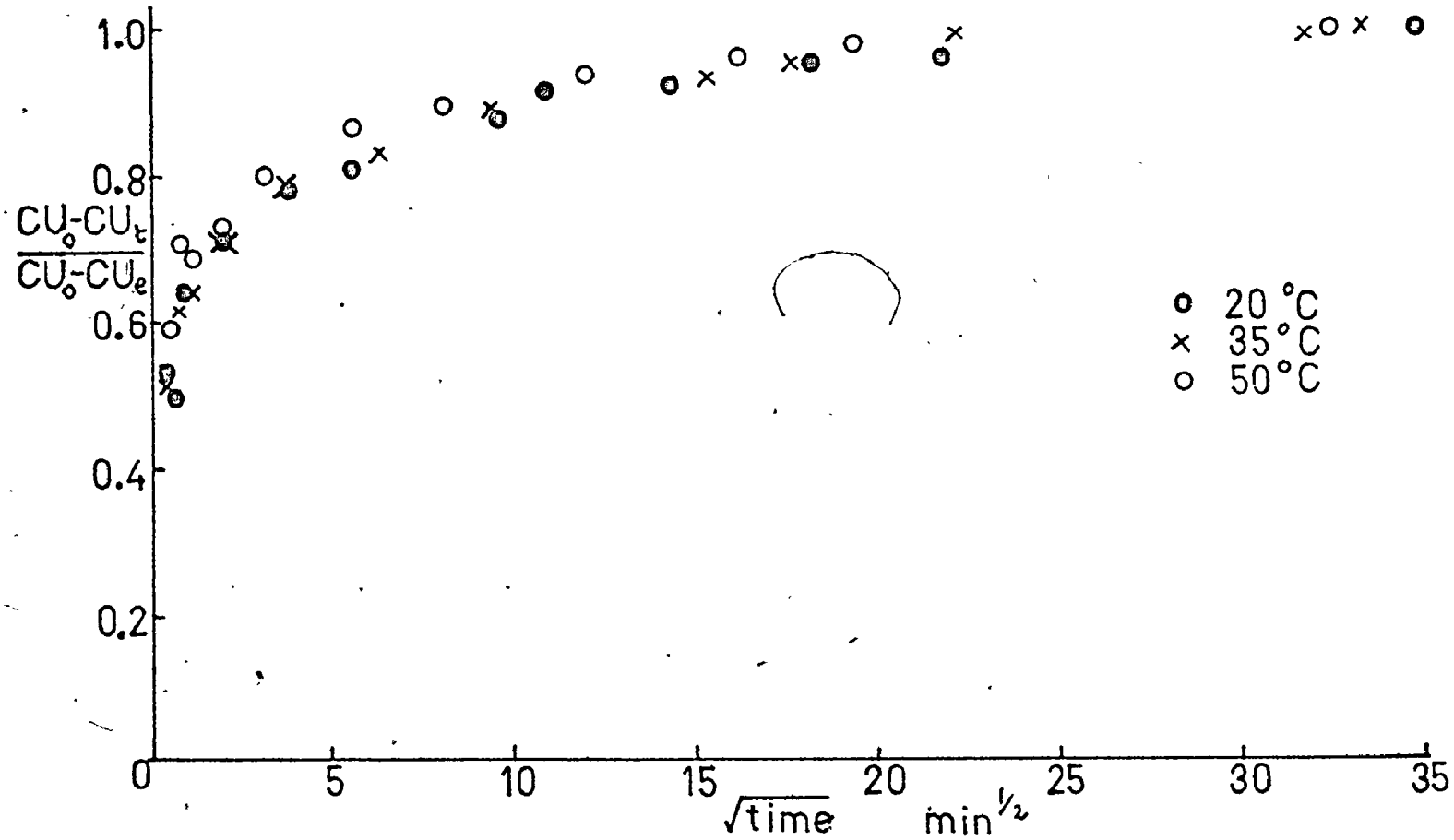

Fig.I.8 TOC ADsorption Kinetics at Different Temperatures

500 mg/l Indulin, $TOC_o$ = 335 mg/l, pH=10., 4 g/l Darco KB

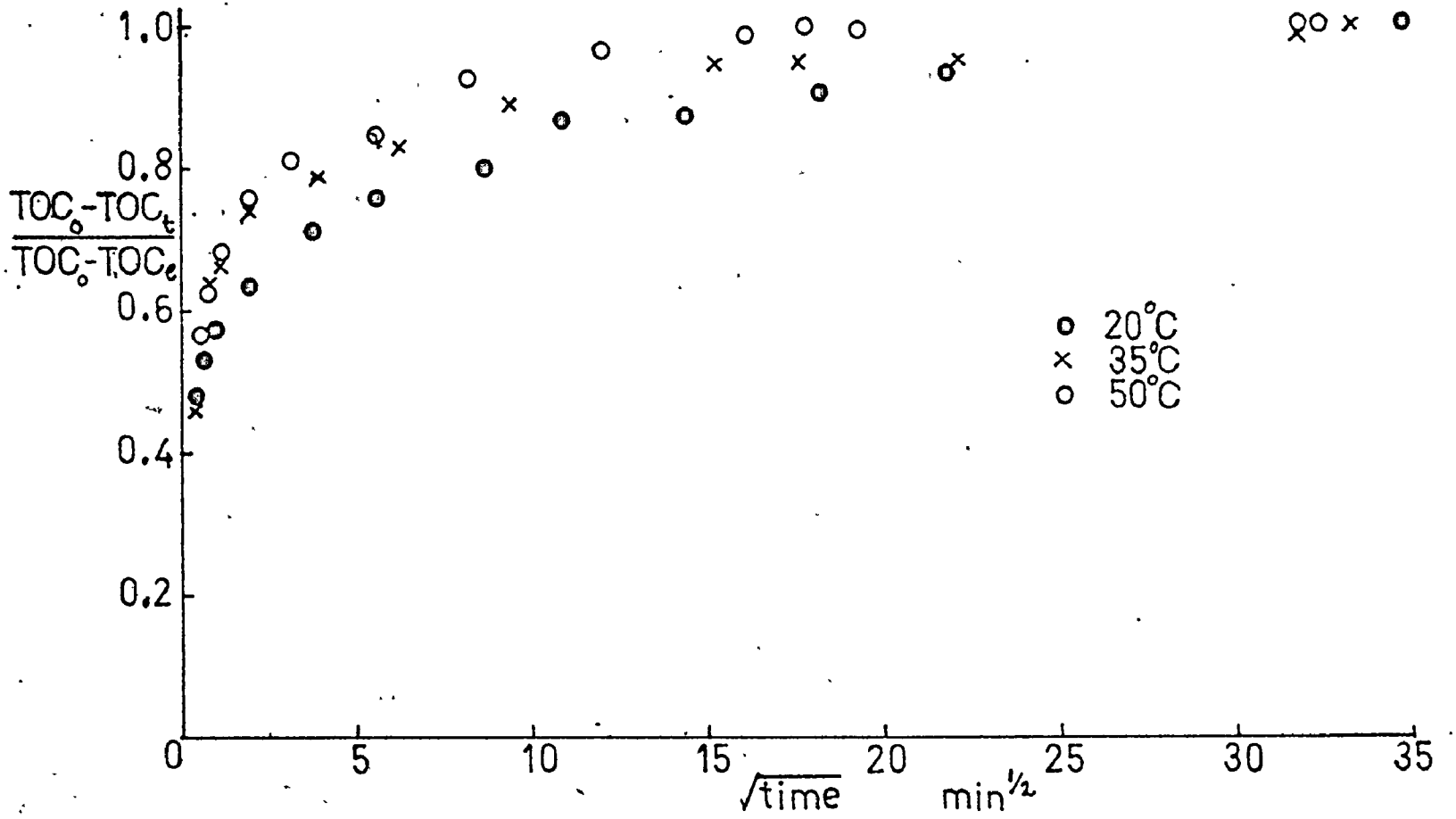

solvent viscosity with temperature increase in this range. Conversely, in view of Weber's (1972) statement that in liquid/solid adsorption systems, heats of adsorption are generally small and of the same magnitude as heats of crystallisation, it seems unlikely that the temperature effect is a result of radical changes in the lignin adsorption reaction.

I.4.1 (ii) pH Effect

The effect of inital solution pH on the overall adsorption rate of Indulin from aqueous solution is shown in Figs. I.9 and I.10. Here the adsorption rate of color and TOC is observed to decrease with decrease in inital solution pH. This effect is associated with alteration of the molecular distribution of Indulin components in solution with pH change. As indicated by the results of the ultrafiltration experiments outlined in Part III (see Figs. III. 12 and III. 13 ), the average molecular weight $\overline{M}_n$ of Indulin in solution increases with pH decrease. This is associated with an increase in the number of larger molecular weight species at the expense of the low molecular weight constituents. At high pH, a significant

Fig.I:9 Color Adsorption Kinetics at Different pH

500mg/l , $CU_o$= various , 35°C , 4 g/l Darco KB
Indulin

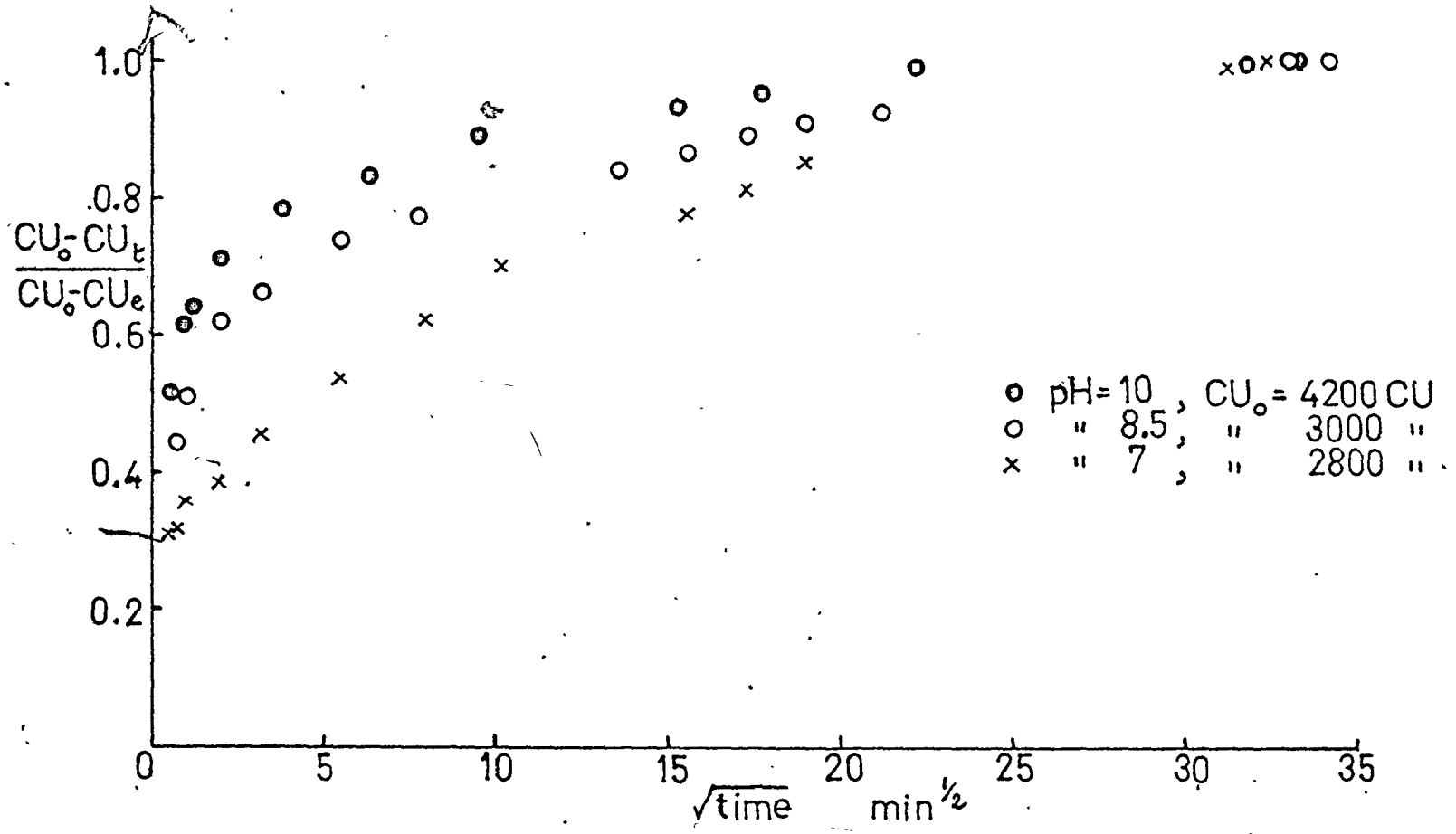

Fig.I.10 TOC Adsorption Kinetics at Different pH

500 mg/l Indulin, $TOC_o$ = 335 mg/l, 35°C, 4 g/l Darco KB

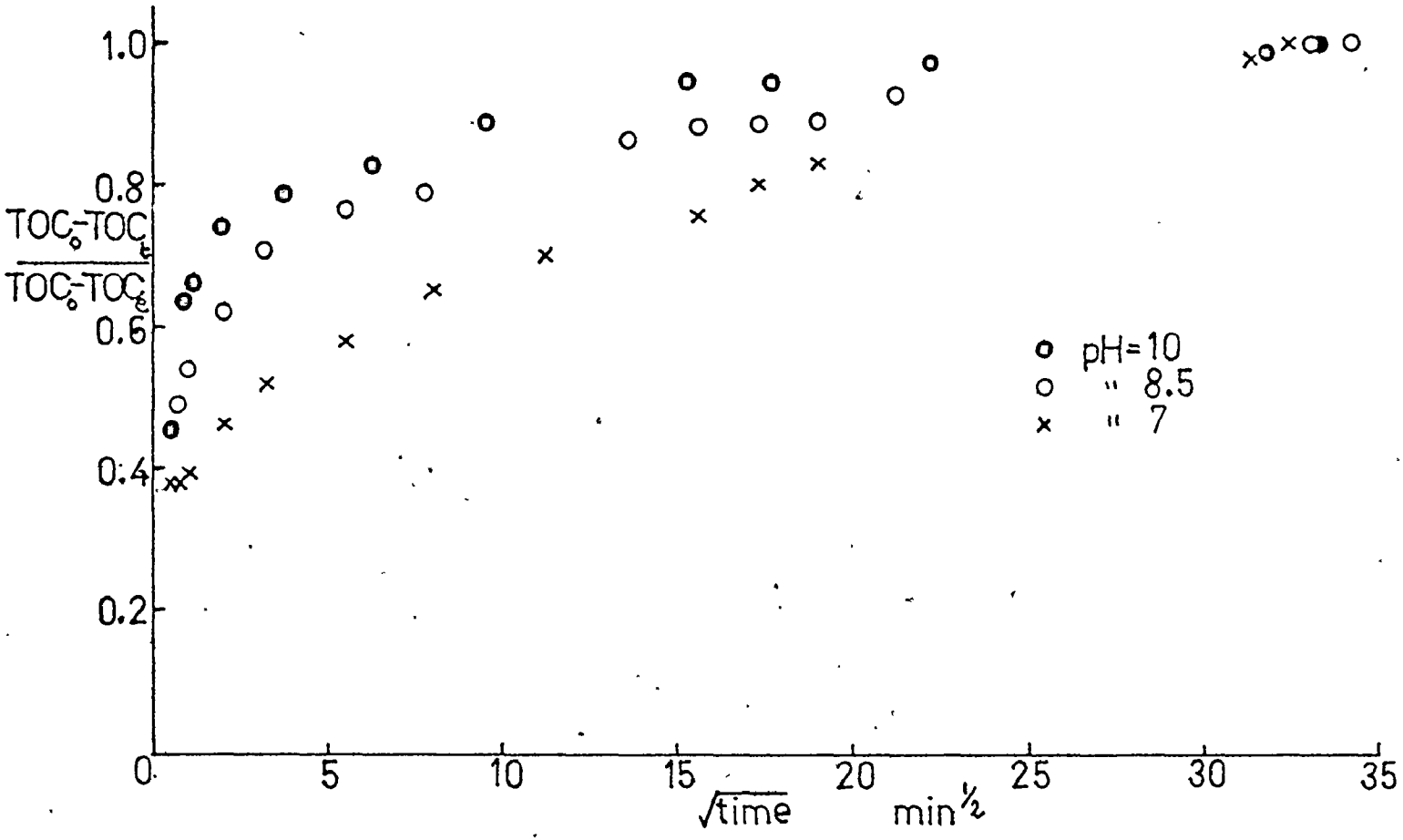

portion of the overall solution color and TOC content is exerted by relatively small molecular weight solutes. Such species have relatively high mobilities and hence overall adsorption rate will be relatively fast. Conversely, at pHs approaching neutral, the bulk of overall solution color and TOC is contained in much larger molecular weight Indulin solutes. Since such solutes have correspondingly lower mobilities, the overall rate of adsorption will be slower.

It should be noted here that although the overall adsorption rate of Indulin decreases, equilibrium adsorption capacity correspondingly increases as discussed later.

I.4.1 (iii) Carbon Dosage Effect

The effect of carbon dosage on the overall adsorption kinetics of Indulin from aqueous solution is shown in Figs. I.11 and I.12. Here the overall adsorption rate of color and TOC is seen to generally increase with carbon dosage. This behaviour is due to the increased absorbent surface area that is presented to the adsorbate with increase in carbon dosage. At low carbon dosages - corresponding to relatively few adsorbent particles in the system - the time taken for adsorbate to diffuse from bulk solution to a surface adsorption site may be relatively long. In addition, competition of adsorbates for adsorption sites at the surface may be significant. Realisation of more adsorbent particles and increased available surface area by increasing carbon dosage will result in faster arrival of adsorbates at the carbon surface, and also minimise competition for adsorption sites, producing faster overall adsorption rates.

The results in Figs. I.11 and I.12 indicate that comparison of adsorption kinetic data for

Fig.I.11 Color Adsorption Kinetics at Different Carbon Dosages

500 mg/l Indulin, $CU_o$=4200 CU, pH=10, 35°C, Darco KB carbon

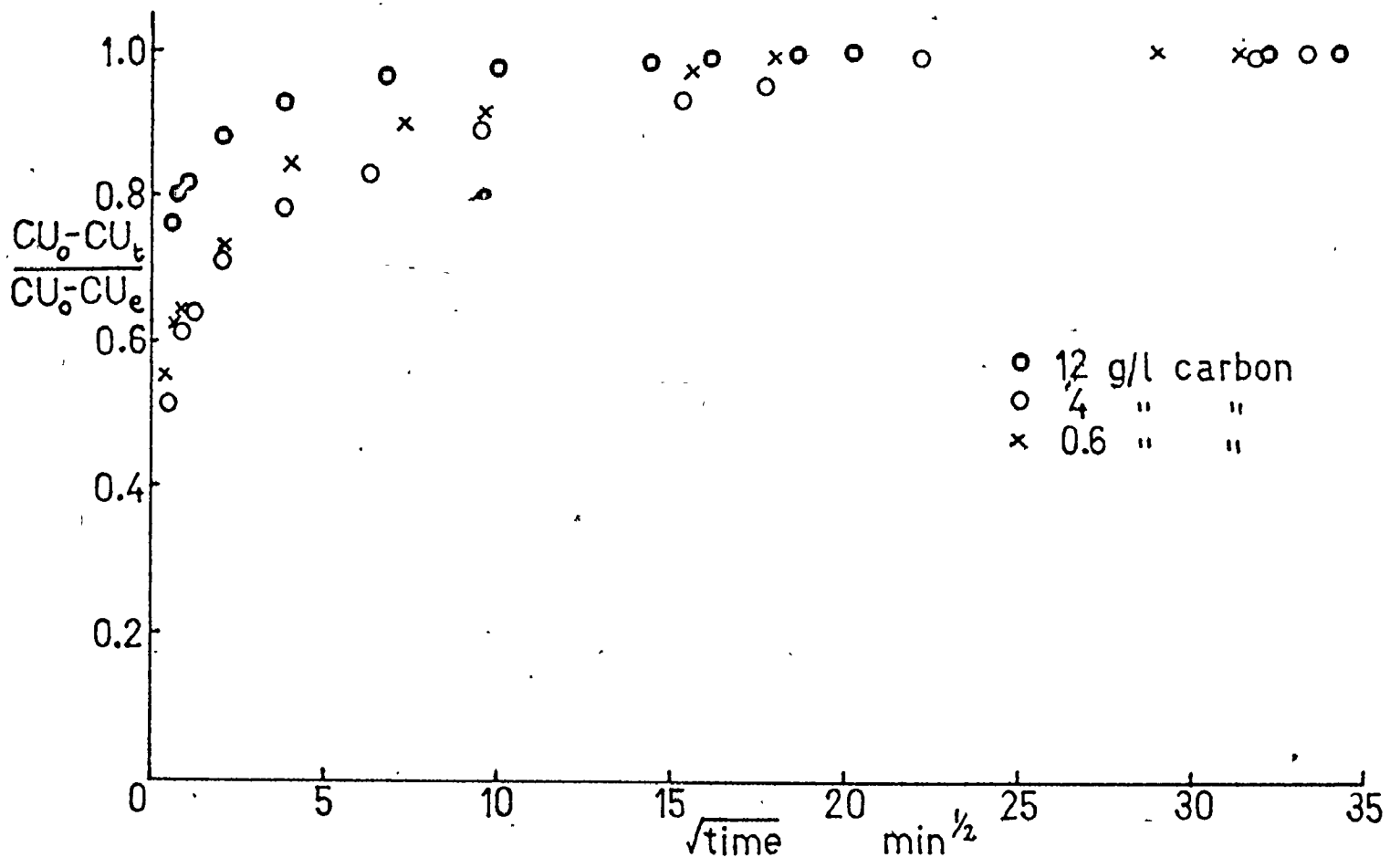

Fig.I.12 TOC Adsorption Kinetics at Different Carbon Dosages

500 mg/l Indulin, $TOC_o$ = 335 mg/l, pH=10, 35°C, Darco KB carbon

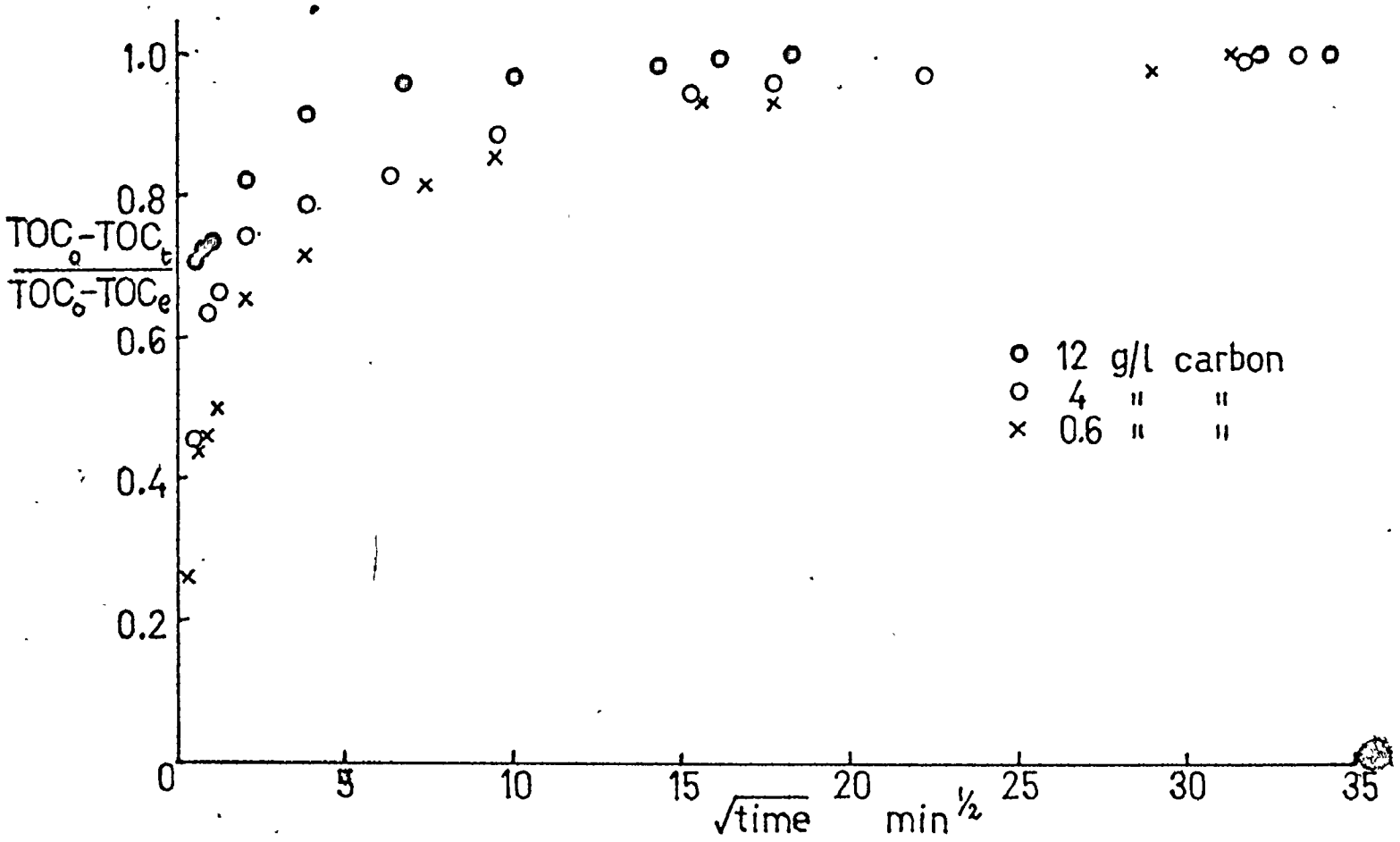

different carbons is only meaningful when applied to adsorption systems using identical carbon dosages.

I.4.1. (iv). Adsorption Selectivity

I.4.1.(iv). a. The Color/TOC ratio of Adsorbed Indulin Components

The cumulative color/TOC ratio of adsorbed Indulin components at any contact time t can be calculated from kinetic adsorption data using the relationship

$$\left[\frac{CU}{TOC}\right]_t^{ads} = \frac{CU_o - CU_t}{TOC_o - TOC_t} \qquad (1.16)$$

where $CU_o$, $TOC_o$, $CU_t$, $TOC_t$ are the solution color and TOC contents at t=0 and t=t respectively, as measured at original solution pH. Fig. I.13 shows how this ratio varies with contact time for the adsorption system studied. For all carbons, this ratio is evidenced to increase from a value of zero at t=0 to a maximum value at low values of t, thereafter decaying to a lower 'equilibrium' value at longer contact times. This suggests a selective adsorption process, wherein Indulin solutes possessing a relatively high color/TOC ratio in solution are adsorbed preferentially at short contact times, followed by

Fig.I.13 Cumulative Color/TOC Ratio Of Adsorbed Indulin Components - Granular Carbon Kinetics

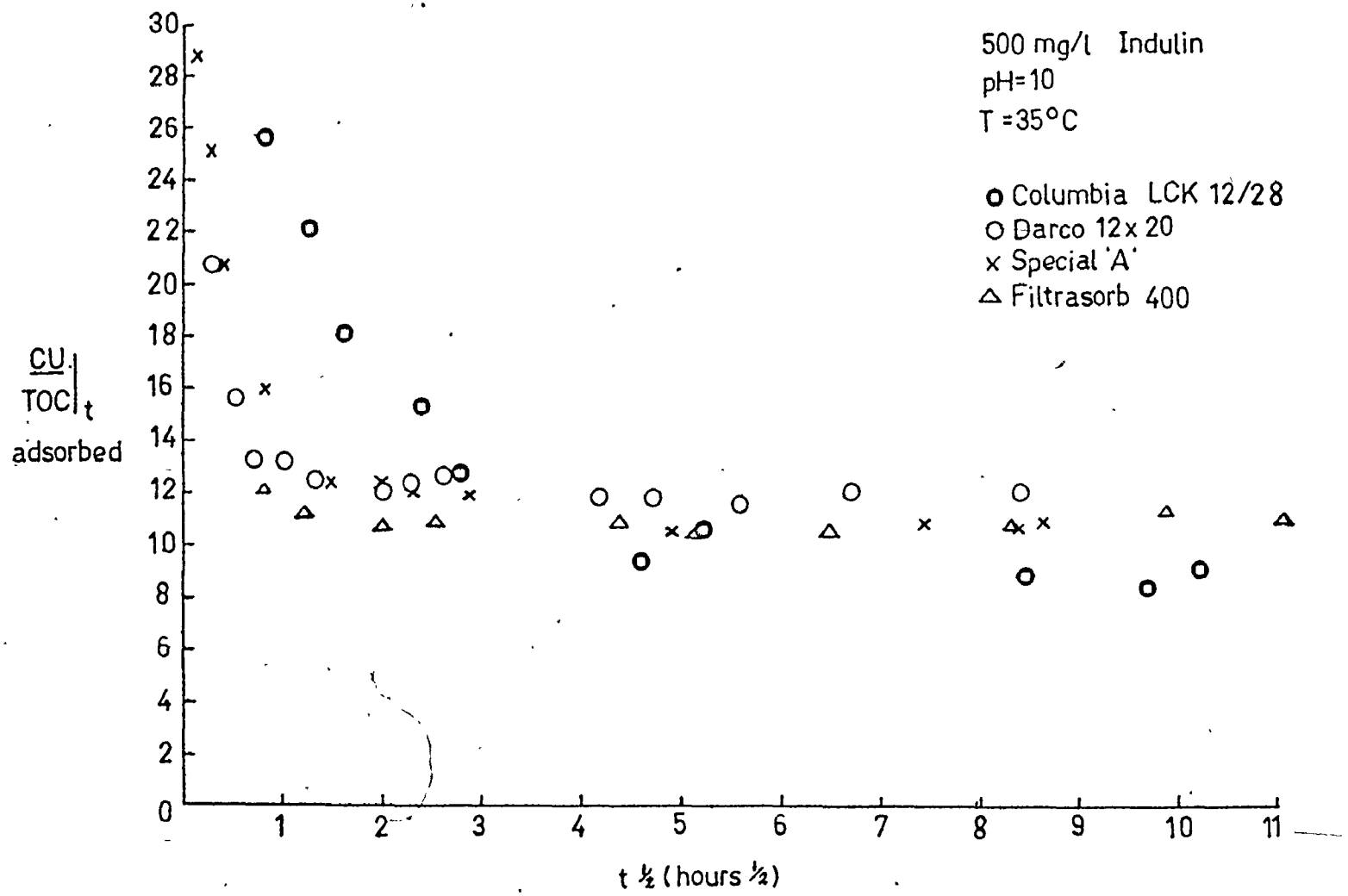

progressive adsorption of solutes of ever decreasing color/TOC ratio at increasingly longer contact times. In view of studies outlined in Part III, which tend to indicate that the color/TOC ratio of Indulin solutes decreases as solute molecular weight - and size - increase, the results in Fig. I.13 support the hypothesis that the kinetics of adsorption of Indulin from aqueous solution incorporates a selective adsorption process, involving initial rapid preferential adsorption of the smallest adsorbable lignin solutes, followed by progressive adsorption of increasingly larger lignin solutes as contact time is increased.

I.4.1. (iv).b. Gel Filtration Analysis of Adsorption Kinetic Residual Solutions

Selected adsorption residuals from kinetic studies were analysed by Gel Filtration as outlined in Part III and Section I.3.3. The molecular distributions of Indulin components remaining in residual solutions after various contact times are shown for two carbons in Figs. I.14 and I.15. Here it is evident that the kinetic adsorption process is

Fig.I.14 GPC Analysis of Adsorption Residual Solutions

Darco KB Kinetics

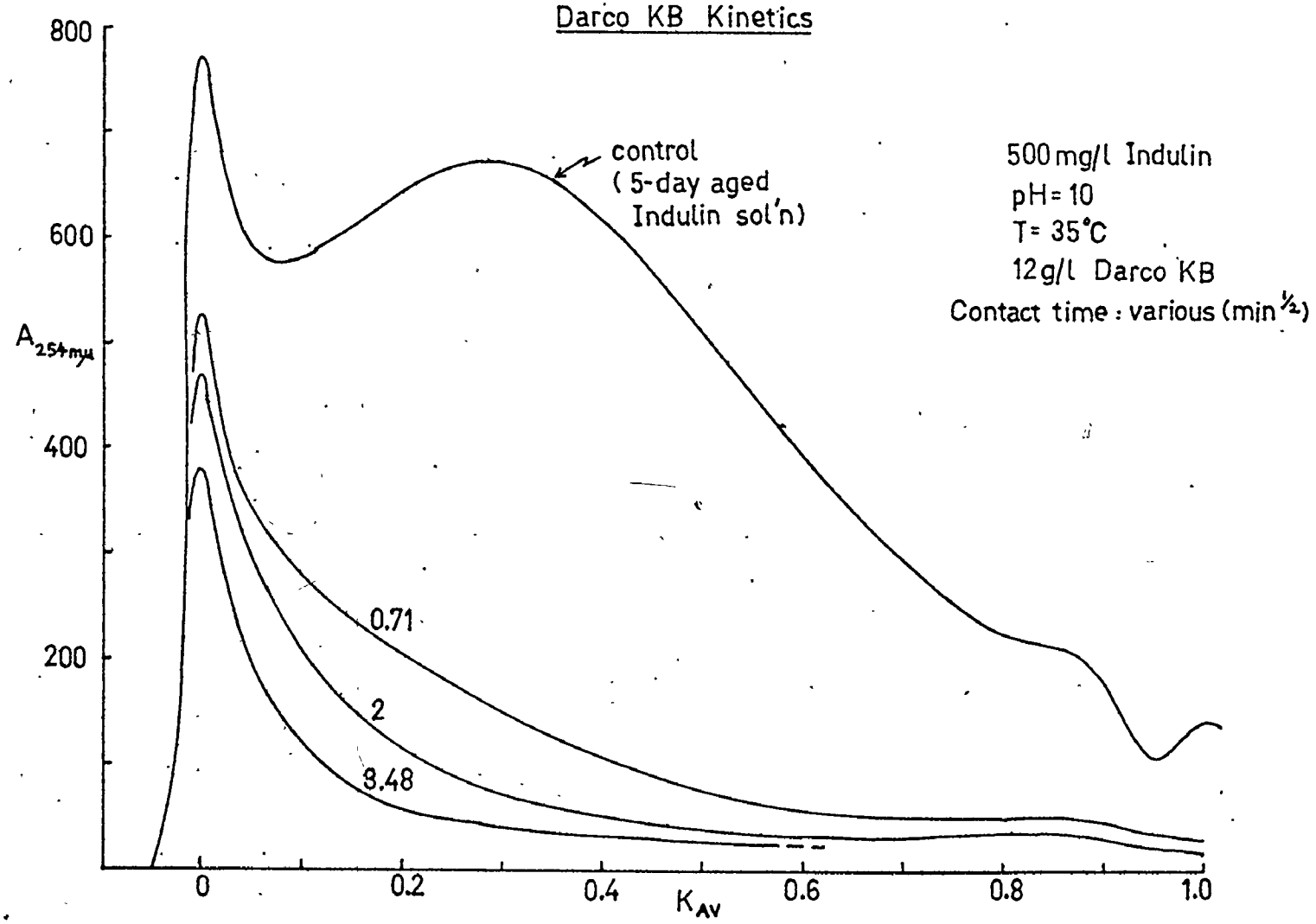

Fig.I.15 GPC Analysis Of Adsorption Residual Solutions

Special 'A' Kinetics

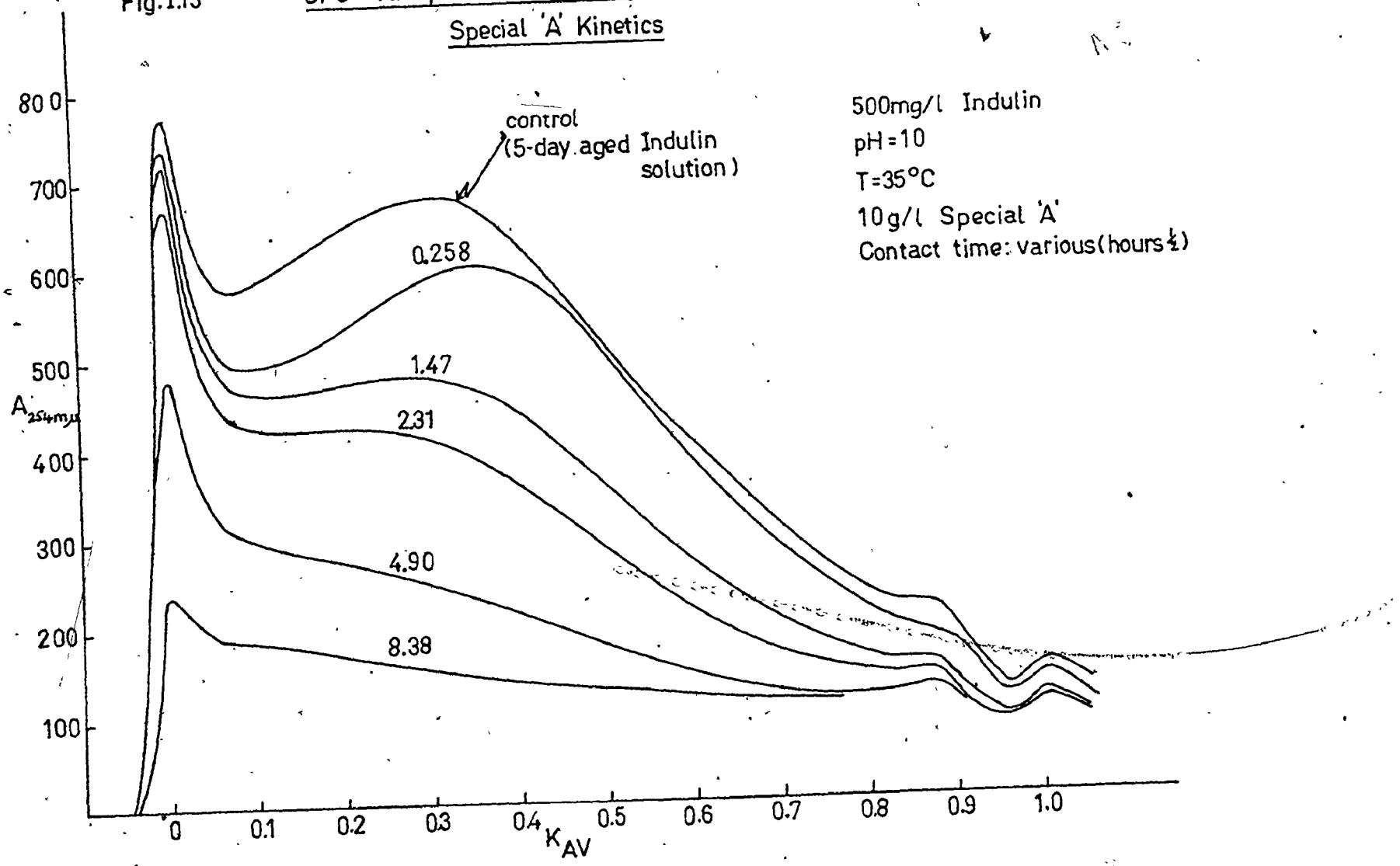

associated with adsorption of each molecular species to an extent determined by contact time and carbon properties. However, it is difficult to determine the relative removals of each species from solution at different contact times directly from Figs. I.14 and I.15.

It is possible, however, to determine the percent removal of each species with contact time from Figs. I.14 and I.15 by comparing the height of the distribution curve of the original - or control - Indulin solution to the corresponding height in the residual solution at the same $K_{AV}$ value. In this manner the percent removal of a given Indulin solute characterised by $(K_{AV})_i$ after a contact time t is given by

$$\%R_{i,t} = 100 \left[1 - (A_{i,t}/A_{i,o})\right] \qquad (1.17)$$

where $A_{i,o}$ and $A_{i,t}$ are the values of 254 mμ absorbance at $(K_{AV})_i$ in the original and residual Indulin solution respectively. Figs. I.16 and I.17 display the results of application of equation (I.17) to the residual distributions in Figs. I.14 and 15 for each $K_{AV}$ value.

Fig.I.16 Removal of Lignin Species at Different Contact Times Using Darco KB

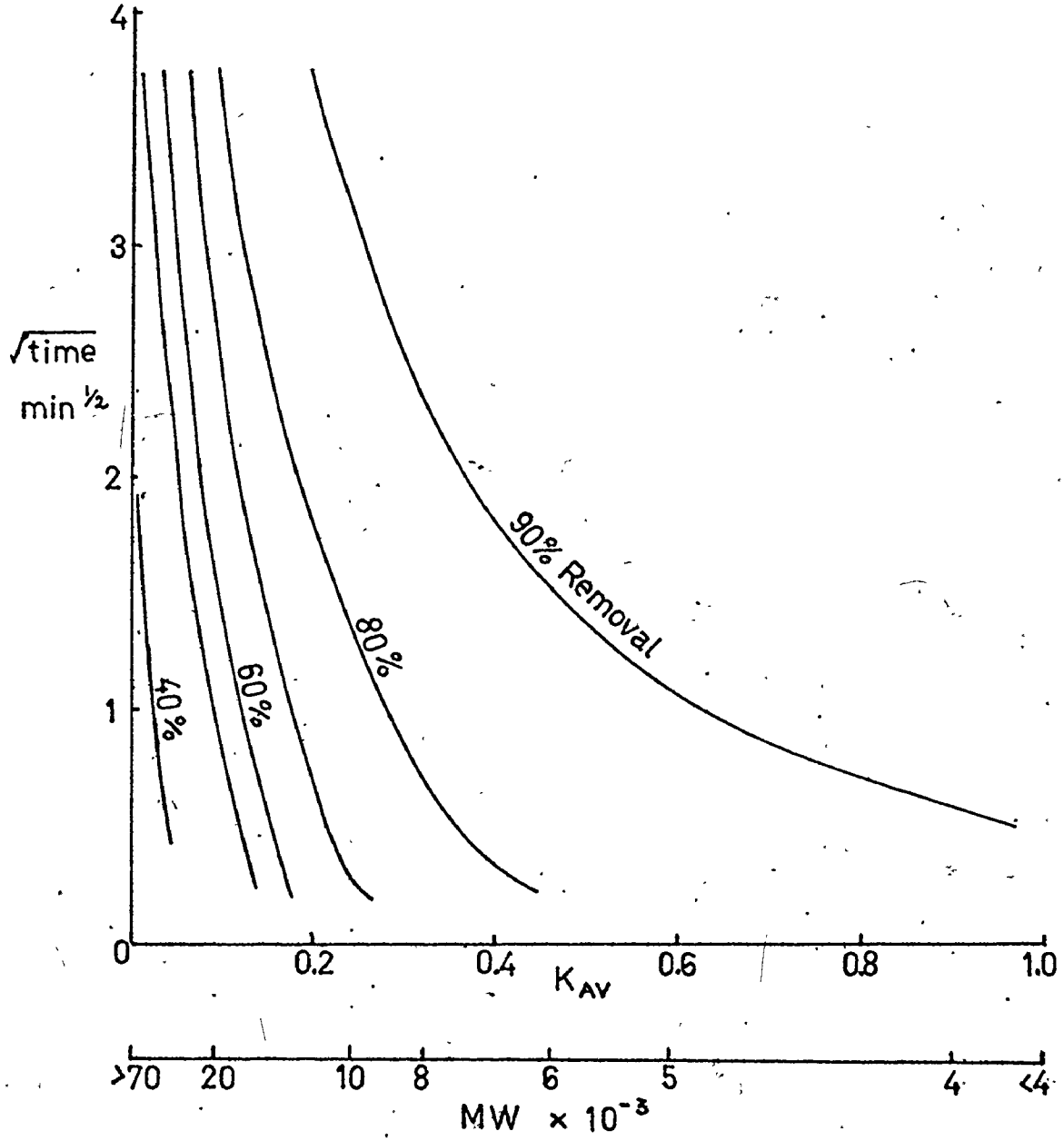

Fig. I.17 Removal of Lignin Species at Different Contact Times Using Special 'A'

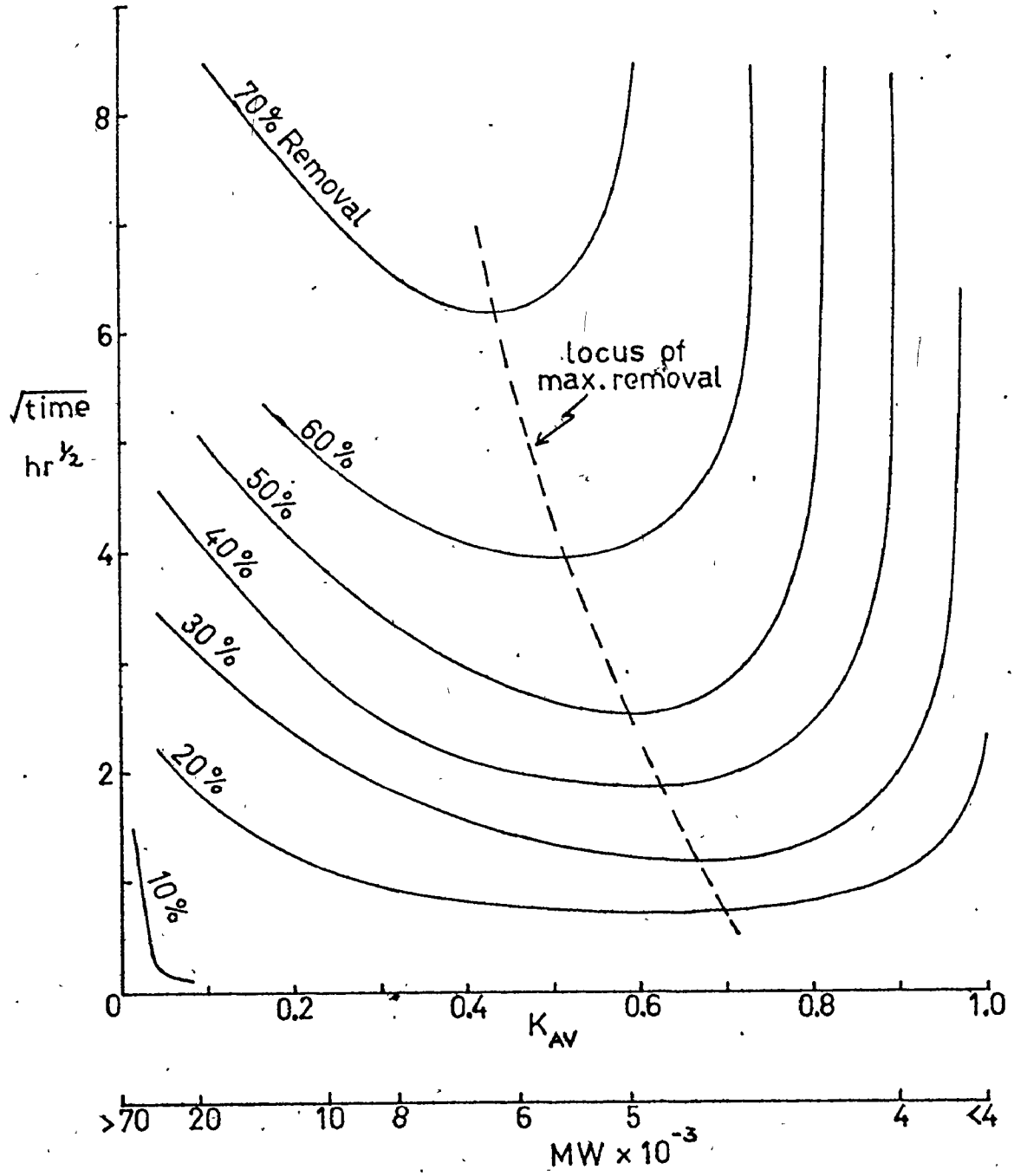

For Darco KB, Fig. I.16 indicates that at short contact times, maximum adsorption of the smallest molecular weight Indulin species occurs, with progressive decrease in adsorption of higher molecular weight species. For example, after 1 minute contact, greater than 90% removal of species of less than about 5000 MW is achieved, but only about 50% removal of species of approximately 20,000 MW. As contact time increases, however, removal of higher molecular weight species becomes significant. For example, after approximately 14 minutes contact, approximately 80% removal of species of about 20,000 MW has occured. The results in Fig. I.16 thus support the selective adsorption hypothesis of the Indulin kinetic adsorption process outlined in Section I.4.1.(iv).a.

The selective adsorption of components during kinetic adsorption process using Special "A" carbon, as depicted in Fig. I.17, tend at first sight to contradict the selective adsorption hypothesis described earlier. Here, very little adsorption of

low molecular weight species of less than approximately 5000 MW occurs, even after long contact times. Furthermore, significant removal of intermediate molecular weight solutes of about 5000 - 10,000 MW occurs at relatively short contact times, and removals increase as contact time is increased. It thus appears that preferential adsorption of intermediate molecular weight Indulin solutes occurs on Special "A" carbon. This phenomenon arises from the pore structural nature of Special "A". In contrast to the pore structure of Darco KB, which contains a sizeable and well distributed pore structure in all pores up to 1000 Å radii, Special "A" contains practically all its pore structure in the approximately 20 - 200 Å pore radii range (see Part II, Figs. II.14 and II.15). It is thus apparent that the relative inability of Special "A" to adsorb Indulin solutes of less than approximately 5000 MW associated with absence of adsorbent pore structure in pores of radii less than approximately 20 Å. This fact alone does not, however, explain the comparative lack of

adsorption of low molecular weight Indulin species onto Special "A". Such species, having high mobilities, certainly have the ability to arrive at the adsorption sites in pores of greater than 20 Å radii before their larger cousins, and intuitively have the potential to be adsorbed in these larger pores. Nevertheless, they are not evidenced to be adsorbed in the larger pores. This may be explained by considering equation (I.10) - see Section I.2 - for each Indulin solute species. If it is assumed that $V^o$ and $\sigma$ in equation (I.10) are approximately independent of pore radius r, and that the constant K in equation (I.10) is relatively independent of solute molecular weight, then equation (I.10) becomes for species i

$$\ln\left[\frac{C'_i}{C^o_i}\right] = \frac{K'}{r} \qquad (1.18)$$

Since the concentration at which the solubility limit is exceeded will decrease as solute molecular weight increases, equation (1.18) will predict preferential adsorption of larger molecular weight species in cases where two or more species may

penetrate the same pore, assuming identical initial concentration $C_U^o$ of each species in solution. Since initial concentrations of the various Indulin species in solution are evidenced to roughly decrease with increase in solute molecular weight, this effect is enhanced in the Indulin solution studied here. From this analysis it is apparant that the Indulin solutes are not significantly adsorbed in adsorbent pores of greater than about 20 Å radii since the pore concentration effect is not sufficient to bring about precipitation, and hence adsorption, in the pores.

The original hypothesis of the selective adsorption mechanism in the kinetic adsorption process is thus not contradicted when using Special "A". In this case, adsorption commences with preferential adsorption of the lowest adsorbable species, i.e. solutes of approximately 5000 - 10,000 MW at low contact times, followed by progressive adsorption of increasingly higher molecular weight solutes at longer contact times. The nature of the 'locus of maximum removal' depicted in Fig. I.17 exemplifies that the aforementioned hypothesis holds even when

carbon pore structural limitations restrict adsorption of certain lignin solutes.

Since selective adsorption of Indulin solutes occurs in the kinetic adsorption process, the average molecular weight $\overline{M}_n$ of Indulin in solution would be expected to change during adsorption. This is evidenced to be the case, as shown in Figs. I.18 and I.19. Here $\overline{M}_n$ was estimated from gel filtration experiments on adsorption residuals as outlined in Part III. The increase of $\overline{M}_n$ with contact time using Darco KB is in agreement with the hypothesised selective adsorption mechanism in the kinetic adsorption process. The change in $\overline{M}_n$ with time using Special "A" carbon is unusual in that $\overline{M}_n$ actually decreases at long contact times. Here the initial increase in $\overline{M}_n$ at short contact times is associated with preferential adsorption of species having molecular weights greater than the largest 'unadsorbable' species, i.e. about 4000-5000 MW, but lower than the average molecular weight $\overline{M}_n$ of about 5900-7600 in the 'uncontacted' Indulin solution (see Part III, Section III.4.3 ). The $\overline{M}_n$ decrease at long contact times is associated

Fig. I.18 Variation of $\bar{M}_n$ with Contact Time Using Darco KB

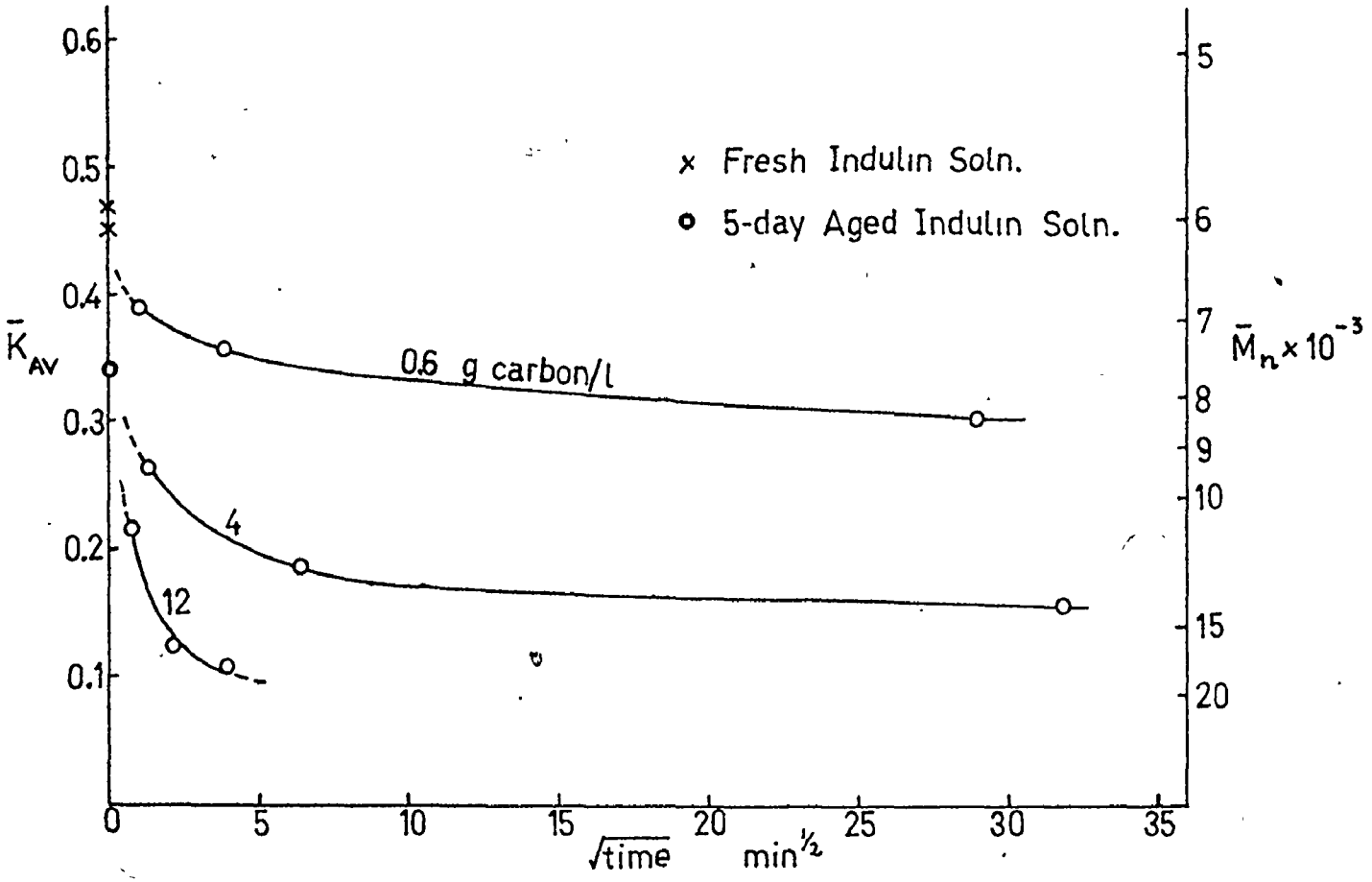

Fig.I.19 Variation of $M_n$ with Contact Time Using Special 'A'

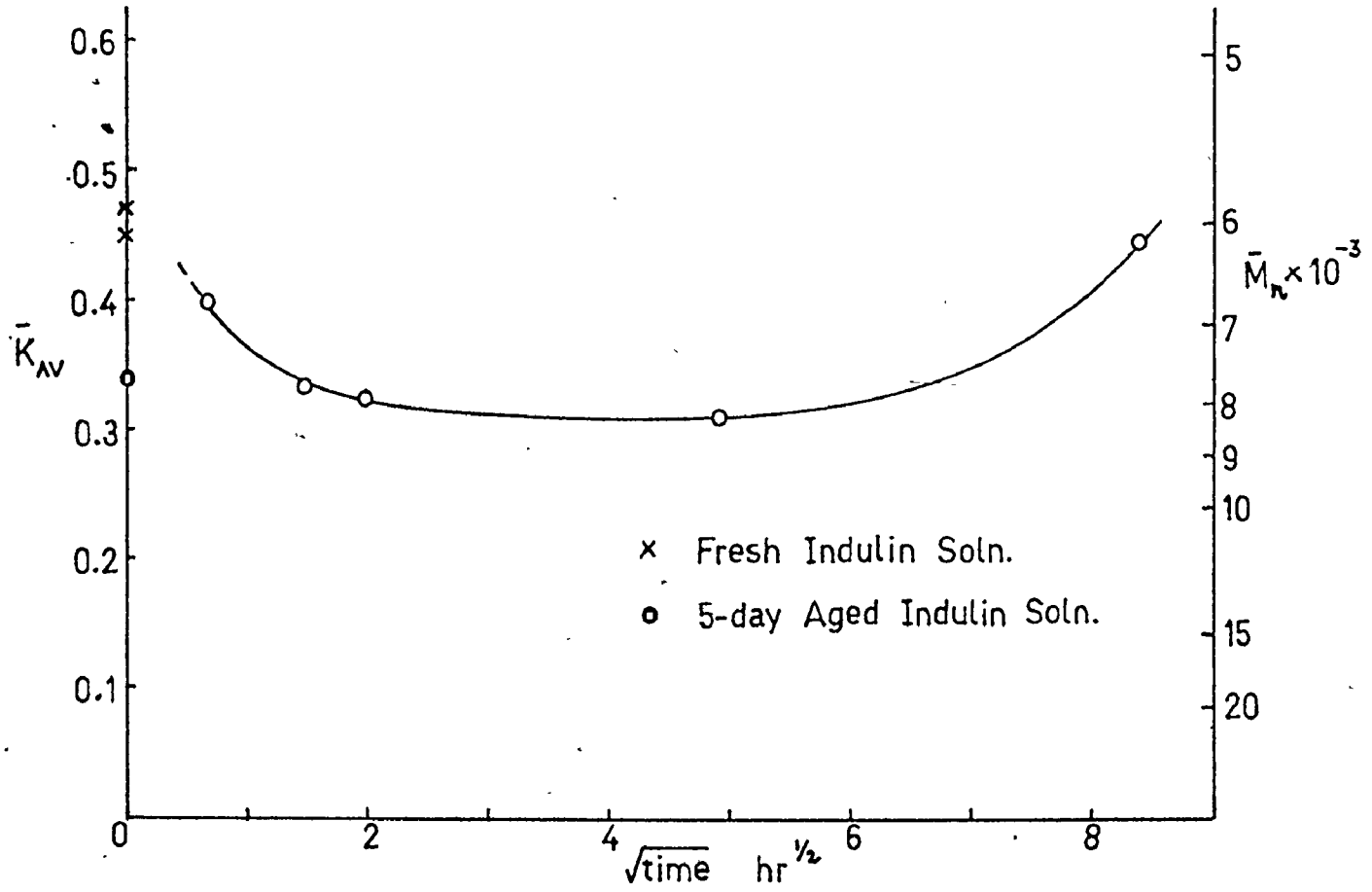

with preferential adsorption of higher molecular weight species having molecular weights in excess of 5900-7600. At such times the residual unadsorbed low molecular weight species predominate in solution and so $\overline{M}_n$ falls.

I.4.1. (v) Interrelation of Indulin Adsorption and Degradation Reactions

The lignin studies outlined in Part II have shown that in alkaline solution, Indulin will degrade with time, resulting in loss of solution color and an increase in the average molecular weight of Indulin solutes. This effect can influence adsorption behaviour, since the adsorbent is presented with adsorbates of dynamically changing characteristics. The effects of both adsorption and degradation on the molecular weight distributions in residual Indulin solutions are amply indicated in Fig. I.20. Here increased adsorption of lignin species having $K_{AV}$ values less than about 0.2 is seen to occur with increase in contact time. However, the degradation reaction is also simultaneously taking place, as evidenced by

Fig. I.20 Gel Filtration Analysis of Adsorption Residual Solns.
Darco KB Kinetics

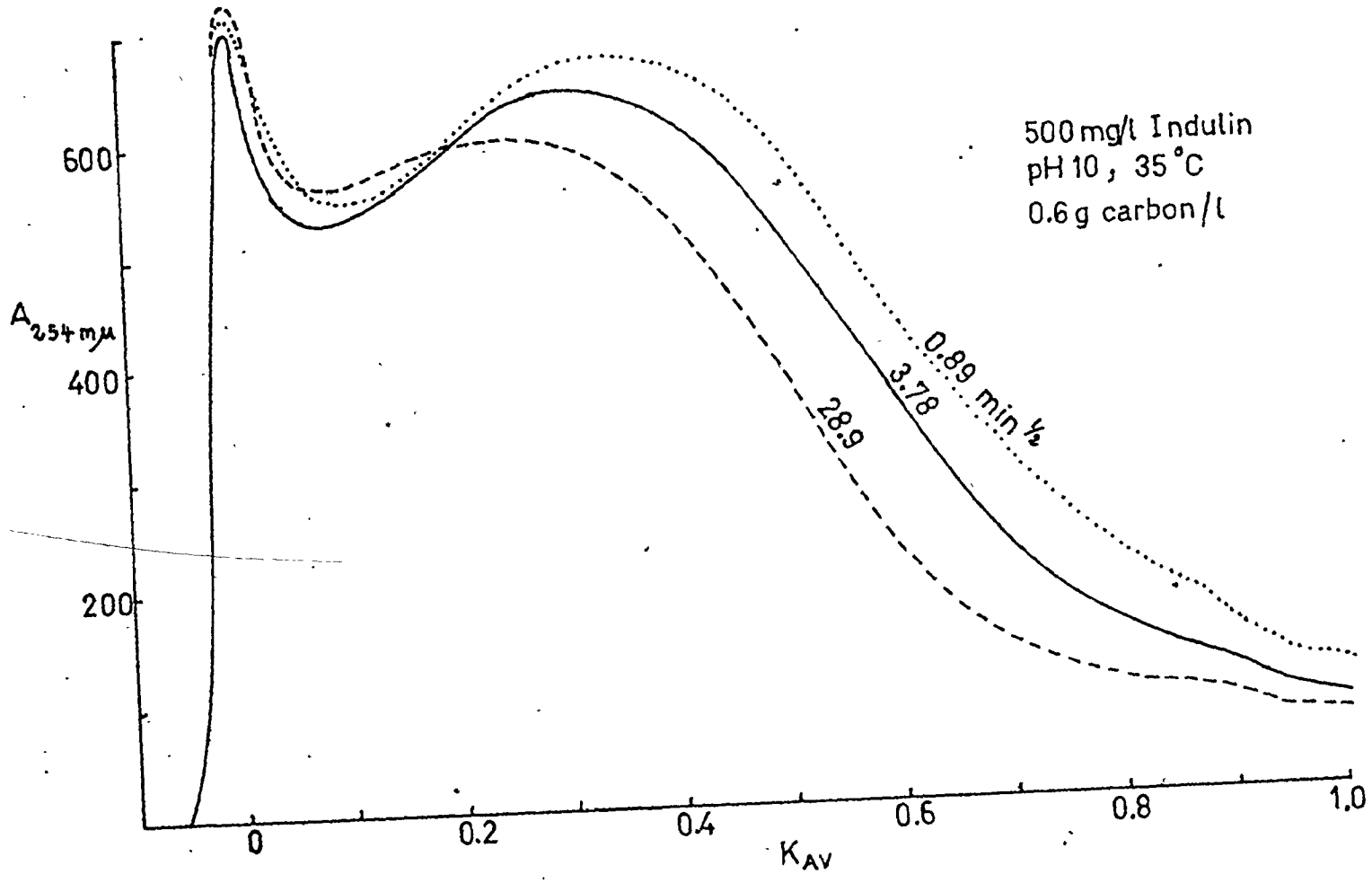

the shift in the intermediate peak of the distribution from a $K_{AV}$ value of 0.5 in the original Indulin solution (see Part III, Fig. III.17) to values of 0.35 and 0.25 after 0.8 mins. and 14 mins. contact respectively. This observation indicates that both adsorption and degradation of lignin occurs simultaneous during the kinetic adsorption process, and furthermore, that the two effects cannot be segregated.

The presence of the lignin degradation reaction gives rise to uncertainties regarding which lignin molecular distribution to use - viz. the distribution in a freshly prepared or 5-day old Indulin solution - as an initial distribution for the purposes of calculating the percent removals of species in Section I.4.1 (iv).b. The 5-day aged distribution was used for this purpose, although the limitations of use of either distribution are clearly recognised here.

I.4.2 Equilibrium Studies - Adsorption Isotherms

Equilibrium adsorption studies on adsorption of Indulin from alkaline solution were conducted by the procedures outlined in Section I.3.2, using

contact times of 15 hours and 4 days for the powdered and granular carbons respectively. The results are expressed in terms of the adsorption isotherm (see Section I.2.3 ), which describes the distribution of Indulin color and TOC between adsorbed and un-adsorbed phases. The color and TOC adsorption isotherms for the carbons studied are shown in Figs. I.21 and I.22.

Generally the isotherms are observed to be similar in shape. They exhibit characteristics of an unfavourable isotherm at high values of relative equilibrium concentration in solution $C^*/C_o$, and favourable isotherm characteristics at low values of $C^*/C_o$. Generally, at low carbon dosages, adsorption intensity of color and TOC, as indicated by the adsorption term (x/m), is high, although the portion of color and TOC removed from solution is relatively small. This suggests that the smaller molecular weight Indulin species, which appear to have a higher color and TOC content per molecule than their larger cousins, but exist in alkaline solution at much

Fig.I.21 Indulin Color Adsorption Isotherms

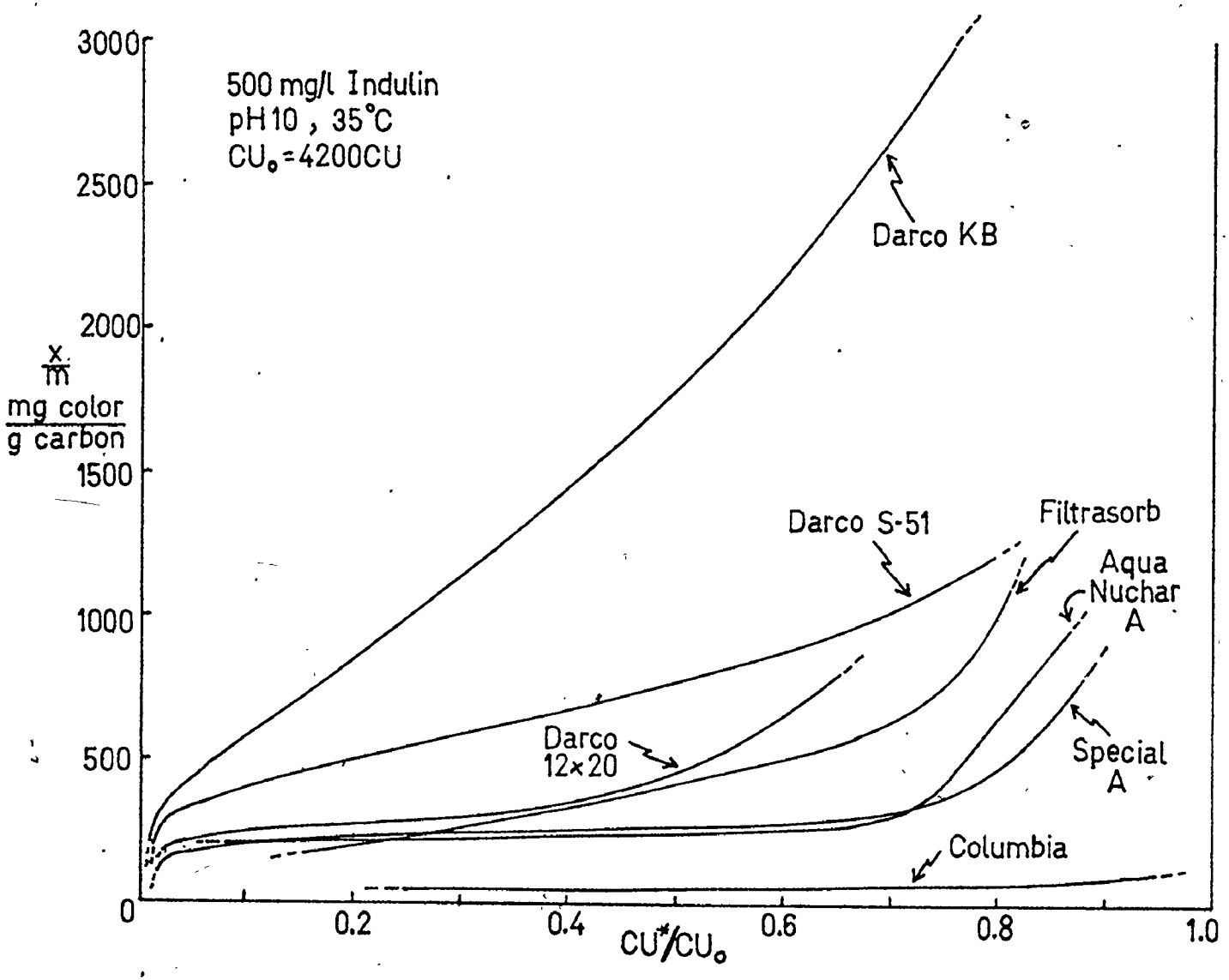

Fig.I.22 Indulin TOC Adsorption Isotherms

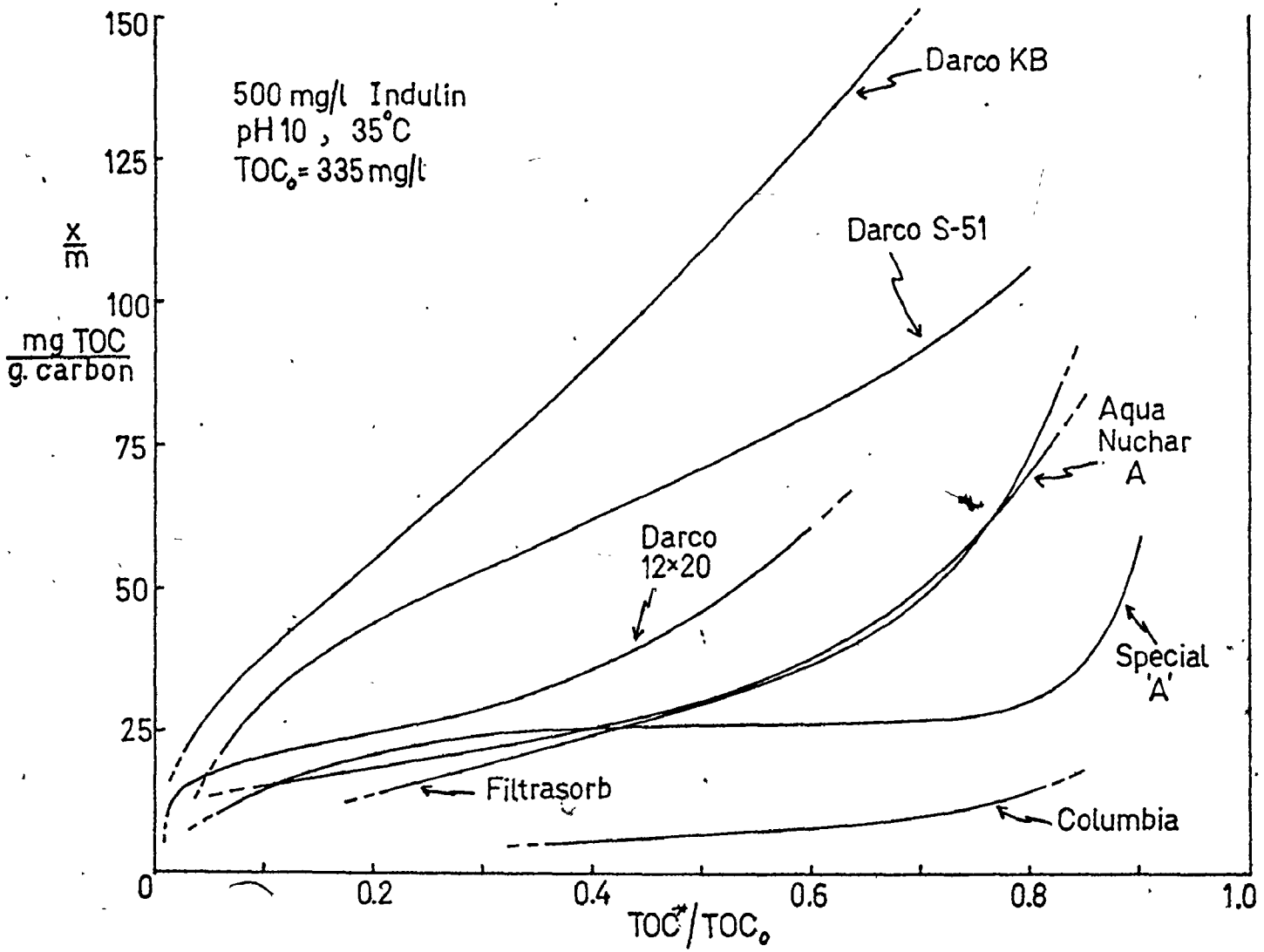

lower concentrations, are adsorbed preferentially at low carbon dosages. As carbon dosage is increased, the cumulative adsorption intensity term (x/m) decreases, together with a significant decrease in $C^*/C_o$. This is associated with progressive preferential adsorption of larger molecular weight solutes, which have a lower color and TOC content per molecule than their smaller cousins, but because of their relatively high concentrations in solution, contribute the main portion of overall solution color and TOC. At values of $C^*/C_o$ about 0.2, the isotherm again becomes favourable, although the cumulative adsorption intensity term (x/m) is low. This region of the isotherm, if present, is associated with removal of the largest molecular weight Indulin solutes, which have the lowest color and TOC per molecule of all components and, because their concentrations in the solution studied are low, do not contribute a large portion of the overall solution TOC and color, noticeably the latter.

In view of Chen's (1970) findings regarding the concentration-precipitation nature of the lignin

adsorption process, the shape of the isotherms also suggests that the precipitated (i.e. adsorbed) lignin solutes are not chemically uniform. The 'breakpoint' between the unfavourable and favourable portions of the isotherms may be indicative of significant chemical differences, or multilayer adsorption in the adsorbed Indulin species.

The shape of the adsorption isotherms suggest that they are linearisable in terms of the B.E. T. model. However, B.E.T. linearisation proved to be unrepresentative, as illustrated in Fig. I.23. The Freundich model also proved inadequate for linearisation of isotherm data. It should be noted here that Langmuir-type models are inappropriate to description of adsorption characteristics of the system studied since adsorption does not attain a finite 'equilibrium' value at high carbon dosages, corresponding to a constant residual concentration of color or TOC in solution.

In contrast to the color isotherms presented by Timpe (1970) and Kabeya (1971), the lignin color adsorption isotherms do not exhibit a well defined

Fig.I.23 B.E.T. Linearisation of Isotherm Data

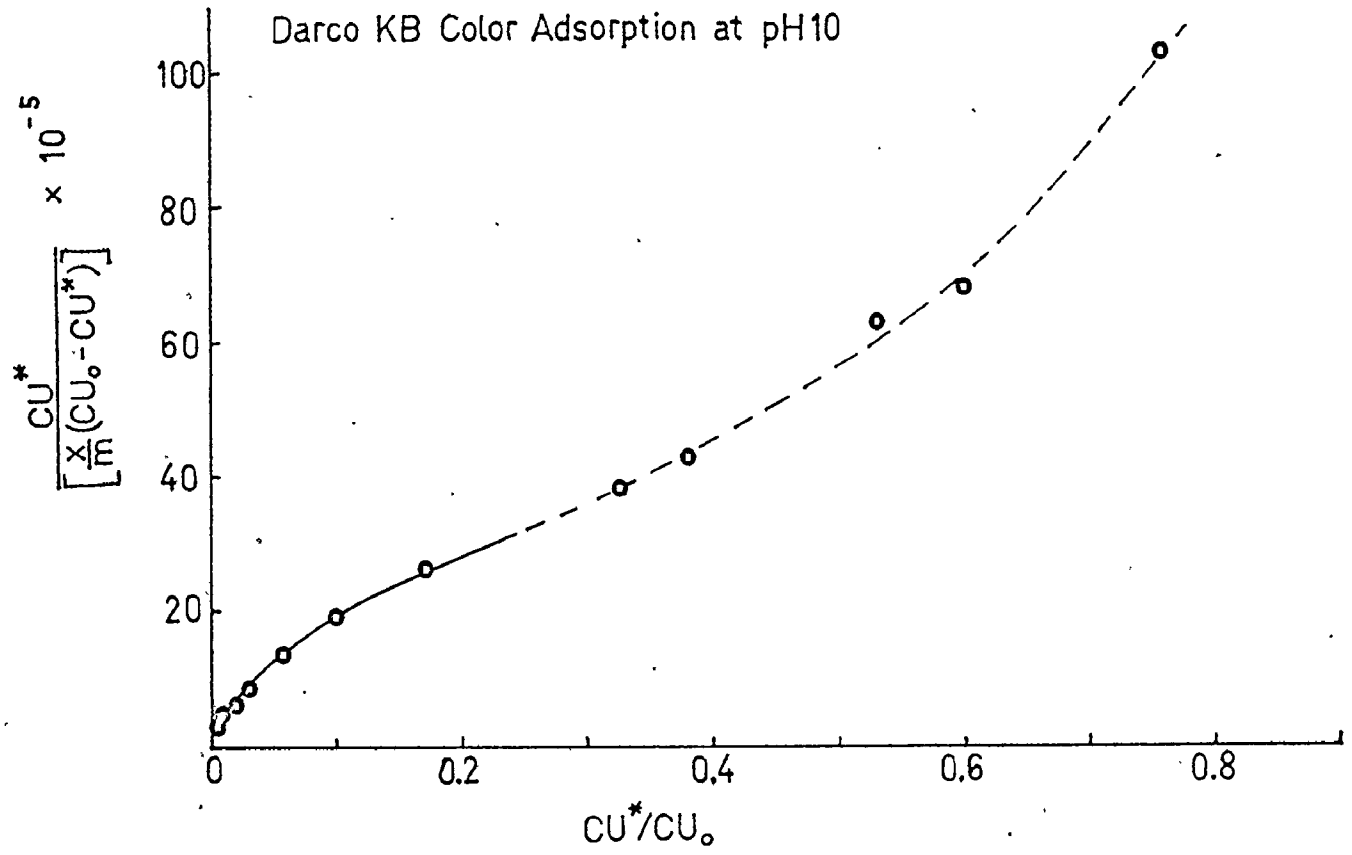

Fig. I. 24 Freundlich Linearisation of Isotherm Data

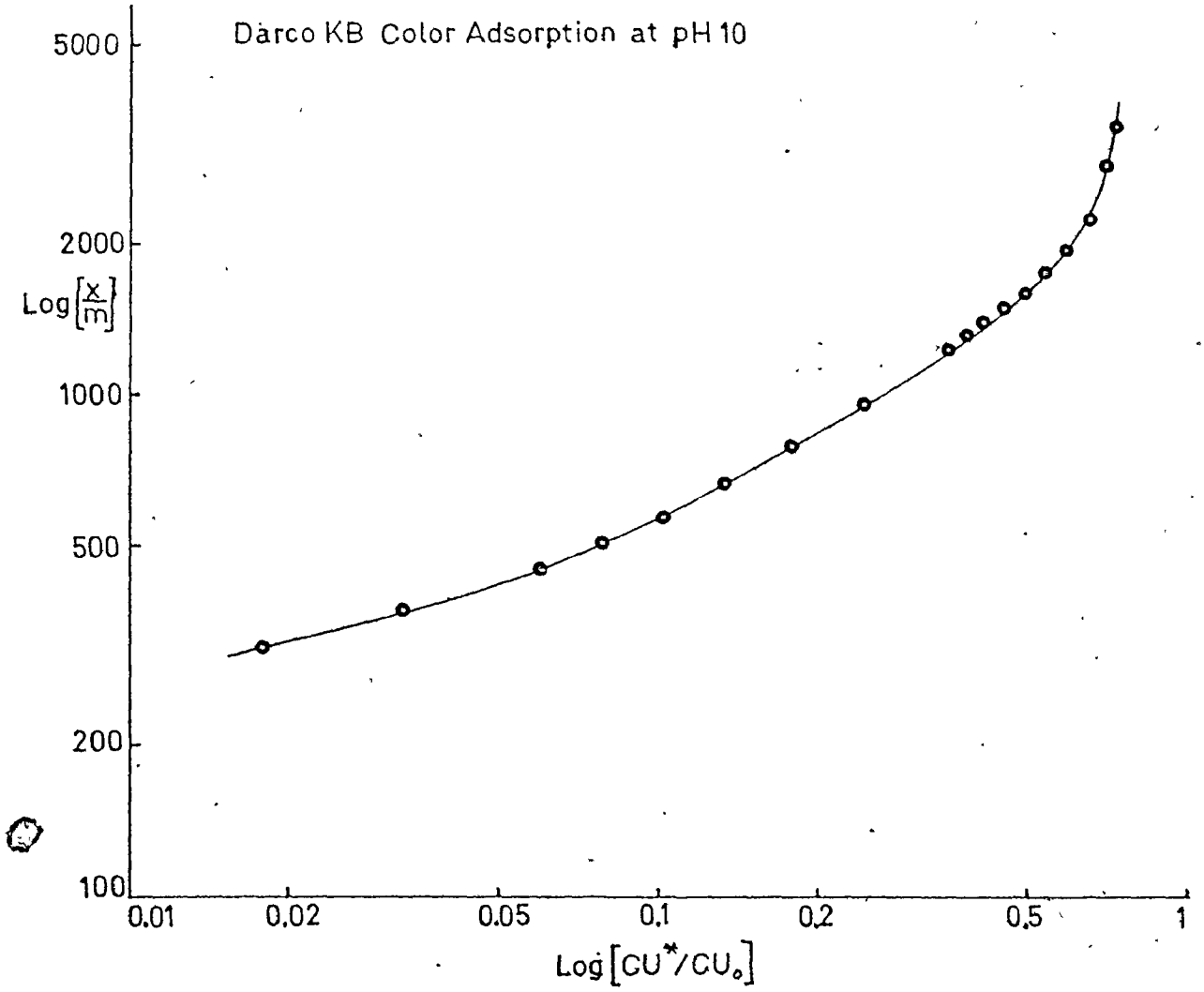

'breakpoint' when subjected to a Freundlich analysis. Instead a smooth transition is noted, as illustrated in Fig. I.24. The discrepancy arises because of differences in lignin solution used in adsorption experiments. Both Timpe and Kabeya used lignin-containing pulp mill effluents, which in addition to lignin, also contain many other adsorbable constituents which may interfere with lignin adsorption.

Two additional facts should be noted regarding the adsorption isotherms in Figs. I.21 and I.22. Firstly, these isotherms may not exactly represent true equilibrium adsorption conditions, due to excessively long contact times required to attain equilibrium in polymer adsorption systems. Chen (1970) has noted that significant differences between the lignin adsorption isotherms based on 10 and 20 days contact are evident. The choice of contact times in this study represents a compromise between practicality and closeness to equilibrium adsorption conditions. Secondly, the adsorption isotherms depicted here are calculated on the assumption that negligible adsorption of the solvent, i.e. water, occurs. This may not necessarily be a good assumption in the case

of lignin adsorption, where significant numbers of chemically or mechanically inbound water molecules may be associated with the large Indulin macromolecules in the adsorbed layer. In such instances, the term $V_o$ in equation (I.3 ) may not be constant and assumed equal to the initial solution volume. However, measurements of the residual solution volume after adsorption have shown that $V_o$ only decreases slightly during adsorption.

The adsorption isotherms also indicate the relative efficiences of each carbon in removing Indulin, as color and TOC, from solution. In this respect, Darco KB is the most efficient of the carbons studied at all carbon dosages. Columbia is the least efficient carbon. As will be seen later, the relative efficiences of the various carbons are related primarily to carbon pore structural characteristics. It is possible to calculate the percent removal of color and TOC at a given carbon dosage directly from the isotherm from a knowledge of (x/m) and $C^*/C_o$. Tables I.8 and I.9 summarize these calculations.

Table I.8. 'Equilibrium' Color Removal Versus Carbon Dosage For Various Carbons

500 mg/l Indulin
pH = 10
T = 35°C
Initial Color = 4200 CU

| Carbon | Carbon Dosage (g/l) Required to Achieve a Given Percent Color Removal | | | | |
|---|---|---|---|---|---|
| | 25% | 50% | 75% | 90% | 100% |
| Columbia LCK | 13.5 | 31.5 | 40 | -- | -- |
| Darco KB | 0.34 | 1.15 | 2.9 | 6.0 | 16.0 |
| Darco S-51 | 1.16 | 2.5 | 5.4 | 9.2 | 18.0 |
| Darco 12x20 | < 2 | 4.6 | 11.5 | 16.5 | 26.0 |
| Aqua Nuchar A | 2.8 | 8.1 | 14.0 | 18.0 | > 20 |
| Filtrasorb 400 | 1.3 | 4.0 | 13.5 | > 20 | > 20 |
| Special "A" | 3.0 | 7.7 | 13.5 | 20 | 33 |

Table I.9. Equilibrium TOC Removal Versus Carbon Dosage For Various Carbons

500 mg/l Indulin
pH = 10
T = 35°C
Initial TOC = 335 mg/l

| Carbon | Carbon Dosage (g/l) Required to Achieve a Given Percent TOC Removal | | | | |
|---|---|---|---|---|---|
| | 25% | 50% | 75% | 90% | 100% |
| Columbia LCK | 8.0 | 27.0 | > 40 | -- | -- |
| Darco KB | 0.5 | 1.4 | 3.6 | 7.2 | 20.0 |
| Darco S-51 | 0.84 | 2.35 | 5.3 | 10 | > 20 |
| Darco 12x20 | < 2 | 3.7 | 9.2 | 15.5 | 32.0 |
| Aqua Nuchar A | 1.25 | 4.5 | 11.5 | 18.5 | > 20 |
| Filtasorb 400 | 1.65 | 6.0 | 15.5 | > 20 | > 20 |
| Special "A" | 2.7 | 6.4 | 11.5 | 21.0 | > 32 |

I.4.2. (i) pH Effect

The effect of initial solution pH on the extent of adsorption of Indulin, as TOC, from aqueous solution onto different activated carbons is shown in Fig. I.25. Here with all carbons, adsorption capacity decreases with decrease in solution pH, an effect noted earlier by Fuchs (1965), McGlasson (1967) and Kabeya (1971). This is attributed to the decrease in solubility of lignin components with pH decrease, a fact supported by the results of the ultrafiltration experiments outlined in Part III, where pH decrease is associated with the presence of larger Indulin solutes in solution. The magnitude of the pH effect on adsorption capacity is dependent on carbon pore structural properties. In this respect, the sizeable increase of adsorption capacity with Special "A" carbon stems from the fact that the change in Indulin molecular distribution with initial solution pH decrease results in formation of molecular weight solutes that are preferentially adsorbed in the pore structure of Special "A", i.e. in pores of 20-200 Å radii. Conversely, the relative insensivity of the adsorption

Fig.I.25 pH Effect on Adsorption Equilibrium

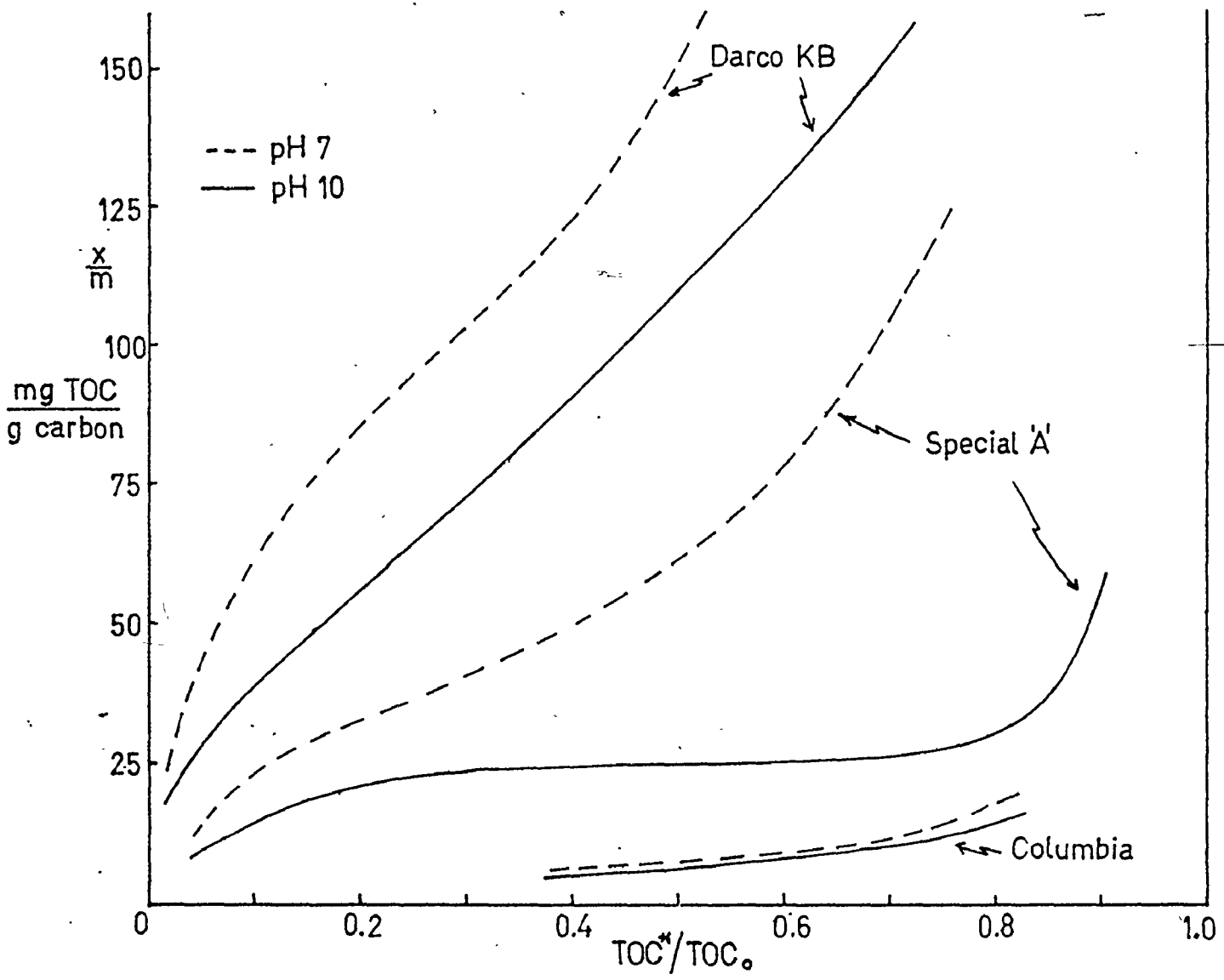

isotherm to initial pH using Columbia carbon arises because this carbon contains negligible pore structure in pores of greater than approximately 15 Å radius. Since, as will be demonstrated later, pores of greater than 15 Å radii play a major role in adsorption of Indulin solutes, molecular weight changes in the distribution of the intermediate and larger molecular weight Indulin solutes caused by pH variations will have negligible effect on Columbia adsorption capacity, since this carbon does not posess the necessary pore structure specific to their adsorption.

The percent removals of color and TOC from pH 7 Indulin solutions are shown in Tables I.10 and I.11 respectively.

Table I.10 Equilibrium Color Removal Versus Carbon Dosage For Various Carbons

500 mg/l Indulin
pH = 7
T = 35°C
Initial Color = 2800 cu

| Carbon | Carbon Dosage (g/l) Required to Achieve a Given Percent Color Removal | | | | |
|---|---|---|---|---|---|
| | 25% | 50% | 75% | 90% | 100% |
| Columbia LCK | 23.0 | >40 | - | - | - |
| Darco KB | 0.3 | 1.1 | 2.4 | 4.5 | 12.0 |
| Darco S-51 | 1.0 | 2.1 | 3.5 | 5.9 | 16.0 |
| Darco 12x20 | <2 | 3.0 | 6.1 | 9.2 | 19.0 |
| Aqua Nuchar A | <0.6 | 2.8 | 5.3 | 7.6 | >10 |
| Filtrasorb 400 | 2.2 | 7.2 | 11.5 | 19.0 | >20 |
| Special "A" | 1.8 | 4.4 | 8.9 | 15.5 | >28 |

Table I.11. Equilibrium TOC Removal Versus Carbon Dosage For Various Carbons

500 mg/l Indulin
pH = 7
T = 35 °C
Initial TOC = 335 mg/l

| Carbon | Carbon Dosage (g/l) Required to Achieve a Given Percent TOC Removal | | | | |
|---|---|---|---|---|---|
| | 25% | 50% | 75% | 90% | 100% |
| Columbia LCK | 6.4 | 25.0 | > 40 | - | - |
| Darco KB | 0.25 | 1.05 | 2.4 | 4.7 | 14 |
| Darco S-51 | 0.66 | 1.85 | 3.2 | 5.5 | 14.5 |
| Darco 12x20 | < 2 | 2.1 | 4.8 | 7.5 | 15.5 |
| Aqua Nuchar A | 2.2 | 4.3 | 5.8 | 7.1 | 10.5 |
| Filtrasorb 400 | < 2 | 5.4 | 10.0 | 16.0 | > 20 |
| Special "A" | 0.8 | 2.85 | 6.8 | 12.5 | > 20 |

I.4.2.(ii ). Adsorption Selectivity

I.4.2.(ii ).a. The Color/TOC Ratio of Adsorbed Indulin Components

The cumulative color/TOC ratio of adsorbed Indulin components at equilibrium as a function of carbon dosage m can be calculated from equilibrium adsorption data by an equation analogous to equation (1.16), i.e.

$$\left[\frac{CU}{TOC}\right]_m^{ads} = \frac{CU_o - CU_m}{TOC_o - TOC_m} \qquad (1.19)$$

where $CU_m$, $TOC_m$ are the residual solution color and TOC respectively after equilibrium contact with m grams carbon. The variation of the color/TOC ratio with m using different carbons is shown in Fig. I.26. This ratio appears to change with carbon dosage in a manner similar to the corresponding curves derived from kinetic data, as outlined in Section I.4.1 (iv).a, although the change is not so pronounced here. However, Fig. I.26 does indicate that selective adsorption of Indulin components occurs in the equilibrium adsorption process. Furthermore, the shape of the curves generally tend to suggest that preferential

Fig.I.26 Cumulative Color/TOC Ratio of Adsorbed Indulin Components at Equilibrium

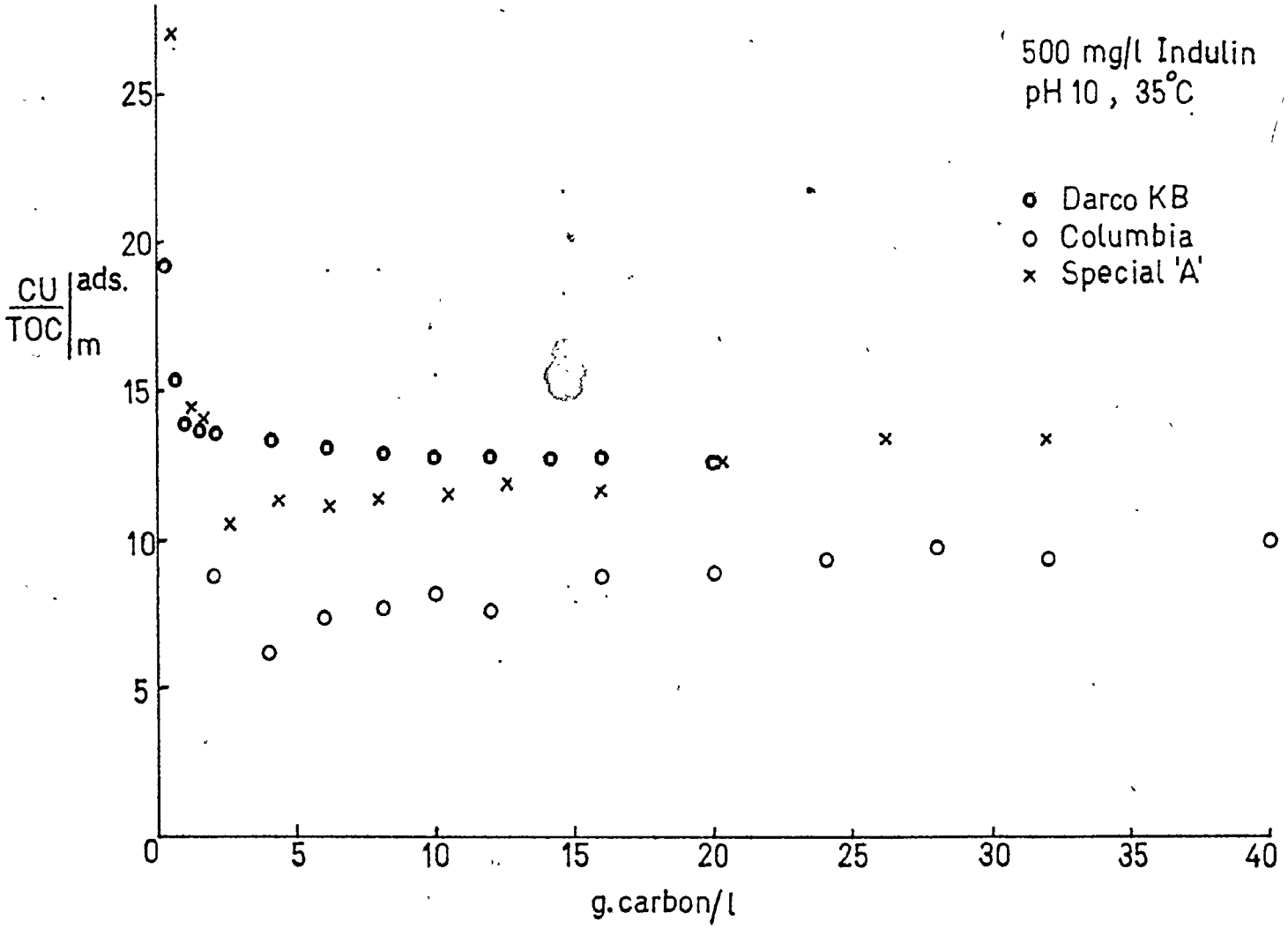

adsorption of low molecular weight Indulin solutes is evident at low carbon dosages.

I.4.2.(ii).b Gel Filtration Analysis of Adsorption Equilibrium Residual Solutions

The molecular weight distributions of Indulin components remaining in selected equilibrium adsorption residual solutions were determined by Gel Filtration experiments as outlined earlier, and are shown in Appendix I.1, Figs. (i) to (v). By a method analogous to the procedure outlined in Section I.4.1.(iv).b, the equilibrium percent removal of each molecular weight Indulin solute characterised by $(K_{AV})_i$ was calculated at different carbon dosages m from the relationship

$$\%R_{i,m} = 100 \left[1 - (A_{i,m}/A_{i,o})\right] \qquad (1.20)$$

where $A_{i,m}$ is the value of 254 mμ absorbance at $(K_{AV})_i$ in the equilibrium residual solution after contact with a carbon dosage m. The results of these calculations are shown graphically in Appendix I.1, Figs. (vi) to (xi), for six different carbons. A synopsis of this data is presented in Table I.12..

Table I.12 Removal of Various Indulin Molecular Weight Species as a Function of Carbon Dosage Using Different Carbons

| Carbon Dosage (g/l) | Carbon Used | Percent Removals of Given Molecular Weight Species | | | | | Composite Percent Removal From Solution | |
|---|---|---|---|---|---|---|---|---|
| | | $K_{AV}$= 0.1 | 0.3 | 0.5 | 0.7 | 0.9 | | |
| | | MW= 18,500 | 8,400 | 5,600 | 4,400 | 4,000 | Colour | TOC |
| 2.0 | Columbia LCK | 0 | 0 | 10* | 30* | 50* | 6 | 8 |
| | Darco KB | 14 | 44 | 78 | 87 | > 90 | 66 | 59 |
| | Darco S-51 | < 20 | 28 | 70 | 82 | 89 | 42 | 45 |
| | Darco 12x20 | 9* | 47* | 72* | 81* | 87* | 34 | 37 |
| | Aqua Nuchar A | 18 | 15 | 30 | 60 | 85 | 23 | 33 |
| | Special "A" | < 10 | 20 | 26* | 20 | < 10 | 20 | 20 |
| 8.0 | Columbia LCK | 0 | 6 | 20 | 43 | 60 | 16 | 25 |
| | Darco KB | 83 | > 90 | > 90 | > 90 | > 90 | 94 | 92 |
| | Darco S-51 | 80 | > 90 | > 90 | > 90 | > 90 | 86 | 86 |
| | Darco 12x20 | 40 | 80 | > 90 | > 90 | > 90 | 63 | 71 |
| | Aqua Nuchar A | 70* | 83 | > 90 | > 90 | > 90 | 49 | 65 |
| | Special "A" | 56 | 74 | 76 | 60 | 43 | 52 | 61 |
| 16.0 | Columbia LCK | 0 | 20 | 42 | 60 | 77* | 28 | 38 |
| | Darco KB | > 90 | ~100 | ~100 | ~100 | ~100 | 100 | 99 |
| | Darco S-51 | > 90 | ~100 | ~100 | ~100 | ~100 | 99 | 94 |
| | Darco 12x20 | > 90 | ~100 | ~100 | ~100 | ~100 | 89 | 91 |
| | Aqua Nuchar A | > 90 | ~100 | ~100 | ~100 | ~100 | 83 | 85 |
| | Special "A" | 97 | 98 | 95 | 85 | 55 | 82 | 85 |
| 26.0 | Columbia LCK | 7 | 41 | 61 | 76 | 84* | 42 | 49 |
| | Darco KB | ~100 | ~100 | ~100 | ~100 | ~100 | 100 | 100 |
| | Darco S-51 | ~100 | ~100 | ~100 | ~100 | ~100 | 100 | 100 |
| | Darco 12x20 | ~100 | ~100 | ~100 | ~100 | ~100 | 100 | 99 |
| | Aqua Nuchar A | ~100 | ~100 | ~100 | ~100 | ~100 | 100 | 100 |
| | Special "A" | 100 | 100 | 99 | 93 | 65 | 96 | 93 |

* extrapolated value

Here increase in carbon dosage is seen to produce a corresponding increase in removal of all components. Furthermore, as removals with Darco carbons at high carbon dosages indicate, total removal of overall solution color and TOC is associated with complete removal of all Indulin components.

The efficiency of each carbon in removing the various molecular weight solutes from solutions is primarily a function of the carbon pore size distribution and dosage. In this respect, Darco KB is the most efficient carbon. This is associated with the large total surface area (approximately 1500 $m^2/g$) and pore volume (approximately 1.8 $cm^3/g$) possessed by this carbon, which is evenly distributed throughout its entire pore size range. Darco KB is thus capable of effecting removal of all species at relatively low carbon dosages (i.e. approximately 10 g/l carbon).

The other Darco carbons, and Aqua Nuchar A, also have the ability to remove all Indulin solutes from solution, but require higher carbon dosages of

about 16 g/l. This is becuase although these carbons have a well diversified pore structure, the magnitude of their pore structure as indicated by total surface areas (approximately 650-900 $m^2/g$) and pore volumes (approximately 0.6-0.8 $cm^3/g$) is considerably less than Darco KB.

In contrast to the Darco and Nuchar carbons, Table I.12 indicates that Columbia LCK is incapable of removing a major portion of larger Indulin solutes of greater than approximately 8,000 MW, even at high carbon dosages. Furthermore, removals of the smaller Indulin solutes of less than 8,000 MW, although resonable, are still not as great as those achievable with the Darco carbons at equivalent dosage. These observations, coupled with a knowledge of Columbia pore structural characteristics (this carbon contains virtually all its pore structure in pores of less than approximately 15 Å radius), indicate that the pore structure of Columbia carbon is available for adsorption of only a small portion of the smaller molecular weight Indulin solutes. The bulk of overall solution

color and TOC, which is contained in larger Indulin solutes, is sterically excluded from pores of less than about 15 Å radius.

Preferential adsorption of specific molecular weight solutes is also evident with Special "A" carbon. Here Table I.12 indicates that this carbon is specific to adsorption of intermediate molecular weight solutes of approximately 5000-10,000 MW, especially at low carbon dosages. At higher dosages significant removals of the very large solutes can, however, occur. In comparison, only low removals of the small molecular weight solutes of less than about 5000 MW are attained. Since the pore structure of Special "A" is almost exclusively contained in the approximate 20-200 Å pore radii range, it appears that this pore size range is specific to adsorption of intermediate molecular weight solutes. The low molecular weight species are not adsorbed in this pore structure (although such species can penetrate such pores, they will not adsorb for reasons discussed earlier, see Section I.4.1 (iv)b). A combination of

Columbia and Special "A" data thus appears to indicate that the small molecular weight solutes are probably best adsorbed in pores of approximately 15-20 $\mathring{A}$ radii.

The results in Table I.12 also provide insight into the mechanism of adsorption in the equilibrium adsorption process. Here, Special "A" excepted, it can be seen that adsorption is always at a maximum for the smallest species. As carbon dosage is increased the percent removal of all species increases accordingly. Hence the smallest molecular weight species $MW_1$ will be adsorbed at a relatively low carbon dosage $m_1$ and each successively higher molecular weight species $MW_2$, $MW_3$.....$MW_n$ will be completely adsorbed at higher dosages $m_2$, $m_3$.....$m_n$, until the largest species $MW_n$ is completely adsorbed corresponding to total Indulin removal. Thus the adsorption mechanism is similar to that evident in the kinetic adsorption process, viz. initial preferential adsorption of the smallest adsorbable species at low carbon dosage, followed by progressive preferential adsorption of increasingly larger molecular

weight solutes as carbon dosage is increased. Naturally this mechanism is modified, but not contradicted, in instances where carbon pore structural considerations restrict adsorption of one or more species. In this respect, adsorption on Columbia carbon virtually ceases after the initial preferential adsorption of the smallest species. Correspondingly, with Special "A" carbon, initial preferential adsorption is not associated with the smallest solutes, but rather with solutes of about 5,000-10,000 MW.

Two additional features have been recognized from Gel Filtration results. Firstly, as can be seen in Appendix I.1, Aqua Nuchar A is capable of removing a significant portion of the large molecular weight solutes of greater than approximately 50,000 MW at low carbon dosages. This phenomena also occurs to a lesser extent with Darco S-51, and cannot be explained by pore structural considerations. In view of the very small average particle diameters of these powdered carbons, viz. approximately 15-25$\mu$ (see Part II, Table II.8 ), and the large diameters of the

high molecular weight lignin solutes, which may be in excess of 100 Å (Clark 1969, Bailey 1972), it is suggested that 'anchor segment' adsortpion of these components occurs on the external surface of the carbon particles, with the unadsorbed 'strands' tailing into solution. It is also feasible that two or more functional groups of the lignin solute may be attached to different adsorbent particles, creating a bridging and flocculation effect. If such a mechanism occurs, it is possible that a given particle could be coated by a film of strands of considerable thickness, each adsorbed molecule being attached by only one functional group, as shown in Fig. I.27.

The second feature, as noted from Table I.12 , is that Darco S-51 appears to remove a significantly higher percentage of solutes having molecular weight greater than about 15,000 than Darco 12x20 at similar dosages, even though the pore structures of the two carbons are very similar (see Part II, Figs. II.14 and II.15 ). This may be due to either external surface

Fig. I.27. External Surface Anchor Segment Adsorption of High Molecular Weight Indulin Solutes on Powdered Carbons

1. No Bridging Between Adsorbent Particles

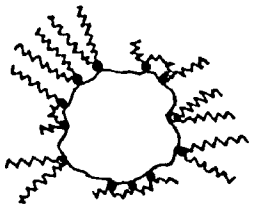

2. Bridging and Flocculation Between Adsorbent Particles

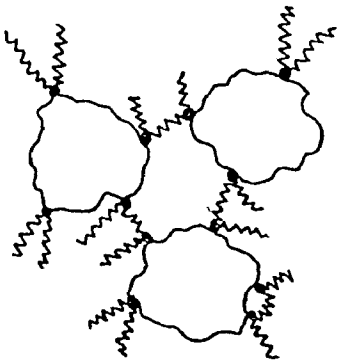

'anchor segment' adsorption of high molecular weight solutes onto Darco S-51 as discussed previously, or equilibrium considerations. If the latter is true, this suggests that the choice of 15 hours contact for powdered carbons represents a closer proximity to true equilibrium conditions than the 4 day contact time allowed for granular carbons.

The number average molecular weight $\overline{M}_n$ in equilibrium residual solutions was obtained from Gel Filtration data as outlined earlier. The variation of this parameter with carbon dosage is shown in Fig. I.28 for several carbons. Generally, $\overline{M}_n$ increases with carbon dosage in a manner governed primarily by carbon pore structural characteristics. This observation is consistent with the hypothesis of the adsorption mechanism in the equilibrium adsorption process summarised previously.

The exception using Special "A", where the initial increase in $\overline{M}_n$ is followed by decrease at dosages in excess of approximately 6 g/l, arises from the inability of this carbon to adsorb the

Fig.I.28 Variation of $M_n$ with Carbon Dosage for Several Carbons

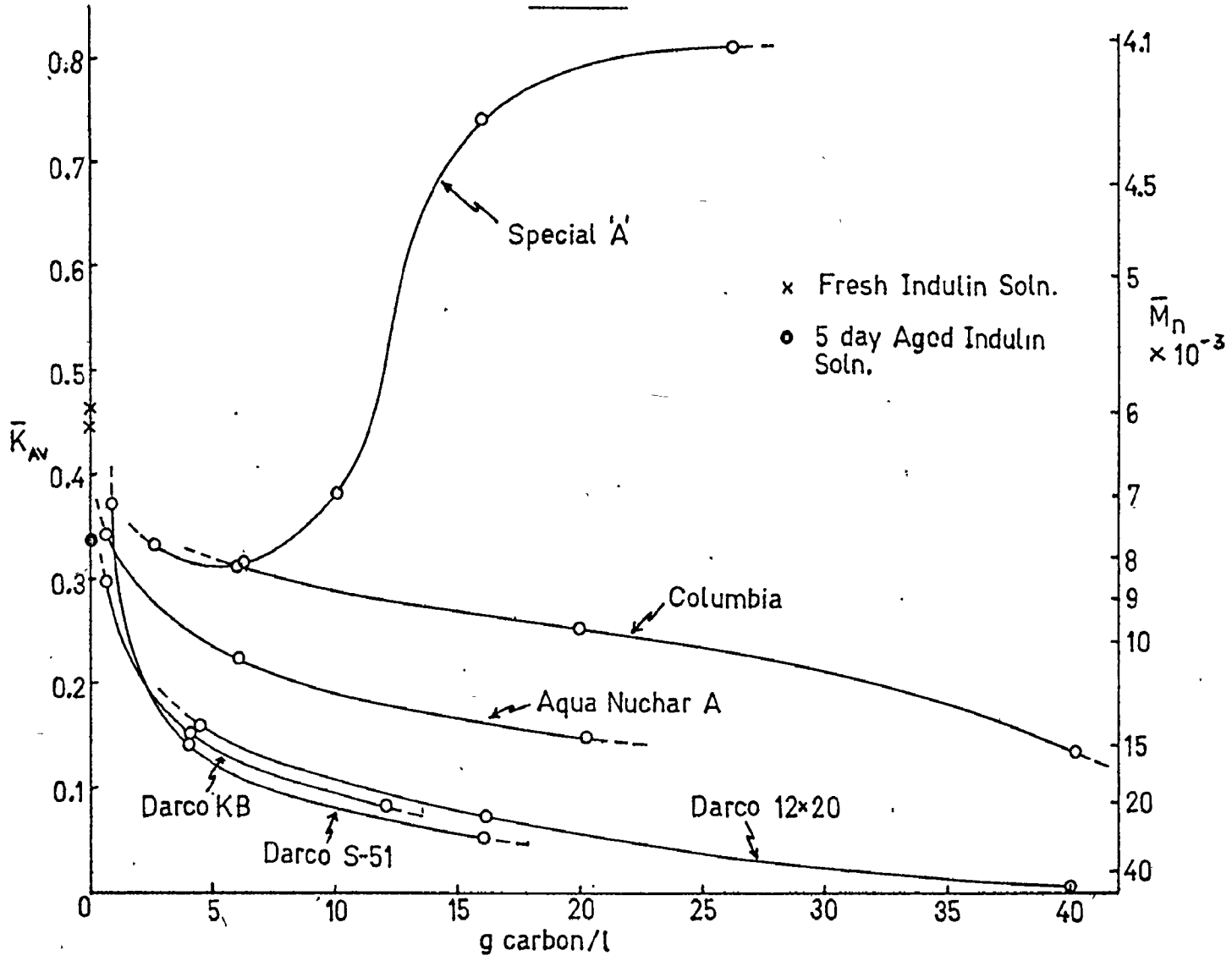

small molecular weight solutes as discussed earlier. Here, a decrease in $\bar{M}_n$ will inevitably occur when all other species are significantly removed from solution.

I.4.3 Correlations

The preceeding discussion has indicated that adsorption of Indulin from alkaline solution onto activated carbon is a selective adsorption process. Here, for each specific molecular weight solute, there exists a specific adsorbent pore size range in which preferential adsorption of this species over all other components occurs. Chen's work has inferred that a pore volume-dependent, concentration-precipitation mechanism occurs in lignin adsorption, wherein each solute is preferentially adsorbed in pores of radii approximately 3.3 to 6.1 times the solute hydrodynamic radius. Chen's findings can thus be checked by correlating observed adsorption data with carbon pore structural characterics. However, the analysis requires a knowledge of the molecular size range of Indulin solutes. Unfortunately, as discussed at length in Part II, these cannot be

accurately estimated from the Gel Filtration analyses employed in this work, due to the high pH eluant used. However, if it is assumed that gel properties do not change with pH, then the approximate hydrodynamic radius r of each molecular weight species can be calculated from equation (3.3), i.e.

$$K_{AV} = \exp\left[-\pi L\,(r+r_r)^2\right] \qquad (3.3)$$

where L, $r_r$ are constants having values of $2.9\times10^{12}$ $cm^{-2}$ and $7\times10^{-8}$ cm respectively (see Part III, Section III.4.1) The results of these calculations are shown in Appendix I.2, where virtually all the Indulin color and TOC appears to be concentrated in solutes of approximately 5-50 Å radii. This range corresponds to that found by Clarke (1969) and Bailey (1972) in similar lignin solutions. Using Chen's formula with the above values, a pore radii range of approximately 16-305 Å is determined as the specific range in which adsorption of Indulin solutes is concentrated. The surface area and pore volume of several carbons in this pore radii range was then determined from carbon pore size distribution data (see Part II, Figs. II.14 and II.15) and correlated with observed Indulin

adsorption behaviour, i.e. (x/m), corresponding to different overall Indulin removals. The correlations were obtained using a computer library program. The results are depicted in Table I.13, with an example of the data correlation at 75% TOC removal shown in Figs. I.29 and I.30. Here good correlations between specific pore structure and adsorption for the carbons studied are evident, tending to give support to Chen's postulation of the range of pore sizes responsible for lignin adsorption.

It is somewhat surprising that the correlations based on specific surface areas and pore volumes are similar. Although the reason for this observation is not known, it may indicate that in addition to a concentration-precipitation mechanism, which is pore volume-dependent, significant surface adsorption of lignin adsorbates may also be evident.

In addition, a knowledge of the molecular size distributions in adsorption residual solutions - as determined by Gel Filtration - provides the means to relate adsorption of each Indulin species to its

Table I.13 Correlation Coefficients Between Adsorption Capacity and Specific Pore Structure * for the Carbons Studied

a) Pore Volume

| % Removal | Correlation Coefft. |
|---|---|
| 25% color | 0.9587 |
| 50% color | 0.9615 |
| 75% color | 0.9522 |
| 25% TOC | 0.9260 |
| 50% TOC | 0.9479 |
| 75% TOC | 0.9078 |

b) Surface Area

| % Removal | Correlation Coefft. |
|---|---|
| 25% color | 0.9590 |
| 50% color | 0.9724 |
| 75% color | 0.9782 |
| 25% TOC | 0.9103 |
| 50% TOC | 0.9587 |
| 75% TOC | 0.9487 |

* contained in the 16 - 305 Å radii range

Fig.I.29 Adsorption Capacity Versus Specific Surface Area for the Carbons Studied

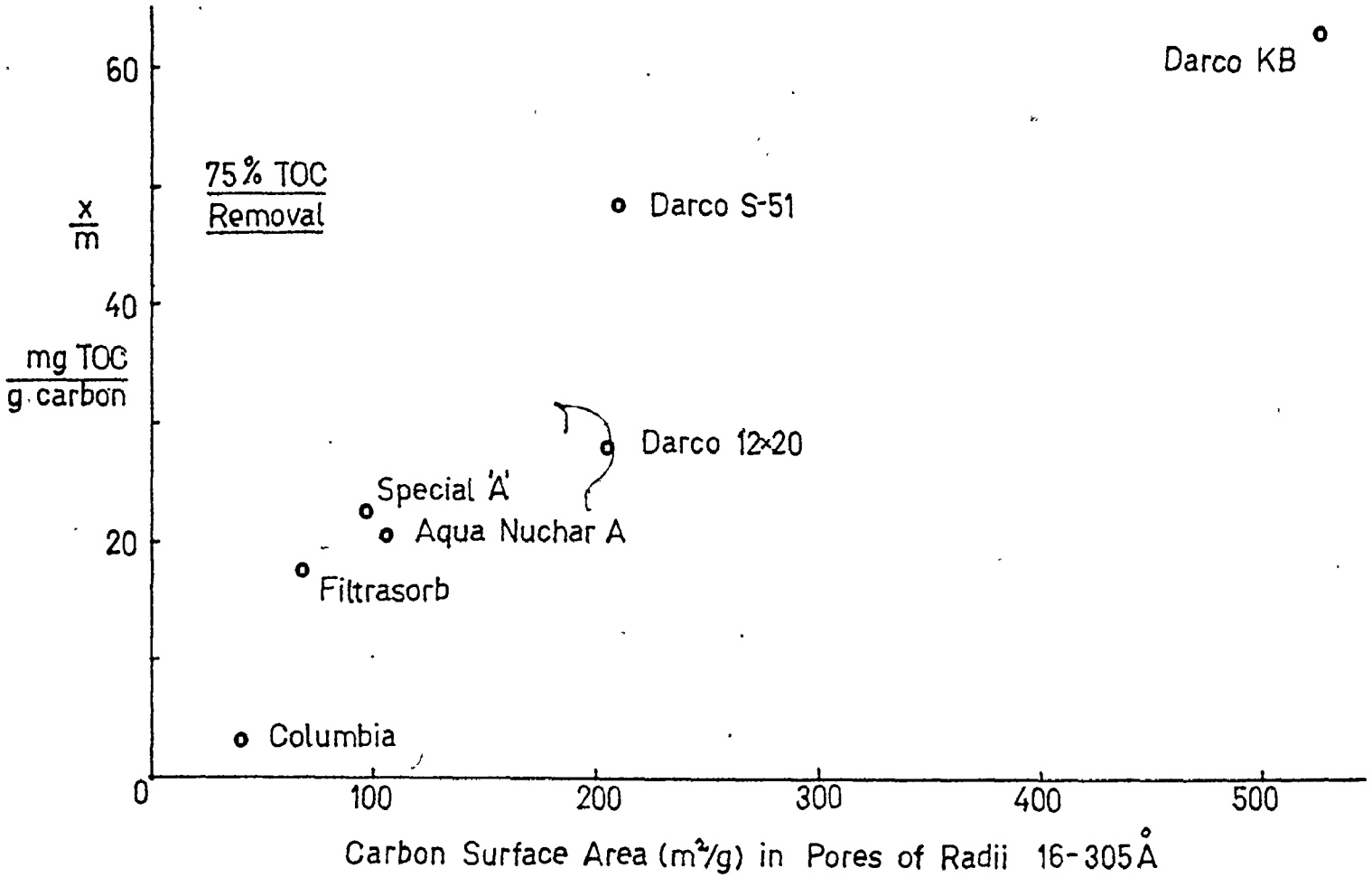

Fig.I.30 Adsorption Capacity versus Specific Pore Volume for the Carbons Studied

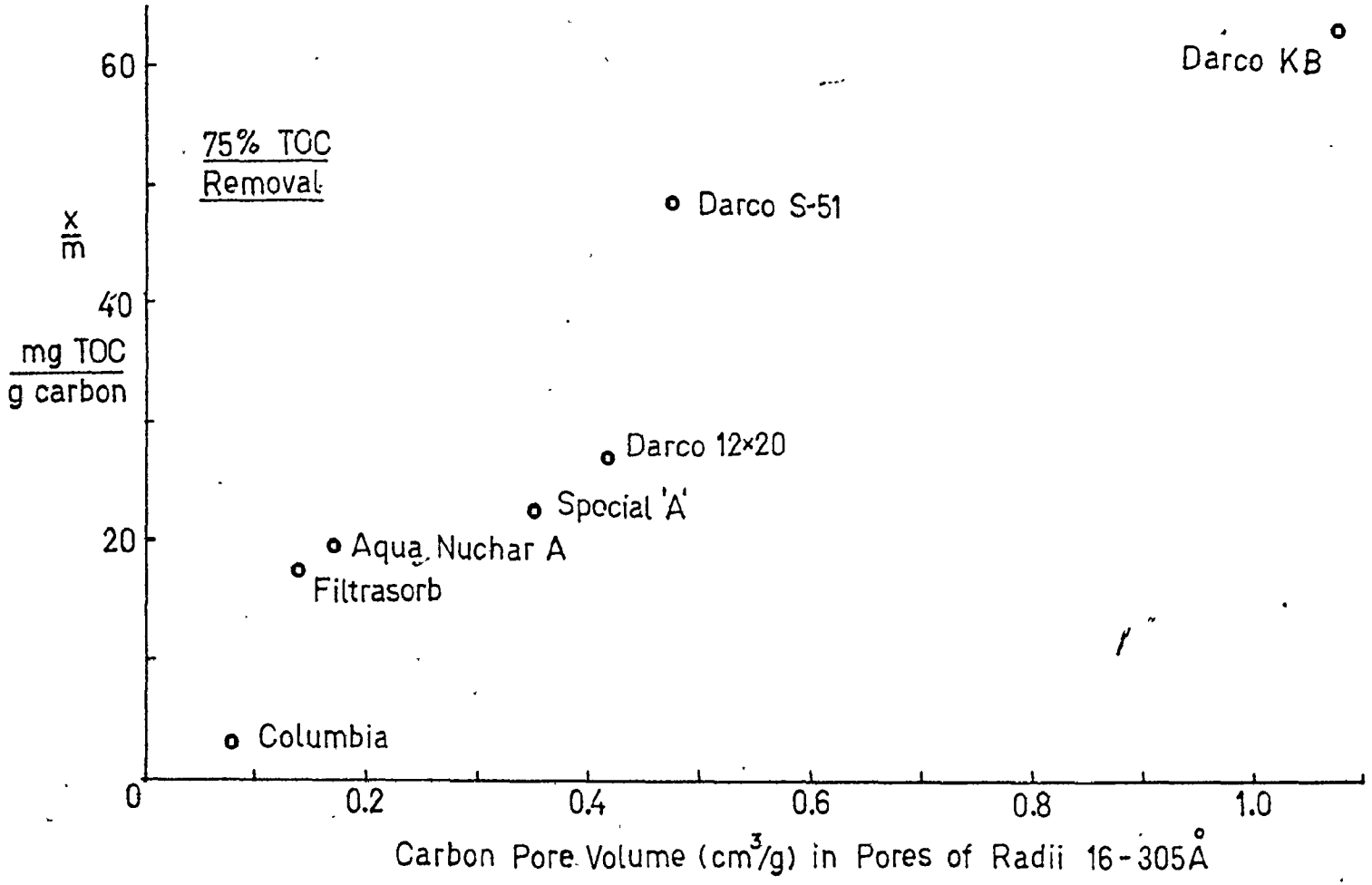

appropriate specific pore structure for various carbons. Here, the approximate hydrodynamic radius and specific pore radii range were calculated from equations (3.3 ) and (1.11) for a given molecular weight species having $K_{AV} = i$. The adsorption of species $i$ at a given percent removal of that species from solution was obtained from the data in Appendix I.1 for each carbon, the adsorption term at a given percent adsorbance removal being calculated by

$$\left(\frac{x}{m}\right)_{K_{AV}=i} = \left[\frac{(A_o)_{K_{AV}=i} - (A)_{K_{AV}=i}}{m}\right] \qquad (1.21)$$

where $A_o$, A are the values of 254 mμ absorbance of species $i$ in the control solution, and the residual solution after equilibrium contact with m g/l carbon, respectively. The adsorption term has units of $l\,g^{-1}$. The results of the calculations and correlations are shown in Table I.14. Here in all cases reasonable correlation coefficients are obtained, suggesting that the indicated preferential pore size range for each species is reasonably representative. These correlations are, however, not as good as those in Table I.13, a fact that arises probably from the

Table I.14 Correlation Coefficients Between Adsorption Capacity and Specific Pore Structure for Adsorption of Various Lignin Components

| Lignin Component | | | | Correlation Coefficients | |
|---|---|---|---|---|---|
| $K_{AV}$ | Molecular wt. MW | Molecular Radius r (Å) | Calculated Specific Pore Radii Range $\Delta R$ (Å) | Based on Specific Pore Volume in $\Delta R$ | Based on Specific Surface Area in $\Delta R$ |
| 0 | 70,000 | 50.0 | 165 - 305 | -- | -- |
| 0.1 | 18,500 | 40.0 | 132 - 244 | 0.7530 (1) | 0.8024 (1) |
| 0.2 | 11,500 | 34.0 | 112 - 207 | -- | -- |
| 0.3 | 8,500 | 28.5 | 95 - 177 | 0.8090 (1) | 0.8381 (1) |
| 0.4 | 6,700 | 24.0 | 79 - 146 | -- | -- |
| 0.5 | 5,700 | 19.7 | 66 - 122 | 0.8030 (1) | 0.8747 (1) |
| 0.6 | 4,900 | 15.7 | 52 - 96 | -- | -- |
| 0.7 | 4,400 | 12.2 | 40 - 74 | 0.8619 (2) | 0.8699 (2) |
| 0.8 | 4,200 | 9.0 | 28 - 55 | -- | -- |
| 0.9 | 4,000 | 6.0 | 20 - 36 | 0.9704 (2) | 0.9623 (2) |
| 1.0 | 4,000 | 5.0 | 16 - 30 | -- | -- |

(1) at 50% removal of lignin species
(2) at 70% removal of lignin species

greater accuracy in calculating adsorption from color and TOC measurements as opposed to Gel Filtration measurements.

The data in Table I.14 relates well to observed Indulin solution characteristics and subsequent adsorption behaviour using various carbons. In this respect, virtually all the pore structure of Columbia, which is contained in pores of less than about 15 Å radius, is seen to be amenable to preferential adsorption of possibly only the very low molecular weight species. Conversely, the bulk of solution color and TOC, which is contained in species of approximately 5000-10,000 MW, (see Part III), is significantly adsorbed by Special "A", even though the total pore structure in this carbon is very much less than in the other carbons studied (see Part II, Figs. II.14 and II.15). This is because the derived pore size range specific to preferential adsorption of these species as shown in Table I.14, i.e. approximately 60-190 Å, falls within the range of pore radii in which virtually all Special "A"'s pore structure is contained, viz. pores of approximately

20-200 Å.

The preceeding discussion has indicated, via correlation coefficients, that the 16-305 Å pore radii range is reasonably representative as the specific pore size range for Indulin adsorption. However, this may not be the only valid range. In order to confirm this range, an analysis similar to the Westvaco (1969) study, wherein correlation coefficients were evaluated using different pore size ranges, would be required.

In view of the limitations regarding the representativeness of Gel Filtration - derived molecular distributions in describing the actual molecular distribution of Indulin in a pH 10 solution as discussed in Part III, it seems extremely likely that pores in excess of 305 Å radii could play a role in Indulin adsorption. Here Ultrafiltration experiments have shown that species in excess of 50Å radius exist in pH 10 solutions. It is thus probable that any pore structure in pores of greater than 16 Å radius would be specific to adsorption of one or more Indulin species, although significant adsorption would still occur in the 16-305 Å pore size range.

I.4.4. Solution pH Drop During Adsorption

A decrease in residual solution pH with adsorption was observed to occur in both kinetic and equilibrium studies. The effect of contact time and carbon dosage on residual solution pH is shown in Figs. I.31 and I.32. Since a comparable pH drop is not observed in control solutions of either lignin or solvent alone, it cannot be explained by possible solution effects such as the lignin degradation reaction, or atmospheric $CO_2$ dissolution in the solvent. Conversely, the magnitude of the pH decrease in a control solution of solvent and carbon alone is similar to that noted in adsorption residual solutions, indicating that the pH drop is due to an adsorption effect, possibly involving an exchange adsorption mechanism. Several adsorption mechanisms may be responsible. These are

a) exchange adsorption involving adsorption of $OH^-$ (and $Na^+$) ions from the solvent.

b) precipitation and adsorption of Indulin solutes in the pore volume, with subsequent release of $H_3O^+$ ions.

Fig. I.31 Solution pH Drop during Adsorption — Kinetic Studies

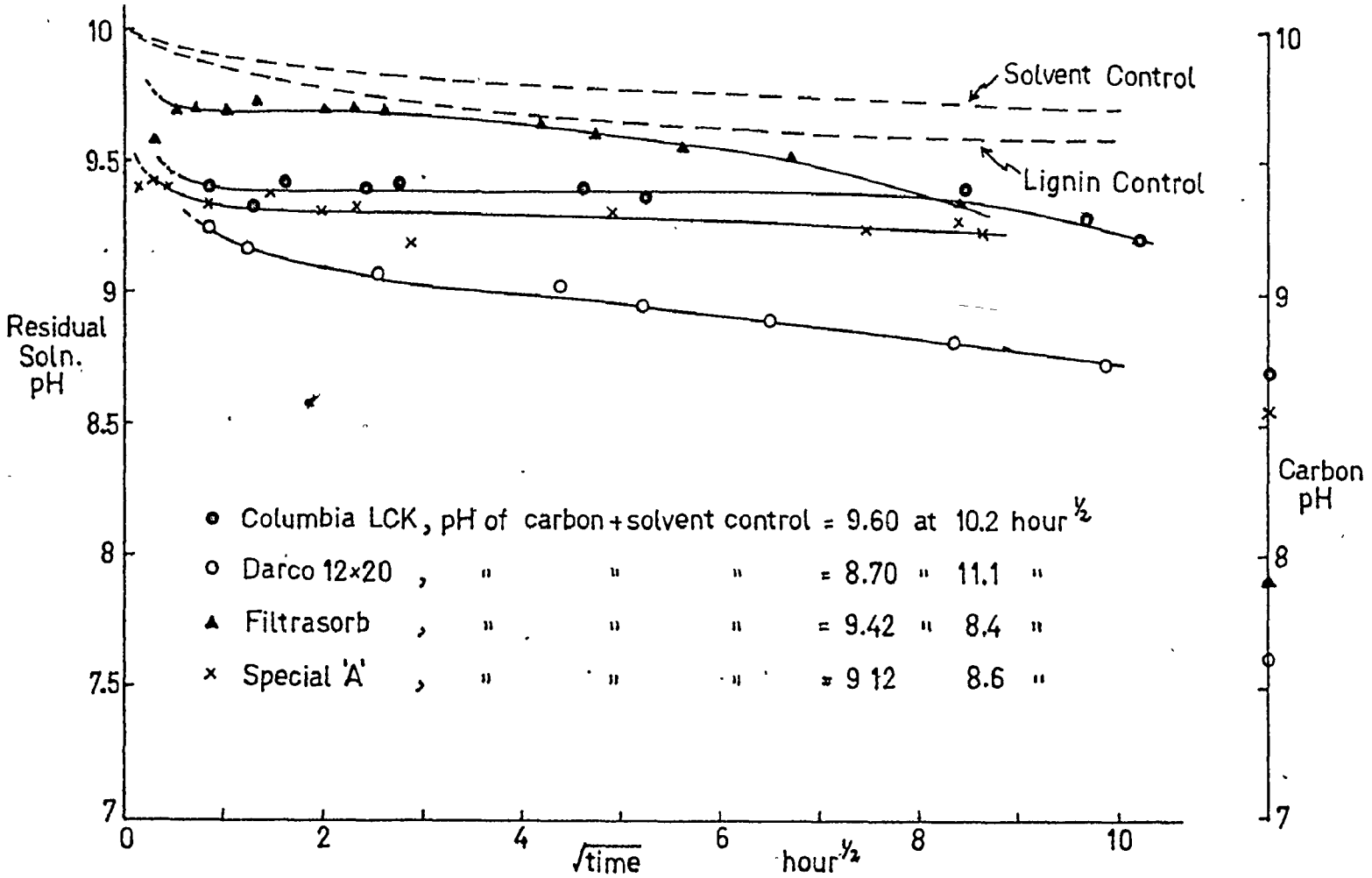

Fig.I.32 Solution pH Drop during Adsorption — Equilibrium Studies

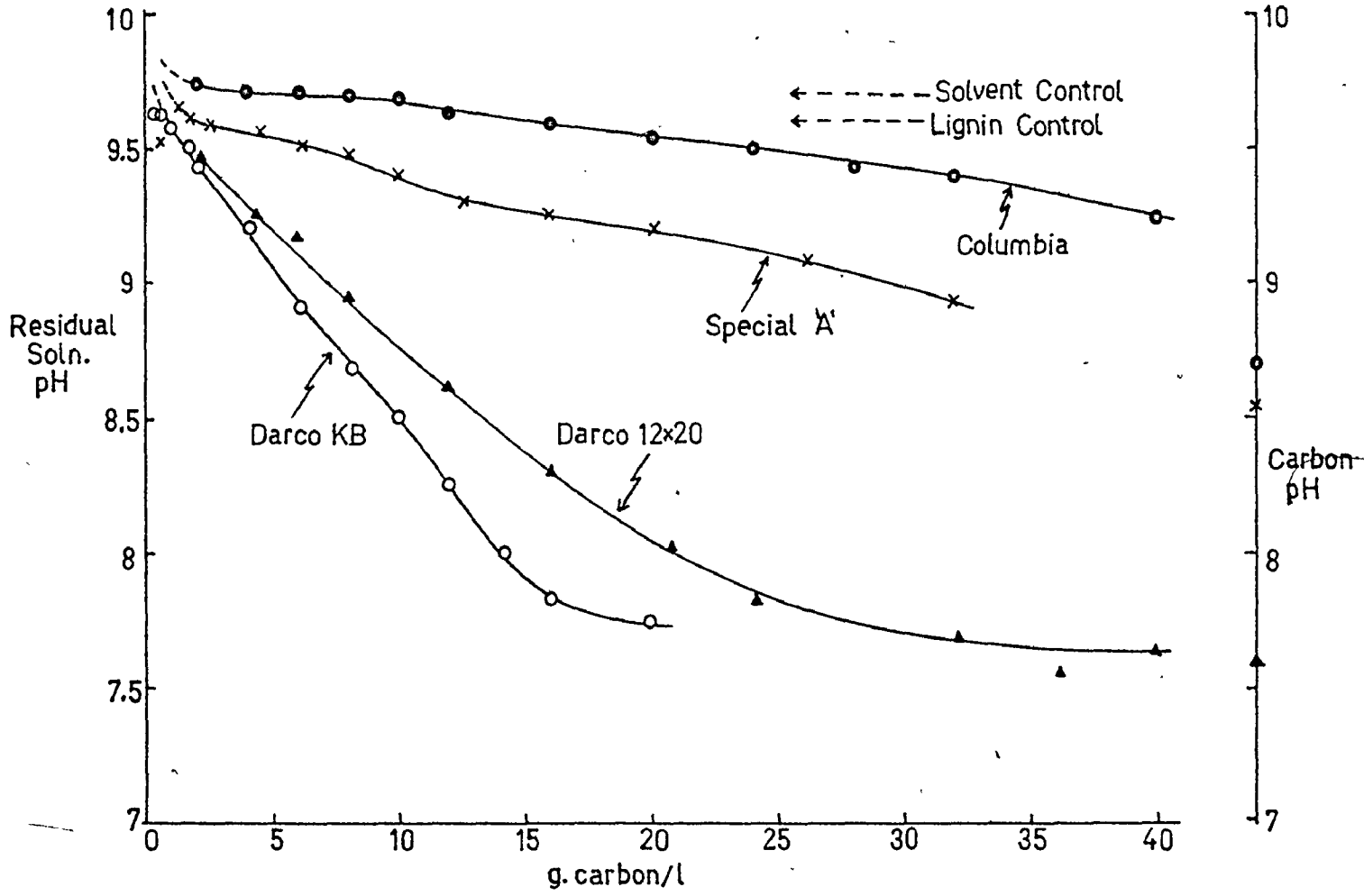

c) exchange adsorption of Indulin components on the carbon internal surface area of the type

$$[\text{lignin}]^- + [\text{adsorbent}]^+ \quad [\text{surface group}]^- \rightarrow [\text{adsorbent}]^+ \quad [\text{lignin}]^- + [\text{surface group}]^-$$

where adsorption of basic lignin components is accompanied by release of surface groups of lower basicity.

d) oxidation of adsorbed lignin components at the carbon surface.

This study does not, however, provide sufficient information for determination of the predominant mechanism involved.

Since, as can be seen from Fig. I.31, the carbon pH appears to influence the extent of the observed pH drop and hence the adsorption mechanism, it may be argued that overall adsorption of color and TOC is dictated by carbon pH. However, it must be realised that this is only of secondary importance in comparison to carbon pore structural considerations: only if a given species can penetrate a carbon pore will adsorption take place. Conversely, adsorption will

not occur if carbon pore structural considerations limit pore penetration of adsorbates, even though carbon pH may be very favourable to an exchange adsorption mechanism. However, for 'equivalent pore structure' carbons, the nature of the carbon surface, as indicated by carbon pH, may become a significant factor in determining relative adsorption capacities, due to variations in carbon surface nature and its associated exchange adsorption potential.

## I.5 CONCLUSIONS

Adsorption of a lignin, Indulin, from alkaline solution onto different activated carbons has been studied in batch reactors. The following conclusions regarding this complex adsorption system may be drawn from this work.

1. The overall adsorption rate of Indulin adsorption is slow, and governed by pore diffusion rate characteristics. Overall adsorption rate is increased by reduction in carbon particle size, and by increase in solution pH, system temperature, and carbon dosage. Carbon pore structure also influences the kinetic adsorption process.

2. Most carbons studied are able to achieve virtually complete equilibrium adsorption of Indulin, as color and TOC, from pH 10 solution at dosages of 16-33 g carbon/litre, this value depending on carbon pore structural characteristics and, to a lesser extent, carbon surface nature. Equilibrium adsorption

capacity is increased with decrease of solution pH.

3. Gel Filtration analyses of adsorption residual solutions has indicated the selectivity of the polymeric Indulin adsorption process. Here preferential adsorption of the smallest adsorbable lignin solute initially occurs, followed by progressive preferential adsorption of increasingly larger lignin solutes as contact time (in the kinetic process) or carbon dosage (in the equilibrium adsorption process) is increased. The extent of adsorption of each molecular species is primarily dependent on its initial concentration in solution, and carbon pore structural considerations. Usually adsorption is accompanied by an increase in solution average molecular weight $\overline{M}_n$.

4. Carbon pore structural deficiencies can limit the extent of Indulin removal, as color and TOC, from solution by restricting

adsorption of one or more molecular species. The low color and TOC removals attainable with Columbia LCK arise because this carbon contains virtually all its pore structure in pores of less than 15 Å radii, this pore structure being accessible to only the very small lignin solutes. Conversely, the good color and TOC removals attainable with Special "A" arise because the very limited pore structure in this carbon, which is contained in the 20-200 Å pore radii range, is specific to preferential adsorption of the bulk of Indulin species present in solution.

5. Correlations of observed adsorption data with Chen's preferential pore size range have tended to support Chen's hypothesis that adsorption of a lignin solute will occur preferentially in pores of approximately 3.3 to 6.1 times the solute hydrodynamic radius. For the solution studied here, this corresponds to a specific carbon pore size

range of approximately 16-305 Å. This, however, may not be the only valid range; it appears likely that all pores of greater than 16 Å radius play a role in Indulin adsorption.

6. It seems probable that adsorption of lignin components occurs mainly by a concentration-precipitation mechanism in the adsorbent pores. However, the observed pH drop in adsorption suggests that an exchange adsorption process may also occur.

7. Lignin adsorption is always accompanied by a simultaneously occuring lignin degradation reaction in solution.

## I.6 RECOMMENDATIONS

1. The economic and technological feasibility of lignin removal from alkaline solution in continuous reactors using powdered carbon should be investigated. Darco KB and Darco S-51 carbons appear to show the greatest promise here. It is unlikely that economic lignin removals can be achieved in granular carbon columns due to the slow overall lignin adsorption rate.

2. Work should be conducted on the development of an activated carbon with pore structural characteristics most suitable for lignin adsorption. In this respect, activation procedures should be developed to maximise the carbon pore structure in pores of greater than approximately 16 Å radii.

3. The effect of carbon surface nature on lignin adsorption should be investigated. From such a study it may be possible to determine a carbon pretreatment program

commensurate with maximum lignin removals in a given pore structure.

4. The effect of lignin molecular weight on adsorption should be studied. Here adsorption studies using narrow molecular weight lignin fractions could be conducted to determine the adsorption characteristics of such fractions.

5. The effect of other organic adsorbates present in lignin solutions on subsequent lignin adsorption should be investigated. From such studies, it may be possible to determine the effects of other dissolved organics on the adsorption of lignin from industrial effluents.

# APPENDIX I.1

## Gel Filtration Analysis of Equilibrium Adsorption Residuals

Fig.(i) Gel Filtration Analysis of Equilibrium Adsorption Residuals

Columbia LCK 12/28

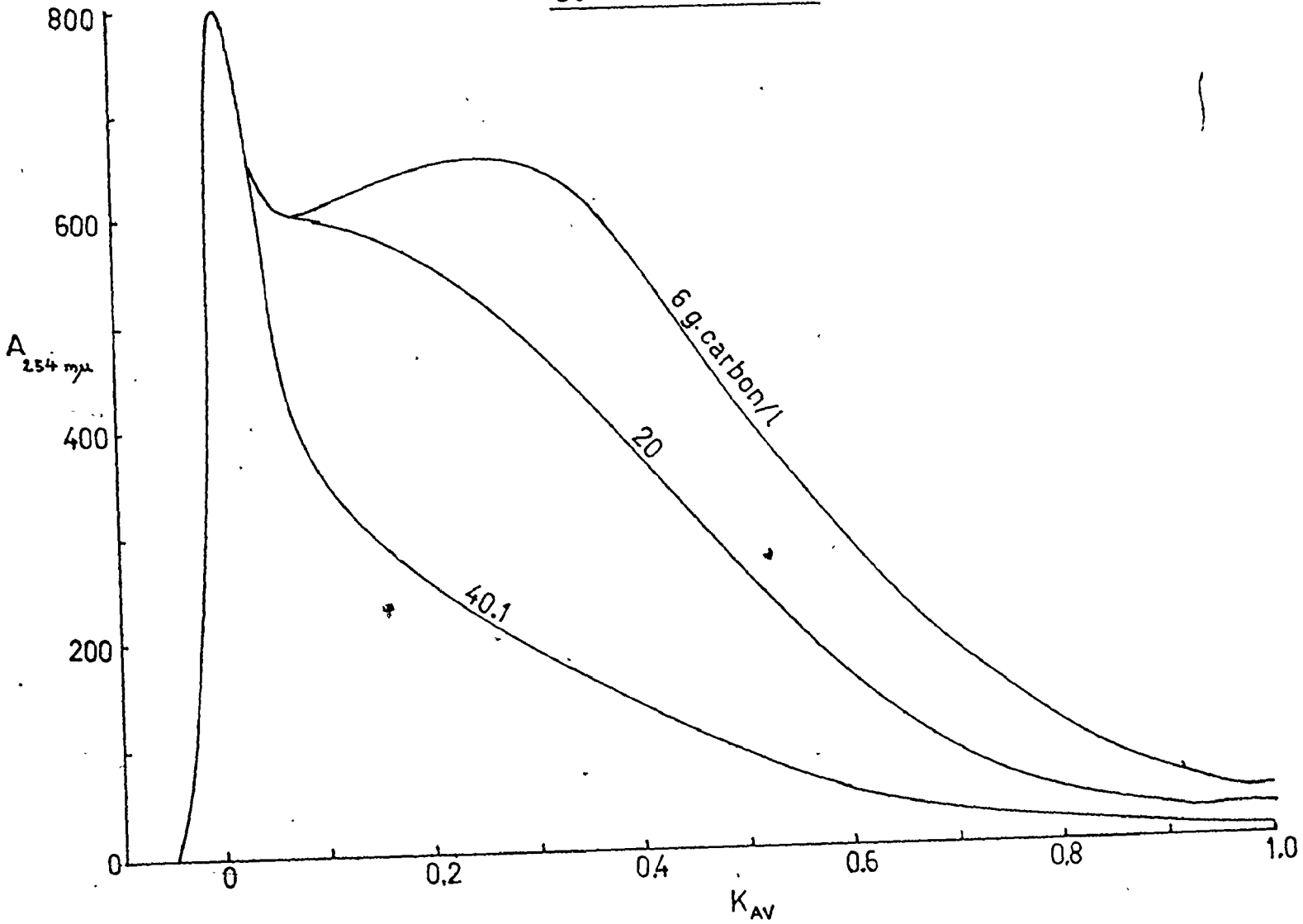

Fig.(ii) Gel Filtration Analysis of Equilibrium Adsorption Residuals

Darco S-51

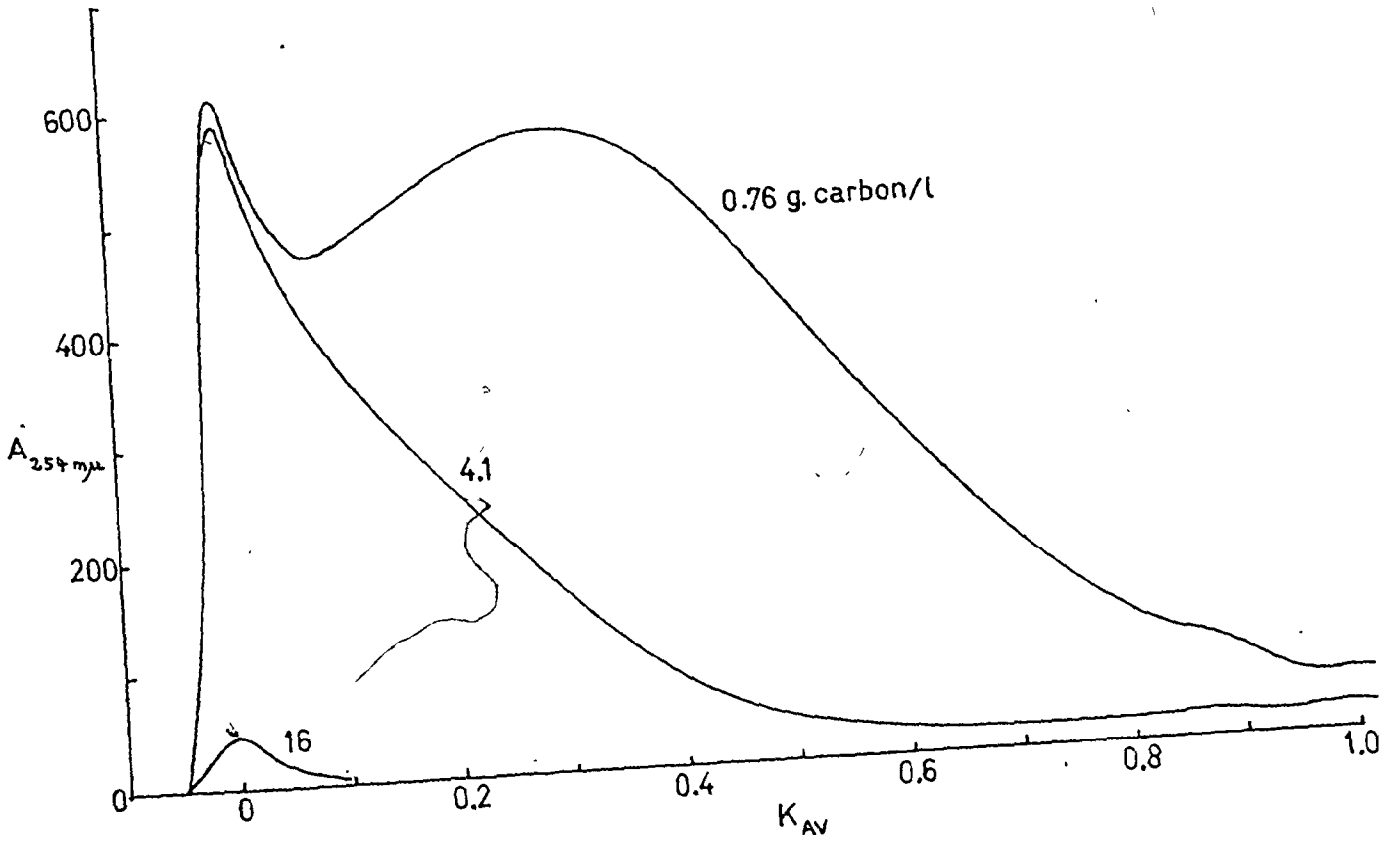

Fig.(iii) Gel Filtration Analysis of Equilibrium Adsorption Residuals

Darco 12×20

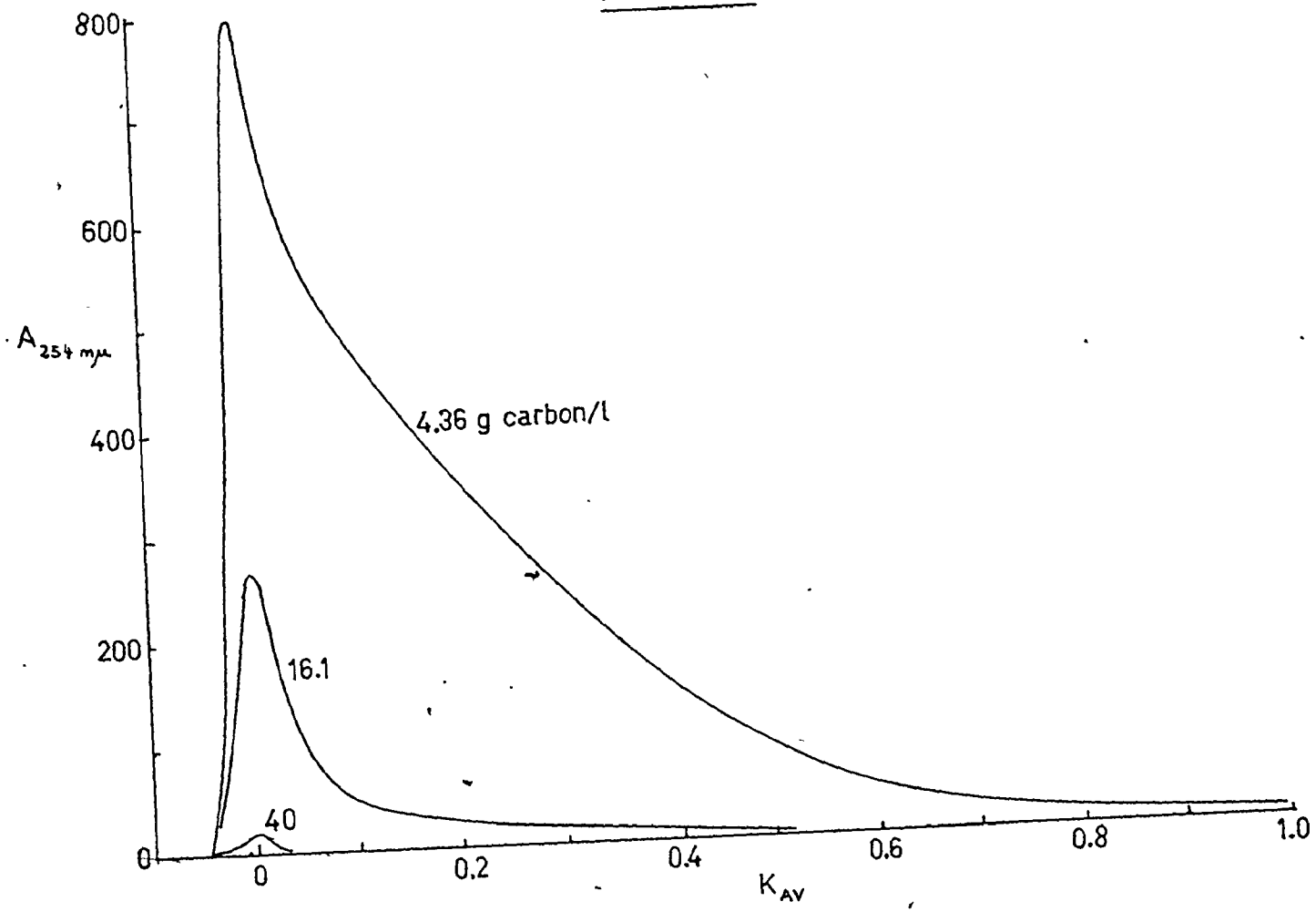

Fig. (iv) Gel Filtration Analysis of Adsorption Equilibrium Residuals

Aqua Nuchar A

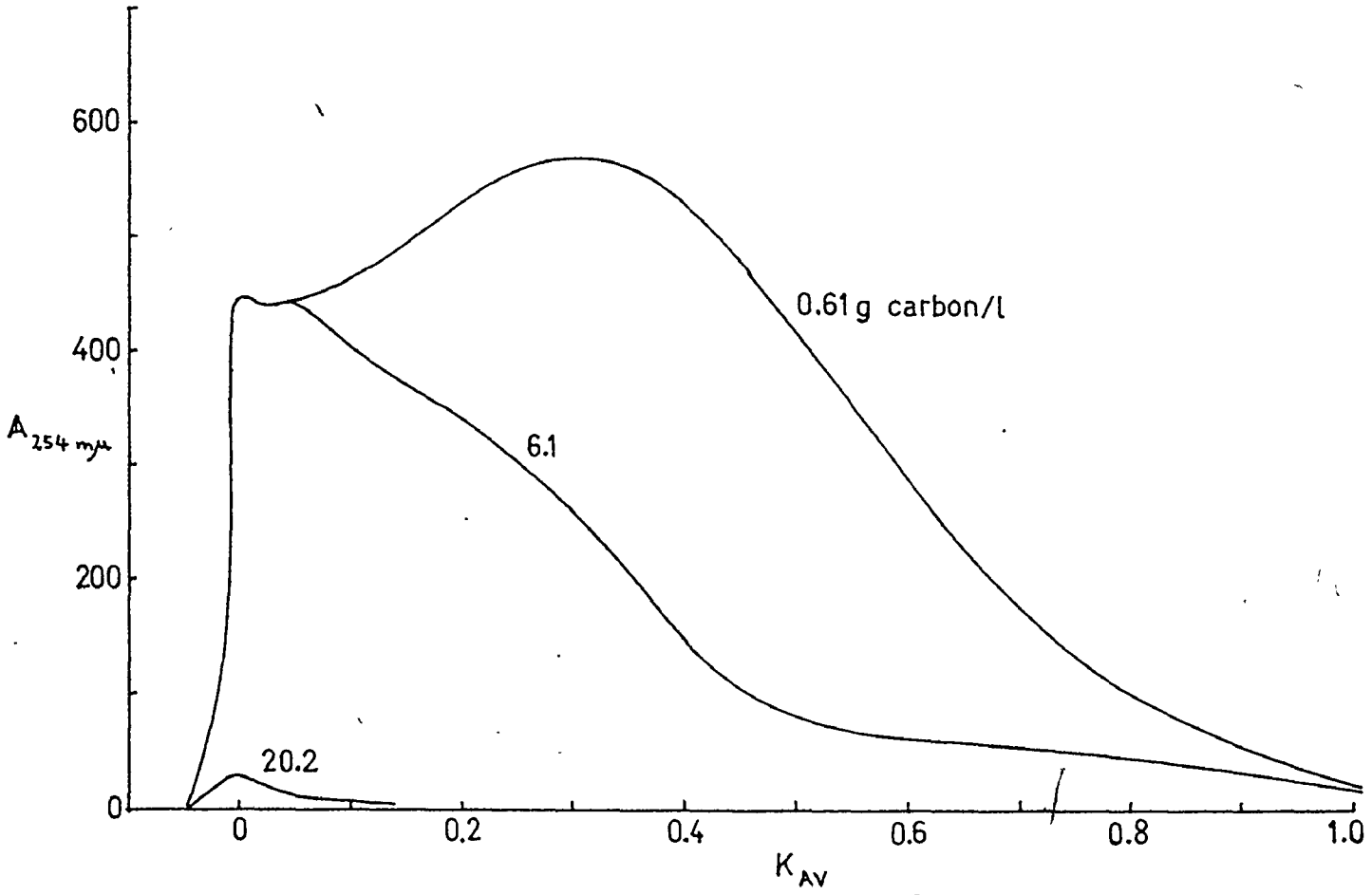

Fig.(v) Gel Filtration Analysis of Equilibrium Adsorption Residuals

Special 'A'

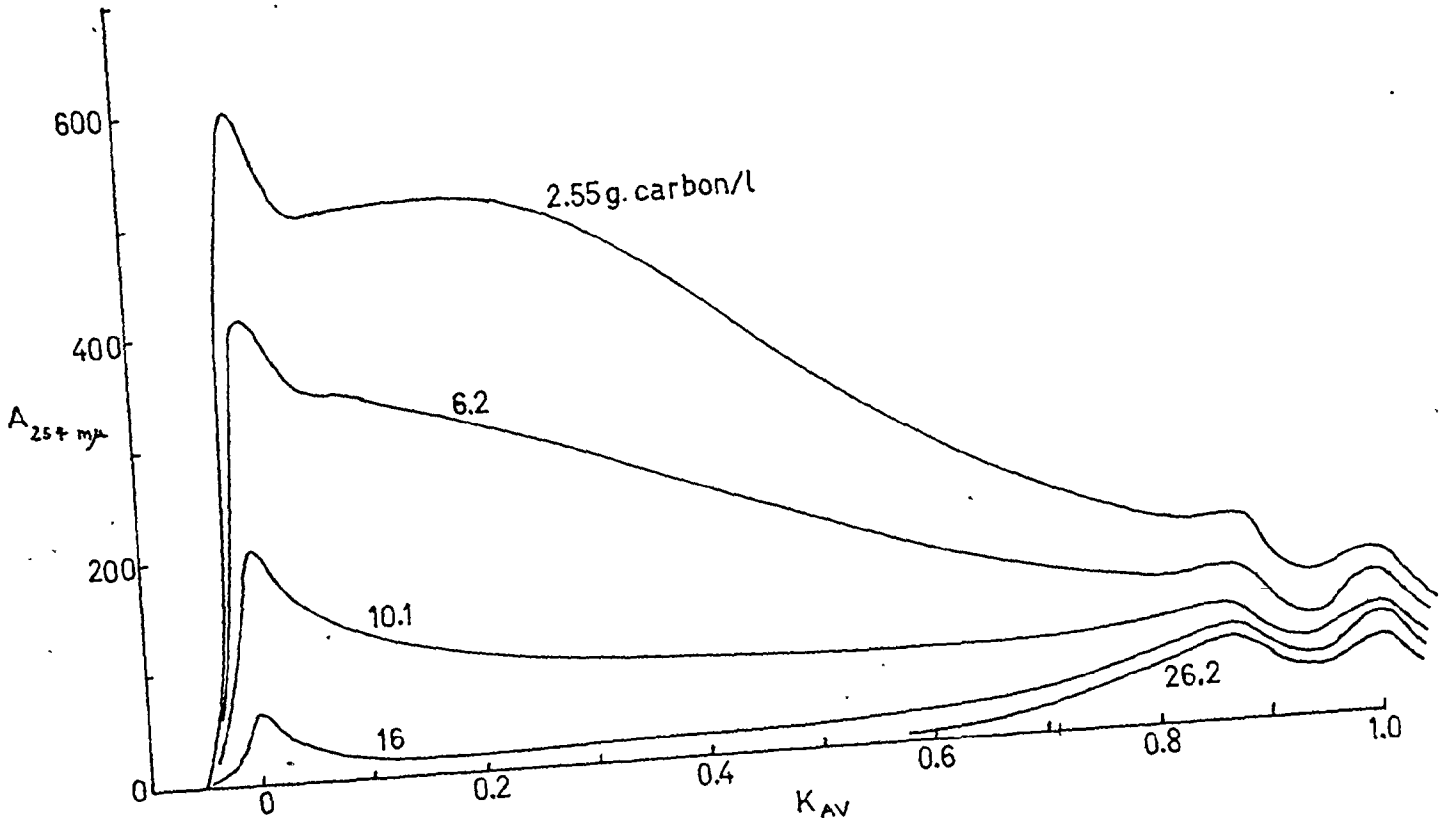

Fig.(vi) Removal of Lignin Species At Equilibrium

Columbia LCK 12/28

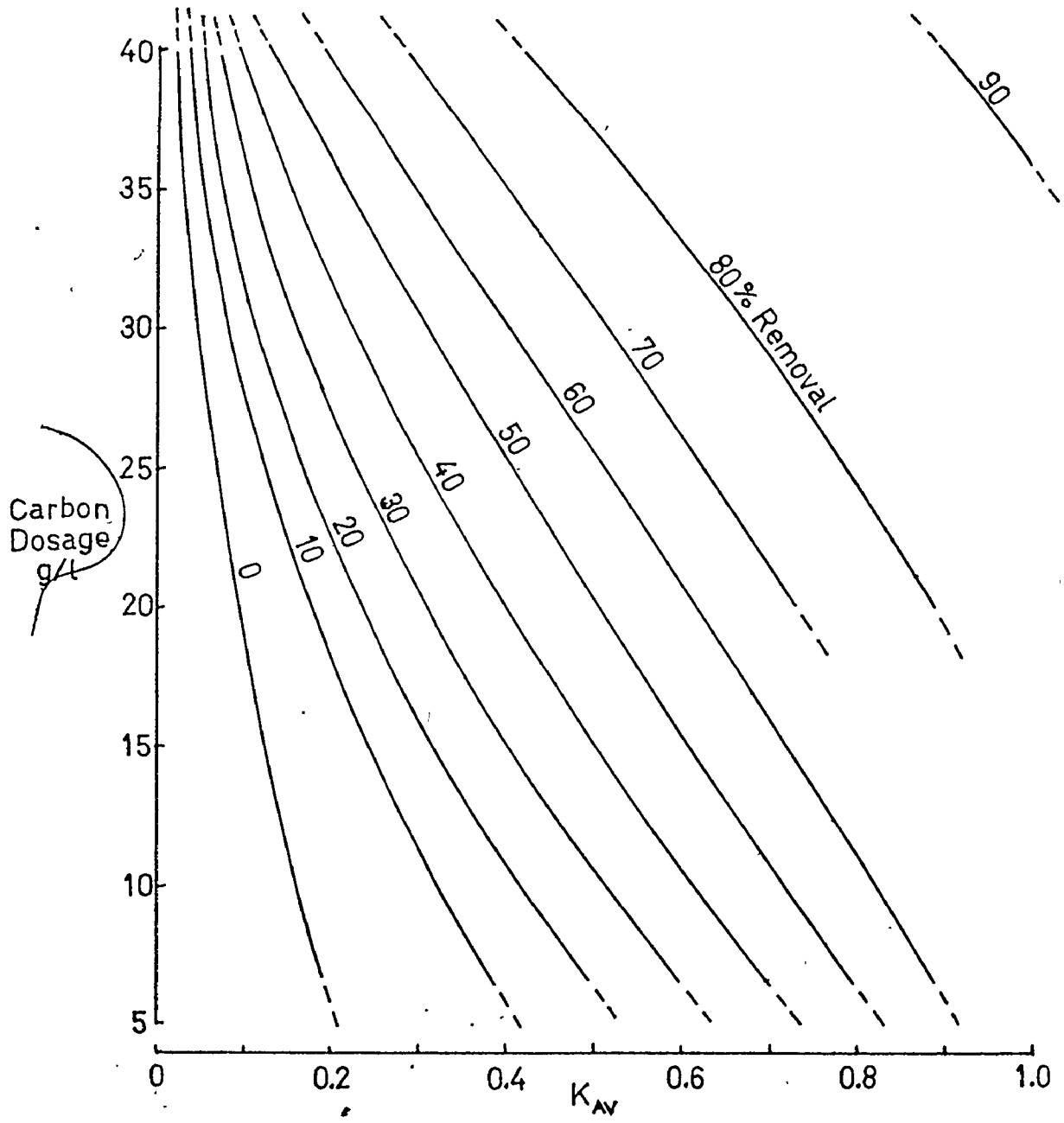

Fig.(vii) Removal of Lignin Species at Equilibrium

Darco KB

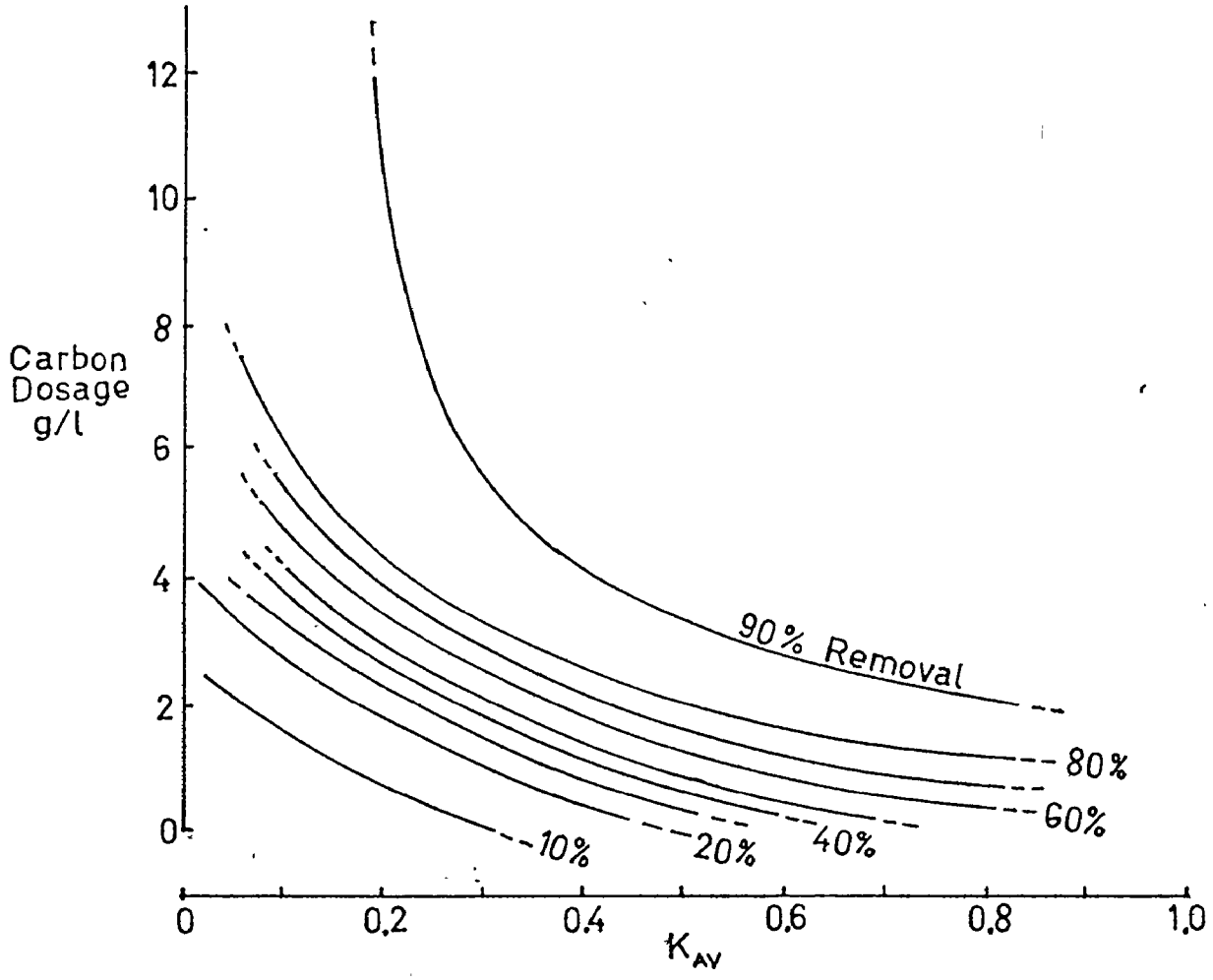

Fig.(viii) Removal of Lignin Species at Equilibrium

Darco S-51

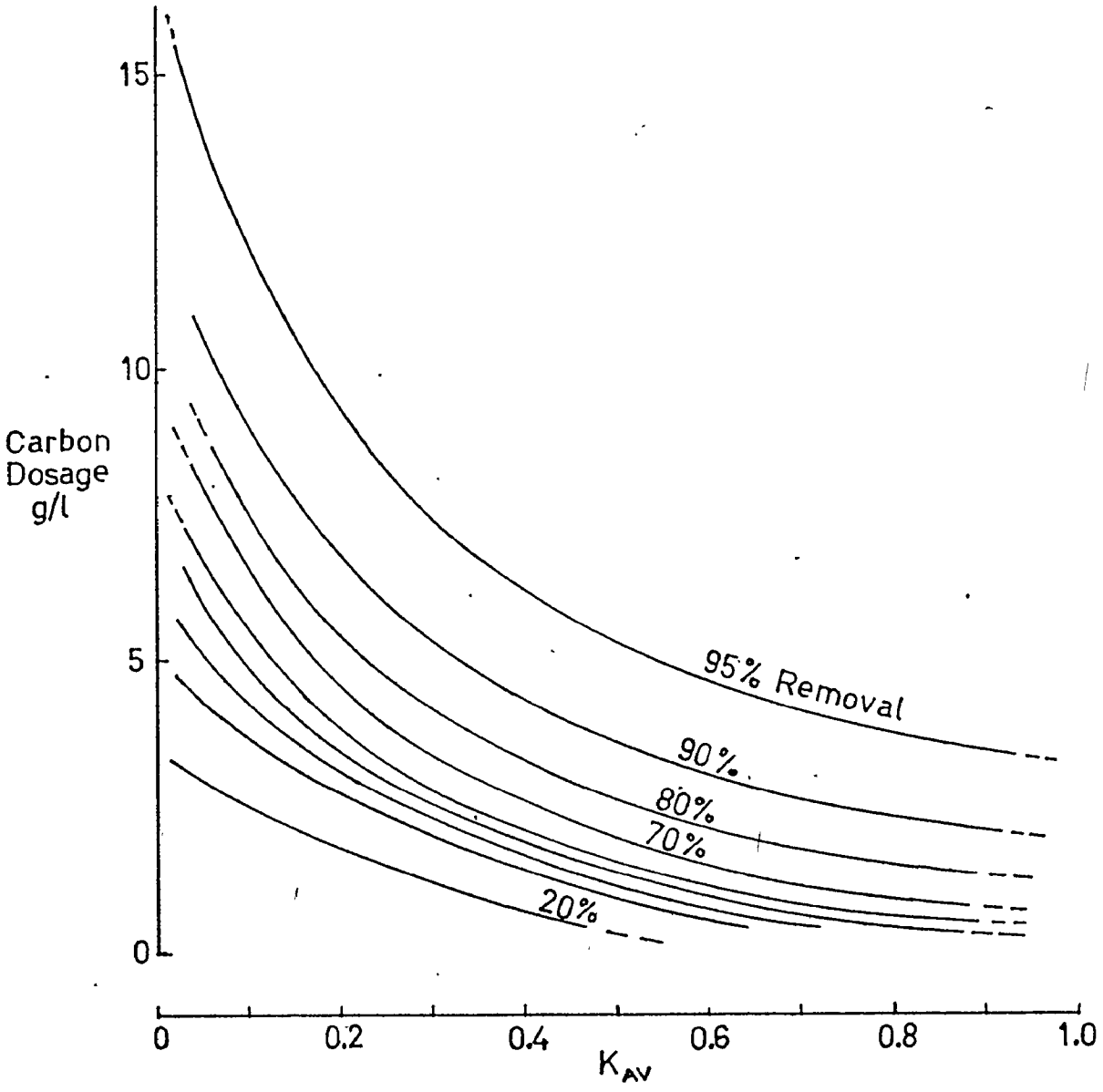

Fig.(ix) Removal of Lignin Species at Equilibrium

Darco 12×20

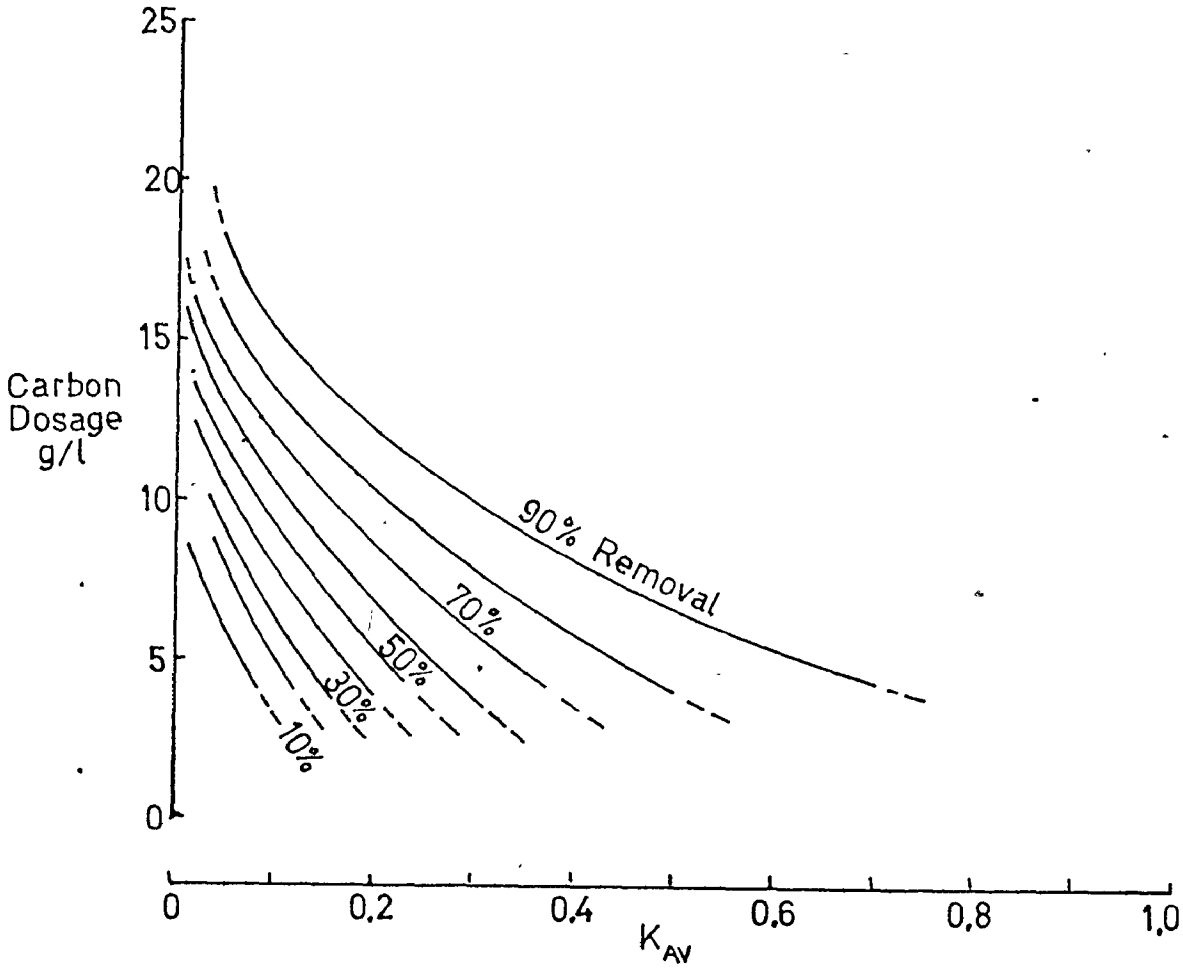

Fig.(x) Removal of Lignin Species at Equilibrium

Aqua Nuchar A

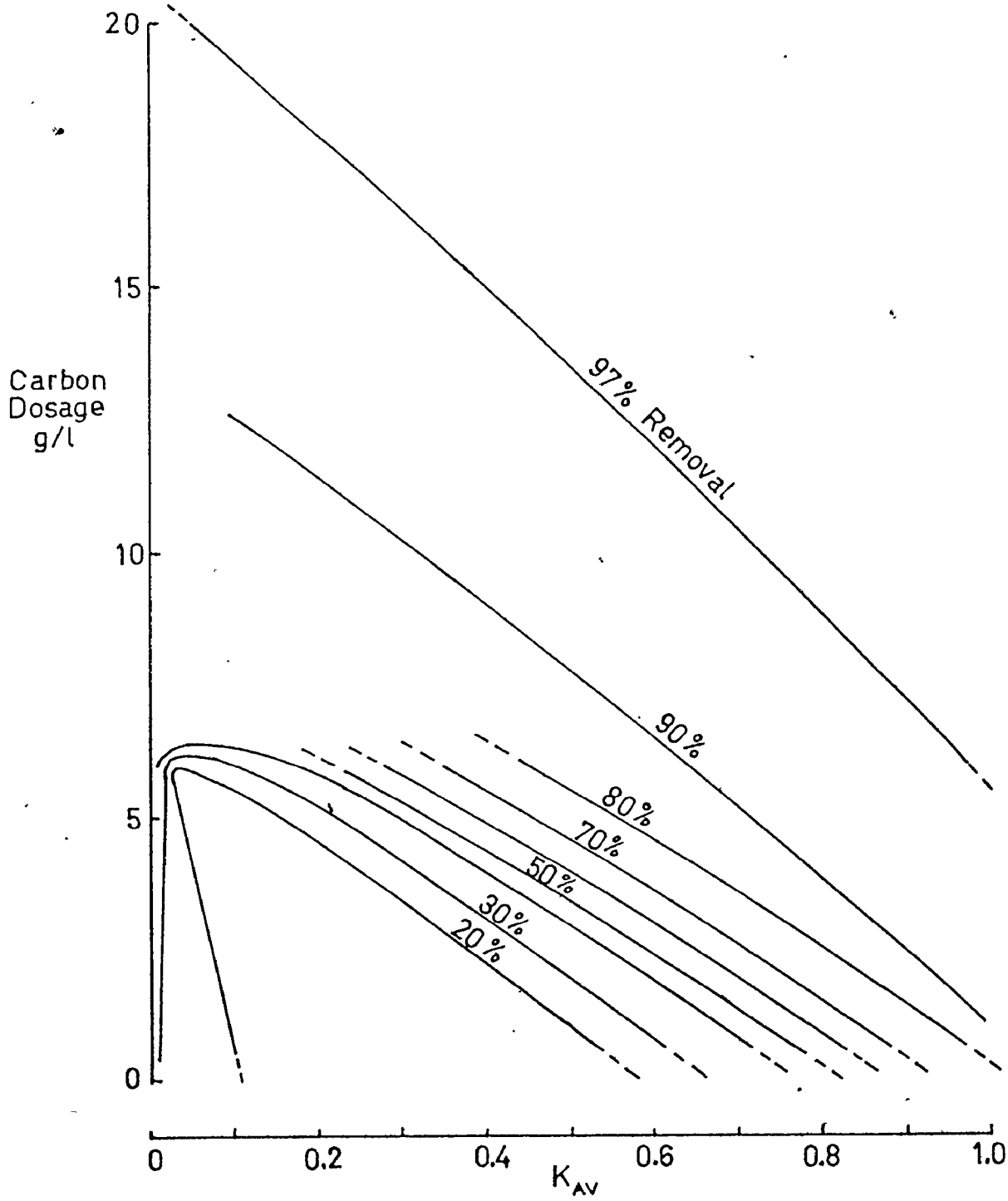

Fig. (xi) Removal of Lignin Species at Equilibrium

Special 'A'

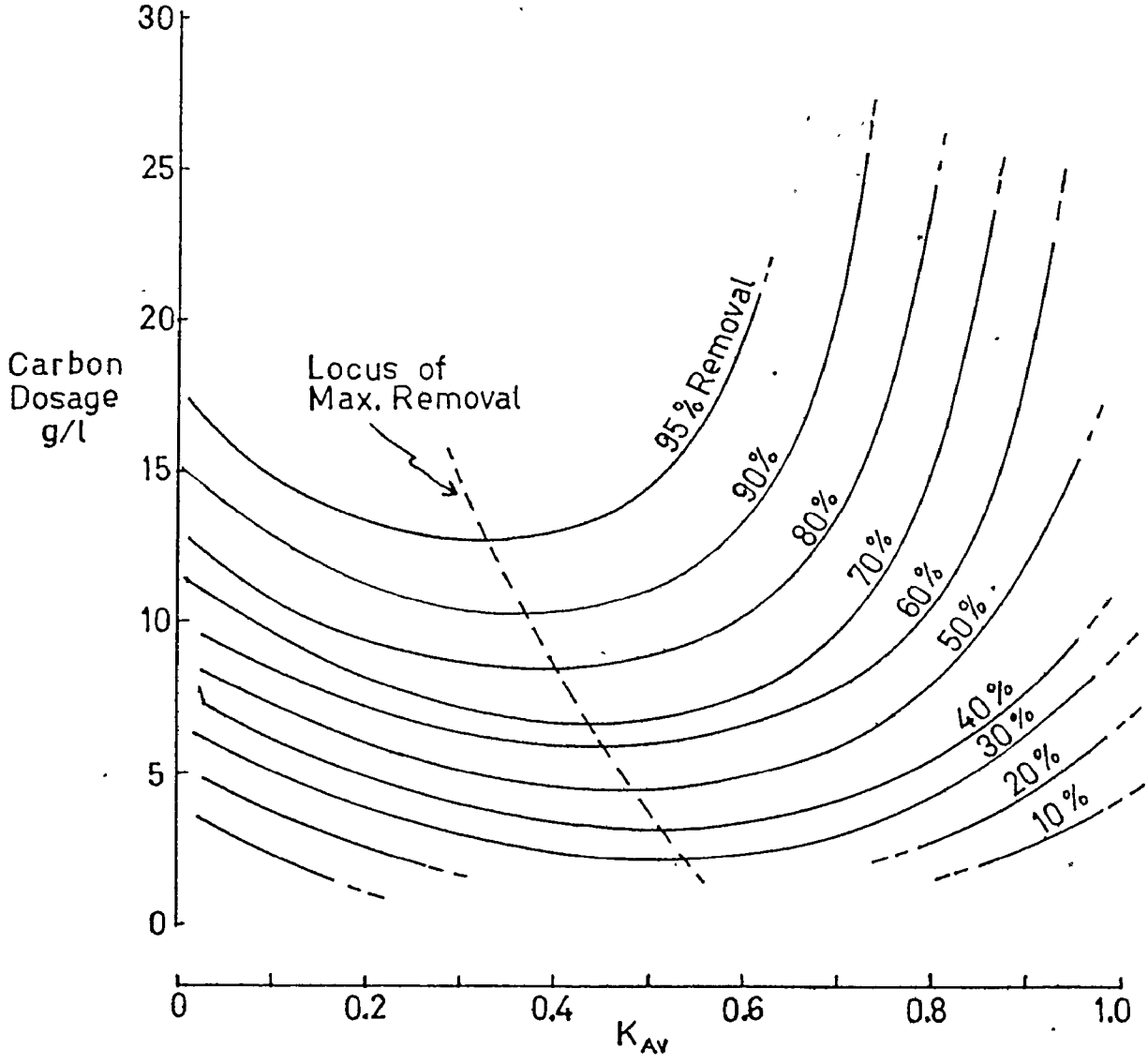

# APPENDIX I.2

## Relationship Between Molecular Weight and Molecular Size (Bailey, 1972).

Fig (i) Relationship Between Molecular Weight and Size

[after Bailey (1972)]

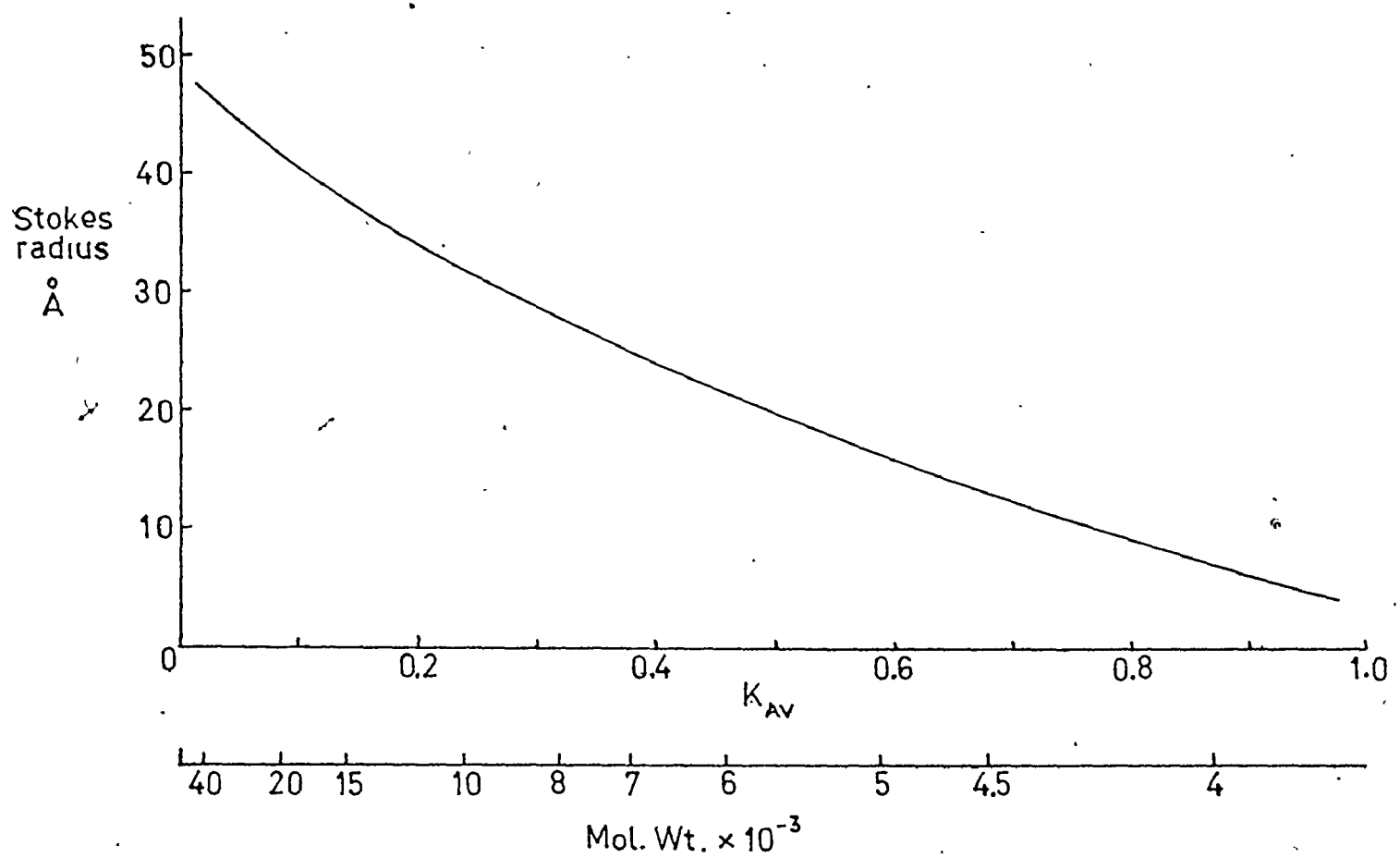

# PART II

# ACTIVATED CARBON CHARACTERISATION STUDIES

## II. 1. INTRODUCTION

Generally when carbon, as a solid porous carbonaceous material, is formed by carbonization of the starting material the result is usually a carbon of low adsorptivity and reactivity. Chaney (1919) proposed that this is because there is a stabilized complex of hydrocarbons adsorbed on the carbon surface. These hydrocarbons lessen its power to combine with or adsorb other substances. Activation of the 'primary' carbon is achieved by selective oxidation of the residual hydrocarbons on the surface, either to produce free surface sites or sites containing active adsorbed groups such as carboxylic, carbonyl or hydroxyl groups. (Hassler, 1967)

The two general methods of activation are (a) high temperature oxidation of a previously charred carbonaceous substance such as coke, char or charcoal and (b) lower temperature chemical dehydration and/or chemical reaction of a carbonaceous raw material. The former process is usually carried out above 800$^{o}$C using steam as an oxidant (Atlas Chemical Industries Inc. 1968) although carbon dioxide or air may also be used (Mantell, 1968). The latter procedure

involves somewhat lower processing temperatures (250°C - 650°C). Many chemical activating agents are employed but all are strong dehydrating agents. The three most commonly used are phosphoric acid, zinc chloride, or sulphuric acid, although alkali can also be used (Mantell, 1968).

Activated carbon is in essence a rigid sponge, formed as a result of the manufacturing procedure. During the charring or carbonization of any carbonaceous substance, considerable volatile matter is given off. In the course of this evolution a large number of internal spaces, or pores are formed, the exact nature of which depends on both the raw material and activation procedure employed.

The activation procedure realizes a very large surface area per unit weight of activated carbon formed; with values of the order 450-1800 $m^2/g$. (Calgon Corp., 1971). The bulk of this surface area is contained in the extensive pore volume of the carbon, with pore volumes in the range 0,4 - 2,2 cc. /g being typical (Timpe, 1970). Thus the high adsorption potential exhibited by activated carbons arises predominantly from the extensive surface areas and pores volumes that they possess. Due to their highly

developed micropore* and/or macropore structure, the availability of the total surface area or pore volume for adsorption of a given adsorbate from the contact phase depends, among other things, strongly on the nature of the adsorbate, and in particular the size of the adsorbate molecules. For example, if an activated carbon, with a surface area of 1300 $m^2/g$ but with pore openings at the particle surface of only 20Å diameter, is used for adsorption of adsorbate molecules of 30Å diameter, any adsorption will be restricted to the external surface of the particle and hence be negligiable. Thus a good adsorbent is a combination of large surface area and sufficient pathways to that area.

To present an adequate picture of the adsorptive capability of a particular carbon, a knowledge of total surface area, total pore volume and pore size distribution must be obtained.

---

* the distinction between a micropore and macropore is an arbitrary one. West Virginia Pulp and Paper Company (1969) define a micropore as being of 0-100Å radius, whereas Fuchs (1965) and Calgon Corporation (1971) state it to be of 5-500Å radius. Macropores are pores with radii greater than these values.

Adsorption may also be influenced by the chemical nature of the surface and adsorbate. For instance it can be generally said that polar surfaces adsorb polar adsorbates, with non-polar surfaces preferring non-polar adsorbates. A pure activated carbon surface is considered to be non-polar, but in practice activated carbons have some carbon-oxygen and carbon-hydrogen-oxygen complexes on the surface which exhibit acid-base properties and can undergo hydrogenation, halogenation and oxidation (Boehm, 1964). An indication of the presence and nature of functional groups on the carbon surface can be obtained from parameters such as the carbon pH.

The previous discussion has been limited to those carbon characteristics which may have an effect on the adsorption capacity of the carbon in a given adsorbent/adsorbate system. However, in order to evaluate adsorption rate, the particle size characteristics of the carbon must be elucidated. A variation in particle size can radically affect the overall adsorption rate, especially if the overall rate process is controlled by an internal transport rather than an external transport or reaction mechanism, whioh is often the case with activated carbon (McGlasson, 1967). A knowledge of adsorption rate processes is particularly valuable in the sizing

of contacting equipment for the adsorption process, notably in continuous adsorbers.

II. 1.1 Carbons Used in the Study

Altogether eight activated carbons were used in this study, and were carefully selected so as to represent a wide range in base-material, mode of preparation, surface area, pore volume and particle size. These are listed, together with manufacturers' specifications, in Table II.1. In the case of Special 'A', no specifications regarding carbon properties were available from the manufacturers, although it is reputed to have most of its total pore volume contained in a narrow pore size range. Furthermore it is not available for use commercially.

Where values in Table II.1 are not the manufacturers values, the source is referenced.

TABLE II.1

Specification Properties of Activated Carbons Investigated

| rbon | Desig-nation | Base Mat. | Form | Pore Volume cc/g | Mean Pore Dia. Å | Nitro Surf. area $m^2/g$ | Particle Size (US mesh) | % Moisture | % Ash | Iodine Number | Molasses de-oolorizing index | Price in car load lot $/lb | Application |
|---|---|---|---|---|---|---|---|---|---|---|---|---|---|
| ua (a) char | AN | Black Liquor | Powder | 0,4-0,6 | 20 | 754 (1) | thru 100 99% (min)<br>thru 200 97% (min)<br>thru 325 90% (min) | 5 (max) | 7 (max) | 703 (1) | 8.1 | 0,085 (1) | taste & odor removal from water. |
| char (a) | WV-G | Coal | Granular | - | - | 1100 | 12 x 40<br>oversize 5% (max)<br>undersize 5% (max) | 2 (max) | 8,5 (max) | 1050 (min) | 8.0 (min) | - | waste water ttmt. chem. & pharmaceutical processing |
| lumbia (b) | LCK | Petroleum | Granular | 0,7 | 17 | 1100 | 14 x 30<br>oversize 5% (max)<br>undersize 5% (max) | 1,5-2 (max) | - | - | - | - | taste,odor removal from water. Alcohol purification. |
| rco (c) | KB | Wood | Powder | 2,2 (1) | 26 (1) | 1200 (1) | thru 100 95%<br>thru 325 50% | 33 (max) | 3-6 | 1200 (1) | - | 0,435 (2) | color,taste & odor removal in treating oils & waxes. |
| rco (c) | S-51 | Lignite | Powder | 1,0 (1) | 30 (1) | 700 (1) | thru 100 95%<br>thru 325 70% | 12 (max) | 17-24 | 1159 (1) | - | 0,140 (2) | general all purpose ttmt. |
| rco (c) | 12x20 | Lignite | Granular | 1,0 | 58 | 700 | 12 x 20<br>oversize 5% (max)<br>undersize 5% (max) | 6 | - | 600-650 | - | 0,43 (2) | food,pharmaceutical industries. |
| ltrasorb (d) | F-400 | Coal | Granular | 0,94 | 35 | 1050-1200 | 12 x 40<br>oversize 5% (max) | 2 (max) | 8,5 (max) | 1100 | - | 0.34 (3) | color,taste & odor removal from waste water. |
| cial A (e) | - | Clay & baked carbon surface | Granular | - | - | - | - | - | - | - | - | | non-commercial carbon |

(a) Westvaco, Chemical Division, Covington, Virginia
(b) Union Carbide Canada Limited, Toronto, Ontario
(c) Atlas Chemical Industries Limited, Brantford, Ontario
(d) Calgon Corporation, Pittsburgh, Pa.
(e) Synthesized for Study

(1) from Timpe (1970)
(2) FOB Brantford, Ontario
(3) FOB Toronto, Ontario

## II. 1.2 Activated Carbon Properties

Each carbon studied was characterized as fully as possible in terms of carbon properties most likely to influence adsorption behaviour. The appropriate properties, coupled with the techniques employed in this study for their evaluation, are summarized in Table II.2.

Table II.2 Carbon Properties and Evaluation Techniques

| Carbon Property | Evaluation Technique |
|---|---|
| Pore structural magnitude and distribution | a. Nitrogen adsorption<br>b. Mercury penetration |
| Particle Size magnitude and distribution | a. Sieving<br>b. Microscopic counting |
| Ash content | High temperature heating |
| Carbon pH | Aqueous Extraction |

## II.2. NITROGEN ADSORPTION AT - 195.8°C

In this experiment the volume of nitrogen gas adsorbed at liquid nitrogen temperature, - 195.8°C, is measured at various applied pressures. The subsequent plot of adsorbed nitrogen volume versus applied pressure at constant temperature is termed the nitrogen adsorption isotherm for the carbon studied.

### II. 2.1. Theory

Nitrogen adsorption onto activated carbon at liquid nitrogen temperature gives rise to a type I or II adsorption isotherm as classified by Brunauer (1943). The latter type of isotherm, depicted in Fig. II.1, occurs as a result of multilayer physical adsorption and can hence be described by

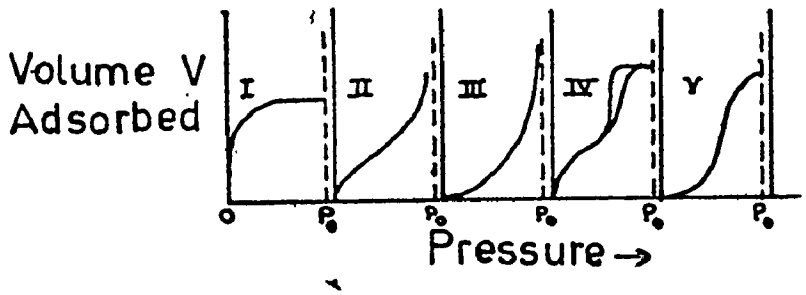


Fig. II.1 The five types of physical adsorption isotherm classified by Brunauer

the Brunauer, Emmett and Teller (B.E.T.) equation, which is

derived from B.E.T. theory (Brunauer, 1938) for multilayer adsorption on a freely accessible surface. Written in its familiar form, the equation is

$$\frac{P/Po}{V(1-P/Po)} = \frac{1}{V_m c} + \frac{(c-1)}{V_m c} \cdot \frac{(P)}{(Po)} \qquad (2.1)$$

Where Po = vapour pressure of nitrogen at adsorption temperature (torr)

P = nitrogen applied pressure (torr)

V = volume of nitrogen adsorbed per gram carbon ($cm^3$(S.T.P.)/g)

$V_m$ = volume of nitrogen per gram adsorbent necessary to form a monolayer ($cm^3$(S.T.P.)/g)

c = a constant related to the net heat of adsorption

Equation (2.1) can be rearranged to the form

$$\frac{1}{V(1-P/Po)} = \frac{1}{V_m} + \frac{1}{V_m c} \cdot \frac{(1-P/Po)}{(P/Po)} \qquad (2.2)$$

If the B.E.T. theory holds, a plot of (P/Po)/(V(1-P/Po)) versus P/Po from equation (2.1) will yield a straight line of slope = $(c-1)/V_m c$ and intercept = $1/V_m c$ at values of P/Po less than 0.3. Likewise from equation (2.2) a plot of $1/(V(1-P/Po))$ versus $(1-(P/Po))/(P/Po)$ will produce a straight line of intercept = $1/V_m$. The use of equation (2.2) is perhaps simpler as this gives $V_m$ directly from the intercept.

An alternate method may be used in determining $V_m$ which is only found to be reliable for type II isotherms with well defined 'knee bends' or plateaux, i.e. when c values in equations (2.1) and (2.2) are high (Thomas, 1967). Called the 'point B' method (Young, 1962), this point marks the change on the isotherm from adsorption predominantly in the first layer to adsorption predominantly in the second layer, and corresponds to the point of inflection of the isotherm. A tangent to the isotherm at this point should cut the y-axis at a volume corresponding to the monolayer adsorption volume $V_m$.

These evaluation techniques enable an adsorbent exhibiting type II nitrogen adsorption behaviour to be characterized in terms of unique adsorption parameters $V_m$ and/or c.

II.2.1. ( i) Evaluation of Adsorbent Total Surface Area

Since the area of adsorbent surface covered by an adsorbed nitrogen molecule in the monolayer is accurately known to be $16.2 \text{Å}^2$ (Atlas Chem. Ind. 1968), the total surface area, $\Sigma$, of the adsorbent covered by the monolayer can be shown (Anderson, 1970) to be given by

$$\Sigma = 4.37\ V_m \qquad (2.3)$$

Where $\Sigma$ is in $m^2/g$ and $V_m$ is in $cm^3$(S.T.P.)/g.

Adsorbent total surface area can also be estimated from the nitrogen adsorption isotherm by the universal t-plot method suggested by DeBoer (1964). This method does not depend on direct determination of $V_m$ but is based on a knowledge of the thickness of the adsorbed nitrogen layer, t, as a function of applied relative pressure P/Po. The t-plot values obtained by Pierce (1959) and reproduced in Fig. II.2 have been shown to be more applicable to carbon adsorption than the alumina-based t-plots of DeBoer. Here it is possible to relate values of V to the corresponding value of t from the adsorption isotherm via Fig. II.2 at given values of relative pressure P/Po. A subsequent plot of V versus t should, at values of P/Po less than 0.25, give a straight line passing through the origin. It can be shown (Anderson, 1970) that the total adsorbent surface area $\Sigma_t$ by this method is given by

$$\Sigma_t = 15.47 \frac{V}{t} \qquad (2.4)$$

Where $\Sigma_t$ is in $m^2/g$, V is in $cm^3$(S.T.P.)/g and t is in Å.

II.2.1 (ii) Evaluation of Adsorbent Total Pore Volume

The total pore volume exhibited by an adsorbent may be estimated from nitrogen adsorption data from a knowledge of the volume of nitrogen gas adsorbed at saturation pressure,

Fig. II.2

Universal 't' values as a function of relative pressure.

(Adapted from Pierce for high C values)

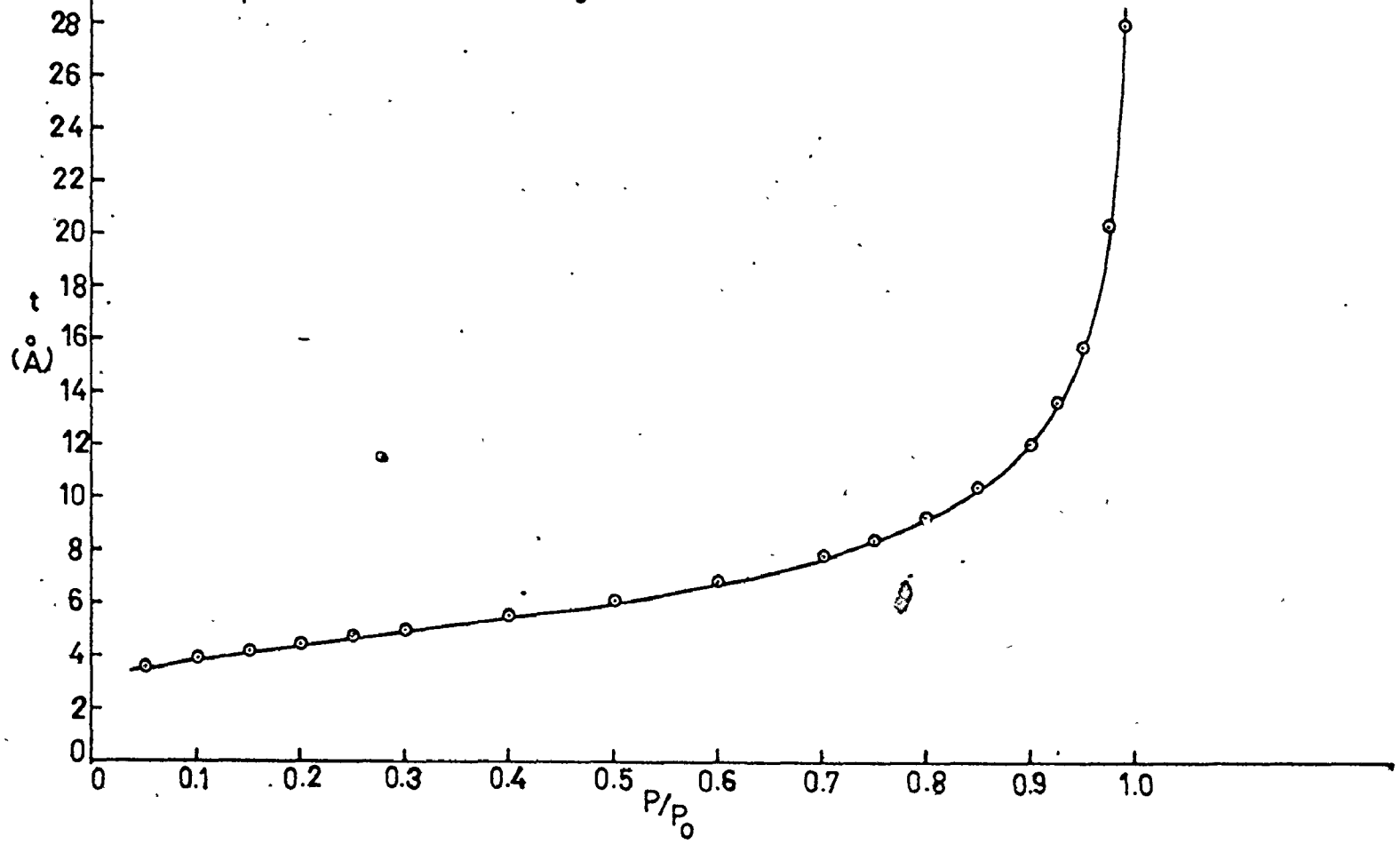

i.e. at P/Po = 1. If it is assumed that at saturation, all adsorbed nitrogen exists as a condensed liquid in the adsorbed phase, then the total adsorbent pore volume is given by

$$P.V. = \frac{V_s M}{\bar{V} \varrho a} \qquad (2.5)$$

Where $V_s$ = the volume of adsorbate per gram adsorbent at saturation pressure ($cm^3$(S.T.P.)/g)

$M$ = molecular weight of adsorbate (g/g mol)

$\bar{V}$ = molar volume of adsorbate ($cm^3$/g mol)

$\varrho a$ = density of adsorbed phase ($g/cm^3$)

For nitrogen adsorption, Anderson (1970) has shown that equation (2.5) reduces to

$$P.V. = \frac{V_s}{\varrho \frac{}{646}} \qquad (2.6)$$

and hence the total carbon pore volume can be obtained from a knowledge of $V_s$ from adsorption data in combination with equation (2.6).

II.2.1 (iii) Evaluation of Adsorbent Average Pore Radius

For nitrogen adsorption on a porous adsorbent, Anderson (1970) has shown that the average adsorbent pore radius $\bar{r}$ may be determined by the relationship

$$\bar{r} = 7.08 \frac{V_s}{V_m} \qquad (2.7)$$

Where $V_s$ and $V_m$ are determined from adsorption data.

II.2.1. (iv) Adsorbent Pore Size Distributions

In order to assess pore sizes and pore size distributions in an adsorbent from nitrogen adsorption data the Kelvin equation (Thomas and Thomas, 1967) is generally used. This equation is derived from thermodynamic considerations of the free energy changes involved in transferring liquid from the unadsorbed phase to the adsorbed phase in fine capillaries, and relates the relative vapour pressure of the adsorbate to pore radius by

$$\ln(P/Po) = - \frac{2 \sigma \bar{V} \cos \sigma}{r R T} \qquad (2.8)$$

Where $\sigma$ = adsorbate surface tension (dynes/cm)

$R$ = universal gas constant (dyne-cm/$^{o}$K g mole)

$r$ = radius of curvature of liquid meniscus (cm)

$\sigma$ = liquid contact angle (radians)

$T$ = absolute temperature ($^{o}$K)

If cylindrical pores and zero contact angle are assumed, then r may be considered equal to pore radius.

However, multilayer adsorption usually accompanies capillary adsorption in the adsorbent pores. Thus the Kelvin equation will not predict the correct pore radius, since this

will have been effectively reduced by the thickness of the adsorbed multilayer. The maximum pore radius which will be filled by capillary condensation at an applied pressure P is thus given by

$$r = t + \frac{2\sigma\bar{V}}{R\,T\,\ln\,(P/Po)} \qquad (2.9)$$

Where t can be estimated from the values of Pierce (1959) or calculated directly from the equation

$$t = 3.54\,\frac{V}{V_m} \qquad (2.10)$$

Equation (2.9) is satisfactory in predicting pore size distributions based on nitrogen desorption and water desorption isotherms (Juhola, 1949) but does not give a representative picture of adsorbent the pore size distribution based on nitrogen adsorption data. This is because, above relative applied pressures of about 0.2, porous adsorbents such as activated carbon desorb a larger quantity of vapour at a given relative pressure than that corresponding to adsorption. Zsigmondy's adsorbed impurity theory (1911) and McBain's ink-well pore theory (1935) attempted to explain the observed hysteresis effect. Cohan (1938) provided a useful mathematical expression for this phenomena by considering the relation between adsorption and desorption pressures for condensation in open-ended cylindrical capilaries at the same adsorbed volume V.

He showed that the pressures can be related by the equation

$$\left[\frac{(Pa)}{(Po)}\right]^2 = \frac{(Pd)}{(Po)} \qquad (2.11)$$

Where Pa = nitrogen pressure on adsorption isotherm (torr)

Pd = nitrogen pressure on desorption isotherm (torr)

Therefore in terms of the Kelvin equation (2.8), the radius corresponding to Pa is twice that corresponding to Pd, and experiments in the adsorption of vapours on glass (Coelingh, 1949) have confirmed this statement. Thus the maximum radius filled by capillary condensation at an applied relative pressure P/Po in adsorption experiments is given by the Cohan equation, i.e.

$$r = t + \frac{\sigma \bar{V}}{RT \ln (P/Po)} \qquad (2.12)$$

The adsorbed phase is thus a composite of multilayer adsorption and capillary condensation. An increase in applied relative pressure $\Delta(P/Po)$ results not only in a filling of pores due to capillary condensation in pores having radii between r and $r + \Delta r$, but also an increase in the thickness of the physically adsorbed layer in pores of radii greater than $r + \Delta r$. As applied relative pressure is increased this process of adsorption continues into increasingly larger pores.

For nitrogen adsorption, equation (2.12) reduces to (Anderson, 1970)

$$r = t + 2.025 \log \left[\frac{Po}{P}\right] \qquad (2.13)$$

By utilizing equation (2.13) in conjunction with the universal t-plot data of Pierce (1959) and nitrogen adsorption data, it is possible to evaluate adsorbent pore size distribution as a function of pore radius.

Here, at a given P/Po, r is calculated from equation (2.13), where t (r) is obtained from Pierce's data (Fig. II.2). An equivalent adsorbed nitrogen gas volume V at the same P/Po value can be obtained from the adsorption isotherm. Hence V can be related to r at a given P/Po value. The resultant plot of V versus r from several P/Po values from P/Po = 0 to P/Po = 1 represents the relationship between the cumulative amount of nitrogen gas adsorbed into pores of radius up to and including r, as a function of pore radius r. However, such a plot does not represent the pore size distribution in the adsorbent, since the adsorbed nitrogen is not adsorbed as a gaseous phase. If it is assumed that the volume of adsorbed gas, both as capillary condensate and adsorbed multilayer, may be represented by condensed nitrogen, then the effective cumulative pore volume $P.V._r$ contained in pores up to and including those of radius r

can be obtained from equation (2.6) for each V. The subsequent plot of $P.V._r$ versus r then represents the cumulative pore volume distribution in the adsorbent as a function of maximum pore radius r filled.

Unfortunately, in nitrogen adsorption experiments, a type I or II adsorption is usually encountered using activated carbons (see Appendix II.3, Figs. (i) to (ix)), with the bulk of adsorption occurring at values of P/Po less than approx. 0.05. As can be seen from Fig. II.2, t values are not accurately known and so values of r calculated by this method will be erroneous at low values of P/Po.

The alternative is to perform the analysis in reverse, i.e. use the identical procedure commencing at $V_s$ (where P/Po = 1) and progressing with decreasing values of V. As before, this procedure also has limitations since, at Vs, the value of t is infinite and hence from equation (2.13), r is also equal to infinity. However, for a slight decrease in P/Po values from saturation, t-values decrease rapidly, as Fig. II.2 shows. Since, as will be seen later, pore volumes and surface areas exhibited by larger pores are usually small compared to the pore structure contained in smaller pores when dealing with activated carbon adsorbents, the error caused by an incorrect estimation in the value of t at $V \rightarrow Vs$ is small when

considering total carbon pore structure.

The latter procedure for estimation of adsorbent pore size distribution is the basis of the Barrett, Joyner and Hallenda (1955) or B.J.H. approach. Briefly, this procedure assumes cylindrical pores and exclusively physical adsorption on the pore walls coupled with capillary condensation in the remaining pore volume. If the total volume of pores occupied by adsorbate at saturation is $V_s$, and at an equilibrium relative pressure less than unity the corresponding total volume of occupied pores is V, then the volume of unfilled pores corresponding to $V_s$-V has been shown by Wheeler (1955) to be given by

$$V_s - V = \int_{(r-t)}^{\infty} \pi (r-t)^2 \, L(r) \, dr \qquad (2.14)$$

Where $L(r)$ is a pore size distribution function defining pore lengths in pores of radii between r and r + dr. The B.J.H. approach solves equation (2.14) by means of a numerical stepwise integration, starting with the differentiated form of equation (2.14), i.e.

$$\Delta V = \pi (r-t)^2 L(r) \Delta r + 2\pi \Delta t \int_{r}^{\infty} (r-t) L(r) \, dr \qquad (2.15)$$

Where values of the distribution function $L(r_1)$, $L(r_2)$....$(r_n)$ corresponding to a given r and $\Delta V$ are evaluated by the integration procedure. In this approach, values of V, r and t at a

given P/Po value are obtained from the adsorption isotherm, equation (2.13) and Fig. II.2. respectively. This analysis yields a distribution of volume of gas adsorbed versus pore radius, but by utilization of equation (2.6) a distribution of pore volume with respect to pore radius may be obtained as discussed earlier.

The BJH method also enables determination of the distribution of adsorbent surface area with respect to pore radius, since Wheeler (1955) has shown that

$$S(r) = \int_{r}^{\infty} 2\pi r \; L(r) \; dr \qquad (2.16)$$

The BJH approach is amenable to rapid analysis using an electronic computer, and recently more advanced methods of calculation have been proposed by Cranston and Inkley (1957) and Roberts (1967), together with details of computer calculation procedures. Such computations enable determination of both surface area and pore volume distributions based on the modified BJH approach. In this work, such distributions are obtained from the computer program developed by Eagan, Shaw and Anderson (1971) at McMaster University, Hamilton Ontario, which is based on the BJH approach. This program is shown in Appendix II.1.

## II.2.2 Experimental

### II.2.2 (i) Preparation of Carbon Sample

Approximately 0.25g of activated carbon was weighed in a previously weighed sample tube. The weight of 'wet' carbon ($W_w$) was thus calculated by difference. The sample tube was then sealed with black wax to a connector having a stop cock (S1) and the assembly was again weighed. The carbon was then evacuated at 250°C overnight under high vacuum ($< 10^{-5}$ torr) by attaching the connector to a vacuum line and immersing the sample tube in a cylindrical furnace, whose temperature was controlled by a variac resistance. Care was taken when opening S1 and exposing the carbon initially to vacuum, as the sudden rush of gases from the carbon surface and from the voids tended to mechanically agitate the carbon sample, causing entrainment and carbon loss into the vacuum line. A very slow and deliberate opening of S1, especially with powdered carbon samples, prevented this. After the high temperature evacuation, which removes adsorbed gases and water, S1 was closed and the apparatus removed from the vacuum line and allowed to cool. Surplus vacuum grease was wiped off the nipple with hexane and the assembly again weighed. The difference in assembly weight before and after evacuation gives $W_A$, the weight of adsorbed gases and water on the sample.

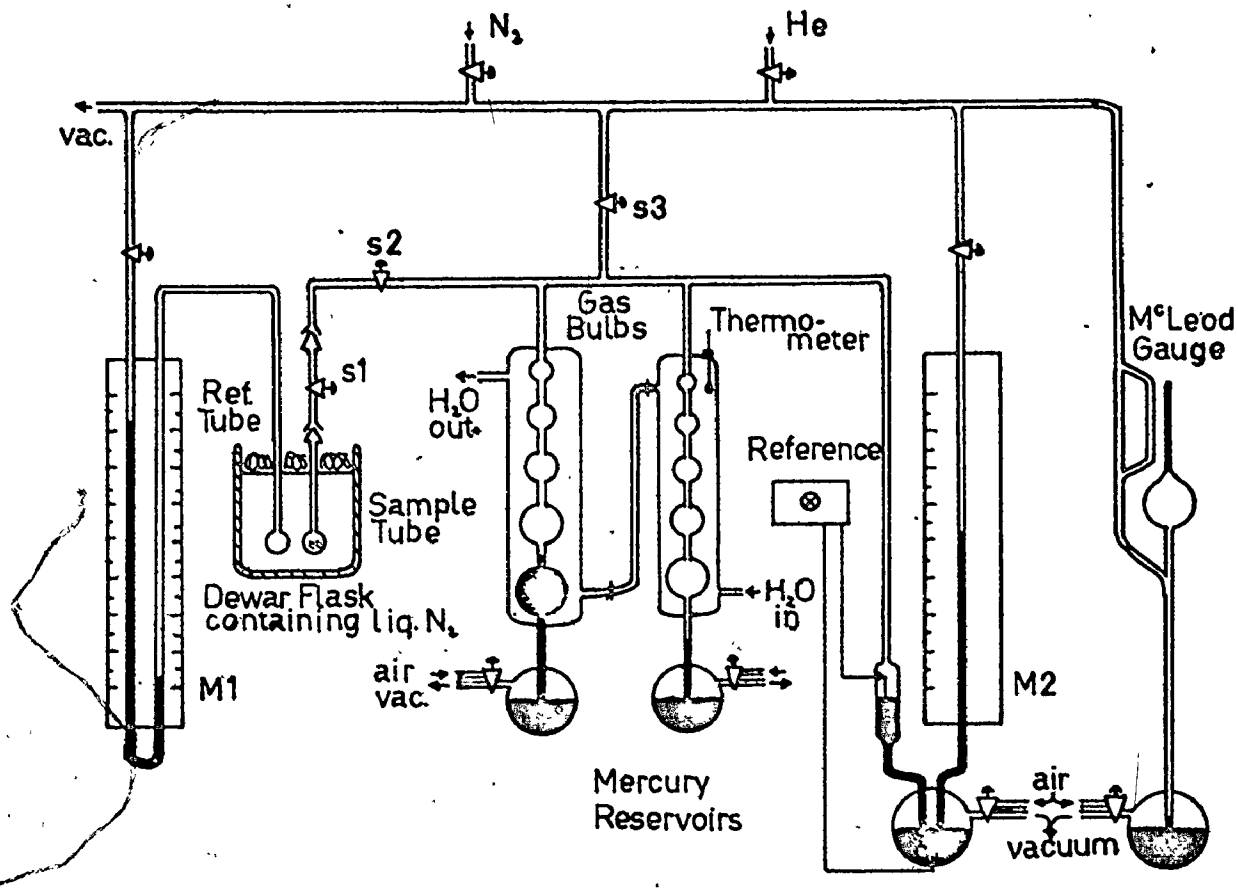


Fig.II.3. Diagram of Nitrogen Adsorption Apparatus.

By difference the weight of 'dry' carbon is thus given by

$$W = W_w - W_A \qquad (2.16)$$

II.2.2. (ii) Description of the Adsorption Apparatus

A sketch of the adsorption apparatus is shown in Fig. II.3. The apparatus is in essence a chamber of known volume where the enclosed volume can be varied by filling or emptying a series of glass bulbs of known volume with mercury from a reservoir by means of external pressure or vacuum. The pressure in the system is recorded on the manometer M2. The assembly containing the adsorbent to be studied is attached to the socket on the left of S2 and the sample tube immersed in a Dewar flask containing liquid nitrogen, together with a bulb full of nitrogen which is attached to manometer M1, for measurement of the nitrogen vapour pressure. By manipulation of valves S1, S2 and S3 it is possible to perform adsorption experiments as outlined later. The whole system can be evacuated through S3 and the vacuum measured on a McLeod gauge, and by the same pathway the adsorbate gas can be allowed into the system from its reservoir.

II.2.2. (iii) Helium Dead Space Factor

Before performing adsorption experiments on the sample,

it is first necessary to evaluate the 'dead space' i.e. the space to the left of S2, with S1 open, which includes the void volume of the sample.

The sample assembly is joined to the adsorption apparatus, which has been previously evacuated, and S2 is then opened to evacuate the volume between S1 and S2. After attainment of good vacuum, as evidenced by the McLeod gauge, S1 is opened and S2 is closed. The temperature of the water jacket around the gas bulbs is checked to be 30°C: the bulb volumes are referred to this temperature.

A Dewar flask is then placed under the sample tube, and filled to the mark with liquid nitrogen. This level should be maintained constant throughout the helium dead space and nitrogen adsorption determinations, and the flask should also be covered with glass wool to minimize dissolution of $O_2$ in the liquid $N_2$.

The gas bulbs are then emptied of mercury and the mercury level carefully set to the reference mark. Approximately 70 torr of Helium is then allowed to enter the system via S3, and then S3 is closed. The pressure of Helium is determined with manometer M2, and the appropriate correction factor for Hg density is subtracted in order to arrive at the actual pressure P. The number of bulbs in each jacket filled with gas are noted

(5 large, 5 small for the first setting). Some helium is then displaced from one of the bulbs by filling it with Hg from the reservoir, and the new pressure and bulb setting is recorded. This is repeated for several (~5) combinations of bulbs filled in order to cover a series of helium pressure ranges. Each recorded pressure is corrected for mercury density.

For each reading the corresponding volume factor ($f_A$) is read from calibration charts for this particular apparatus, where

$$f_A = \frac{(V_T\ (273.16)}{(760.0)} \quad \frac{cm^3(S.T.P.)\ ^oK}{torr} \qquad (2.17)$$

and $V_T$ is the total volume in $cm^3$ to the right of S2, beneath S3 and down to the zero reference of M2. The inlet volume of Helium ($V_I$) is given by

$$V_I = \left[\frac{(f_A \times P\ corrected)}{(\quad 303.16 \quad)}\right] \text{ S2 closed} \quad cm^3(S.T.P.) \qquad (2.18)$$

for each bulb setting and corresponding Helium pressure.

An average value of $V_I$ is then obtained from the 5 or so determinations.

The stopcock S2 is then opened and the procedure repeated for several bulb settings in order to determine the residual volume ($V_R$) of Helium remaining to the right of S2 for

each new pressure P, where

$$V_R = \left[\frac{(f_A \times P \text{ corrected})}{303.16}\right]_{S2 \text{ open}} \text{cm}^3(\text{S.T.P.}) \qquad (2.19)$$

Separate values of the dead space factor (F) were obtained, where

$$F = \left[\frac{((V_I)_{AVE} - V_R)}{P \text{ corrected})}\right]_{S2 \text{ open}} \frac{\text{cm}^3(\text{S.T.P.})}{\text{torr}} \qquad (2.20)$$

Since Helium is reputed not to be adsorbed on carbon, the dead space factor is the volume of gas at S.T.P. per unit pressure contained to the left of S2, including the void volume of the sample.

III.2.2. (iv) Nitrogen Adsorption

The Helium is evacuated from the system through S3 until a good vacuum is obtained, with the liquid nitrogen bath removed from the sample. When a good vacuum is obtained, S2 is closed and the nitrogen bath replaced. With all gas bulbs empty of mercury, approx. 120-200 torr* of Nitrogen is allowed into the system. The inlet volume ($V_I$) of nitrogen is determined in the

---

* The value depends on the expected surface area of each carbon, i.e. for carbons with relatively high surface areas, more nitrogen is required corresponding to a high initial pressure.

same way as for Helium, by taking the average of a few determinations. Then, with all bulbs empty of mercury, nitrogen is admitted to the sample by opening S2. The mercury level in M2 is continually adjusted until a constant pressure is achieved over a period of about 5 minutes. The pressure is then recorded as well as the nitrogen vapour pressure Po from manometer M1, which may change in the experiment due to dissolution of $O_2$ in the liquid nitrogen bath.

The procedure is then repeated for ever increasing pressure P by filling the gas bulbs with mercury as desired, and then allowing sufficient time for adsorption equilibrium. The equilibrium pressure P is then recorded together with the number of bulbs filled with gas. Six or more readings should be obtained at less than 200 torr because these data are used to determine the surface area.

Readings at pressures other than those possible with integral numbers of bulbs filled can be made by partially filling a certain bulb up to a fixed level, and allowing time for equilibration before recording P and Po. Then S2 is immediately closed and the bulb is filled with, or emptied of, mercury to the next integral bulb reference mark, and the pressure P again recorded, together with the number of bulbs filled with mercury. Before re-opening S2, one must make sure

that the pressure P is equal to, or slightly greater than, the pressure before S2 was closed.

After filling all bulbs it is usually necessary to admit more nitrogen into the system in order to reach higher pressures. If this is required, S2 is closed and the number of bulbs filled with mercury is recorded, together with the pressure P. From this, the residual volume of nitrogen to the right of S2 is calculated from equations (2.17) and (2.19). Then all bulbs are emptied of mercury and enough nitrogen is allowed into the system, via S3, to yield a pressure slightly greater than that before S2 was closed, and then S3 is closed. The amount of nitrogen to the right of S2 is then found by stepwise filling of the bulbs with mercury, at the same time recording the pressure P, and then using the equations (2.17) and (2.18) to calculate the separate $V_I$'s for each bulb setting. The average $V_I$ gives the volume of nitrogen to the right of S2. By subtracting the residual nitrogen volume remaining before more nitrogen was added, one can arrive at the volume of nitrogen which has just been added to the system. The stopcock S2 is again opened and the procedure continued by filling the bulbs with mercury, corresponding to increasing values of

P until a final reading of P as close as possible, but not exceeding* Po is obtained.

The residual Volume $V_R$ is then calculated for each setting by use of equations (2.17) and (2.19). The dead space factor F calculated from equation (2.20) was determined with helium, which obeys the ideal gas law even at - 195.8°C. This is not true of nitrogen, and so a correction factor for F must be applied, i.e.

$$F_{N_2} = F_{H_e} (1+ (0.05P/760.0)) \frac{cm^3(S.T.P.)}{torr} \quad (2.21)$$

and hence the volume of nitrogen contained in the 'dead space' to the left of S2, but not adsorbed, is given at any pressure P by

$$V_A = P \left[ (F_{H_e} (1+ (0.05P/760.0)) \right] cm^3(S.T.P.) \quad (2.22)$$

where P is corrected pressure.

Thus the amount of nitrogen adsorbed at any pressure P (or relative pressure P/Po) is given by

$$V_c = \left[ V_I - (V_A + V_R) \right] cm^3(S.T.P.) \quad (2.23)$$

---

* a value of $P \geq Po$ will give rise to significant nitrogen condensation and hence equilibrium will be very difficult to achieve.

or in terms of volume adsorbed per unit weight of dry carbon (V) by

$$V = \frac{Vc}{W} \qquad cm^3(S.T.P.)/g.\ dry\ carbon \qquad (2.24)$$

From the data obtained a plot of V versus P/Po gives the adsorption isotherm for the system, and the calculations needed to arrive at this plot for nitrogen adsorption on a typical carbon are shown in Appendix II.2.

## II.2.3. Results and Discussion

### II.2.3. (i) The Adsorption Isotherm

The nitrogen adsorption isotherms for the carbons studied are shown in Appendix II.3, Figs. (i) to (ix). Generally these isotherms appear at first sight to exhibit a type I isotherm as classified by Brunauer (1943). The clear exceptions are those of Darco KB and Special 'A', which obviously more clearly resemble a type II case.

The type I isotherm can be described by the well known Langmuir equation, which is developed from adsorption theory on the prime assumption of monolayer physical adsorption and/or chemisorption, in which each adsorption site can accommodate only one adsorbed entity, and where all adsorption sites exhibit equal adsorption energies. However linearization of the isotherms depicted in Appendix II.3 using the Langmuir model (see Part I. ) was unsuccessful. Closer scrutiny of the isotherms reveals that the tendency to deviate from type I behaviour is only slightly evident at low relative pressures, but at higher relative pressures the deviation is very noticeable. At relative pressures in excess of 0.95, the isotherms generally tend to a vertical assymptote. Hence it is evident that multilayer adsorption is occurring, i.e. adsorption does not cease with monolayer formation. Thus in

Fig. II.4 BET Plot for Columbia LCK 12/28

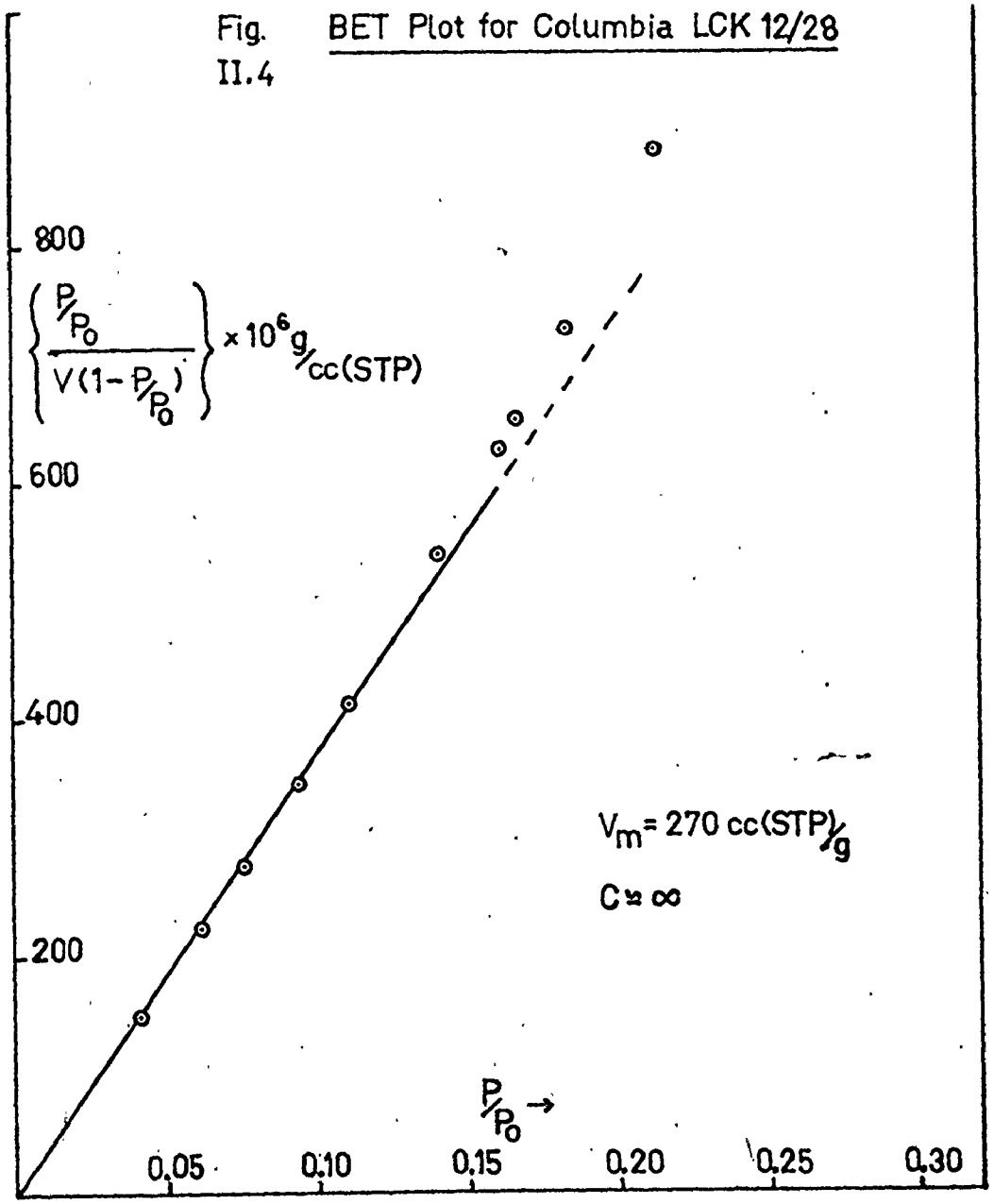

Fig. II.5 BET Plot for Special 'A'

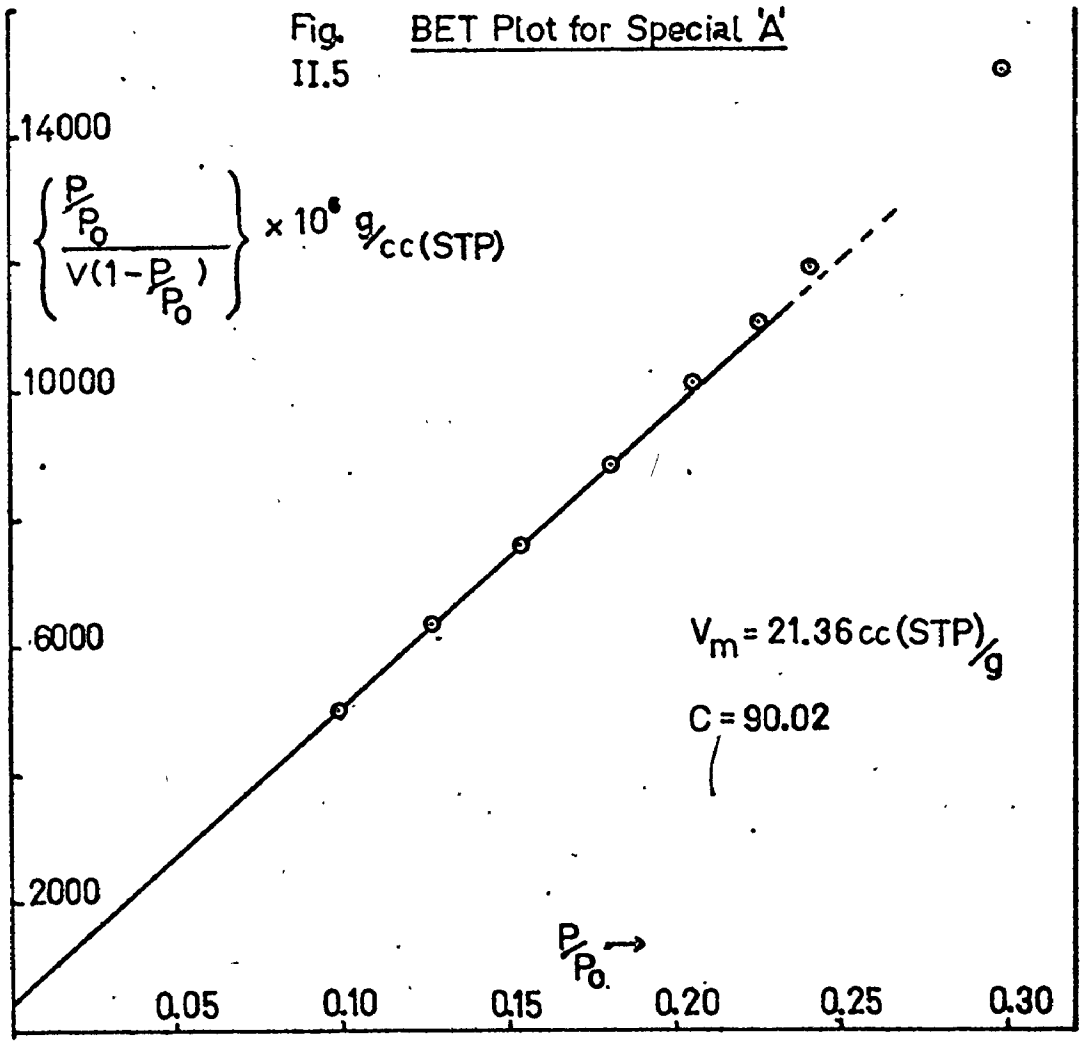

reality the typical activated carbon nitrogen adsorption isotherm is a type II isotherm where the generally high initial adsorption at low relative pressures due to an almost exclusive abundance of very small pores gives rise to the appearance of a type I isotherm. Linearization of the isotherms in Appendix II.3 by the B.E.T. approach* for type II isotherms using equation (2.1) was successful, for adsorption data at relative pressures less than 0.3. Figs. II.4 and II.5 illustrate the appropriateness of this model for linearization of adsorption isotherm data in the case of isotherms obtained for Columbia and Special 'A' carbons respectively. It was however noted that carbons exhibiting pseudo-type I behaviour gave B.E.T. plots which passed through the origin (see Fig. II.4) whereas

---

* The B.E.T. theory is based on Langmuir assumptions, but in addition assumes that monolayer treatment can be extended to multilayers. Thus each adsorbed species in the first layer (monolayer) serves as an adsorption site into the second layer, and each species in the second layer as a site into the third layer etc.. The assumption is also made that the heats of adsorption into second and subsequent layers are all equal, and are equal to the heat of liquefaction of the adsorbed vapour.

the obvious type II isotherms exhibited by Special 'A' and Darco KB produced B.E.T. plots with y-axis intercepts. This behaviour may be explained by consideration of equation (2.1), which at very high values of c reduces to

$$\frac{P/Po}{V(1-P/Po)} = \frac{1}{Vm}\left[\frac{P}{Po}\right] \qquad (2.25)$$

which is a straight line of slope = 1/Vm. Thus the more evident the type I behaviour, the higher the value of c will be. The c value is related to the net heat of adsorption $H_1 - H_\ell$ by (Brunauer 1943)

$$c = \frac{a_1 b_2}{a_2 b_1} \exp\left(\frac{H_1 - H_\ell}{RT}\right) \qquad (2.26)$$

where $H_1$ = heat of adsorption in the first layer
$H_\ell$ = heat of liquefaction of the gas
$a_1, b_1, a_2, b_2$ = pre-exponential teams for evaporation and condensation kinetic expressions from the first and second layers respectively
R = universal gas constant
T = absolute temperature

Thus Special A, where $c \simeq 90$, and Darco KB, where $c \simeq 153$, display a lower net heat of adsorption than do the other carbons.

From the B.E.T. plots for each carbon, Vm was estimated and the total surface area, $\Sigma$, was subsequently calculated using equation (2.3). Similarly for each carbon, determination of Vm by the 'point B' method, and hence the corresponding value of surface area, $\Sigma_B$, via equation (2.3) was also calculated. The value of total surface area $\Sigma_t$ using the universal t-plot

procedure as outlined earlier was also determined for each carbon. A comparison of the results of total surface area determination by these 3 procedures are shown in Table II.3.

Here the t-plot analysis of adsorption data is seen to give values of total surface area $\Sigma t$ which correspond well with values of $\Sigma$ obtained from B.E.T. analysis for each carbon. However the 'point B' method produces values of $\Sigma_B$ that are in general higher than those derived by the other two methods. This discrepancy probably arises from the difficulty in exact estimation of the position of the inflection point in the pseudo - type I adsorption isotherms.

It is important to note here that the representativeness of the adsorption isotherms, shown in Appendix II.3, in describing true nitrogen adsorption behaviour are limited by the experimental technique employed in their determination. In this respect two points are worth mentioning regarding the experimental procedure used here as outlined in section II.2.2.

Firstly, due to limitations of the adsorption apparatus, there were experimental difficulties connected with accurate determination of V values at P/Po values in excess of 0.95 (the implications of this difficulty are discussed more fully later - see Section II.2.3. (iii)).

TABLE II.3

Comparison of Surface Areas, as Evaluated by Nitrogen Adsorption Experiments, For the Carbons Under Study

| Carbon | Surface Area ($m^2/g$) | | | |
|---|---|---|---|---|
| | Point 'B' $\Sigma_B$ | BET $\Sigma_{BET}$ | t-plot $\Sigma_t$ | Manuf. Spec. |
| Powdered | | | | |
| Nuchar Aqua A | 1092 | 909 | 897 | 754 |
| Darco S-51 | 673 | 632 | 650 | 700 (1) |
| Darco KB | 1569 | 1503 | 1464 | 1200 (1) |
| Pulverized Darco 12 x 20 | 695 | 658 | 660 | 700 |
| Granular | | | | |
| Nuchar WV-G 12 x 40 | 1350 | 1157 | 1187 | 1100 |
| Filtrasorb F-400 | 1027 | 901 | 961 | 1050-1200 |
| Darco 12 x 20 | 712 | 698 | 672 | 700 |
| Columbia LCK 12/28 | 1333 | 1180 | 1236 | 1100 |
| Special 'A' | 89.6 | 93.4 | 88.4 | - |

(1) Values of Timpe (1970)

Secondly, there was experimental evidence to suggest that helium is adsorbed onto activated carbon during the dead space determinations (see section II.2.2. (iii)). This was based on a comparison of the calculated dead space volume with a corresponding visual estimation. It appeared that the latter was somewhat smaller than the calculated quantity. If this is in fact the case, then the subsequent corrections for dead space used in calculation of adsorbed volumes in equations (2.22) to (2.24) would give rise to erroneously low values of V. However, since the adsorbed volumes at all relative applied pressures were high for all the carbons studied, and the approximate discrepancies between estimated and calculated dead space volumes were low (est. 2-5 $cm^3$ (S.T.P.)), the error in the calculated V values is considered negligible. Since the helium adsorption was found to be completely reversible, a possible explanation would be that of weak physical adsorption of helium on the carbon surface. It is suspected that all 'inert' gases may be subject to a small amount of adsorption onto activated carbon, and accordingly dead space factor determinations may still be subject to a small error if other 'inert' gases are used in its evaluation. This point should be further investigated by surface chemists.

II.2.3. (ii) Fundamental Carbon Properties

For each carbon, the total surface area was calculated from the appropriate nitrogen adsorption isotherm by the three different methods as outlined in section II.2.1 and summarized in Table II.3. The representative carbon total surface area was then taken to be an arithmetic average of $\Sigma_{BET}$ and $\Sigma_t$ (see Table II.3). Similarly, total pore volume and average pore radius for each carbon were determined from nitrogen adsorption data in conjunction with equations (2.6) and (2.7). Table II.4 summarizes these fundamental carbon properties for each carbon studied.

Table II.4 Carbon Fundamental Properties Evaluated from Nitrogen Adsorption Isotherms

| Carbon | Surf.Area ($m^2/g$) | Pore Vol. ($cm^3/g$) | Ave.Pore Radius (Å) |
|---|---|---|---|
| Columbia LCK 12/28 | 1208 | 0.585 | 9.5 |
| Darco KB | 1484 | 1.402 | 19.5 |
| Darco S-51 | 641 | 0.775 | 23.8 |
| Darco 12 X 20 | 685 | 0.712 | 20.4 |
| Pulverized Darco 12 x 20 | 659 | 0.523 | 15.8 |
| Filtrasorb 400 | 931 | 0.449 | 9.3 |
| Nuchar Aqua A | 903 | 0.594 | 13.2 |
| Nuchar 12 x 40 | 1172 | 0.724 | 12.2 |
| Special 'A' | 90.9 | 0.331 | 74.9 |

From this table it is noticed that there is a large variation in total surface area for the various carbons, ranging from 90.9 $m^2/g$ for Special 'A' to 1484 $m^2/g$ for Darco KB. Similarly, total pore volumes and average pore radius are also seen to vary quite significantly, total pore volumes ranging from 1.402 $cm^3/g$ (Darco KB) down to 0.331 $cm^3/g$ (Special 'A') and average pore radius from 9.33 Å (Filtrasorb 400) up to 74.9 Å (Special 'A')

These values may be explained in terms of physical properties and activation procedure for a particular carbon. Darco KB is claimed by the manufacturers to be a carbon of extra high adsorptive capacity, in which the chemical activation procedure involving the activation of wood char with phosphoric acid leads to a highly developed pore structure, wherein the total volume of pores formed is large compared with steam activation. The high values of surface area (1484 $m^2/g$) and total pore volume (1.402 $cm^3/g$) confirm this. The average pore radius of 19.5 Å indicates that the pore size distribution includes a significant contribution of both large and small pores to the total pore volume, i.e. that the bulk of the pore volume is not supplied by very small micropores (less than 10 Å in radius). In comparison, Special 'A' appears to be a carbon or very little total adsorptive capacity, as evidenced by the

very small surface area (90.9 $m^2/g$) and total pore volume (0.331 $cm^3/g$) exhibited. However the high average pore radius (74.9 Å) displayed suggests that the bulk of the pore structure is realized by large pores, with the existence of little or no small micropores, as indicated by the small surface area. Thus this would appear to be an unusual carbon in which the bulk of its pore volume and hence adsorptive capacity would appear to be concentrated in a narrow pore size range of large micropores. This deduction may be explained by consideration of the physical nature of Special 'A'; it is actually a pseudo-activated carbon, the granules consisting of a clay-alumina inner core with a layer of carbon baked onto surface in the activation procedure. Thus particle surface properties will be dictated by the carbon coating whereas bulk particle properties, including pore structure, will be governed by alumina-clay properties. This is evidenced by the form of the adsorption isotherm (see Appendix II.3 Fig. (ix)), which approximates a typical alumina-type adsorption isotherm (Anderson 1970) at the low relative pressures.

Columbia LCK 12/28 is an example of a carbon in which the volume of very small micropores (less than 10 Å radius) contributes a sizeable portion of the total pore volume. This is evidenced by the high surface area (1208 $m^2/g$) and pore volume (0.585 $cm^3/g$), coupled with the very small average pore

radius (9.46 Å), found from isotherm analysis. These findings are again found to be in accordance with the manufacturer's specifications, where this carbon is stated "to have been designed especially for use in adsorption of relatively small molecules from solution, as contrasted to the decolorizing operation".

The other carbons studied display pore structural properties within the three extreme cases quoted, the nature and extent of contained pore structure being evident from the values in table II.4. In general there is no trend between the pore structures of granular versus powdered carbons, since each carbon is prepared and activated in a unique manner from a unique base material. However for a granular carbon prepared by stabilization of a powdered activated carbon agglomerate with a binding agent; a trend in pore structure alteration may exist, whereby some larger pores may be formed between adjacent carbon particles in the agglomerate. Conversely, pulverization of a granular carbon to produce a powdered carbon may be expected to yield a decrease in the number of larger pores. This suggestion is confirmed by comparing the values in table II.4 for granular Darco 12 x 20 with its pulverized form, in which the granules were pulverized

to give a powdered carbon where 97.6 wt.% of the particles passed through a #325 U.S. mesh screen. It can be seen that, although surface area is relatively unaffected (685 versus 659 $m^2/g$) pulverization gives rise to a decrease in total pore volume (0.712 versus 0.523 $cm^3/g$) and average pore radius (20.4 - 15.8 Å). This signifies that pulverization destroys some of the pore structure, with the bulk of the destruction occurring in the larger pores. Similarly, from table II.4 one might expect that Nuchar 12 x 40 should exhibit a larger pore volume and average pore radius than Aqua Nuchar A, whereas the reverse case is evidenced. However this would not necessarily follow, since the base materials are different.

In general, the experimental values shown in table II.4 agree quite well with those in Table II.1 as specified by the manufacturers and/or other researchers. The exception here is Filtrasorb 400, where the experimental values of surface area, pore volume and average pore radius are significantly lower than the manufacturers specifications. Assuming both sets of values are correct, (a duplicate isotherm on this carbon confirmed the findings of this study), this would suggest that some of the pore volume became plugged in transit or by previous laboratory use of the same carbon sample as an

adsorbent. The discrepancy could also arise if there were a temporary malfunction in the activation procedure at the manufacturing plant, resulting in loss of generated pore volume.

II.2.3.(iii) Pore Size Distributions

The surface area and pore volume distributions with respect to pore radius were calculated for each carbon from nitrogen adsorption data by utilization of the computer program reproduced in Appendix II.1 and based on the BJH approach. These distributions are shown in Appendix II.4, Figs. (i) to (viii) and Appendix II.5, Figs. (i) to (viii) respectively.

The pore size distributions obtained by the aforementioned procedures suffer inherent inaccuracies. Firstly, the assumption of cylindrical pores may not be a good one: the same may be said for the assumption of open-ended capillary condensation.

Secondly, the procedure used for arrival of a pore size distribution from nitrogen adsorption isotherm data will influence the nature of the obtained distribution. In this respect, Figure II.6 shows the distribution obtained by application of the BJH approach to the nitrogen adsorption isotherm of Darco KB:

Fig. II.6 Pore Volume Distribution

for Darco KB as derived from the $N_2$ Adsorpt'n Isotherm

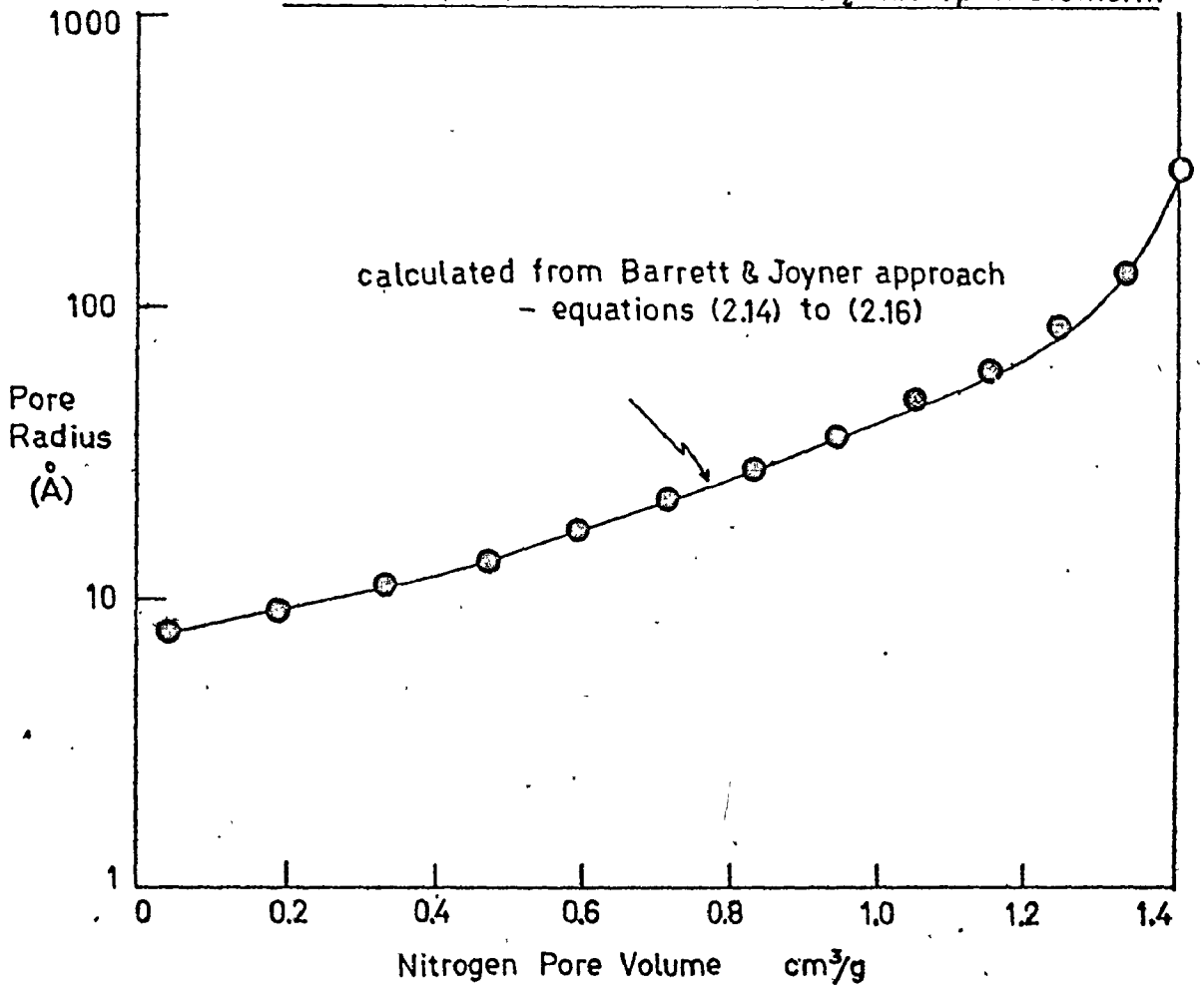

Thirdly, the shape of the adsorption isotherms generally obtained in this study by their nature do not lend themselves to accurate determination of pore size distributions. This is because the isotherms, especially the pseudo type-I isotherms, display very high adsorption capacity at both very low and very high applied relative pressures. Since Pierce's t-plot data (Fig. II.2) is uncertain in regions of low (less than 0.05) and high (greater than 0.95) applied relative pressures, any pore size distribution analysis incorporating t-plot data will yield a pore size distribution that would be inaccurate at its lower and upper limits, i.e. for pore radii less than approx. 10 Å and greater than approx. 1000 Å. The error in the pore size distribution obtained in the large (greater than approx. 1000 Å) pore radii range is further compounded by the experimental difficulties connected with determination of a true value of V at high (greater than 0.95) relative applied pressures. These difficulties arise from

a) The long time (approx. 2 hours) required to obtain a true equilibrium value of V at the high P/Po values.

b) The rapid change of V with small changes in P/Po at the high P/Po values (see Appendix II.3)

c) The danger, with the apparatus used, of momentarily exceeding at P/Po value greater than unity when determining V at relative pressures approaching unity, which would lead to dew point nitrogen condensation in the system.

[Due to the difficulties in determining V at high values of P/Po, it also follows that the extrapolated value of Vs at P/Po = 1 (see Appendix II.3) may also be subject to error. Since the total pore volume and average pore radius calculated for each carbon from nitrogen adsorption data are calculated from a knowledge of Vs (see equations (2.6) and (2.7)), it is apparent that the values of these parameters in Table II.4 may be slightly inaccurate.]

A further limitation in evaluating pore size distributions from nitrogen adsorption data is one of physical limitation. The smallest pore that can theoretically penetrated is one whose diameter is equal to that of a condensed nitrogen molecule, i.e. of radius 4.32 Å (Atlas Chem. Ind. 1968). Thus the physical restriction imposed by the size of a nitrogen molecule determines that the pore size distribution in pores of less than about 4.32 Å radius cannot be estimated from nitrogen adsorption data.

Desorption rather than adsorption isotherms are generally considered more suitable for obtaining a more representative adsorbent pore size distribution. In general, porous adsorbents such as activated carbon desorb a larger quantity of vapour at a given relative pressure P/Po than is adsorbed at that same relative pressure. This hysteresis effect may be explained naïvely in terms of the inkwell pore theory. For a pore such as that depicted in Fig. II.7,

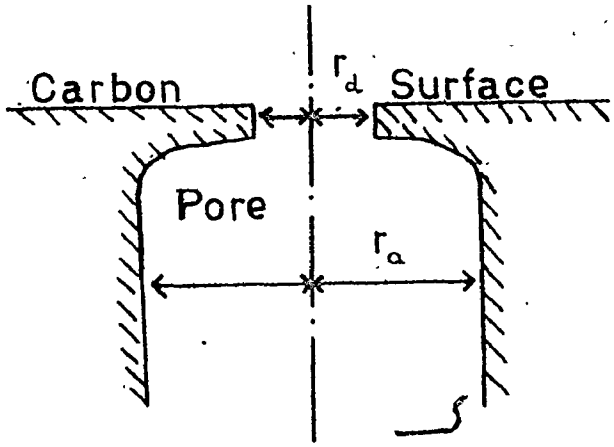


Fig.II.7 An inkwell pore

the volume of gas adsorbed V by the pore will occur at a relative pressure $(P/Po)_a$, corresponding to a pore radius $r_a$ as given by equation (2.9), but the same volume V of gas desorbed will occur at a different relative pressure $(P/Po)_d$,

corresponding to a pore radius $r_d$ from equation (2.12). It is hence obvious that the BJH analysis will yield different pore size distributions when applied to adsorption rather than desorption isotherm data. In general, pore size distributions obtained from adsorption data relate to radii of pore necks whereas distributions based on desorption data relate to radii of pore interiors, according to inkwell pore theory. Since in this work the effect of adsorbate molecular size on its adsorption into carbon pores will be studied, it is evident that a pore size distribution based on pore necks, and hence on adsorption data, may be more meaningful than a distribution based on pore interiors. However, in the BJH pore size distribution evaluation procedure, (see Appendix II.1) the Cohan rather than the Kelvin equation was used in order to endeavour to account for the hysteresis effect and hence the obtained distributions in Appendicies II.4 and II.5 are more closely based on radii of pore interiors rather than pore necks. In retrospect, it would have been interesting to compare BJH pore size distributions for a given carbon based on (a) the desorption isotherm/Kelvin equation and ~~(b)~~ the adsorption isotherm/Cohan equation approaches, in order to obtain an indication of the differences in the obtained distributions.

## II.3 MERCURY PENETRATION UP TO 50,000 PSIA

By means of mercury penetration experiments it is possible to determine the volume of mercury that will penetrate the pore structure of a porous solid at various applied pressures. The mercury penetration volume - applied pressure relationship obtained may be used to yield important information concerning pore structural characteristics of the solid.

### II.3.1 Theory

The force tending to impede the entry of a 'non-wetting' liquid such as mercury into a narrow cylindrical channel of radius r is given by

$$F = 2 \pi r \sigma \cos \alpha \qquad (2.27)$$

where $\sigma$ = liquid surface tension (dynes/cm)

$\alpha$ = liquid-solid contact angle (radians)

If a pressure is imparted to the mercury, the force tending to drive mercury into the cylindrical channels, such as may be present as pores or voids in a porous solid, is given by

$$F = \pi r^2 P \qquad (2.28)$$

Equating these two forces gives

$$P = - \frac{2 \pi \sigma \cos \alpha}{r} \qquad (2.29)$$

Equation (2.29) indicates that at zero applied pressure, no pores or interparticle voids are penetrated by mercury, and that increasingly smaller pores are penetrated as applied pressure is increased.

Reported measurements of contact angles between mercury and a large variety of solids range from $112^{o}$ to $142^{o}$ (Orr, 1959). The contact angle between mercury and carbon is taken to be $140^{o}$ (Atlas Chem. Ind., 1968). The surface tension of mercury at ambient temperature has been quoted as 480 dynes/cm (Thomas and Thomas, 1967), 474 dynes/cm (Micromeritics Inst. Corpn., 1970) and 474 dynes/cm (Atlas Chem. Ind., 1968). Assuming $\sigma$ = 474 dynes/cm and $\alpha$ = $140^{o}$, then equation (2.29) becomes

$$P = \frac{1.074 \times 10^{6}}{r} \qquad (2.30)$$

where P is measured as psia and r as angstroms.

II.3.1 (i) Evaluation of Adsorbent Total Pore Volume and Pore Volume Distribution

From mercury penetration experiments a plot of penetration volume $V_p$ versus applied pressure P is obtained (see Section II.3.2). Conversion of P to an equivalent r is accomplished by utilization of equation (2.30), and enables a plot of $V_p$ versus r to be constructed. The latter plot represents the cumulative pore volume distribution of pores as

a function of pore radius for the solid studied, assuming cylindrical pores. However, as obtained, the distribution fails to distinguish the contribution of pore volume arising from (a) pore structure (b) interparticle void spaces.

The range of pore sizes in which an accurate picture of the pore volume distribution can be obtained is dependent on the range of applied pressures that can be applied in the experimental method. By use of a 50,000 psia mercury penetration porosimeter, with a 1-50,000 psia applied pressure range, the pore volume distribution in pores of approx. 20-1,000,000 Å radii can be obtained. [There are limitations in applying pressures greater than 50,000 psia corresponding to penetration of pores of less than approx. 20 Å radius, one being that too high pressures may crush the porous solid particles]. Thus mercury penetration porosimetry is incapable of evaluating the pore structure of a solid contained in micropores less than approx. 20 Å radius.

The total pore volume of a solid as determined by mercury penetration experiments may be obtained from the Vp versus P or Vp versus r curves. There the total pore volume $(Vp)_{Total}$ is given by

$$(Vp)_{Total} = (Vp)_{P_{max}, r_{min}} - (Vp)_{P_{min}, r_{max}} \qquad (2.31)$$

where $(V_P)_{Total}$ is the difference in mercury penetration volume values (in $cm^3/g$) taken at the highest and lowest applied pressures.

It is again evident that the total pore volume determined from experimental data using a 50,000 psia porosimeter will only represent the pore volume contained in pores of radii between 20 and 1,000,000 Å. This may be accurate in quantitising the total pore volume of solids containing no micropores, but obviously will not represent the true total pore volume in solids which contain a sizeable pore structure in pores of less than approx. 20 Å radius, as do most activated carbons.

II.3.1 (ii) Evaluation of Adsorbent Total Surface Area and Surface Area Distribution

The applied pressure - mercury penetration volume curve obtained for a particular solid from mercury penetration experiments can also be used to calculate the surface area of that solid (Rootare, 1967).

The work required to immerse an area dS of a non wetting powder in mercury is given by

$$dW = \sigma \cos \alpha \, dS \qquad (2.32)$$

Since this work is suppled when the applied external pressure P forces a volume of mercury $d(V_P)$ into the pores of the powder, equation (2.32) becomes

$$-P \, d(V_P) = \sigma \cos \alpha \, dS \qquad (2.33)$$

Assuming that $\sigma$ and $\prec$ do not vary with pressure, then equation (2.33) may be written

$$dS = \frac{-P \; d(V_P)}{\sigma \cos \prec} \tag{2.34}$$

or in integrated form

$$S = \int_{(V_P)_{min.}}^{(V_P)_{max}} \frac{P \; d(V_P)}{\sigma \cos \prec} \tag{2.35}$$

For $\prec = 140^{o}$ and $\sigma = 474$ dynes/cm, equation (2.35) becomes

$$S = 0.0189 \int_{(V_P)\,min.}^{(V_P)max.} P \; d(V_P) \tag{2.36}$$

Where S is the total surface area ($m^2/g$) in pores exhibiting a total penetration volume equal to $(V_P)_{max} - (V_P)_{min}$

Similarly, the contribution to the total surface area of a small increment $\Delta(V_P)_n$ of penetration volume equal to $(V_P)_n - (V_P)_{n+1}$ can be approximated from equation (2.36) by

$$\Delta S_n = 0.0189 \; \bar{P} \; \Delta(V_P)_n \tag{2.37}$$

Where $\bar{P}$ (taken equal to $P_n$) is the mean pressure that must be applied in order to bring about an increase in penetration volume $\Delta(V_P)_n$.

Thus by means of a graphical integration procedure commencing at $(V_P)_{max}$ and employing equation (2.37) for successive decreasing values of $V_P$, one can obtain, by relating $\bar{P}$ to r via

equation (2.30), a cumulative distribution of surface area with respect to pore radius for the solid studied. Additionally, the cumulative value of S at the lowest value of $V_p$, i.e. at $P_{min}$, represents the total surface area as estimated from mercury penetration.

However, the surface area distributions and total surface areas obtained from mercury penetration data may not reflect the entire picture of the adsorbent pore structure due to the applied pressure limitations of the penetration apparatus used, as discussed earlier (see section II.3.1 (ii)).

II.3.2 Experimental

II.3.2 (i) Preparation of the Carbon Sample

A sample of the carbon to be tested is pre-dried for 12 hours in an oven at approx. 103°C. Just before use, the carbon is weighed in a clean dry sample cell whose weight is known accurately. By difference the weight of dry carbon is obtained. Experience has shown that for powdered and granular carbons the best sample weights to use are 0.15-0.3g and 1-2.5g respectively.

II.3.2 (ii) Description of the Mercury Penetration Apparatus

A schematic diagram of the apparatus is shown in Figs. II.8 and II.9, and a full description can be found in the instruction manual. (Micromeritics Instrument Corp. 1970)

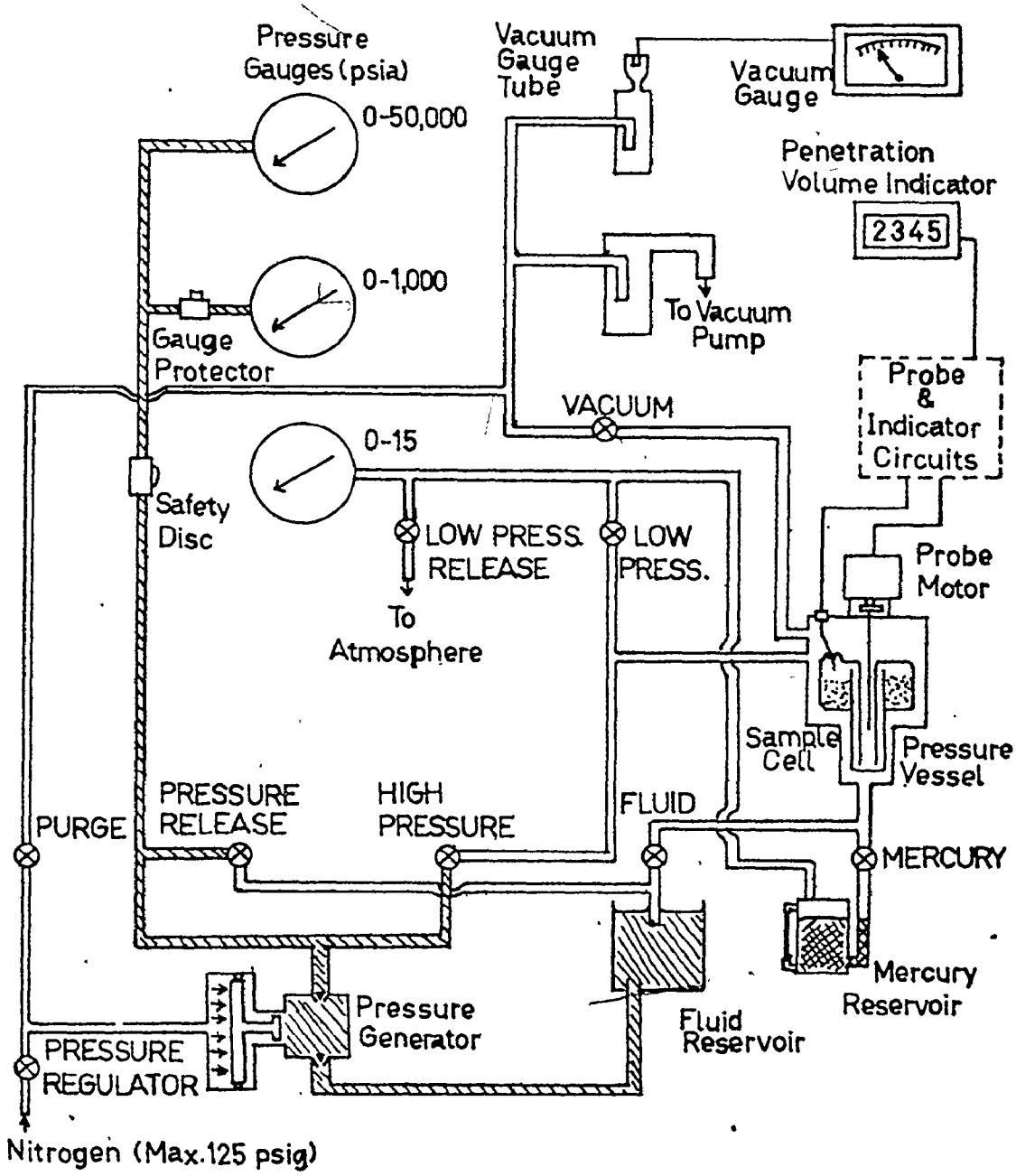


Fig.II.8 Schematic Diagram of Porosimeter

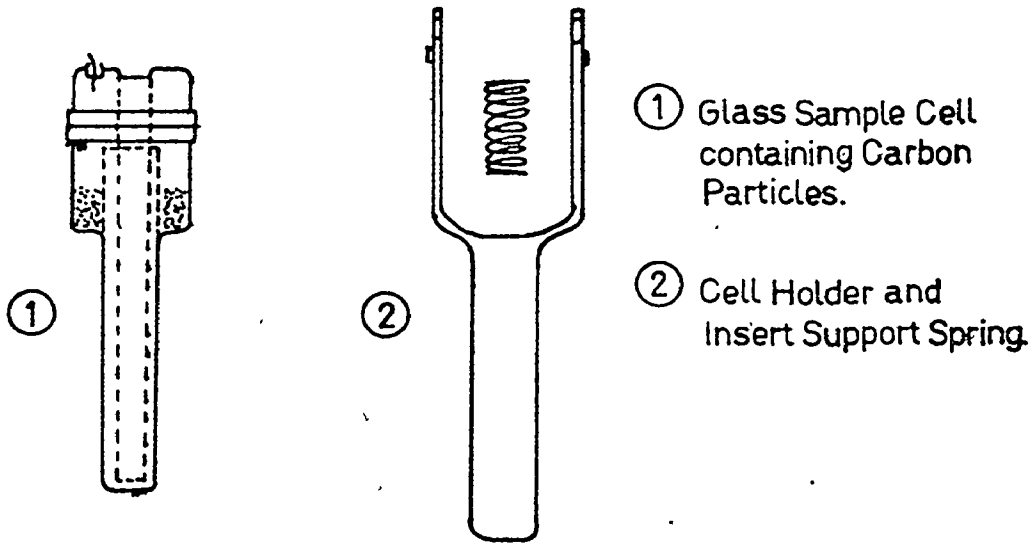


Fig.II.9 Cell Arrangement for Penetration Test.

In brief, the apparatus consists essentially of a pressure chamber in which the sample tube plus contents are placed. This chamber can be evacuated via a vacuum line or pressurized by means of air or hydraulic fluid. The pressure on the fluid is generated pneumatically with a pressure generator and gas line. The retractable probe mechanism and counter enable one to record small changes in mercury level in the sample cell during the experiment and provision is also made for recording the pressure on a series of pressure gauges.

II.3.2 (iii) Mercury Penetration Experiments

Experiments were carried out using a model 900/901 Mercury Penetration Porosimeter*, following the procedure laid down in the instruction manual. In brief, the sample cell containing a known weight of dry carbon is introduced into the pressure chamber, and the system evacuated. After attainment of a good vacuum (less than 20 microns of Mercury), mercury is allowed to fill the sample cell from the mercury reservoir, and afterwards excess mercury is drained off. The level of mercury in the sample cell is then noted by the automatic probe mechanism. Air is then allowed to enter the pressure chamber at various pressure increments from 0.5-14.7 psia as recorded on

---

* Micromeritics Instrument Corporation, Norcross, Georgia, U.S.A.

the low pressure gauge and the subsequent depression of mercury level in the sample cell caused by mercury penetration of large pores and voids is recorded by the automatic probe as a number of 'counts', where each count can be related to an equivalent penetration volume of mercury by the equation

$$V_P = k\, N_C \qquad (2.38)$$

Where $V_P$ = penetration volume of mercury at pressure P ($cm^3$)

$N_C$ = number of counts, corrected for mercury compressibility, at pressure P

$k$ = the cell constant ($cm^3$/count)

After zeroing the counter at a pressure of 0.5 psia, the cumulative number of counts at each increased pressure P is recorded, assuring that sufficient time is allowed for equilibrium at each increased pressure. When atmospheric pressure has been attained, the pressure chamber is evacuated of air and then filled with hydraulic fluid. Pressures above atmospheric are then generated in the fluid, via the pneumatic pressure generator, by means of nitrogen gas at approx. 80 psig pressure. By means of the pressure regulator it is possible, as before for air, to increase the hydraulic pressure in stages from 14.7 psia up to 50,000 psia, at the same time noting the number of counts at equilibrium for each pressure P. The cumulative penetration volumes are calculated from equation (2.38).

Hence by employing air and hydraulic fluid as the pressurizing media on the mercury, it is possible to obtain values of mercury penetration volume $V_p$ versus pressure for pressures ranging from 1 psia to 50,000 psia. The values of Vp must, however, be corrected for mercury compressibility by subtracting the mercury compressibility count at the corresponding pressure. Mercury compressibility counts as a function of pressure are obtained by running a separate experiment with an empty sample cell. The correction factors can thus be applied to $N_C$ values only if the assumption that the actual solid volume (i.e. excluding pores and voids) of the carbon sample is small compared to the total 'internal' volume of the sample cell, is valid. This condition has been met by carbon samples used in the present experiments.

Specific mercury penetration volumes ($cm^3/g$) at each pressure were obtained by dividing $V_p$ values by the original weight of dry carbon used.

II.3.3 Results and Discussion

II.3.3. (i) The Penetration Volume - Applied Pressure Curve

From mercury penetration porosimetry experiments, a plot of applied pressure P versus a 'recorded number of mercury penetration counts' $N_R$ was obtained for each carbon, as outlined in Section II.3.2. However the values of $N_R$ arise not only as

a result of mercury penetration of pores and voids, but also from compression of mercury itself with applied pressure. Each value of $N_R$ was therefore first corrected for mercury compressibility by utilization of equation (2.39), viz.

$$N_C = N_R - N_{Hg} \qquad (2.39)$$

Where $N_C$ = the number of counts at pressure P, corrected for mercury compressibility

$N_R$ = the recorded number of counts at pressure P

$N_{Hg}$ = the number of counts at pressure P due to mercury compressibility.

[ Values of $N_{Hg}$ versus P were determined as outlined earlier by conducting mercury penetration experiments using an empty sample tube. The results of these experiments are shown in Appendix II.6 ]

The appropriate values of mercury penetration volume Vp at each P were then calculated via $N_C$ values from equation (2.38), where k was stated, for the porosimeter and sample tube used, to be 0.00180 $cm^3$/count.

The subsequent penetration volume - applied pressure curves obtained for each carbon, using different amounts of carbon in the sample tube, are shown in Appendix II.7, figs. (i) to (viii).

In contrast to the nitrogen adsorption for a given carbon, the mercury penetration volume - applied pressure curve is immediately indicative of carbon pore volume distribution, since values of P may be directly related to an 'equivalent' minimum pore radius filled r, via equation (2.30). Thus the difference in the shape of the curves in Appendix II.7 between carbons immediately reflects differences in their pore structural characteristics.

However, like analysis of nitrogen adsorption isotherm data, determination of accurate and meaningful pore size distributions for a given carbon from its mercury penetration volume - applied pressure curve can often be very difficult.

Firstly, as mentioned earlier due to limitations on maximum applied pressures that can be achieved, it is only possible from our data to estimate carbon pore structure in the approx. 20 $\mathring{A}$ - 1,000,000 $\mathring{A}$ pore radii range, corresponding to the 1-50,000 psia applied pressure range attainable with the porosimeter used.

Secondly, the nature of mercury penetration experimentation does not provide the means to distinguish between the penetration volume utilized in filling interparticle voids and that genuinely utilized in filling pores. This is in contrast to nitrogen adsorption experiments, where the magnitude of the void space between the carbon particles is evaluated separately

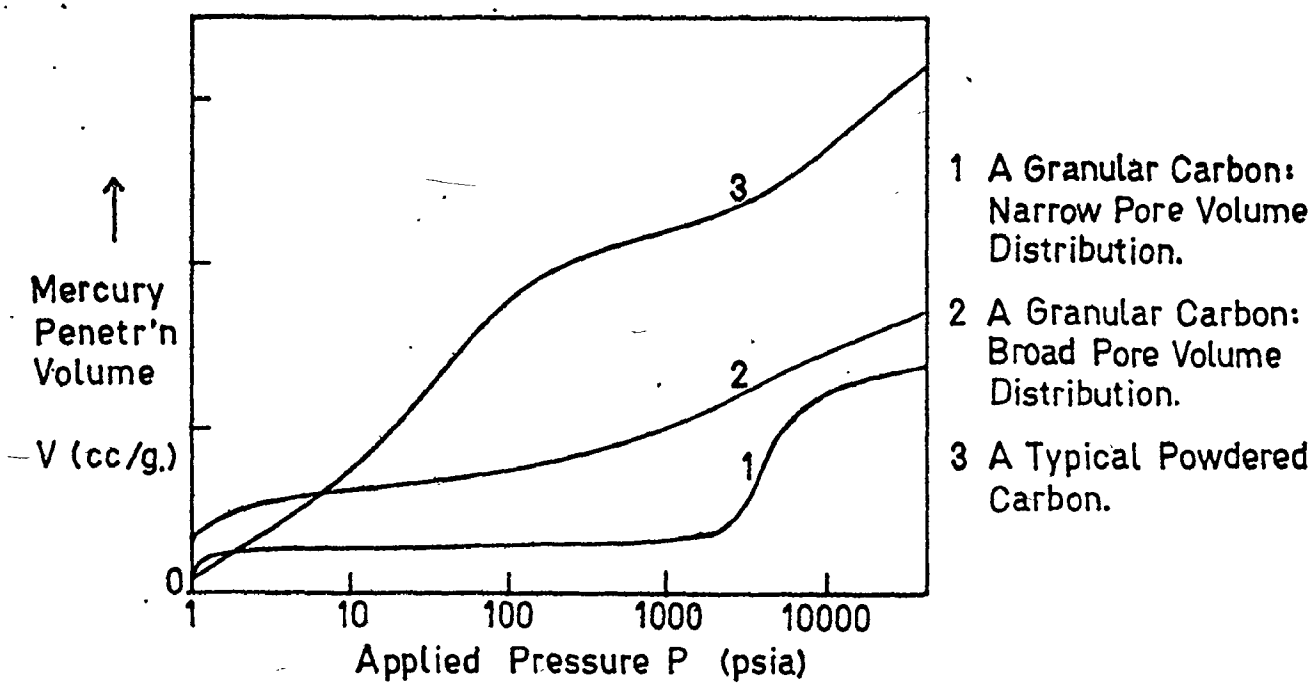


Fig. II.10 Examples of P–V data obtained from mercury penetr'n experiments on different activated carbons.

in the dead space determination, and then subtracted from the total adsorbed volume. However, depending on the shape of the mercury penetration volume - applied pressure curve, an estimation of the contribution of the void penetration volume to the total penetration volume may be made. Consider the curves shown in Fig. II.10. Here curves 1 and 2 have an initial penetration volume at the lower pressures i.e. less than 10 psia, and that in the intermediate pressure range the curves tend to flatten out, suggesting negligible pore volume in the intermediate pore size range. Since, in contrast to nitrogen adsorption, an increase in applied pressure gives rise to mercury penetration of increasingly smaller pores due to the convex nature of the mercury meniscus versus the concave condensed nitrogen meniscus in the pores, it is apparant that the bulk of the pore structure of carbon, which is contained in pores of less than 10,000 Å radii (Atlas Chem. Ind. 1968), will be penetrated at pressures in excess of approx. 100 psia (from equation (2.30)). Although carbons may still contain some pores of greater than 10,000 Å radii, their contribution to total carbon pore structure will be very small. Accordingly, it is reasonable to assume that the initial penetration volume corresponding to attainment of the plateau in curves 1 and 2 is commensurate with filling of interparticle voids. In the

case of curve 3, no such plateau occurs; deciphering of this curve in order to segregate void and pore penetration volumes is thus virtually possible, since one cannot estimate accurately the pressure at which cessation of void filling occurs.

Another indication of the contribution of void penetration volume to the total penetration volume may be obtained from analysis of the penetration volume - applied pressure curves obtained on the same carbon using different sample amounts. As can be seen from Appendix II.7, the amount of carbon sample used in the porosimeter sample cell (Fig. II.9) affects the penetration volumes in the low pressure regimes, but does not alter the obtained incremental penetration volumes in the intermediate and high pressure ranges. Figure II.11 exemplifies this phenomenon in the case of the penetration volume - applied pressure curves obtained for Nuchar 12 x 40 granular carbon. Here, at pressures above approx. 10 psia, the curves are identical with respect to increase of penetration volume with increased pressure, but below 10 psia the penetration volume depends on sample size. From Appendix II.7 it can be seen that, without exception, an increase in carbon sample amount gives rise to a decrease in the initial penetration volume. This is due to the wall effect of the sample tube and the closer packing of the sample with large sample amount. Since it is obvious

FIG. II.11. MERCURY PENETRATION DATA FOR NUCHAR WV-G 12 x 40

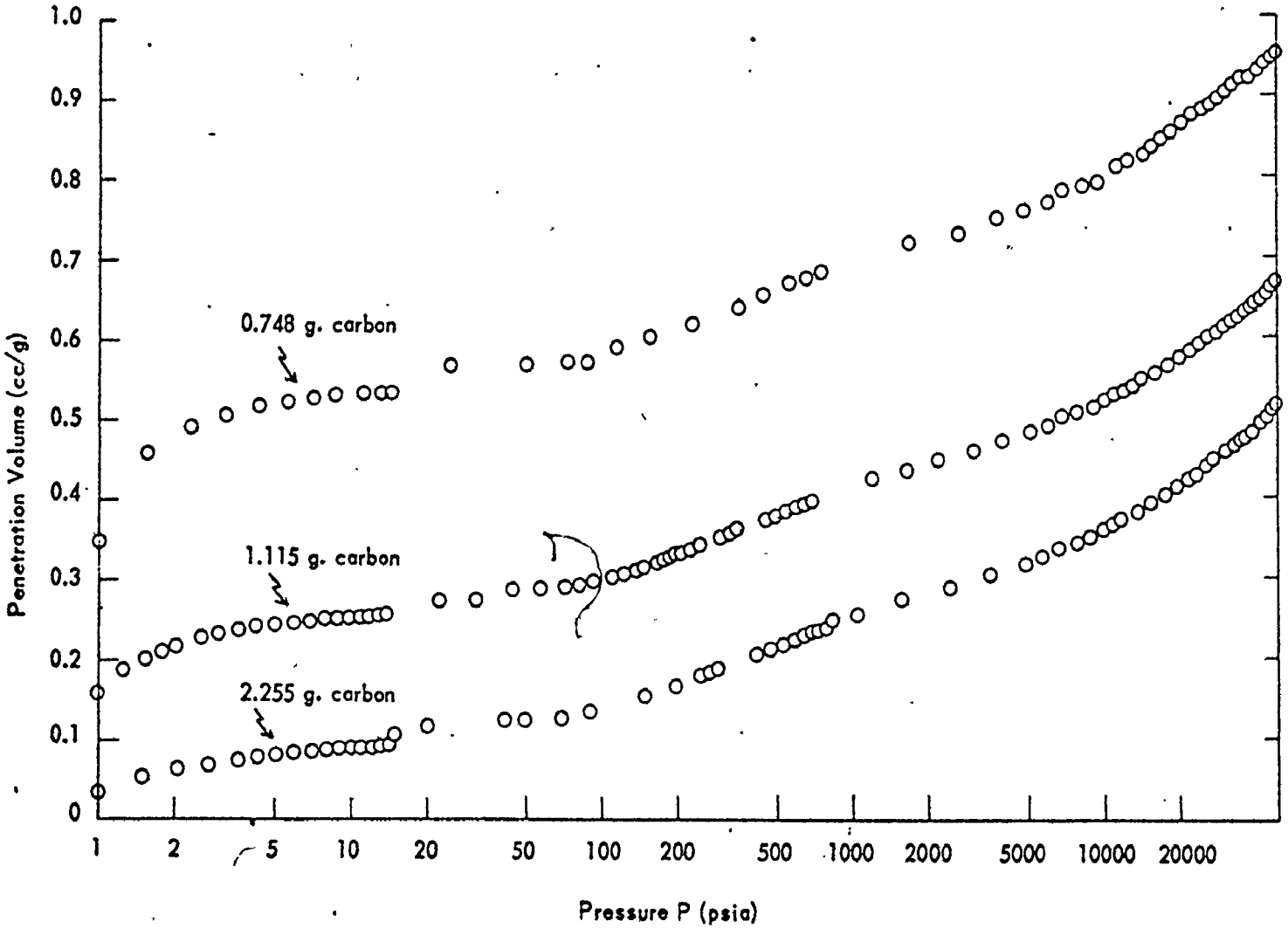

the use of different sample quantities will not change the pore penetration volume - applied pressure curve, provided that sufficient carbon sample quantity is employed and that the specific penetration volume $V_p$ ($cm^3/g$) is used, then the reproducible portion of the curves illustrated in Fig. II.11 will represent the pore penetration volume, and the non- reproducible portion will pertain to the void penetration volume, the latter being dependent on sample quantity. As can be seen in Appendix II.7, the effect of sample size on the penetration volume-pressure curves is in general more evident for granular than powdered carbons.

The size of the particles used in the sample cell is also known to influence the nature of the obtained penetration volume-pressure curves. Mayer and Stowe (1965) introduced the concept of a break through pressure $P^*$, defined as the pressure required to force mercury through a uniform bed of similar sized particles. Its magnitude is a function of bed porosity E and the contact angle $\Theta$ between the particles and mercury, the factors being related as shown in Fig. II.12. At any applied pressure P, the force generated by its application serves both to force mercury into the pores and also to force mercury between adjacent particles. Mayer and Stowe state that the smallest particles forced apart by an applied pressure P is

fig.II.12 Breakthrough Pressure Correlation

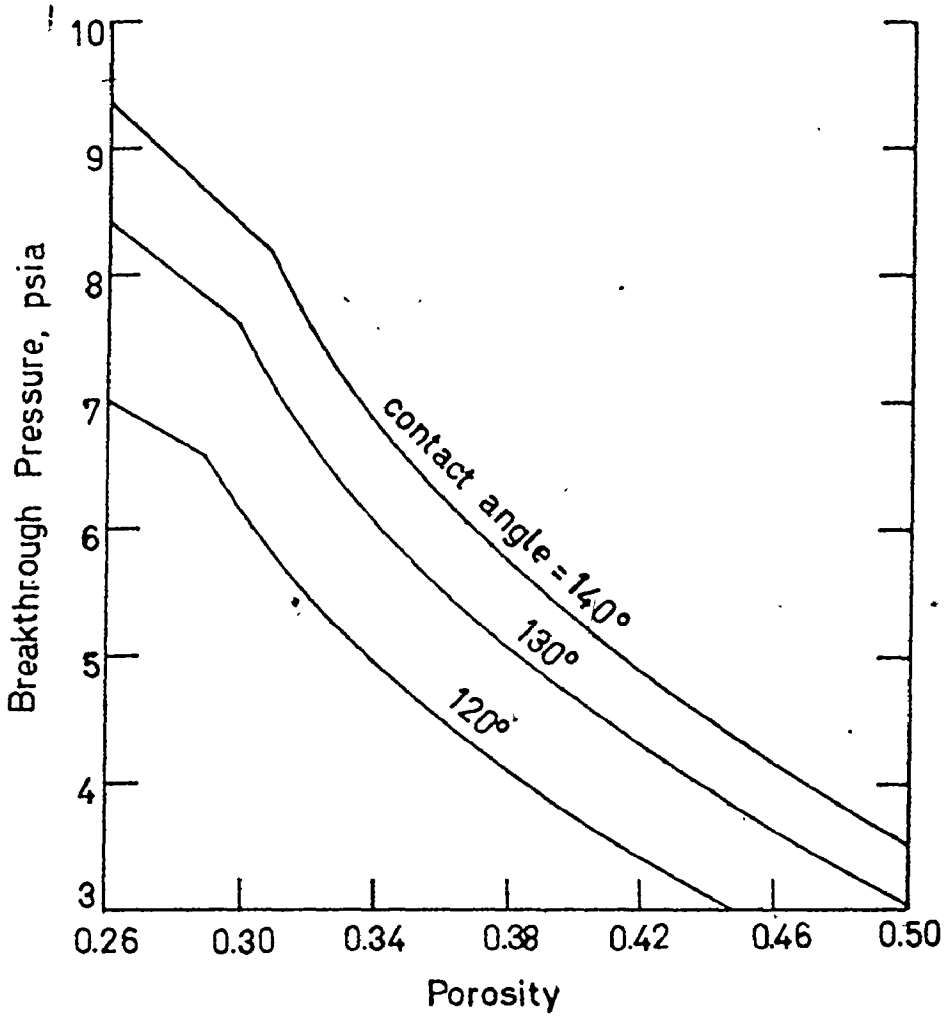

fig.II.13 Minimum Particle Size Separated Versus Applied Pressure (P) For A Contact Angle Of 140° Using Mercury Penetration Porosimetry

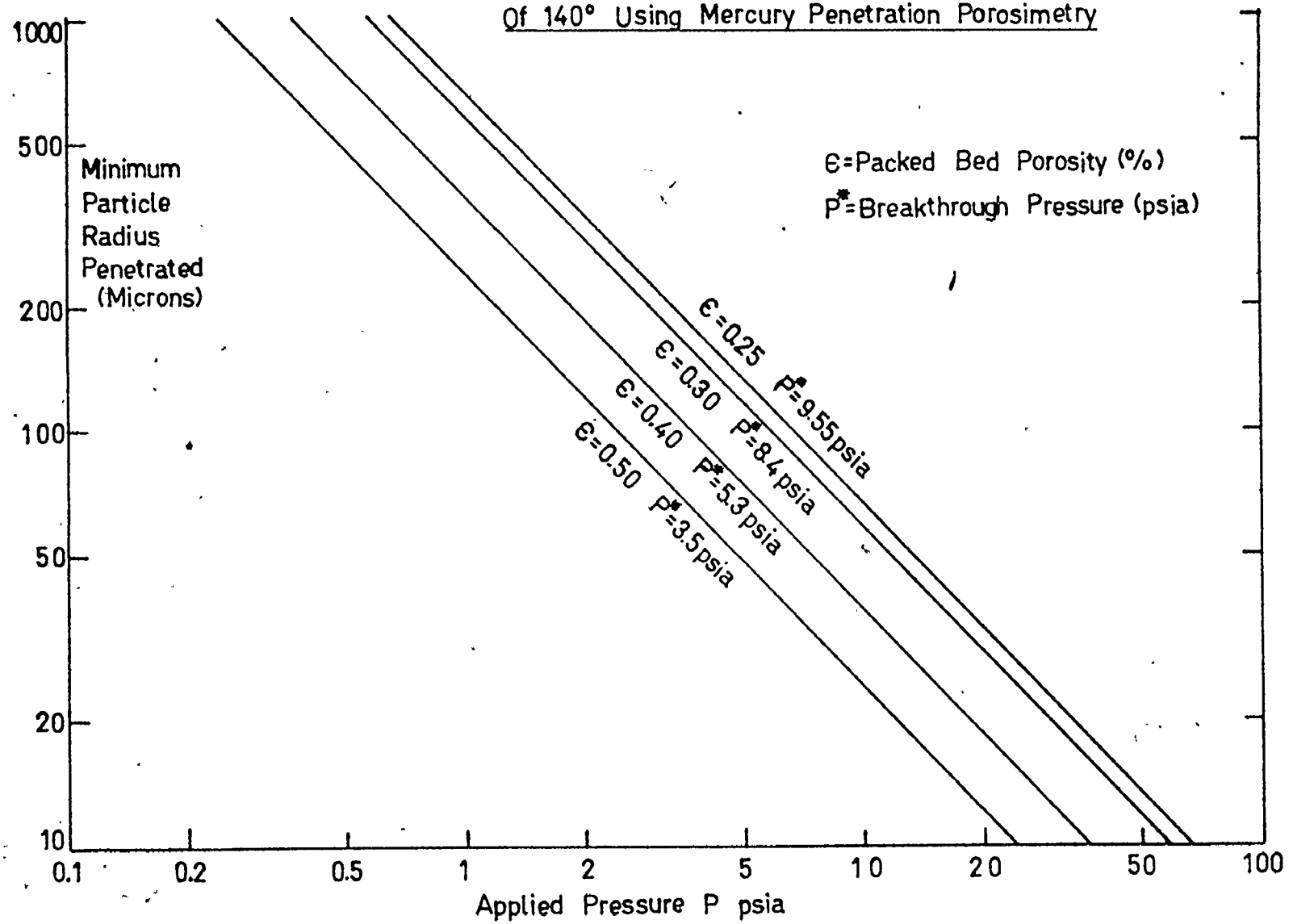

given by

$$r = 68.77 \frac{P^*}{P} \qquad (2.40)$$

Where $r$ = particle radius (microns)

$P^*$ = break through pressure (psia)

$P$ = applied pressure (psia)

Figure II.13 represents graphically an amalgamation of equation (2.40) with Fig. II.12 for substances displaying a contact angle of 140° with mercury, such as activated carbon. By using Fig. II.13 in conjunction with carbon particle size data (see Section II. 5 ), it is possible to ascertain the minimum pressure that must be exerted in order to force mercury between adjacent particles of a given size. This pressure is shown, for each of the carbons studied, as a function of packed bed porosity and carbon particle size characteristics in Table II.5.

Table II.5

Minimum Applied Pressure (psia) Required for Mercury Penetration of Voids between Carbon Particles for the Carbons Studied

| Carbon | * Average Particle Diameter $\langle D_A \rangle_w$ (microns) | * Particle Diameter at Pr ($D_A \leq \langle D_A \rangle$) = 99.5% (microns) | Minimum Applied Pressure (psia) required to penetrate between particles of size = $G \langle D_A \rangle_w$ | | Minimum Applied Pressure (psia) required to penetrate between particles of size at Pr ( $D_A \leq \langle D_A \rangle$) = 99.5% | |
|---|---|---|---|---|---|---|
| | | | E=0.25 | E=0.5 | E=0.25 | E=0.5 |
| Aqua Nuchar A | 14.4 | 1.2 | 91.0 | 33.0 | 1090 | 395 |
| Columbia LCK | 980 | 600 | 1.35 | 0.49 | 2.20 | 0.80 |
| Darco KB | 25.5 | 1.6 | 51.0 | 18.7 | 820 | 300 |
| Darco S-51 | 23.1 | 1.5 | 57.0 | 20.9 | 870 | 320 |
| Darco 12 X 20 | 1190 | 740 | 1.10 | 1.40 | 1.75 | 0.64 |
| Filtrasorb 400 | 900 | 390 | 1.45 | 0.53 | 3.30 | 1.20 |
| Nuchar 12 X 40 | 1040 | 660 | 1.25 | 0.46 | 2.00 | 0.72 |
| Special 'A' | 430 | 200 | 3.00 | 1.10 | 6.50 | 2.40 |

* values obtained from Particle Size Analysis (see Section II. 5 )

It is clearly apparent from table II.5 that the pressures required for mercury penetration of granular carbon interparticle voids are considerably less than the corresponding required pressures using powdered carbons, e.g. Aqua Nuchar A, Darco KB and Darco S-51

For granular carbons, the maximum pressure required to force even the smallest granular carbon particles apart is only 1.75 - 6.5 psia depending on the carbon studied. Hence the penetration volume - applied pressure curve will accurately reflect granular carbon pore structure at applied pressures above these values, corresponding to pores of less than approx. 615,000 - 165,000 Å radius. Since in this study pore structure in the 0 - 100,000 Å pore radii range is of primary interest, subsequent pore size distribution data in this range, obtained from granular carbon penetration volume - applied pressure curves above a pressure of 10.5 psia, will be free of error caused by mercury penetration of voids.

However, in the case of powdered carbons, where particle sizes are approx. $10^{-2}$ times that of the granular forms, it can be seen from table II.5 that packed bed porosity and particle size have a greater effect on the minimum required penetration pressure than for granular carbons. Furthermore the required

penetration pressures are much higher. In considering the smallest particle carbon, Aqua Nuchar A, a pressure of 91 psia would bring about penetration of approx. half the total interparticulate contacts. However in order to force almost all the particles apart an applied pressure of about 1090 psia is required, assuming a bed porosity of 25%. From equation (2.30), these pressures correspond to mercury penetration into pores of radii 11,800 Å and 986 Å respectively. Thus the penetration volume - applied pressure curve for Aqua Nuchar A carbon is only reflective of carbon pore structure at pressures greater than about 1100 psia. Recorded penetration volumes at pressures below this value will represent an indistinguishable summation of void penetration volume and pore penetration volume in pores of greater than approx. 1000 Å radius. It thus follows that for this carbon, only accurate pore size distributions in pores of less than about 1000 Å can be obtained using the penetration volume-applied pressure curve. Similarly, table II.5 indicates that for Darco KB and Darco S-51 carbons, only accurate pore size distributions in pores of less than approx. 1300 Å (corresponding to applied pressures greater than approx. 850 psia) can be obtained from the appropriate penetration volume-applied pressure curves.

The above deductions, coupled with considerations of the minimum pore size that is able to be penetrated with mercury as discussed earlier, indicate that for the powdered carbons studied, only pore structural properties in the approx. 21.5 Å to 1300 Å pore radii range (21.5 Å - 1000 Å in the case of Aqua Nuchar A) can be evaluated from mercury penetration data, whereas for granular carbons an accurate indication of pore structure in the 21.5 Å - 100,000 Å pore radii range can be obtained from mercury penetration data.

One final point is worth noting regarding interpretation of the applied pressure-penetration volume curves, particularly when considering granular carbon pore structure. From the curves in Appendix II.7, it can be seen that there is an apparant discontinuity in the approx. 15-60 psia applied pressure range. This is most apparent in the curve for Columbia LCK and least noticeable for Darco 12 X 20. This is the result of an uncontrollable pressure surge when initially changing over to a hydraulically generated pressure source in order to achieve applied pressures in excess of ambient pressure. [As outlined in Section II.3.2, after attainment of atmospheric applied pressure, i.e. 14.7 psia, increased applied pressures are generated hydraulically by surrounding the sample tube with oil, which is pressurized by nitrogen gas via a pneumatic pres-

sure generator. Unfortunately, due to the design of the porosimeter, it was not easily possible to prevent a surge of pressure due to piston displacement for pressures less than about 60 psia. Accordingly, although the applied pressure gauge may have read 20 psia, this value in fact would represent a pressure surge at approx. 60 psia followed by pressure dissipation through the system, finally equilibrating to 20 psia. In this case it is apparant that voids and/or pores penetrated by 60 psia applied pressure may not have been vacated during pressure dissipation to 20 psia because of hysteresis effects, giving rise to erroneously high recorded penetration volumes at the recorded applied pressure. This holds for all pressures in the 14.7 - 60 psia range, and thus explains the discontinuity just above 14.7 psia on the curves. The control of pressure surges in the system at applied pressures greater than 60 psia was easily achieved.] However, from the curves in Appendix II.7 it is possible to interpolate with good accuracy the shape of the penetration volume- applied pressure curve in the 'discontinuity' range of applied pressures from the shape of the curve at pressures less than 14.7 psia and the corresponding shape at pressures in excess of 60 psia.

II.3.3 (ii) Pore Size Distributions

For each carbon, the penetration volume-applied pressure curve was used in conjunction with equation (2.30) to yield the cumulative pore volume distribution, as outlined in Section II.3.1 (i). These are shown in Appendix II.5, Figs. (i) to (viii) for the carbons studied.

The surface area distribution for each carbon was obtained from the penetration volume-applied pressure curve by a graphical integration procedure utilizing equations (2.30) and (2.37), as outlined in Section II.3.1 (ii). An example of the calculation procedure is shown in Appendix II.8. The surface area distribution obtained for the carbons studied are shown in Appendix II.5, Figs (i) to (viii).

The validity of the pore size distributions obtained for each carbon are naturally subject to the accuracy of the penetration volume-applied pressure curves as discussed in Section II.3.3 (i). Hence the pore size distributions are only representative of carbon pore structure in pores of approx. 21.5 - 1000 $\mathring{A}$ radii for powdered carbons, and in pores of approx. 21.5 - 100,000 $\mathring{A}$ radii for granular carbons. In addition, the obtained pore size distributions are also calculated on the assumptions of cylindrical pores and an 140$^{o}$ mercury/carbon

contact angle. Any significant practical deviations from these assumptions may result in erroneous pore size distributions.

Detailed discussion of the pore size distributions depicted in Appendices II.4 and II.5 will follow in Section II.4.

II.3.3 (iii) Fundamental Carbon Properties

Since the magnitude of carbon pore structure in pores of less than approx. 21.5 Å radii is, in contrast to nitrogen adsorption experiments, not ascertainable using mercury penetration techniques, carbon fundamental properties such as 'total' surface area and 'total' pore volumes obtained from analysis of penetration volume-applied pressure curves as outlined earlier are generally completely unrepresentative of actual total carbon pore structure. This is because most carbons usually contain a significant proportion of their total exhibited pore structure in pores of less than 21.5 Å radii. To illustrate this point, Table II.6 summarizes the 'total' pore volume and surface area calculated as outlined in sections II.3.1(i) and II.3.1 (ii) from mercury penetration data for each carbon studied.

Comparison of Table II.6 with Table II.4 (see Section II.2.3 (ii)) reveals that for the carbons studied (with the exception of Special 'A'), the total pore volumes and surface

Table II.6 Fundamental Carbon Properties Evaluated From Mercury Penetration Data

| Carbon | Surface Area ($m^2/g$) | | Pore Volume ($cm^3/g$) | |
|---|---|---|---|---|
| | (A) | (B) | (A) | (B) |
| Columbia LCK 12/28 | 58.8 | 59.3 | 0.141 | 0.405 |
| Darco KB | 244.9 | - | 0.980 | - |
| Darco S-51 | 161.0 | - | 0.550 | - |
| Darco 12 X 20 | 162.1 | 163.3 | 0.482 | 0.712 |
| Filtrasorb 400 | 86.6 | 87.9 | 0.276 | 0.519 |
| Nuchar Aqua A | 93.9 | - | 0.400 | - |
| Nuchar 12 X 40 | 89.3 | 90.2 | 0.260 | 0.427 |
| Special 'A' | 73.6 | 73.7 | 0.310 | 0.374 |

(A) in pores of radii 21.5 - 1000 Å

(B) in pores of radii 21.5 - 100,000 Å

areas determined from nitrogen adsorption experiments are significantly larger than those evaluated from mercury penetration experiments. This is because the total surface area and pore volume calculated from nitrogen adsorption data pertains to pore structure in the 0 - approx. 1000 Å pore radii range, but the corresponding values obtained from mercury penetration data are representative of pore structure in the pore radii range of 21.5 Å up to approx. 1000 Å for powdered carbons, or up to 100,000 Å for granular carbons. Thus the total surface area and pore volume calculated from mercury penetration data will not include a contribution from pore structure in pores of less than about 21.5 Å radii. The highly developed pore structure in pores of less than 21.5 Å radii evident in most activated carbons thus explains the differences between values in Table II.4 and II.6.

Conversely, for Special 'A' carbon, values of total surface area (90.9 $m^2/g$) and pore volume (0.331 $cm^3/g$) derived from nitrogen adsorption data correspond reasonably well with values of total surface area (73.7 $m^2/g$) and pore volume (0.310 $cm^3/g$) derived from mercury penetration data, for pore structure in pores up to about 1000 Å radius. This is because, as will be seen in Section II.4, this carbon contains very few pores,

and hence negligible pore volume and surface area, in pores of less than about 20-30 Å radius. Hence the total surface area and pore volume in this carbon as derived from both nitrogen adsorption and mercury penetration data would be expected to show good agreement, as evidenced above.

Generally, comparison of the values in Table II.6 support the previous statements made in Section II.2.3(ii) regarding carbon pore structural differences. The large values of surface area and pore volumes for the Darco carbons, particularly Darco KB in Table II.6 confirm the existence of a significant number of larger pores in these carbons. Conversely, the very small values of surface area and pore volume determined for Columbia LCK carbon substantiate the fact that this carbon contains negligible pore structure in pores of greater than approx. 20 Å radius. Although Special 'A' appears to contain negligible pore structure in pores of less than approx. 20 Å radius, Table II.6 indicates that its pore structure in pores of greater than 20 Å radius is comparable to that exhibited by other activated carbons such as the Nuchar and Filtrasorb carbons in the same pore size range.

## II.4 OVERALL PORE SIZE DISTRIBUTIONS

In order to obtain a representative picture of the overall pore size distribution in a given carbon, it is necessary to combine the separate distributions obtained from both nitrogen adsorption and mercury penetration data, since the pore size range in which accurate pore size distributions can be obtained is limited in both procedures. The use of nitrogen adsorption data has been stated to yield pore size distribution data that is only accurate in the approx. 15-125 Å pore radii range (Atlas Chem. Ind., 1968). Similarly pore size distributions obtained from mercury penetration data using a 50,000 psia porosimeter are only accurate in the approx. 21.5 - 1000 Å pore radii range for powdered carbons, and the 21.5 - 100,000 Å range for granular carbons. [West Virginia Pulp and Paper Co. (1969) stated this accuracy range as being 25-100,000 Å radii using a 50,000 psia porosimeter.]

In the WestVaco study (1969), the distributions obtained by the two methods were joined at 1000 Å radius, whereas Atlas Chemical Company (1968) suggest matching at 125 Å radius. However WestVaco used only a 15,000 psia porosimeter, in which the smallest pore that can be penetrated is one of approx. 72 Å radius (from equation (2.30)). Accordingly, in this study it was felt that matching at 50 Å radius was justified, since the

50,000 psia porosimeter used here had a greater resolution with respect to smallest pore radius penetrated. Below 50 Å, the BET data was used. Above 50 Å, the incremental increases in pore parameters obtained from mercury penetration data were added to the BET data.

The combined distributions with respect to surface area and pore volume are shown in Appendix II.4, figs (i) to (viii) and Appendix II.5, figs. (i) to (viii) respectively. Here the distributions match very well for the Darco carbons and Special A, but deteriorate with the Nuchar carbons and Columbia LCK. The distributions do not match well for Filtrasorb 400 carbon. As discussed earlier, the lack of a good 'match' between the two distributions probably arises from the assumptions made regarding pore shape and surface/adsorbate contact angle in determination of pore size distributions. It is feasible that the assumption of cylindrical pores may not be a good one when considering certain carbons. In this respect the pore size distributions calculated from nitrogen adsorption data in the manner outlined earlier (Section II.2.3 (iii)) relate to pore interiors while mercury penetration data gives rise to pore size distributions based on pore necks. Thus carbons with pores of approximately cylindrical shape will give reasonable 'matches' where it is evident that carbons with pores deviating considerably from a cylindrical config-

uration (e.g. inkwell pores) would give rise to different pore size distributions obtained by the two methods, and hence 'poor matches' in the combined distributions.

In addition, it is also feasible that the assumptions of zero and 140° contact angles at the carbon/liquid surface in nitrogen adsorption and mercury penetration respectively may be in error: furthermore, due to differences in carbon surface characteristics between carbons (see Section II.7), this angle may vary from carbon to carbon. Any actual deviation from the appropriate assumed value in the model used for determination of carbon pore size distributions by either procedure could also give rise to a poor 'match' in the combined distribution. Hence it is likely that the poor 'match' in the case of Filtrasorb carbon arises from the presence of essentially non-cylindrical pores and/or an unusual mercury/carbon or liquid nitrogen/carbon contact angle in this carbon.

In the case where a poor 'match' was evident at 50 Å radius, a 'smoothing-out' curve was constructed to by-pass the discontinuity in the overall distribution curve. Figures II.14 and II.15 show the overall 'smoothed-out' pore size distributions with respect to surface area and pore volume for the carbons studied, expressed as the total surface area or pore volume contained in pores up to a given pore radius.

Fig.II.14 Overall Surface Area Distributions For Carbons Studied

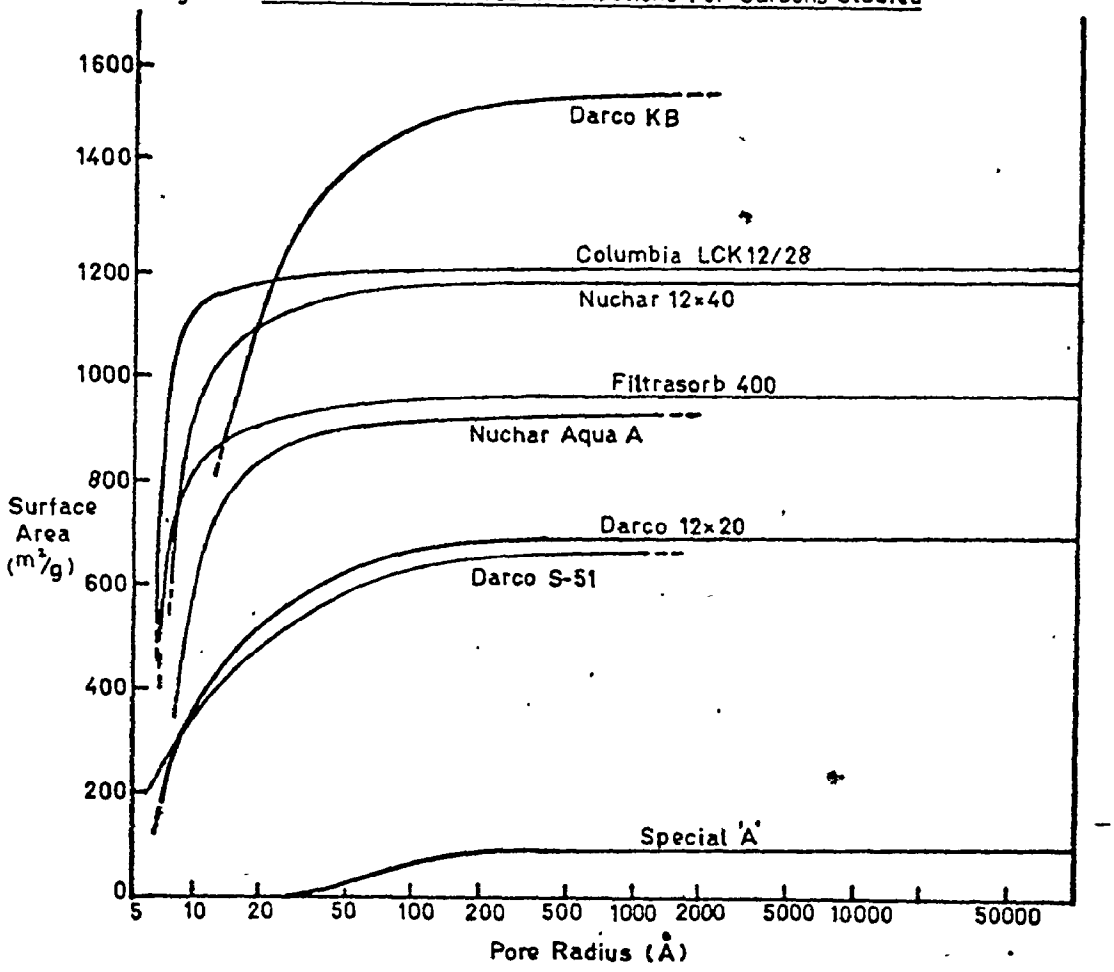

Fig.II.15 Overall Pore Volume Distributions For Carbons Studied

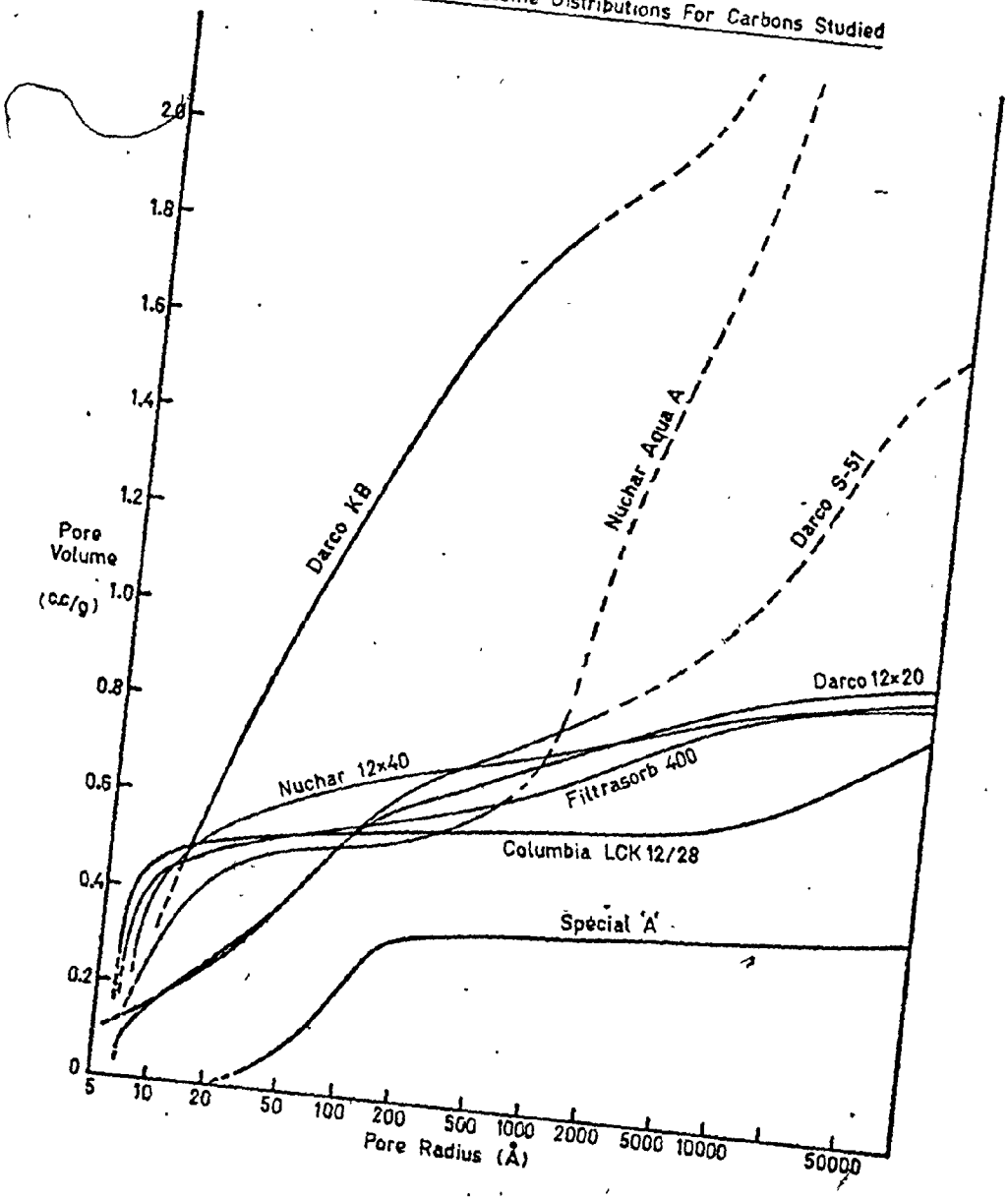

Here it can be seen that there is a wide variation in carbon pore structural properties among the carbons studied. Darco KB carbon is seen to possess the broadest and most highly developed pore structure of all the carbons studied, containing a significant amount of pore structure in all pores of up to approx. 1000 Å radius. Special 'A', on the other hand, contains practically all its exhibited pore structure in pores of approx. 20-200 Å radii. Columbia LCK carbon appears to contain virtually all its highly developed pore structure in very small pores of less than approx. 15 Å radius. (Although from Fig. II.15 it appears that this carbon contains some pore volume in very large pores, it is questionable whether this volume represents true pore volume or interparticle void volume as discussed earlier in Section II.3.3). The other carbons studied display pore structures intermediate between the pore structures of the carbons quoted above.

In general the total pore volumes and surface areas in pores of up to 1000 Å radius obtained from Figs. II.14 and II.15 generally agree well with the corresponding values determined from nitrogen adsorption data and listed in Table II.4. However in the case of Darco KB, the value of total pore volume (approx. 1.85 $cm^3/g$) determined from Fig. II.15 is somewhat higher than the corresponding value (1.40 $cm^3/g$) determined from nitrogen

adsorption data. This discrepancy can arise as a result of three factors, viz.

a) the manner in which the distributions are 'matched'

b) possible errors in determination of $V_s$ in nitrogen adsorption experiments as outlined earlier (see Section II.2.3)

c) possible errors in the pore volumes at larger pore sizes due to the contribution of void penetration volume in mercury penetration data (see Section II.3.3).

and will occur to an extent with all carbons, but particularly with powdered carbons exhibiting highly developed pore structures.

It is also interesting to note from Figs. II.14 and II.15 that, for equivalent pore volumes, the ratio of surface area to pore volume decreases as pore size increases. To illustrate this, it can be seen that in pores below approx. 30 Å radius, Darco KB contains approx. 0.9 $cm^3/g$ pore volume and approx. 1330 $m^2/g$ surface area. However in the approx. 30-1000 Å pore radii range, this carbon contains approximately the same pore volume of approx. 0.9 $cm^3/g$ but only approx. 120 $m^2/g$ surface area. This arises from pore geometry since, assuming cylindrical pores, the ratio of surface area to pore volume is equal to $2\pi r/\pi r^2$, or $1/r$. Hence for equivalent pore volume, the number of surface adsorption sites decreases with increase in pore radius.

## II.5 PARTICLE SIZE ANALYSIS

Activated carbon particle size is an important parameter in determination of adsorption rate. Each of the carbons studied were thus subjected to a particle size analysis. The granular carbons, due to their relatively large size, were characterized by sieving techniques, whereas the powdered carbons were analyzed by a microscopic counting procedure.

### II.5.1. Theory

#### II.5.1. (i) Sieving

By mechanically sieving a sample of granular activated carbon through a sieve array of progressively decreasing aperture openings (i.e. increasing sieve mesh numbers) for a given time, and then weighing the amount of sample retained on each sieve, it is possible to determine carbon particle size as a weight distribution with respect to aperture opening, or carbon characteristic diameter. The amount of sample retained on a given mesh size after shaking is an indication of the weight fraction whose particle geometrical characteristics - generally expressed as a characteristic particle diameter $D_A$ - are greater than or equal to the sieve mesh opening. Usually $D_A$

for a given weight fraction $W_i$ is taken to be the arithmetic average of the sieve aperture openings bracketting the fraction, i.e. for the ith fraction

$$D_{A_i} = 1/2 \left( A_{i-1} + A_i \right) \qquad (2.41)$$

where $A_{i-1}$ = the aperture opening of the sieve above the sample

and $A_i$ = the aperture opening of the sieve on which the sample is retained

For all i values, the above equation enables determination of the <u>incremental</u> weight-size characteristics of the original sample. However, in order to obtain the <u>cumulative</u> weight-size distribution, the cumulative weight fraction $\sum_{i=1}^{i} w_i$ retained on or above sieve i in an array of n sieves is evaluated. The fractional weight term $\sum_{i=1}^{i} w_i \,/\, \sum_{i=1}^{n} w_i$ is then plotted against $D_{A_i}$, where in this case $D_{A_i}$ is taken to be equal to $A_i$. The fractional weight term is an indication of the probability of any particle having a diameter greater, than or equal to, the weight average particle diameter $\langle D_A \rangle_w$, i.e.

$$\frac{\sum_{i=1}^{i} w_i}{\sum_{i=1}^{n} w_i} = \Pr \left( D_{A_i} \geq \langle D_A \rangle_w \right) \qquad (2.42)$$

The form of $\langle D_A \rangle_w$ depends on how the data is distributed. A Gaussian distribution of the data will yield an arithmetic weight average particle diameter ${}_a\langle D_A \rangle_w$, where

$$ {}_a\langle D_A \rangle_w = \frac{\sum_{i=1}^{n} w_i D_{A_i}}{\sum_{i=1}^{n} w_i} \qquad (2.43) $$

Likewise logarithmically normalised data will yield a geometric weight average particle diameter ${}_G\langle D_A \rangle_w$, where

$$ \log {}_G\langle D_A \rangle_w = \frac{\sum_{i=1}^{n} w_i \log D_{A_i}}{\sum_{i=1}^{n} w_i} \qquad (2.44) $$

These are the two principally encountered data normalisation tools, although others may give a more accurate normalisation of highly skewed distribution data.

II.5.1. (ii) Microscopic Counting

By relating the projected form of a particle, as viewed under a microscope, to a circle of equivalent area, it is possible to obtain a number-size distribution of particles in the original sample by successive counting of

particles having the same, equivalent circular diameter.

The number of particles $n_i$ having an equivalent circular diameter $D_{m_i}$ are counted for each i. The cumulative probability function expressing the likelyhood of any particle having $D_{m_i}$ greater than or equal to the number average particle diameter $\langle D_m \rangle_n$ is given by

$$\frac{\sum_{i=1}^{i} n_i}{\sum_{i=1}^{n} n_i} = \Pr\left(D_{m_i} \geq \langle D_m \rangle_n\right) \qquad (2.45)$$

By analogy with section II.5.1.(i), the nature of the number average particle diameter $\langle D_m \rangle_n$ will depend on whether the data are normally or log-normally distributed, giving rise to arithmetically and geometrically weighted number average diameters ${}_a\langle D_m \rangle_n$ and ${}_G\langle D_m \rangle_n$ respectively at $\Pr\left(D_{m_i} \geq \langle D_m \rangle_n\right) = 50\%$.

As a rule, if the number distribution of $D_m$ obeys a normal distribution law, it does not necessarily follow that the weight distribution is normally distributed. However, if the number distribution is log-normal then it can be shown by Kapteyn's transformation (Herdan, 1960) that the weight distribution is also log-normal and with the same

log standard deviation $\sigma_G$. Hence since $(\sigma_G)_w = (\sigma_G)_n$ it can be shown that

$$\ln {}_a\langle D_m\rangle_w = \ln {}_G\langle D_m\rangle_w + 0.5 \ln [\sigma_G]^2 \quad (2.46)$$

it can also be shown that the arithmetic weight average particle diamter ${}_a\langle D_m\rangle_w$ can be related to the geometric number average particle diameter ${}_G\langle D_m\rangle_w$ by the equations

$$\ln {}_a\langle D_m\rangle_w = \ln {}_G\langle D_m\rangle_n + 3.5 \ln [\sigma_G]^2 \quad (2.47)$$

Thus by combining equations (2.46) and (2.47) the relation between the geometric number and weight average particle diameter is given by

$$\ln {}_G\langle D_m\rangle_w = \ln {}_G\langle D_m\rangle_n + 3 \ln [\sigma_G]^2 \quad (2.48)$$

II.5.2. Experimental

II.5.2. (i) Sieving

Approximately 50 - 100 g of granular carbon was weighed and then added in increments to a sieve array containing sieves of numbers 14, 16, 25, 30, 40, 50 and 70 U.S. mesh sizes (when sieving the Special "A" carbon sieve numbers 80, 100 and 200 U.S. mesh were also used in addition to the others.) After addition of the last increment of sample, the array was subjected to 15 and occasionally 30 mins. of shaking. The amount of carbon retained on each

sieve was then weighed as was the contents of the pan. From the weight data and a knowledge of the sieve aperture sizes the weight-size distribution characteristics of each carbon was determined as outlined in Section II.5.1. (i).

II.5.2. (ii) Microscopic Counting

For each powdered carbon, approximately 25 g of sample was screened on a #200 U.S. mesh sieve. Both +200 and -200 mesh fractions was collected and the weight of the +200 fraction was determined. The -200 fraction was then analyzed * by a microscopic counting method using a Quantimet 720 image Analyzer. Approximately 500 particles were counted and their diameter recorded as that of an "equivalent circle" diameter $D_m$. From the data obtained, it is possible to express the characteristic particle sizes of the -200 fraction as a number-size distribution, as outlined in Section II.5.1. (ii).

---

* Analyses performed by Ontario Research Foundation, Sheridan Park, Mississauga, Ontario.

## II.5.3. Results and Discussion

### II.5.3. (i) Evaluation of Particle Size Distributions

#### a) Sieving

For each granular carbon used in this study, the weight-size distribution of particles was calculated from the results of sieving experiments by utilization of equation (2.42). The distributions are shown in Appendix II.9, figs. (i) to (v). The data are assumed to be log-normally distributed. It should be noted, however, that the data can also be adequately described by a Gaussian distribution. This arises because there is lack of a sufficient number of data points in regions where the bulk of particles are concentrated (see Appendix II.9), due to the unavailability of appropriate sieve sizes. However, due to the limitations of sieving procedures such as aperture binding, particle attrition and agglomeration, the experimental errors incurred in determination of the distribution data points are considered to significantly outweigh the error that may be caused by selection of the incorrect normalisation model (i.e. log-normal or normal distribution).

From Appendix II.9, figs. (i) to (v), the geometric weight average particle diamter $_{G}\langle D_{A}\rangle_{w}$ is obtained, being

the value of $D_A$ at Pr $(D_{A_i} \geq \langle D_A \rangle_w)$ = 50%. Similarily the standard deviation $\sigma_G$ can be taken as the difference in $D_A$ values at the 50% and 84% probability values. The values of both $_G\langle D_A \rangle_w$ and $\sigma_G$ for each carbon are shown in Table II.8.

b) Microscopic Counting

The number-size distributions of the -200 U.S. mesh fractions were calculated from microscopic counting data by use of equation (2.45). The data was found to be log-normally distributed, as shown in Appendix II.10, figs. (i) to (iii). The geometric number average particle diameter $_G\langle D_m \rangle_n$ was correspondingly obtained for each carbon from primarily distribution data, being the value of $D_m$ at Pr $(D_{m_i} \leq \langle D_m \rangle_n)$ = 50%. Similarily the standard deviation $\sigma_G$ is the difference in $D_m$ values at the 50% and 84% probability values. However, in order to compare powdered and granular carbon particle size distributions directly, the former must first be converted to weight-size distributions. This is achieved by use of Kapteyn's transformation, as outlined in Section II.5.1. (ii). Here the geometric weight average particle diameter $_G\langle D_m \rangle_w$ - point "A" in Appendix II.10, figs. (i) to (iii) - can be calculated from

equation (2.48), since ${}_G\langle D_m \rangle_n$ and $\sigma_G$ are known. The corresponding weight-size distribution of the original data is thus represented by a straight line passing through point "A" and running parallel to the number-size distribution, as shown in Appendix II.10, figs. (i) to (iii).

[It is also possible to convert individual data points on a number-size distribution to the corresponding points on a weight-size distribution. Here, it can be shown (Herdan, 1960) that if the shape and density of all sized particles are assumed similar, then the weight-size distribution can be calculated from number-size data via the equation.

$$\Pr\left(D_{m_i} \geq \langle D_m \rangle_w\right) = \frac{\sum_{i=1}^{i} n_i D_{m_i}^3}{\sum_{i=1}^{n} n_i D_{m_i}^3} \qquad (2.49)$$

where the number of particles $n_i$ of a characteristic diameter $D_{m_i}$ is known for all i from microscopic counting data. The distributions calculated from equation (2.49) are shown in Appendix II.10.]

The weight-size distributions thus far obtained are still not amenable to direct comparison with granular carbon distribution data, since the former only apply to the -200 U.S. mesh fraction. The powdered carbon weight-size

distributions must be adjusted to incorporate the +200 U.S. mesh fraction. Values of the latter for each powdered carbon are shown in Table II.7.

The values in Table II.7 cannot per se be used in conjunction with -200 U.S. mesh weight-size distribution, since they are characterised by a sieving characteristic particle diameter $D_A$, whereas the weight-size distributions of the -200 mesh fractions are characterised in terms of an equivalent circle diameter $D_m$. Heywood (1947) has developed an equation relating $D_A$ to $D_m$, i.e.

$$\frac{D_A}{D_m} = 0.724 \sqrt{\frac{m^2 + 1}{mn}} \qquad (2.50)$$

where $m$ = particle breadth/thickness ratio

$n$ = particle length/breadth ratio

If it is assumed that all the powdered carbon particles are either spherical, cubic, or rhomboid in shape, then from equation (2.50), $D_A = D_m$. Making this assumption, values of $\Pr\left(D_{m_i} \leq \langle D_m \rangle_w\right)$ from the weight-size distribution of the -200 U.S. mesh fraction may be adjusted to incorporate the +200 mesh fraction by use of the equation

Table II.7 Sieve Analysis of Powdered Activated Carbons

| Carbon | Weight Percentage Retained on a 200 U.S. Mesh Sieve |
|---|---|
| Aqua Nuchar A | 2.0% |
| Darco KB | 29.0% |
| Darco S-51 | 18.4% |

$$\left[\Pr\ (D_{Ai} \leq \langle D_m \rangle_w)\right]_{\text{Total}} = \left[\Pr\ (D_{mi} \leq \langle D_m \rangle_w)\right]_{\text{Total}} = \left[\Pr\ (D_{mi} \leq \langle D_m \rangle_w)\right]_{\substack{-200 \text{ U.S.} \\ \text{mesh fraction}}} \times \frac{(100-y)}{100} \qquad (2.51)$$

where y is the weight percent of sample retained on a 200 U.S. mesh sieve (see Table II.7.) The "total" powdered carbon weight-size particle distributions calculated from equation (2.51) are shown in Appendix II.10, figs. (i) to (iii). The corresponding values of the weight average particle diameter ${}_G\langle D_A \rangle_w$ are shown in Table II.8.

II.5.3. (ii) Carbon Particle Size Characteristics

A summation of carbon particle size characteristics evaluated by the aforementioned procedures is shown in Table II.8.

Here the granular carbons studied generally have average particle diameters of about 1 mm . These values also show good agreement with manufacturers' determined values, where available, although the nature of the average particle diameter stipulated by the carbon manufacturer is not known. Special "A" carbon, however, is seen to exhibit approximately half the average particle diameter of the other granular carbons studied. Examination of granular

Table II.8 Carbon Particle Size Characteristics

| Carbon | Geometric Weight Average Particle Diameter $_{G}\langle D_{A}\rangle_{W}$ (mm) | Geometric Standard Deviation $\sigma_G$ (mm) | Manufacturers Specified Average Particle Diameter $\langle D_p \rangle$ (mm) |
|---|---|---|---|
| **Granular** | | | |
| Columbia LCK 12/28 | 0.98 | 0.32 | -- |
| Darco 12 x 20 | 1.19 | 0.02 | 1.2 |
| Filtrasorb 400 | 0.90 | 0.48 | 0.9-1.1 |
| Nuchar WV-G 12 x 40 | 1.04 | 0.16 | -- |
| Special "A" | 0.43 | 0.18 | -- |
| **Powdered** | | | |
| Darco KB | 0.0255 | ~ 0.014 | -- |
| Darco S-51 | 0.0231 | ~ 0.015 | -- |
| Nuchar Aqua A | 0.0144 | ~ 0.0095 | -- |

carbon $\sigma_G$ values indicates that the representativeness of characterising all the particles in terms of single average diameter ${}_G\langle D_A \rangle_W$ is reasonable for Darco 12x20 and Nuchar 12x40 carbons, but falls off progressively in the case of Columbia, Special A and Filtrasorb carbons.

In comparison, the powdered carbons used in this study are seen to exhibit corresponding average particle diameters approximately fifty times smaller than their granular conterparts. In addition, estimated $\sigma_G$ values for the powdered carbons * are also high, indicating a considerable spread of particle diameter within the carbon sample.

The validity of the particle size distributions and average carbon particle sizes obtained here is dependent on the analytical method used in the evaluation. In this respect, Herdan (1960) has indicated that in sieving techniques, increase in shaking time and decrease of sample weight can give rise to a reduction in the calculated value

---

* due to the nature of the powdered carbon weight-size distributions (see Appendix II.10) - being non-linear - it is only possible to gain an approximate value of the standard deviation by consideration of $D_A$ values at the 50% and 16% probability values.

of ${}_G\langle D_A \rangle_W$ and an increase in $\sigma_G$. This effect is a result of particle attrition, and is particularily evident in sieving characterisation of low abrasion-resistant materials. However, the effect of sample size and shaking time on the weight-size particle distributions of all granular carbons studied here can be seen (Appendix II.9, figs. (i) to (v)) to be negligible. Thus it appears that the granular carbons under study all have a relatively high abrasion resistance, and that the derived values in Table II.8 are representative of original sample particle size characteristics.

The particle size distributions obtained from microscopic counting techniques are to some extent unrepresentative of original sample particle size distributions since the instrument used is not able to count particles of less than approximately 0.0002 mm. diameter.

Hence the actual values of ${}_G\langle D_A \rangle_W$ in Table II.8 may be lower, especially if the number of particles of less than 0.0002 mm diameter in the sample is significant. However, this is not considered excessive for the powdered carbons studied here, with the possible exception of Nuchar Aqua A, and so the values in Table II.8 for these carbons are reasonably representative.

It should be noted here that the characteristic

"sieve hole" particle diameter $D_A$ has been used in the carbon particle size analysis. In respect of adsorption into the pores of a porous adsorbent, the characteristic "volume/surface" diameter $D_{vs}$ of the particle is perhaps more representative in consideration of carbon particle diameter effects on adsorption. However, if it is assumed that all the carbon particles are spherical in shape, then $D_A$ and $D_{vs}$ become identical. Thus making this assumption, one may use the values in Table II.8 in analysis of adsorption data.

## II.6. CARBON ASH CONTENT

The total ash content of an activated carbon is the residue which remains after the carbonaceous portion is burnt off. In acid-washed carbons make from lignite, wood or coal, the ash consists mainly of silica and insoluble silicates of aluminium, iron magnesium and calcium (Atlas Chem. Ind. 1968). Generally the ash content of activated carbon is taken to be an indication of the portion of carbon weight that is not directly utilized in adsorptive capacity. However, this is not necessarily the case. Mantell (1968) has indicated that many "high-ash" activated carbons are more efficient in removing color and odor from solution than those with lower ash content. In order to account for this observation, the terms soluble and insoluble ash content are used. The soluble ash content, which is the water, acid or alkali-soluble portion of the total ash content, is reflective of the amount of inorganic material - mainly metal ions - that is free to participate in an "ion exchange" adsorption mechanism with potential adsorbates in solution. The insoluble portion of the total ash content is more representative of the fraction of carbon that is impotent

in adsorption. In this study, only the total ash content was determined.

II.6.1. Experimental

The procedure followed was similar to that outlined by Mantell (1968). Here an adequate sample of pre-washed carbon was dried for 1 - 2 hours in a 103°C oven. Approximately 1 g of the dried carbon was weighed in a procelain coucible and then heated at 900°C for 5 hours in a muffle furnace. After combustion, the sample was allowed to cool to room temperature in a dessicator. The residue was then weighed, and the total ash content recorded as weight percent of original dried carbon. Triplicate determinations were performed for each carbon.

II.6.2. Results and Discussion

The total ash contents for the carbons studied are shown in Table II.9.

Here carbon total ash contents are generally quite low, and agree well with the manufacturers' specified values, where available. Special "A", however, exhibits an extremely high ash content, this being expected due to the extensive clay-alumina interior of the particles comprising this "pseudo-carbon". The very low total ash content exhibited

Table II.9 Carbon Total Ash Contents

| Carbon | Experimental Values (wt.%) | Manufacturers' Specified Values (wt.%) |
|---|---|---|
| Columbia LCK 12/28 | 0.9 - 1.7 | -- |
| Darco KB | 3.4 - 3.5 | 3 - 6 |
| Darco S-51 | 15.8 - 15.9 | 17 - 24 |
| Darco 12x20 | 10.6 - 10.8 | -- |
| Filtrasorb 400 | 6.4 - 6.8 | 8.5 (max.) |
| Nuchar Aqua A | 1.2 - 1.6 | 7 (max.) |
| Nuchar WV-G 12x40 | 0.7 - 0.8 | 8.5 (max.) |
| Special "A" | 89.9 - 90.0 | -- (max.) |

by Columbia is also expected since the material from which it is derived, viz. petroleum, has virtually no mineral content. It is interesting to note that Darco 12x20 has a lower total ash content than Darco S-51, although both carbons are prepared from the same base material - lignite - by a similar thermal activation procedure. Here granular Darco carbons such as Darco 12x20 are prepared from the powdered Darco S-51 form by agglomeration of powdered particulates with a binding agent. Since the binding agent - usually tar or pitch - is carbonaceous in origin, it is completely volatilised in the muffle furnace, thus explaining the discrepancy.

## II.7 CARBON pH

The carbon pH is in essence the pH of water extract obtained under prescribed conditions. Generally acid-washed steam activated carbons will have a slightly acidic pH in the range 5 - 7. The corresponding water-washed carbons exhibit a slightly alkaline pH of about 7 - 2, whereas unwashed carbons may have pHs as high as 11 - 12 (Atlas Chem. Ind. 1968). The carbon pH is indicative of the nature of carbon surface functional groups. These groups arise from surface reactions during the carbon history, primarily during its preparation and activation. The nature of the surface functional groups may influence carbon adsorptive behaviour in liquid systems, as outlined by Garten and Weiss (1957.) Acidic carbons have been shown to be associated with acidic surface functional groups such as phenols, n-lactones and f-lactones (Garten and Weiss, 1957), carboxyl groups (Kruyt and de Kadt, 1931), oxidised carboxyl groups of the form $C(OH_3)^-$ (Shilov, 1930), or quinone groups (Studebaker, 1956). Alkaline carbons have been shown to be associated with the presence of hydroquinone (Studebaker, 1956) or chromene surface functional groups of the type

>CHR or $-CHR_2$ (Graten and Weiss, 1957). Steenberg (1941) has also shown that activation temperature can influence the nature of the carbon surface functional groups: activation below 400°C will yield an acidic (or L-) carbon, whereas 800°- 1100°C activation will produce an alkali (or H-) carbon.

II.7.1. Experimental

Mantell's (1968) procedure was followed, with slight modification. Here 10 g. carbon were added to 100 ml of freshly boiled distilled and deionized water in a 125 ml Erlenmeyer flask. The stoppered flask was then placed in a water bath shaker at 35°C, and shaken at approximately 80 oscillations per minute for 15 hours. The resultant slurry was then filtered through a well washed 0.45 μ membrane filter, and the filtrate then immediately subjected to pH measurement using a pre-calibrated Accumet Model 120 pH meter.* Any delay in pH measurement resulted in a $CO_2$ interference error as the solution was not buffered.

II.7.2. Results and Discussion

The results of carbon pH determinations are shown

---

* Fisher Scientific Ltd., Don Mills, Ontario

Table II.10 Carbon pH Values

| Carbon | Experimental pH Value | pH Value Quoted by Manufacturer |
|---|---|---|
| Columbia LCK 12/28 | 8.7 | -- |
| Darco KB | 5.5 | 4.5 - 6.5 |
| Darco S-51 | 6.7 | 5 - 7 |
| Darco 12x20 | 7.6 | 6 |
| Filtrasorb 400 | 7.9 | 8 |
| Nuchar Aqua A | 4.2 | -- |
| Nuchar WV-G 12x40 | 8.4 | -- |
| Special "A" | 8.6 | -- |

in Table II.10. Here most carbons can be seen to display either slightly acid or alkaline pHs', with values generally agreeing well with manufacturer's specified values, where available. All powdered carbons, viz. Darco KB, Darco S-51, and Nuchar Aqua A, display acidic pHs' whereas the granular carbons are alkaline. This suggests that all powdered carbons contain a predominance of acidic surface functional groups such as phenol, lactone or carboxyl groups whereas the granular carbons contain an excess of alkali surface functional groups such as chromene groups.

With the exception of Special "A", all carbon water extracts were colorless. In the case of Special "A", the water extract displayed a greenish-yellow tinge after carbon filtration. The reason for this is not known, but may have been caused by dissolution of heavy metal ion impurities held in the lattice structure of the clay-alumina base material as a result of ion exchange with hydrogen ions in the water solvent.

## II.8 SUMMARY

Each of the 8 activated carbons studied has been characterised in terms of the physical and chemical parameters which may influence its adsorptive behaviour in subsequent adsorption of lignier from aqueous solution.

It has been shown that all activated carbons, with the exception of Special "A", exhibit characteristically high total surface areas and pore volumes as calculated from nitrogen adsorption data. Total surface areas are in the range 650 - 1500 $m^2/g$. and total pore volumes in the range 0.45 - 1.8 $cm^3/g$. Special "A" displays a considerably lower total surface area (91 $m^2/g$) and pore volume (0.331 $m^2/g$) than the other carbons.

Overall pore size distributions obtained from a combination of nitrogen adsorption and mercury penetration data have indicated that wide pore structural differences exist between the carbons studied. Columbia LCK 12/28 has been shown to contain virtually all its pore structure in pores of less than 15 Å radius, whereas Special "A" contains practically all its limited pore structure in pores of approximately 20 to 200 Å radius. Darco KB exhibits the

most extensive pore structure of the carbons studied; furthermore, its pore volume is evenly distributed throughout pores up to 1000 Å radius. The other carbons studied exhibit pore structure properties within these three extreme cases outlined above.

Turning to average particle size, it has been shown by sieving techniques that the granular carbons all have average diameters of around 1 mm. Special "A" granules are about half the size of the other granular forms. Analysis of powdered carbon particle characteristics by microscopic counting techniques has indicated that the powdered carbons exhibit much smaller average particle diameters, being in the approximately 0.015 - 0.025 mm size range.

Generally the activated carbons studied exhibit low ash contents. although Special "A" contains close to 90% ash.

Carbon pH, indicative of the nature of functional groups on the carbon surface, was found to be slightly alkaline for the granular carbons, and slightly acidic for the powdered carbons.

The limitations of estimating pore distribution properties from nitrogen adsorption and mercury penetration techniques have been discussed. It has been shown that pore size distributions calculated from nitrogen adsorption data are only reasonably representative in the approximately 5 Å - 200 Å pore radii range, corresponding to applied relative pressures in the range approximately 0.05 - 0.95. Furthermore, it has been shown that different pore size distributions may be obtained from adsorption isotherm data by utilising different analytical procedures. It has also been established that experimental procedures for evaluation of the nitrogen adsorption isotherm may give rise to erroneous values of adsorbed nitrogen volume V in the high relative pressure region, and that the use of helium in dead space determinations may cause errors in calculation of the dead space factor as helium is evidenced to be slightly adsorbed on activated carbon.

The difficulties in estimation of pore size distributions from mercury penetration experiments have also been discussed. It has been shown that the 50,000 psi porosimeter is only capable of evaluating pore structural

characteristics in pores greater than 21.5 Å radius. The amount of carbon sample has also been shown to affect the shape of the penetration volume - applied pressure curve obtained, and is believed to be caused by the wall effect of the sample cell. In addition, the particle size of the carbon has been shown to limit the range of pore sizes in which the evaluated pore structural characteristics may be considered representative. Here the pore size range of accurate data is an inverse function of the particle size. Mercury penetration data for granular carbons may only be taken indicative of pore structural properties in the approximately 21.5 - 1,000,000 Å pore radii range corresponding to 10 - 50,000 psi range of applied pressures, whereas ~~for~~ powdered carbons the accurate pore radii range is reduced to approximately 21.5 - 1,000 Å corresponding to an applied pressure range of approximately 1,000 - 50,000 psi. The invalidity of using penetration data obtained for powdered carbons at pressures less than 1,000 psi corresponding to pores of greater than approximately 1,000 Å radius is due to simultaneous penetration of voids and pores at the lower applied pressures.

Lignin adsorption is expected to be influenced by carbon characteristics. It has been shown that carbons with widely varying characteristics have been chosen so that differences in their adsorptive behaviour, such as adsorption rate and capacity, may be related to differences in carbon properties, particularly pore size distributions.

Finally, it is important to note that in subsequent adsorption studies of the lignin macromolecule from solution, adsorption capacity experiments should not be carried out using pulverised granular carbon forms as the adsorbent. In studies of adsorption from solution, the pulverised form of the carbon adsorbent is usually used to bring about faster attainment of equilibrium conditions due to the well-known increase in adsorption rate with decreased particle size. It has been shown here that pulverisation destroys some of the pore structure contained in larger pores in the activated carbon adsorbent. Although pulverisation of carbon may not give rise to any significant difference in adsorption capacity for small-molecule solutes, it may generate substantial differences in carbon adsorption capacity for the larger sized, high

molecular weight constituents of the lignin macromolecule which may be preferentially or exclusively adsorbed in the larger pores.

# APPENDIX II.1

## Computer Program For Determination of Pore Size Distributions From Nitrogen Adsorption Isotherms

```
                      PROGRAM TST (INPUT,OUTPUT,TAPE5=INPUT,TAPE6=OUTPUT)
                C
                C     PORE DISTRIBUTION BASED ON HORSETROUGH PORE MODEL
                C
                C
000003                DIMENSION X(100),T(100),D(100),S(100),DT(100),B(100),V(100)
                     1,C(100)
000003                DIMENSION A(100),DVDD(100),F(100),FOLD(100),TITLE(13),NCONVG(100)
                C     NO IS THE NUMBER OF DECKS
000003                ND=9
                C     NDATA ARE THE NUMBER OF DATA POINTS
                C     DELV  IS  H  THE STEP SIZE
                C     VS  IS THE FINAL VOLUME
000004                KK=1
000005          200   READ(5,902) TITLE
000013                READ(5,900) NDATA,DELV,VS,NSORB
                C     NSORB ENTERED AS 1 IN COLUMN 32 FOR ADSORPTION
000027                IF(NSORB.EQ.1) GO TO 11
000031                EE=4.05
000033                GO TO 12
000033           11   EE=2.025
000035           12   IF(NDATA.LT.101) GO TO 3
000040                WRITE(6,992)
000043                STOP
000045            3   READ(5,901)(X(I), T(I),I=1,NDATA)
                C     CHECK TO INSURE THAT THE DATA ARE IN DECREASING ORDER OF X
000062          203   DO 5 I=2,NDATA
000064                IF(X(I-1) - X(I).LT.0.0) GO TO 4
000067                GO TO 5
000070            4   WRITE(6,993)
000074                STOP
000076            5   CONTINUE
000101                DO 150 KJ=1,5
000102                LK=(KJ-1)**2
000104                ALPHA=LK
000106                DO 10 I=1,NDATA
000110                E=EE/(-ALOG10(X(I)))
000115                T(I)=1.3*T(I)
000117                D(I)=E*T(I)
000122           10   S(I)=D(I)*D(I)*(1.0+ALPHA)/(E*(E+ALPHA*D(I)))
000134                L = NDATA-1
000136                DO 20 I=2,L
000137           20   DT(I) = (T(I-1)-T(I+1))/2.0
000145                DT(NDATA) = T(NDATA-1) - T(NDATA)
000150                DO 40 I=2,NDATA
000152           40   FOLD(I) = 1.2
000156                DO 45 I=1,NDATA
000157           45   NCONVG(I) = 0
000162                F(1)=S(1)
000163                FOLD(1)=S(1)
000164                B(1)=0.0
000165                C(1)=0.0
000166                CONR=(1.0+0.5*ALPHA)/(1.0+ALPHA)
000174                CONS=1.0/(1.0+ALPHA)
000176                DO 55 J=1,40
000200                NSUM = 1
000201                DO 50 I=2,NDATA
```

```
000203          I1 = I-1
000204          IF(NCONVG(I).EQ.1) GO TO 50
000207          B(I)=(FOLD(I1)/D(I1)+FOLD(I)/D(I))*CORR+B(I1)
000216          C(I)=CORS*(FOLD(I1)/(D(I1)*D(I1))+FOLD(I)/(D(I)*D(I)))+C(I1)
000227          F(I)=S(I)*(1.0-DT(I)*(B(I)-T(I)*C(I)))
000237          IF(F(I).LT.0.0)  F(I) = 0.0
000242          IF(ABS(F(I)-FOLD(I)).LT.0.00001) NCONVG(I) = 1
000251          FOLD(I) = F(I)
000254       50 NSUM = NSUM+NCONVG(I)
000261          IF(NSUM.EQ.NDATA) GO TO 58
000262          IF(J.EQ.40) WRITE(6,994)
000270       55 CONTINUE
             C  V(I)  IS THE VOLUME OF PORES OF SIZE GREATER THAN  D
000272       58 CONTINUE
000272          V(1)=0.0
000273          DO 60 I=2,NDATA
000275          I1 = I-1
000276       60 V(I) = 0.5*DELV*(F(I1) + F(I))+ V(I1)
             C  A(I)  IS THE AREA OF PORES OF SIZE GREATER THAN  D
000307          A(1)=0.0
000310          DO 70 I=2,NDATA
000311          I1 = I-1
000312       70 A(I)=15.46*DELV*(F(I1)/D(I1)+F(I)/D(I))*CORR+A(I1)
             C  DVDD  IS THE DERIVATIVE OF VOLUME WITH RESPECT TO PORE SIZE
000327          DVDD(1) = 0.0
000327          DVDD(2) = (F(2)*2.0*DELV)/(VS*(D(1)-D(3)))
000335          M = NDATA-2
000337          DD = 10.0*DELV
000341          DO 80 I=3,M
000343       80 DVDD(I) = (F(I)*DD)/(VS*(2.*D(I-2)+D(I-1)-D(I+1)-2.*D(I+2)))
000361          DVDD(NDATA-1) = (F(NDATA)*2.0*DELV)/(VS*(D(NDATA-2)-D(NDATA)))
000371          DVDD(NDATA) = .0
000372          WRITE(6,997)  TITLE
000377          WRITE(6,996) VS,DELV,NDATA,ALPHA
000413          WRITE(6,998)
000417          WRITE(6,999) (I,X(I),T(I),F(I),V(I),A(I),D(I),DVDD(I),I=1,NDATA)
000447          CHECK = VS - V(NDATA)
000452          WRITE(6,991) D(NDATA),CHECK
000462          WRITE(6,995)
000466      150 CONTINUE
000470          KK=KK+1
000472          IF(KK.LE.ND) GO TO 200
000474          STOP
             C
             C
000476      900 FORMAT(I10,2F10.3,I2)
000476      901 FORMAT(2F20.3)
000476      902 FORMAT(13A6)
000476      991 FORMAT(///15X, 86H THE DIFFERENCE BETWEEN THE TOTAL VOLUME ADSORBE
                1D, AND THE VOLUME IN PORES LARGER THAN,   /  19X,F8.2, 16H    ANG
                2STROMS IS,  F9.2)
000476      992 FORMAT(2X,111H THE NUMBER OF DATA POINTS MUST BE LESS THAN 101,
                1YOU MUST HAVE READ IN   NDATA   WITHOUT RIGHT-JUSTIFYING IT)
000476      993 FORMAT(2X, 67H THE  X  VALUES MUST BE IN DECREASING ORDER,   CHECK
                1 THE INPUT DATA)
000476      994 FORMAT (2X,* THE CALCULATION OF  F(I) DID NOT CONVERGE IN 40 LOOPS
                1BUT THE PROGRAM IS CONTINIUNG WITH THE LAST VALUE*)
000476      995 FORMAT(1H1)
```

```
000476      996 FORMAT(9X,F9.2,3X,52H CC.(S.T.P.) PER GRAM IS THE MAXIMUM VOLUME A
                1DSORBED/
                2          9X,F9.2,3X,77H CC.(S.T.P.) PER GRAM IS THE STEP SIZE USED F
                3OR THE INPUT  X  VERSUS  T  DATA/
                4          9X,I9,3X,25H DATA POINTS WERE READ IN,5X,10H ALPHA IS,F8.4
                5///)
000476      997 FORMAT(1H-,/42X,49H PORE DISTRIBUTION BASED ON HORSETROUGH PO
                1RE  //// 27X,13A6///)
000476      998 FORMAT(   35X,2H X, 9X,2H T,16X,6H DV/DQ,6X,7H VOLUME,
                16X,5H AREA,5X,9H RADIUS R,6X,6H DV/DR/)
000476      999 FORMAT(22X,I3,F14.4,F12.3,F20.3,2F12.2,F14.2,F13.5)
                C
000476            END
UNUSED COMPILER SPACE
006100
```

# APPENDIX II.2

## Example Analysis of Nitrogen Adsorption Data

Figure Example of Data Analysis on Raw BET Data in Order to Determine Nitrogen Adsorption Isotherm

Carbon: Columbia LCK 12/28 Weight of Sample Tube + Wet Carbon = 12.4962 g Weight of Wet Carbon + Assembly = 62.1810 g Weight of Wet Carbon = 0.2810 g
Date : 19/2/73 Weight of Sample Tube = 12.2152 g Weight of Dry Carbon + Assembly = 62.1632 g Weight Moisture = 0.0178 g
By : P. Rankin Weight Wet Carbon = 0.2810 g Weight Moisture = 0.0178 g Weight Dry Carbon = 0.2632 g

| Gas | S2 | Bulb Setting (empty) Small | Large | Gas Pressure P (torr) Observed | Corrected | Vapour Pressure Po (torr) | Relative Press. P/Po | Inlet Volume $V_I$ ($cm^3$ S.T.P.) | Residual Volume $V_R$ ($cm^3$ S.T.P.) | Dead Space Factor $F=V_I-V_R$ / $P_{corr}$ | $V_I - V_R$ (A) ($cm^3$ S.T.P.) | $V_A=FxP_{corr}x(1+0.05\frac{P_{corr}}{760})$ | Volume Adsorbed ($V_I-V_R-V_A$) | Volume Adsorbed / Gram Carbon $Q(cm^3/g)$ |
|---|---|---|---|---|---|---|---|---|---|---|---|---|---|---|
| He | Closed | 5 | 5 | 120 9 | 120.4 | | | 44.358 | | | | | | |
| | | 4 | 5 | 135.0 | 134 4 | | | 44.366 | | | | | | |
| | | 3 | 5 | 146.4 | 145.7 | | | 44.338 | | | | | | |
| | | 3 | 4 | 283.5 | 282.2 | | | 44.355 | | | | | | |
| | | | | | | | Ave $V_I$ = | 44.354 | | | | | | |
| He | Open | 5 | 5 | 111.5 | 111.0 | | | | 40.895 | 0.0312 | | | | |
| | | 4 | 5 | 123.1 | 122:5 | | | | 40.438 | 0.0321 | | | | |
| | | 3 | 6 | 132.7 | 132.1 | | | | 40.200 | 0.0313 | | | | |
| | | 3 | 4 | 236.6 | 235.5 | | | | 36.984 | 0.0313 | | | | |
| | | | | | | | | | Ave F = | 0.0315 | | | | |
| $N_2$ | Closed | 5 | 5 | 132.3 | 131.7 | | | 48.521 | | | | | | |
| | | 5 | 4 | 220.7 | 219.7 | | | 48.805 | | | | | | |
| | | 4 | 4 | 266.8 | 265.6 | | | 48.824 | | | | | | |
| | | 4 | 5 | 148.0 | 147.3 | | | 48.625 | | | | | | |
| | | 3 | 5 | 160.9 | 160 2 | | | 48.750 | | | | | | |
| | | | | | | | Ave $V_I$ = | 48.705 | | | | | | |
| $N_2$ | Open | 5 | 5 | 0.0 | 0.0 | 775.5 | | | 0.0 (all adsorbed) | | 48.705 (all adsorbed) | 0.000 | 48.705 | 185.049 |
| $N_2$ | Closed | 5 | 5 | 101.2 | 100.7 | | | 37.100 | | | | | | |
| | | 4 | 5 | 113.0 | 112 5 | | | 37.137 | | | | | | |
| | | 3 | 5 | 122 6 | 122 0 | | | 37 126 | | | | | | |
| | | 1 | 5 | 135.0 | 134.4 | | | 37.195 | | | | | | |
| | | | | | | | Ave $V_I$ = | 37.140 | | | | | | |
| $N_2$ | Open | 5 | 5 | 31.2 | 31.1 | 775.2 | 0.0402 | | 11.458 | | 74.387 | 0.988 | 73.399 | 278.872 |
| | | 4 | 4 | 47.1 | 46,9 | 774.9 | 0.0607 | | 8.621 | | 77.224 | 1.491 | 75.733 | 287.739 |
| | | 4 | 3 | 57.9 | 57.6 | 773.7 | 0.0748 | | 7.154 | | 78.691 | 1 833 | 76.858 | 292.014 |
| | | 4 | 1 | 72.1 | 71.8 | 772.9 | 0.0933 | | 5.604 | | 80.241 | 2 287 | 77.954 | 296.178 |
| | | 3 | 1 | 85.3 | 84 9 | 773.6 | 0.1103 | | 4.436 | | 81.409 | 2.706 | 78.703 | 299.024 |
| | | 1 | 1 | 108.3 | 107.8 | 770.1 | 0.1406 | | 2.661 | | 83.184 | 3 441 | 79.743 | 302.975 |
| | | 0 | 0 | 123.9 | 123.3 | 770.4 | 0.1608 | | 1.695 | | 84.150 | 3.940 | 80.210 | 304.749 |
| $N_2$ | Closed | 5 | 5 | 128.0 | 127.4 | | | 46.937 | | | | | | |
| | | 4 | 5 | 142 9 | 142.2 | | | 46.941 | | | | | | |
| | | 3 | 5 | 155.1 | 154.4 | | | 46.986 | | | | | | |
| | | 1 | 5 | 171.0 | 170.2 | | | 47.103 | | | | | | |
| | | | | | | | Ave $V_I$ = | 46.992 | | | | | | |
| $N_2$ | Open | 5 | 5 | 127.3 | 126.7 | 763.8 | 0.1667 | | 46 679 | | 84.463 | 4.050 | 80.413 | 305.520 |
| | | 4 | 5 | 140.0 | 139.4 | 763 7 | 0 1833 | | 46.017 | | 85.125 | 4.460 | 80.665 | 306.478 |
| | | 1 | 5 | 163.0 | 162.3 | 763.7 | 0.2134 | | 44.916 | | 86.227 | 5 200 | 81 026 | 307.850 |
| | | 5 | 4 | 196.1 | 195.2 | 762.5 | 0.2572 | | 43.362 | | 87.780 | 6 267 | 81.513 | 309.700 |
| | | 5 | 3 | 252.7 | 251.6 | 763.2 | 0.3311 | | 40.889 | | 90.253 | 8.108 | 82.145 | 312.101 |
| | | 4 | 3 | 310.8 | 309.4 | 763.1 | 0.4073 | | 38.427 | | 92.715 | 10.008 | 82.707 | 314.236 |
| | | 3 | 3 | 368.1 | 366.4 | 762.8 | 0.4826 | | 36.055 | | 95.087 | 11.895 | 83.192 | 316.079 |
| $N_2$ | Open | 3 | 2 | 456.6 | 454.6 | 763.2 | 0.5983 | | 32.513 | 0.0315 | 98.629 | 14.842 | 83.787 | 318.340 |
| | | 2 | 2 | 536.0 | 533.6 | 763.1 | 0 7024 | | 29.190 | (as average) | 101.952 | 17.509 | 84.443 | 320.832 |
| | | 1 | 2 | 600.8 | 598.1 | 762.4 | 0.7880 | | 26.291 | | 104.851 | 19.706 | 85.145 | 323.499 |
| | open | 1 | 2 | 600.8 | 645.1 | 763.1 | 0.8490 | | - | | - | 21.318 | 85.977 | 326.660 |
| | closed | 1 | 2 | 545.0 | 542.5 | - | - | | 23.847 | | 107.295 | - | | |
| | open | 1 | ? | 689.6 | 686.5 | 762.9 | 0.9039 | | - | | - | 22.745 | 87.227 | 331.410 |
| | closed | 1 | 2 | 483.8 | 481.6 | - | - | | 21.170 | | 109.972 | - | | |
| | open | 1 | ? | 721.1 | 717.8 | 762.6 | 0.9456 | | - | | - | 23.829 | 89.079 | 338.446 |
| | closed | 1 | 1 | 741.9 | 738.6 | - | - | | 18.234 | | 112.908 | - | | |
| | open | 1 | 0 | 740.0 | 736.7 | 762.8 | 0.9701 | | 14.119 | | 117.023 | 24.485 | 92.538 | 351.588 |
| | open | 1 | 0 | 755.9 | 752.5 | 762.6 | 0.9912 | | - | | - | 25.035 | 94.330 | 358.397 |
| | closed | 1 | 0 | 617.3 | 614.5 | - | - | | 11.777 | | 119.365 | - | | |

# APPENDIX II.3

## Nitrogen Adsorption Isotherms

fig.(i) Nitrogen Adsorption Isotherm for Colombia LCK 12/28

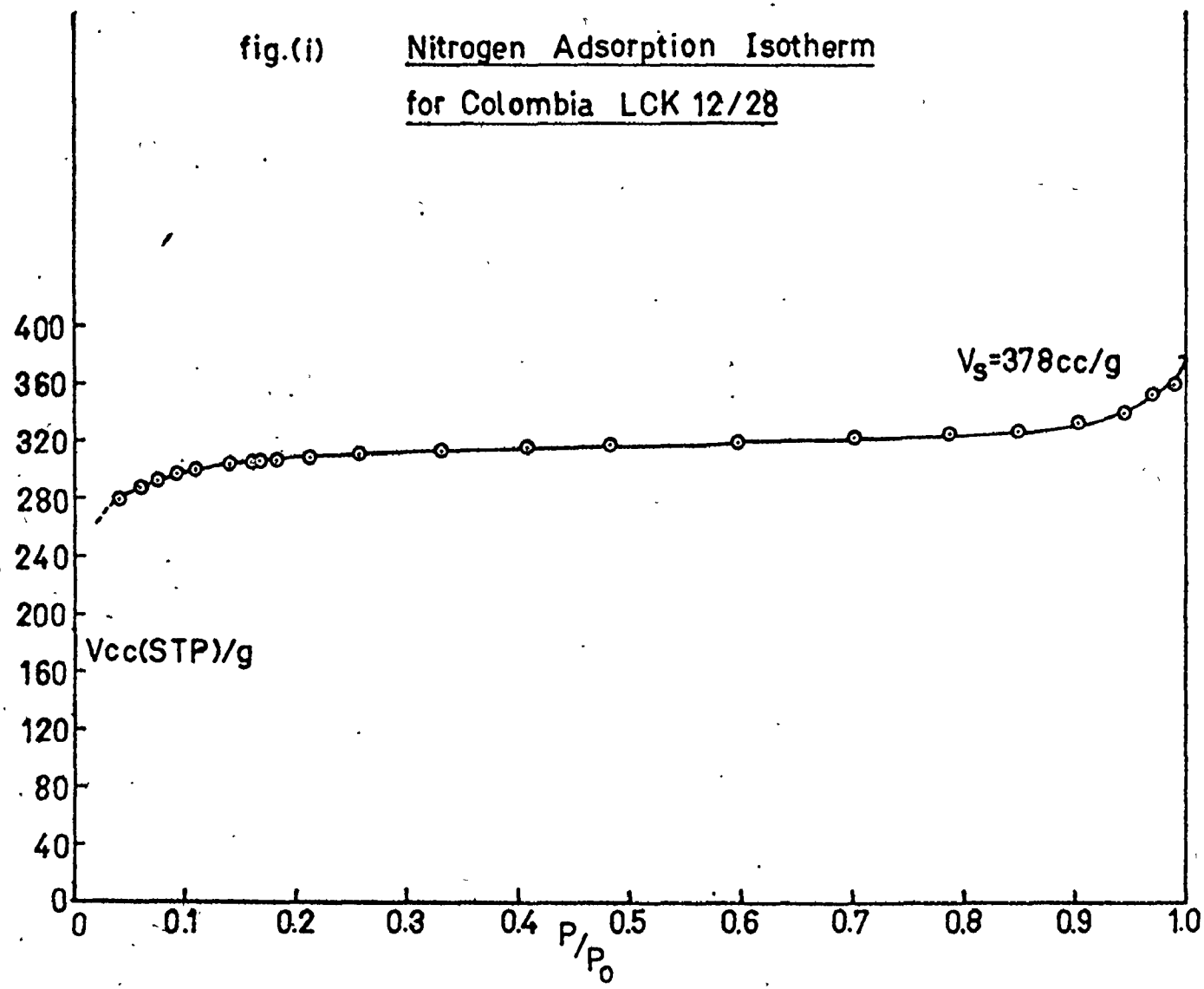

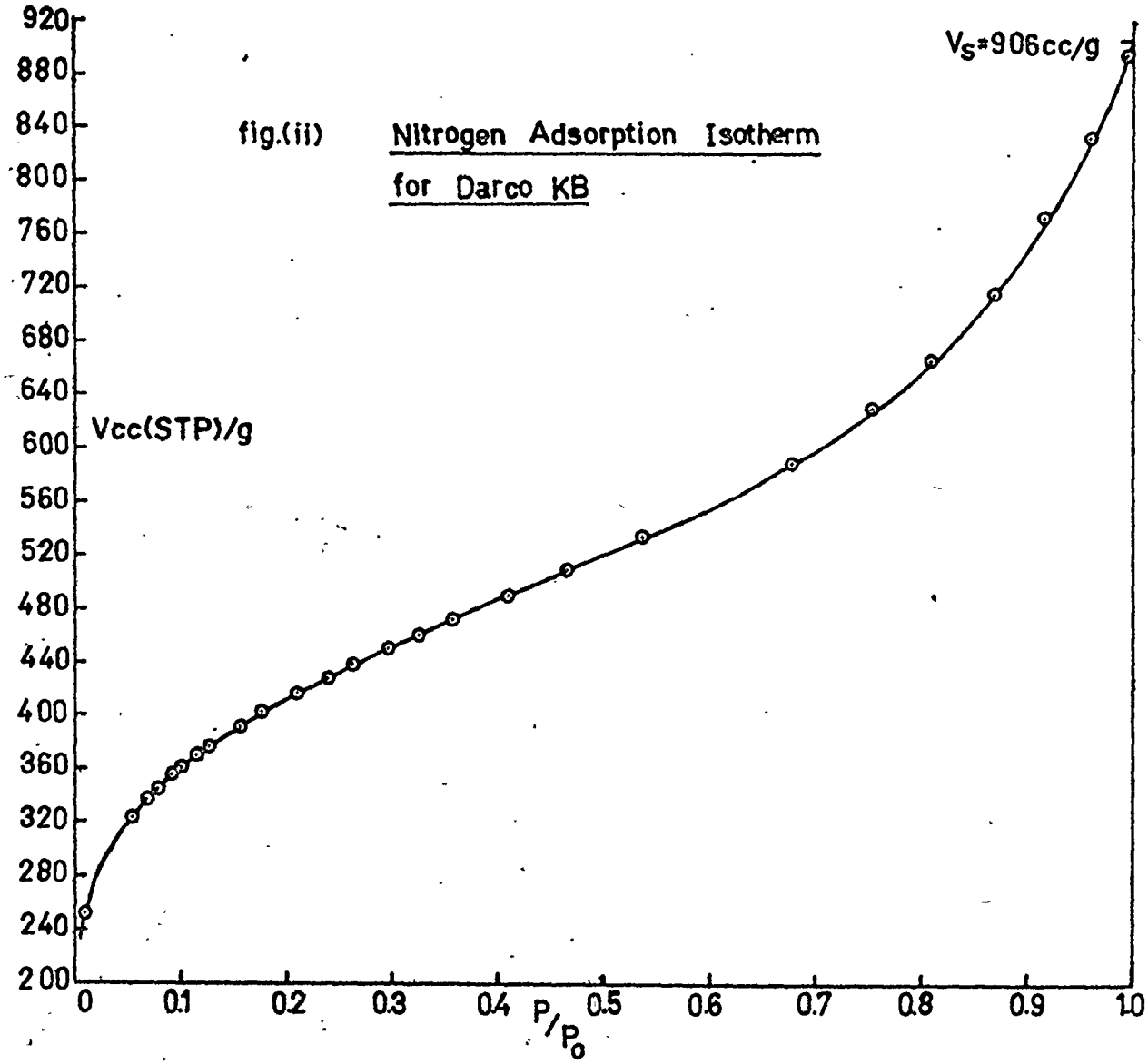


fig.(ii) Nitrogen Adsorption Isotherm for Darco KB

fig.(iii) Nitrogen Adsorption Isotherm for Darco S-51

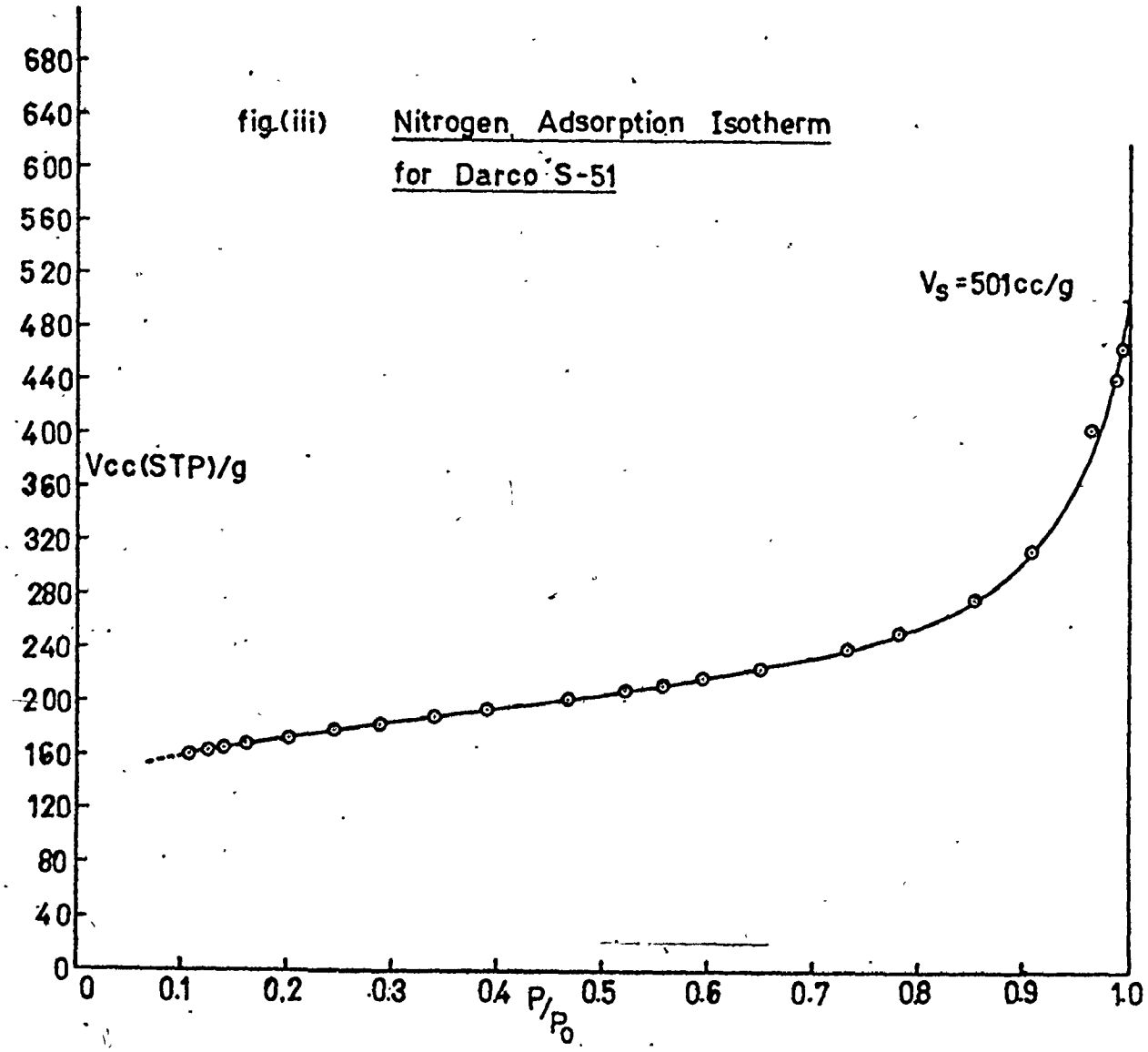

fig.(iv) Nitrogen Adsorption Isotherm for Darco Granular 12x20

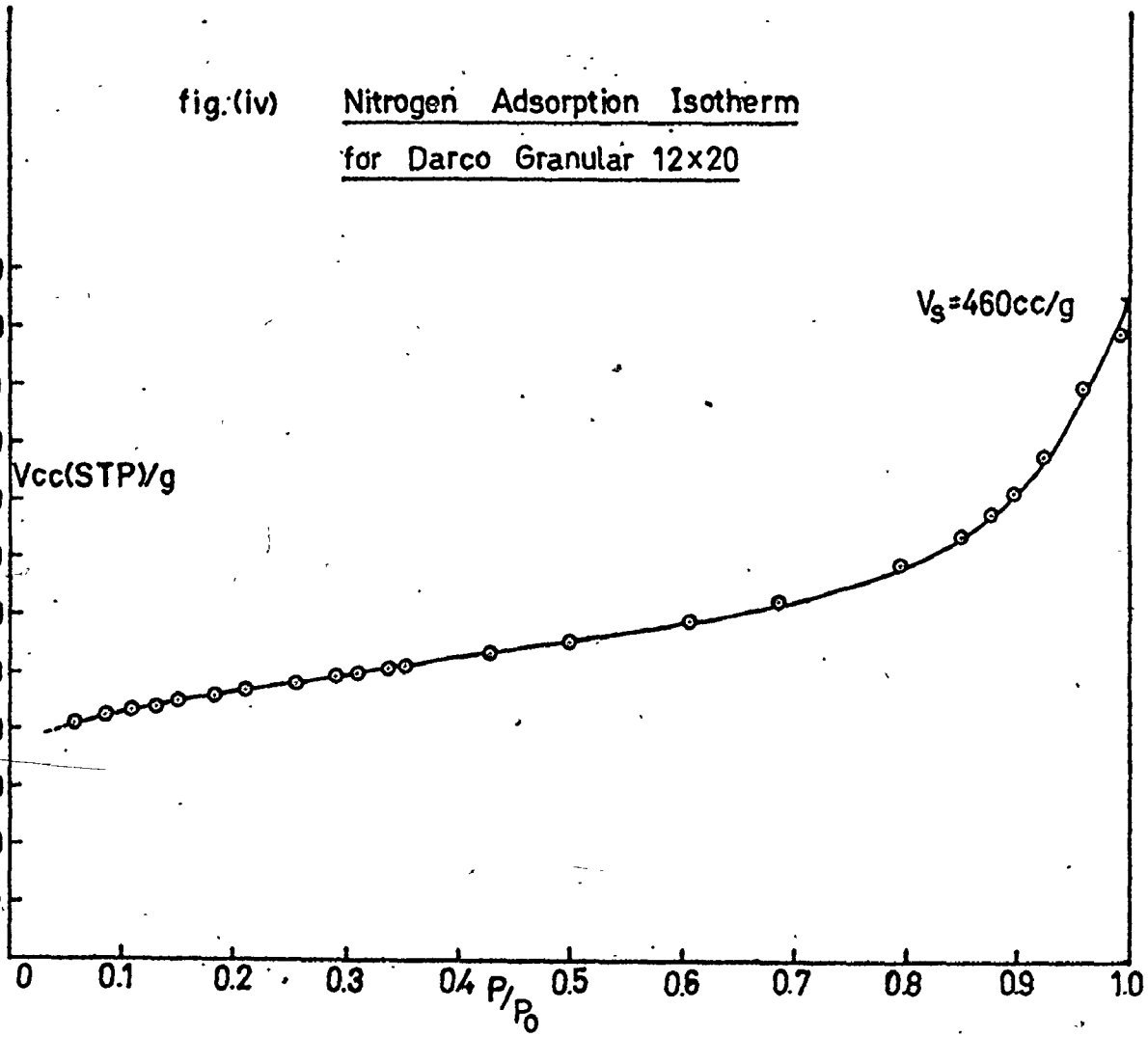

fig.(v) Nitrogen Adsorption Isotherm for Darco 12x20 pulverised to 97.6% thro' 325 U.S. mesh

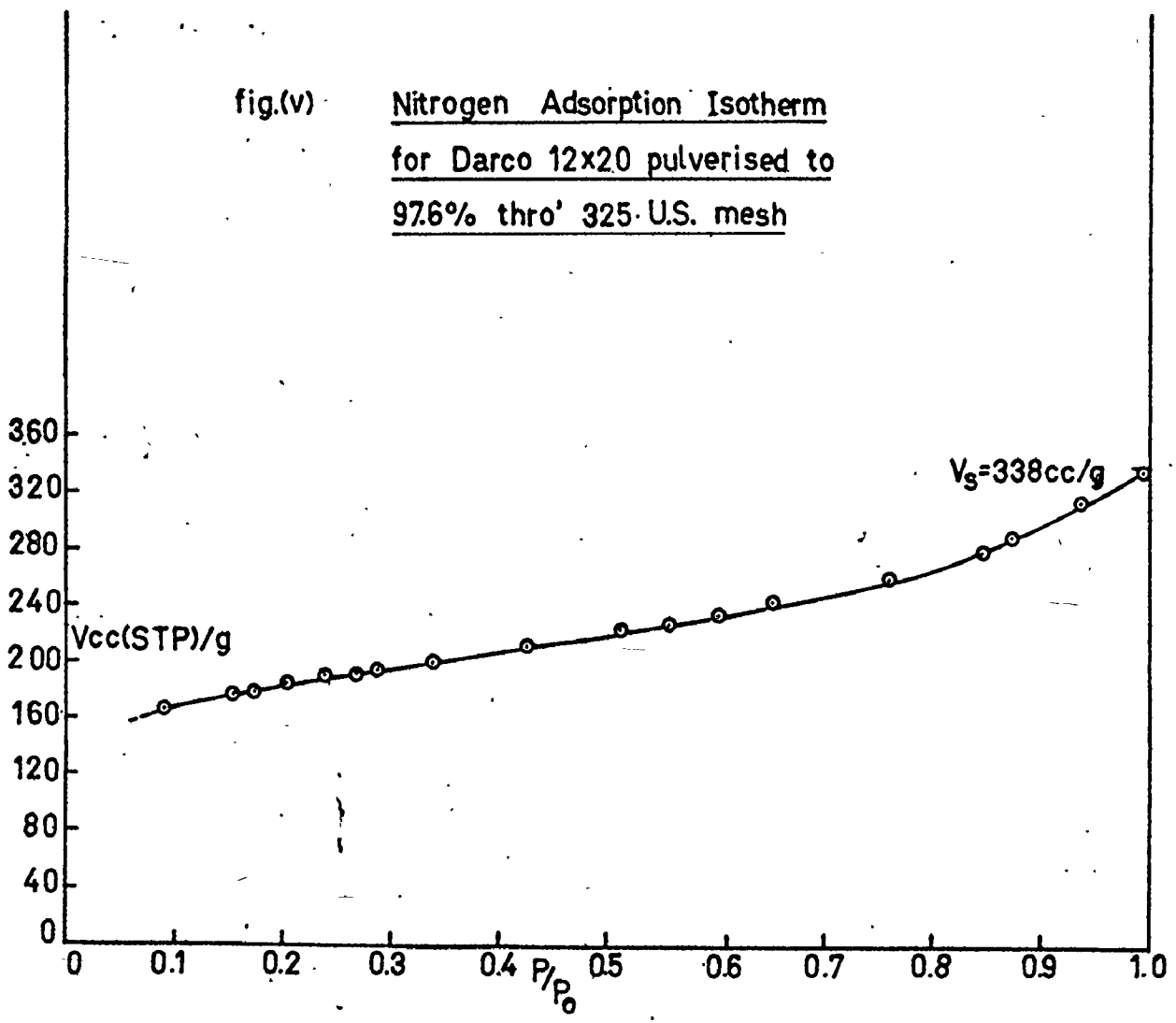

fig.(vi) Nitrogen Adsorption Isotherm for Filtrasorb 400

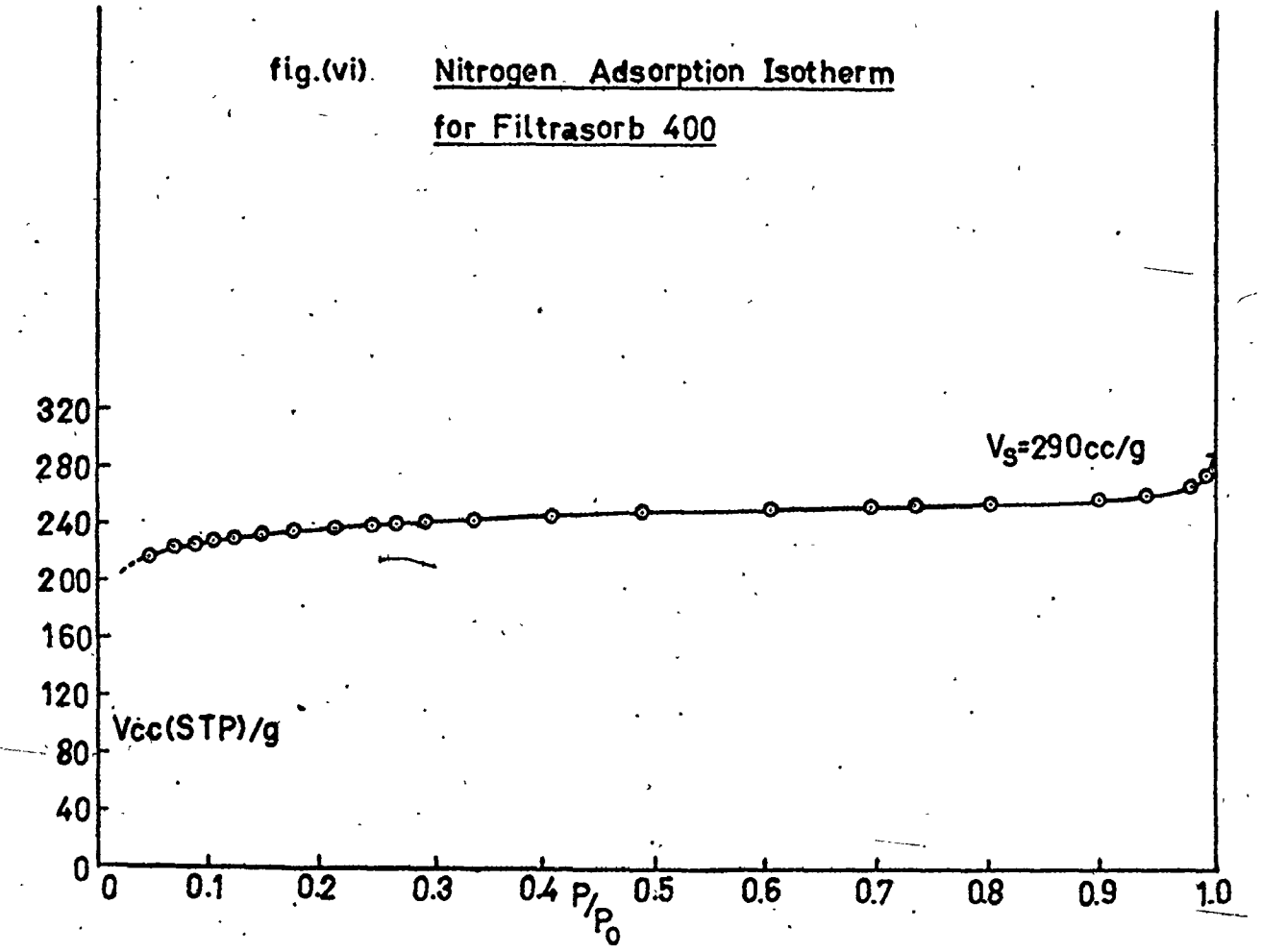

fig.(vii) Nitrogen Adsorption Isotherm for Nuchar Powdered Aqua A

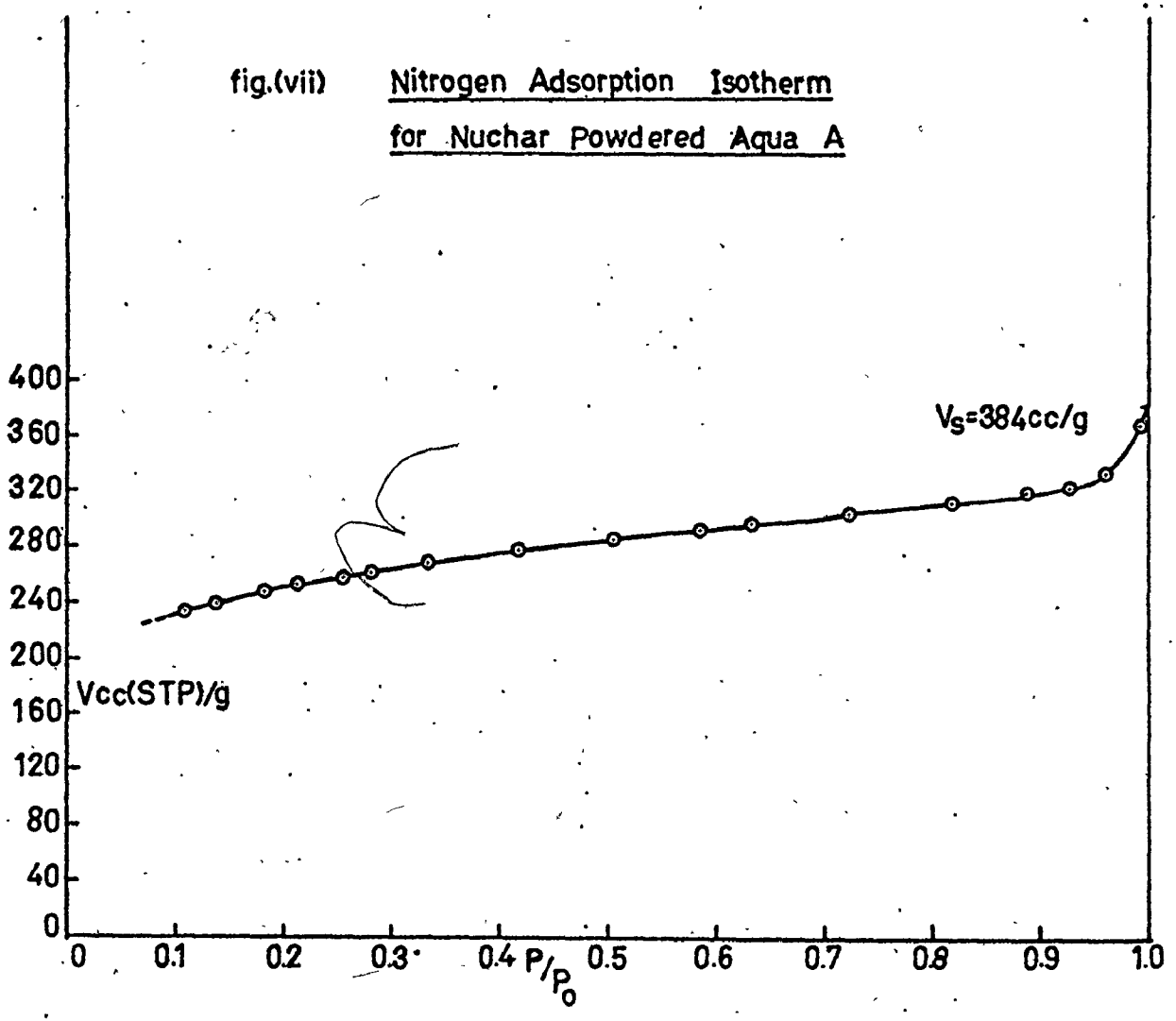

fig.(viii) Nitrogen Adsorption Isotherm for Nuchar Granular WV-G 12x40

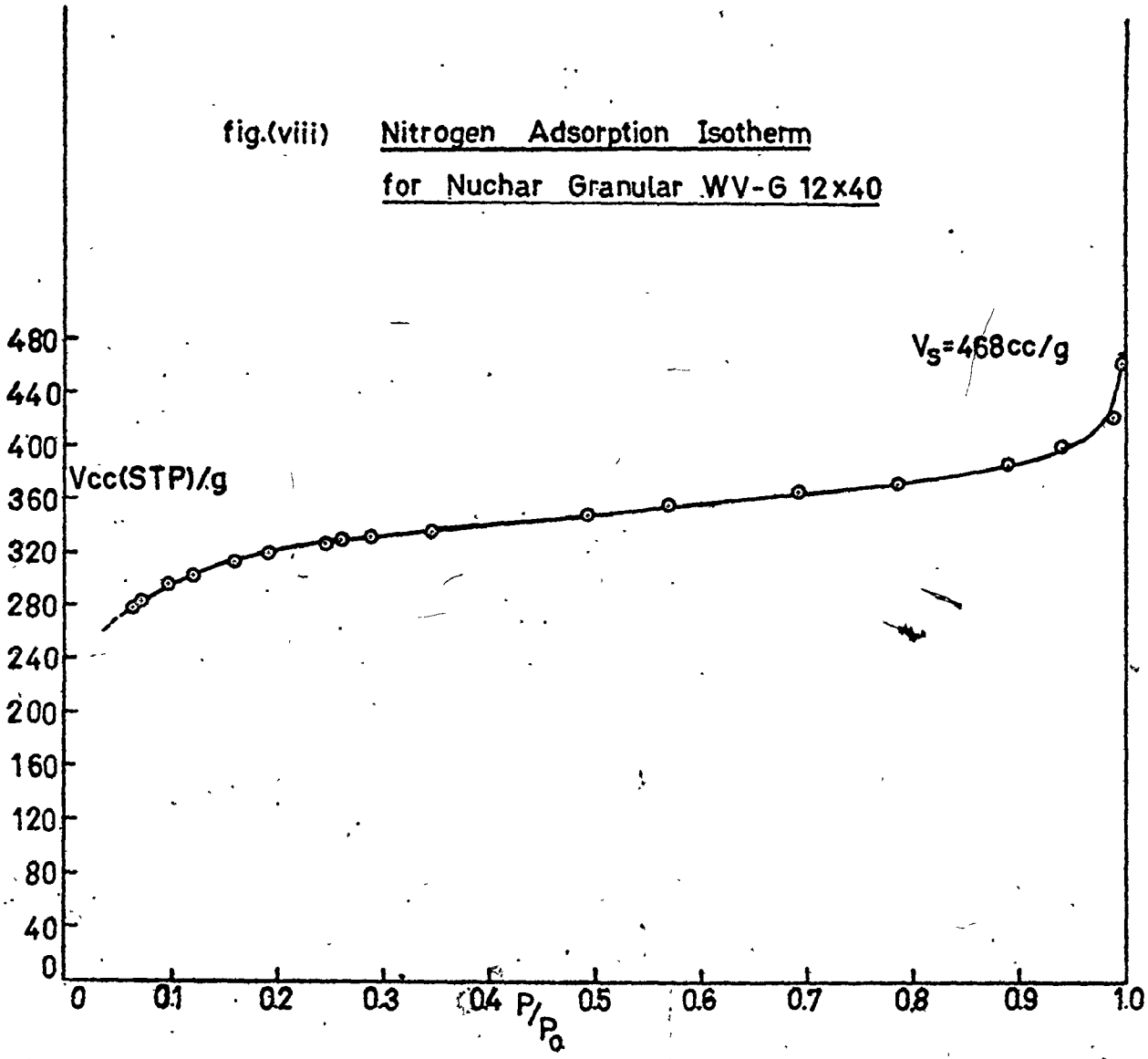

fig.(ix) Nitrogen Adsorption Isotherm for Special 'A' Carbon

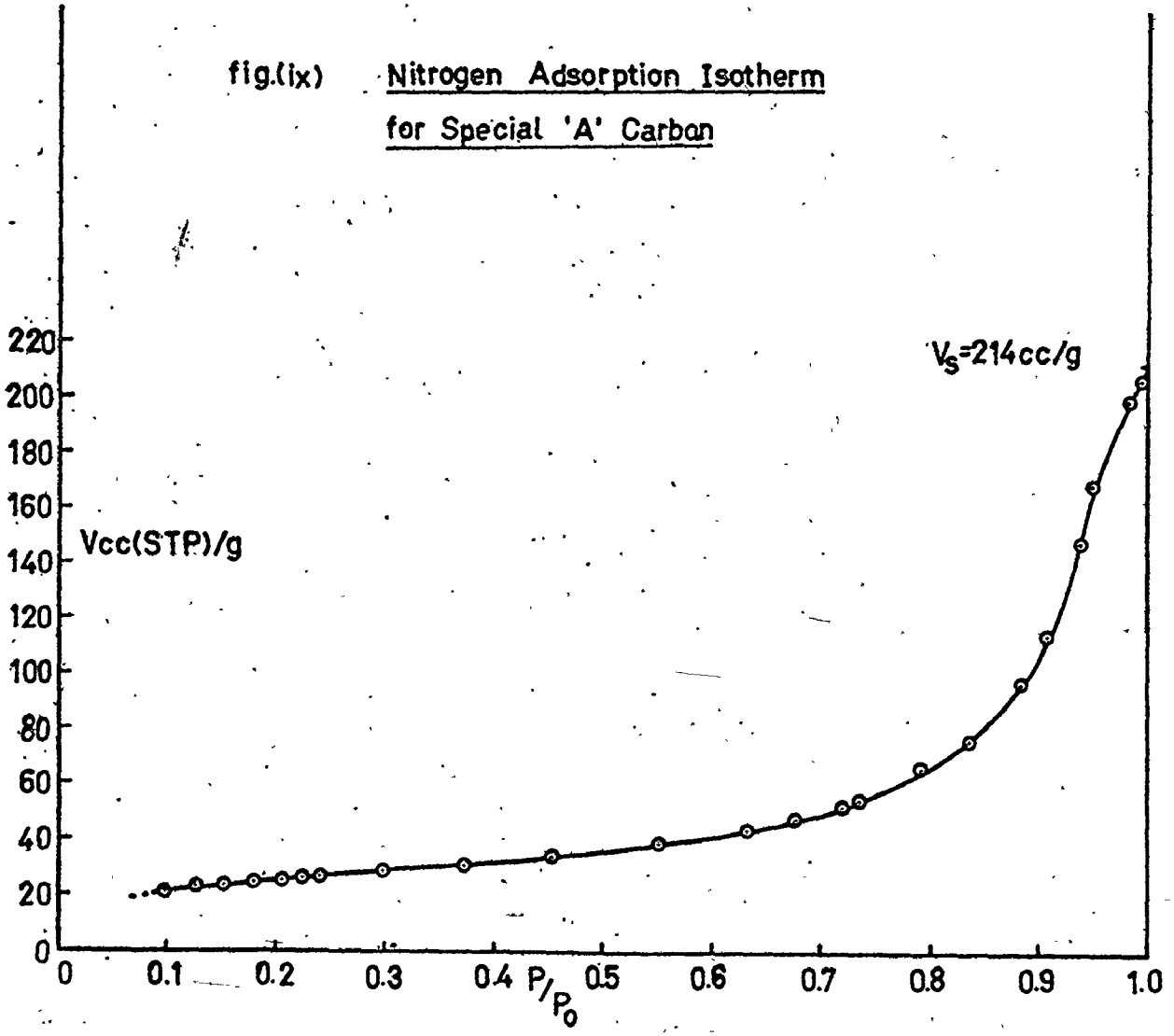

# APPENDIX II.4

## Carbon Pore Size Distributions With Respect to Surface Area

Fig.(i) Surface Area Distribution for Columbia LCK 12/28

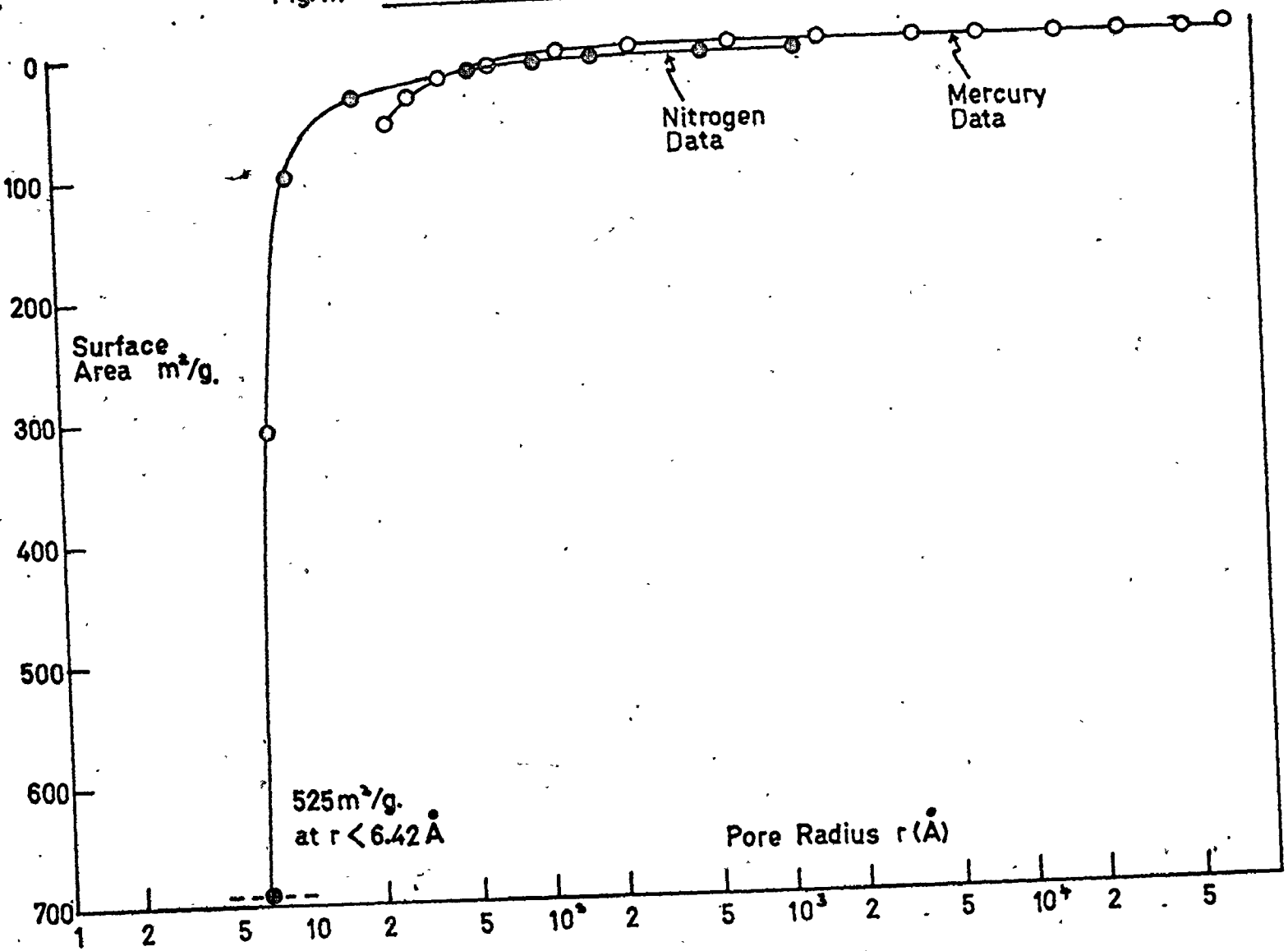

Fig.(ii) Surface Area Distribution for Darco KB

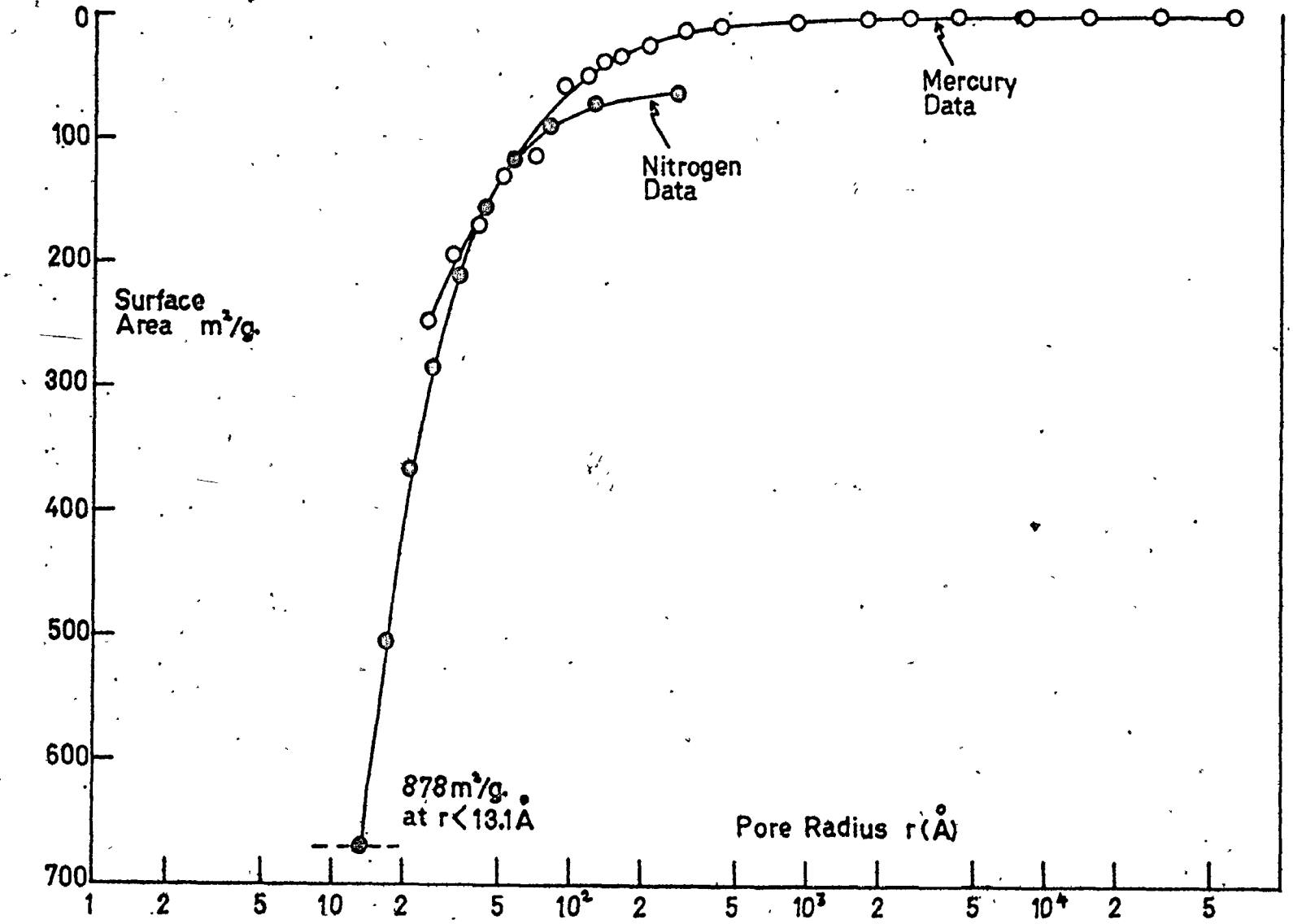

Fig.(iii) Surface Area Distribution for Darco S-51

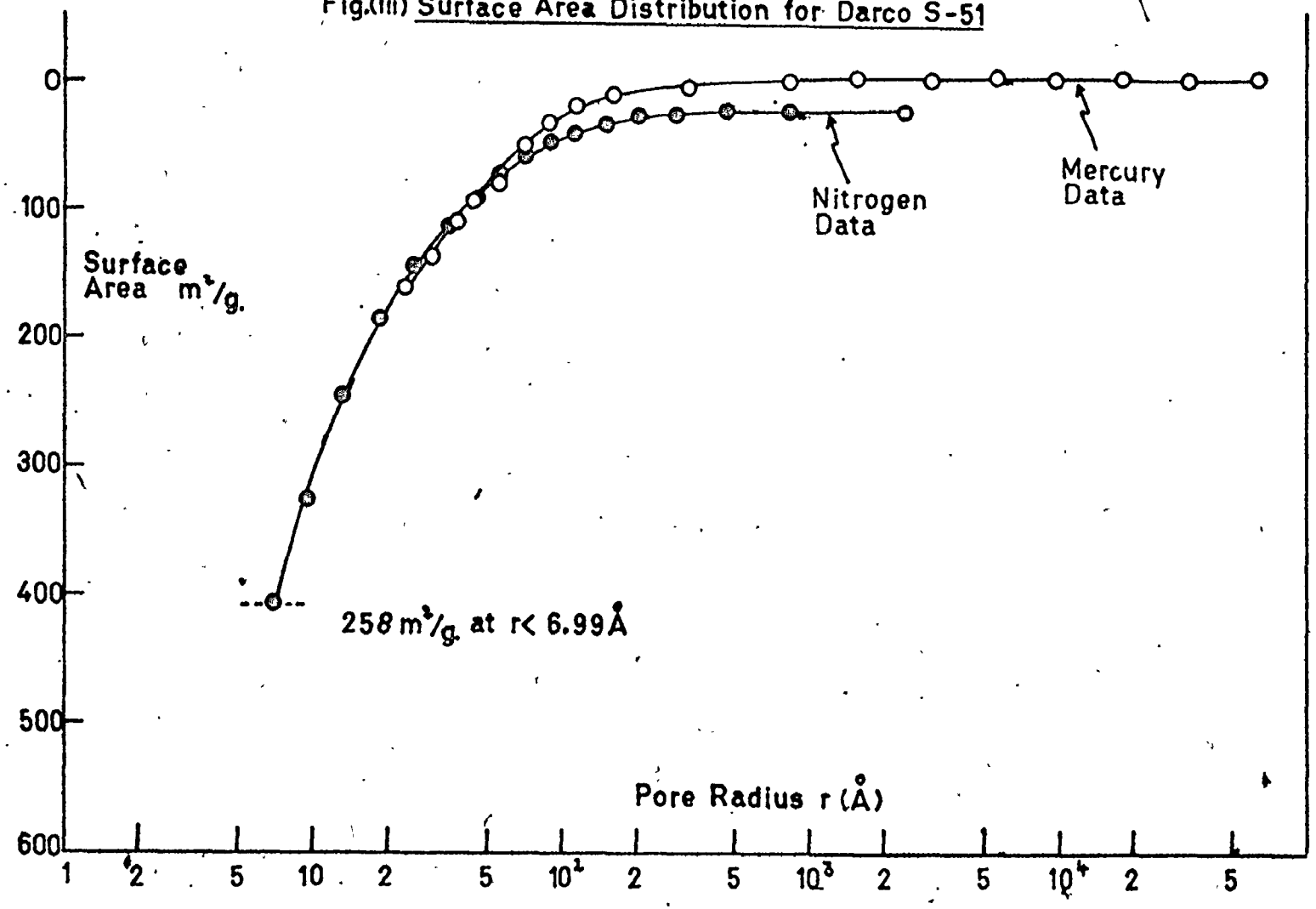

Fig.(iv) Surface Area Distribution for Darco 12×20

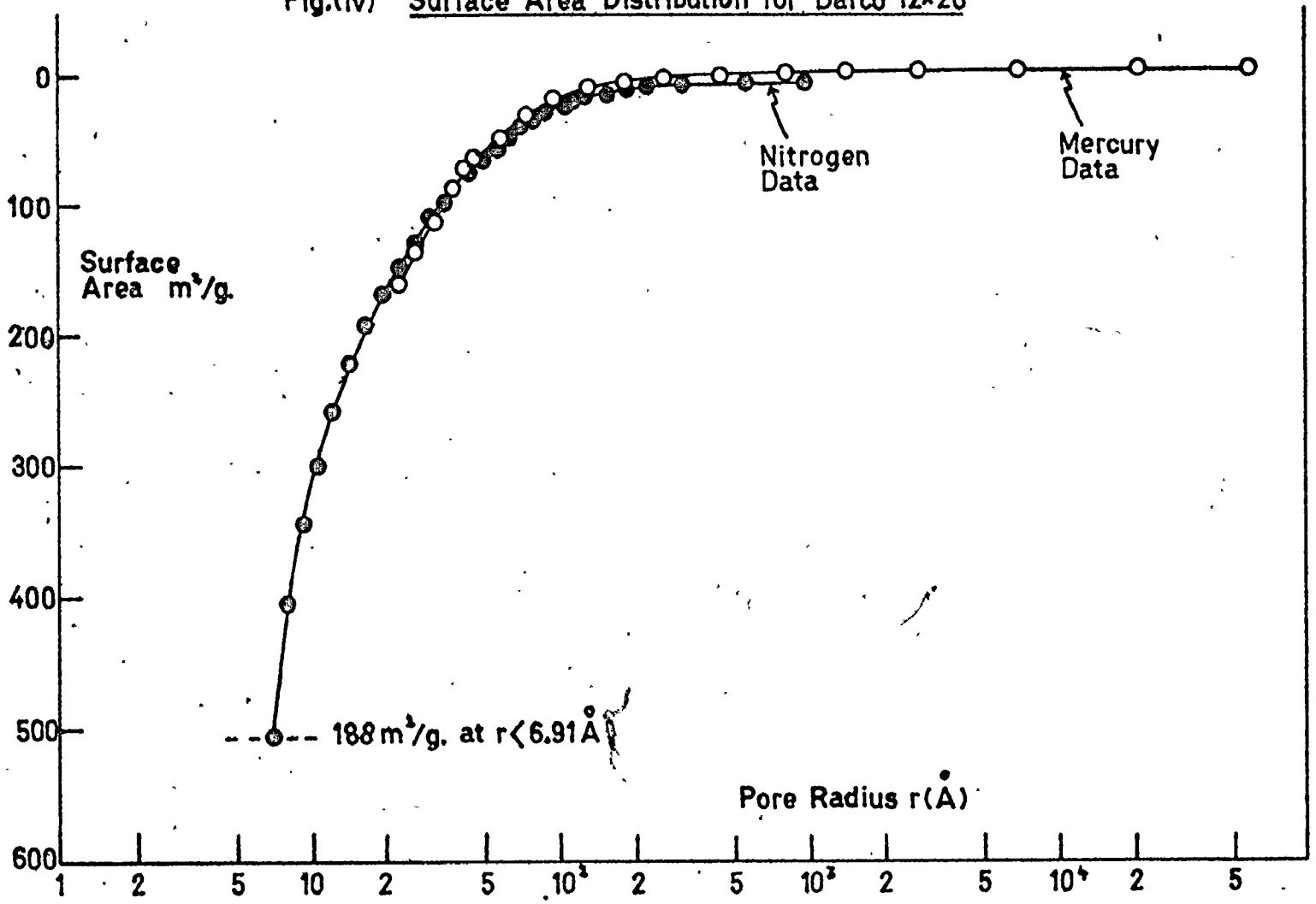

Fig. (v) Surface Area Distribution for Filtrasorb 400

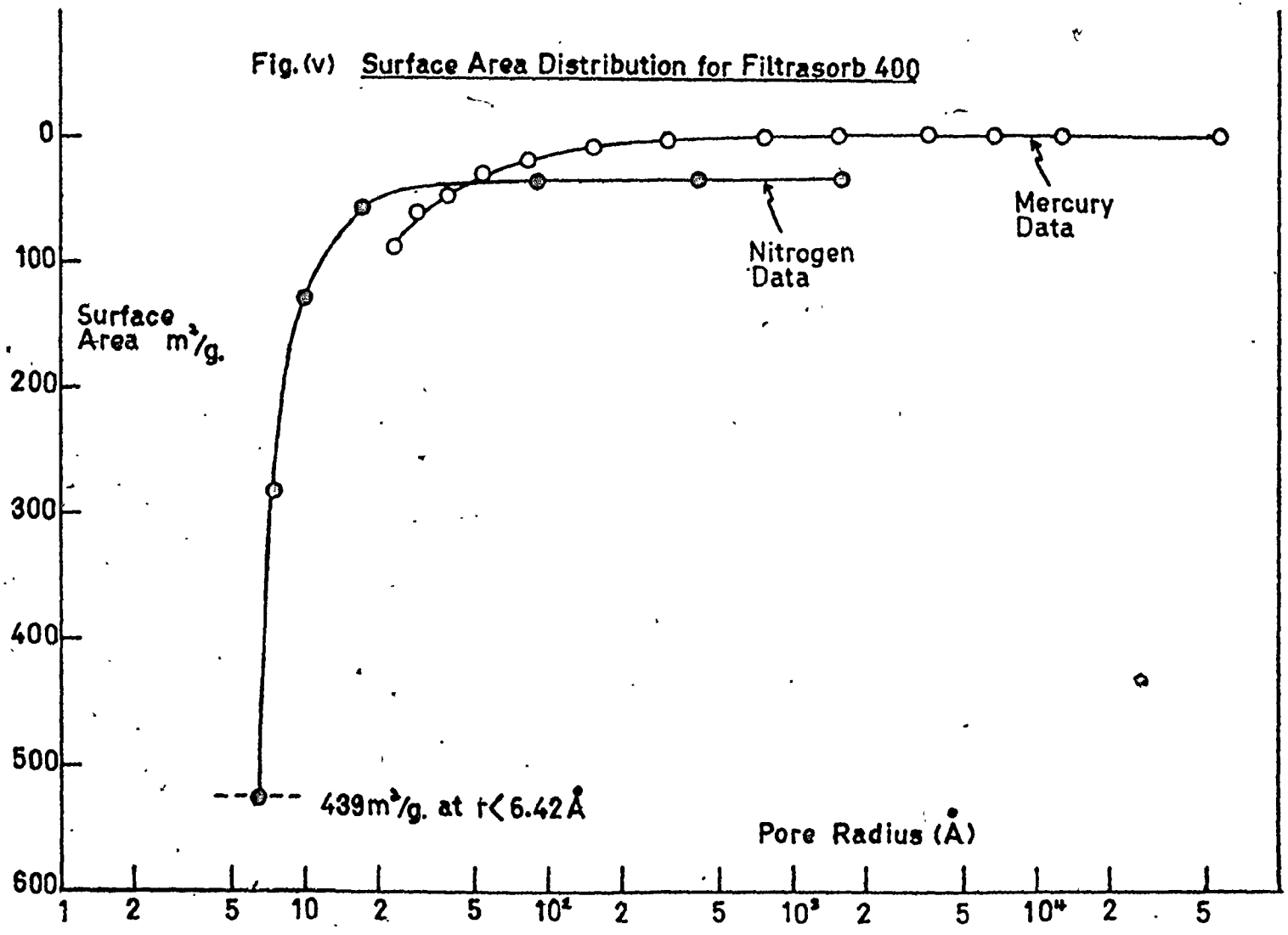

Fig.(vi) Surface Area Distribution for Nuchar Aqua A

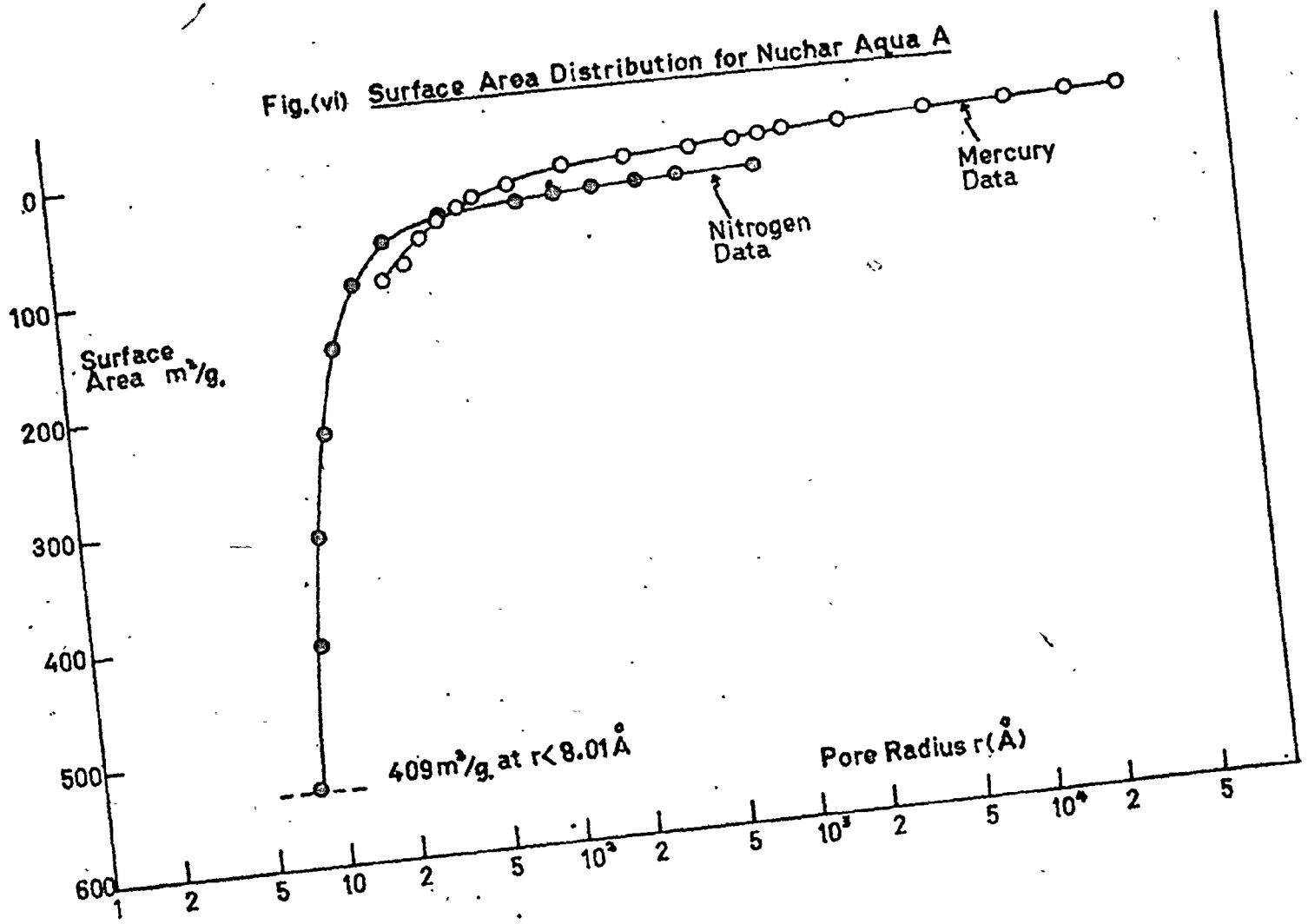

Fig.(vii) Surface Area Distribution for Nuchar WV-G 12×40

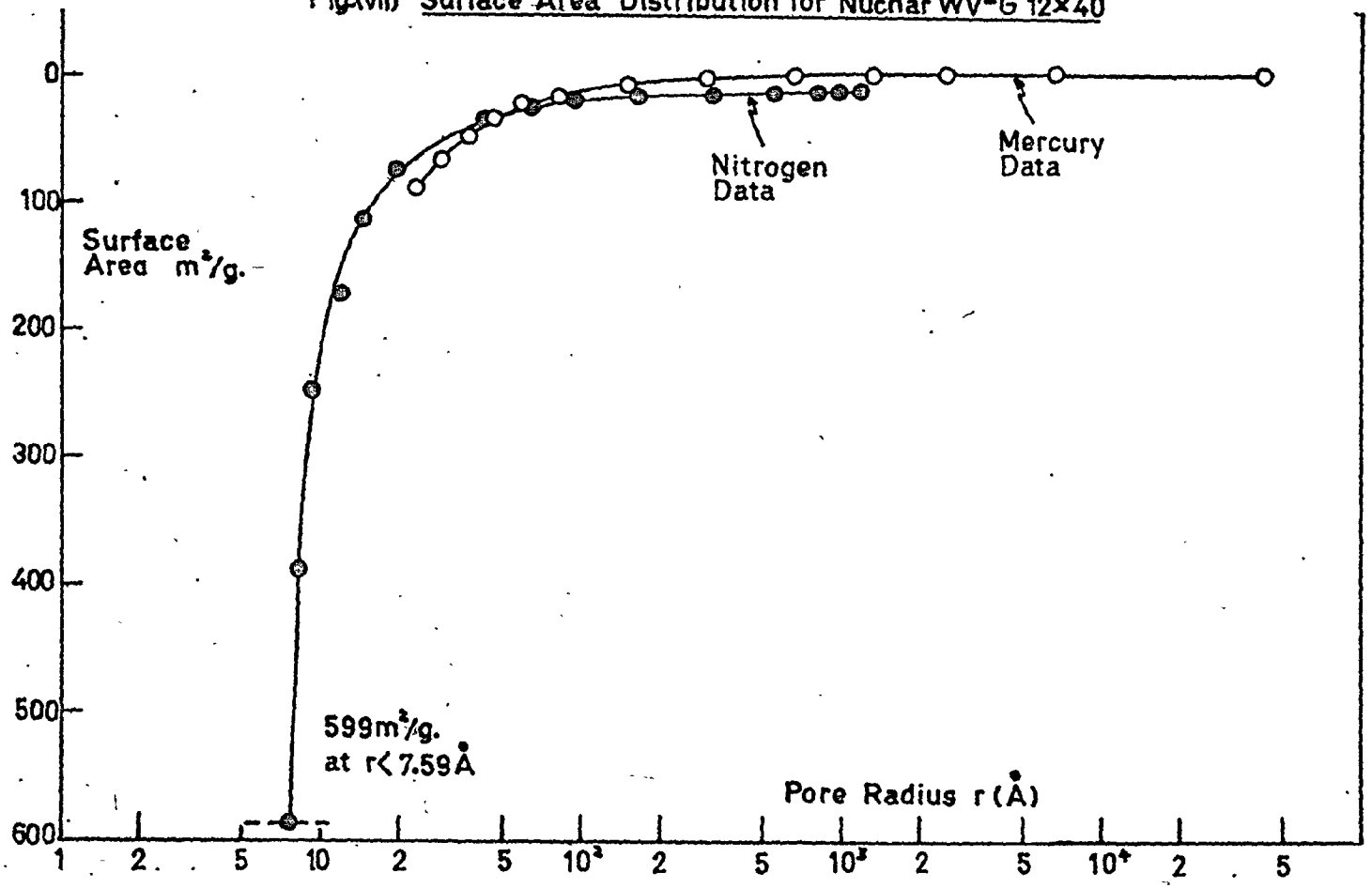

Fig.(viii) Surface Area Distribution for Special 'A'

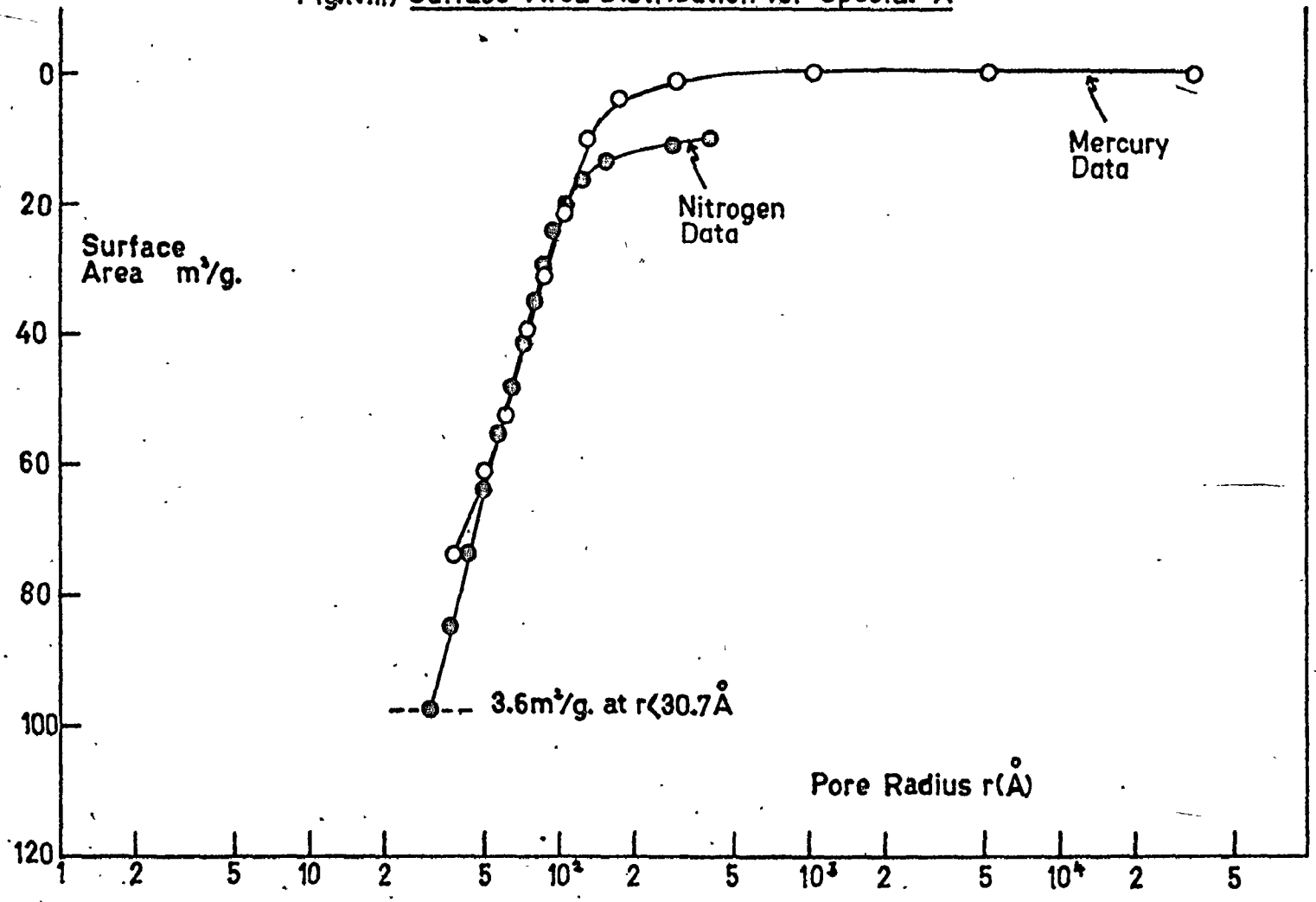

# APPENDIX II.5

## Carbon Pore Size Distributions

## With Respect to Pore Volume

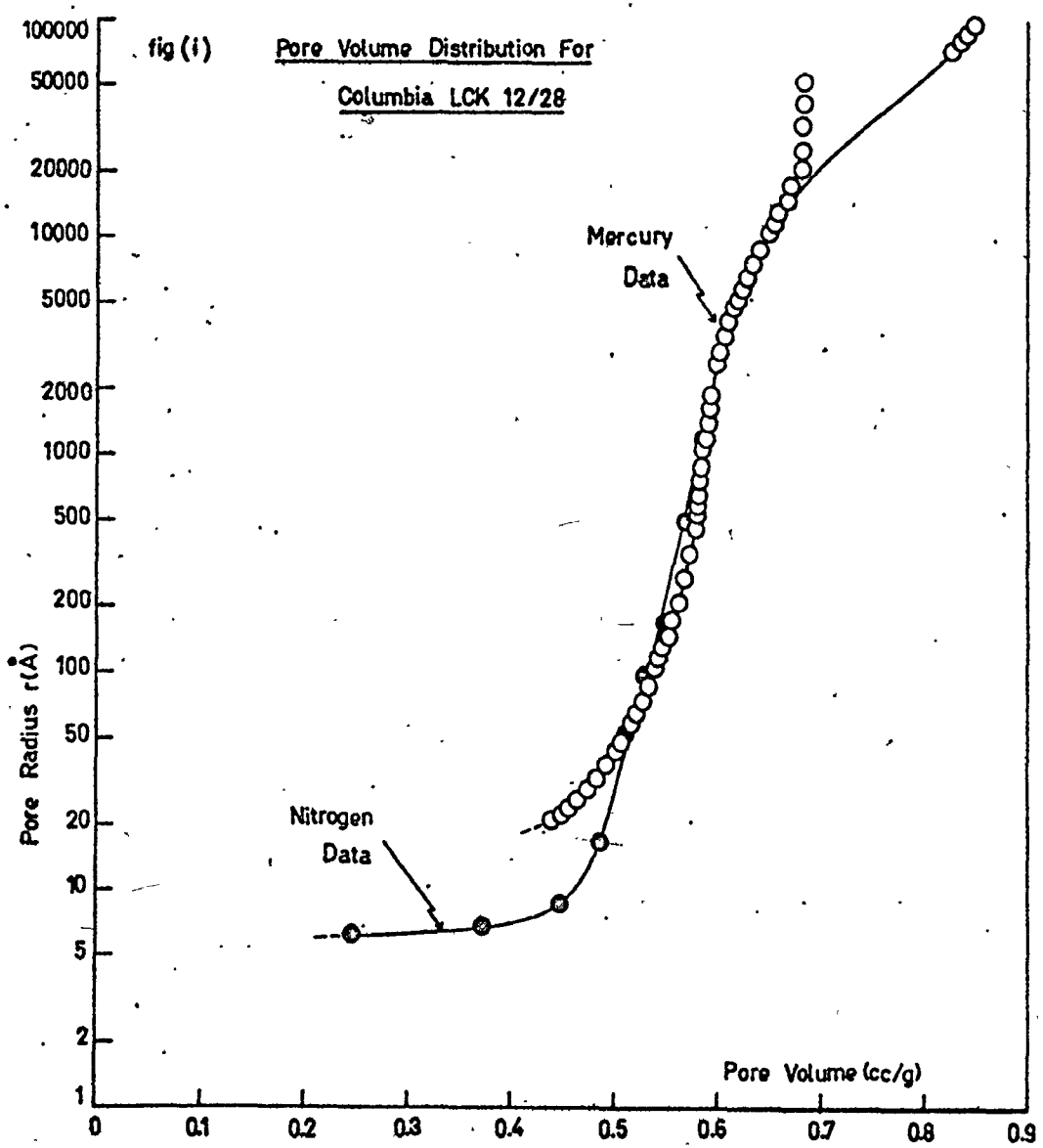
fig (i)
Pore Volume Distribution For
Columbia LCK 12/28
Mercury
Data
Nitrogen
Data
Pore Radius r(Å)
Pore Volume (cc/g)
100000
50000
20000
10000
5000
2000
1000
500
200
100
50
20
10
5
2
1
0
0.1
0.2
0.3
0.4
0.5
0.6
0.7
0.8
0.9

fig (ii) Pore Volume Distribution For Darco KB

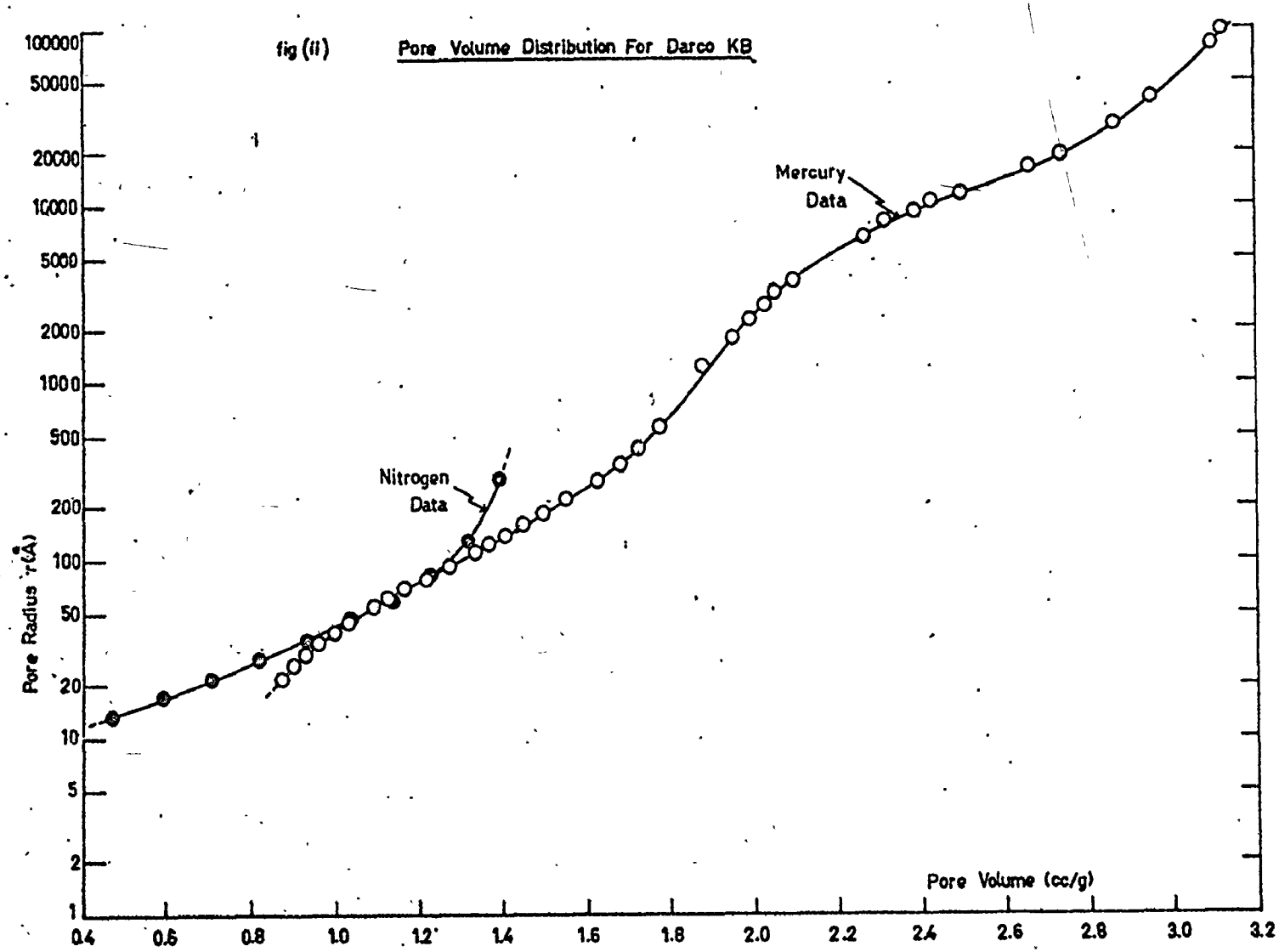

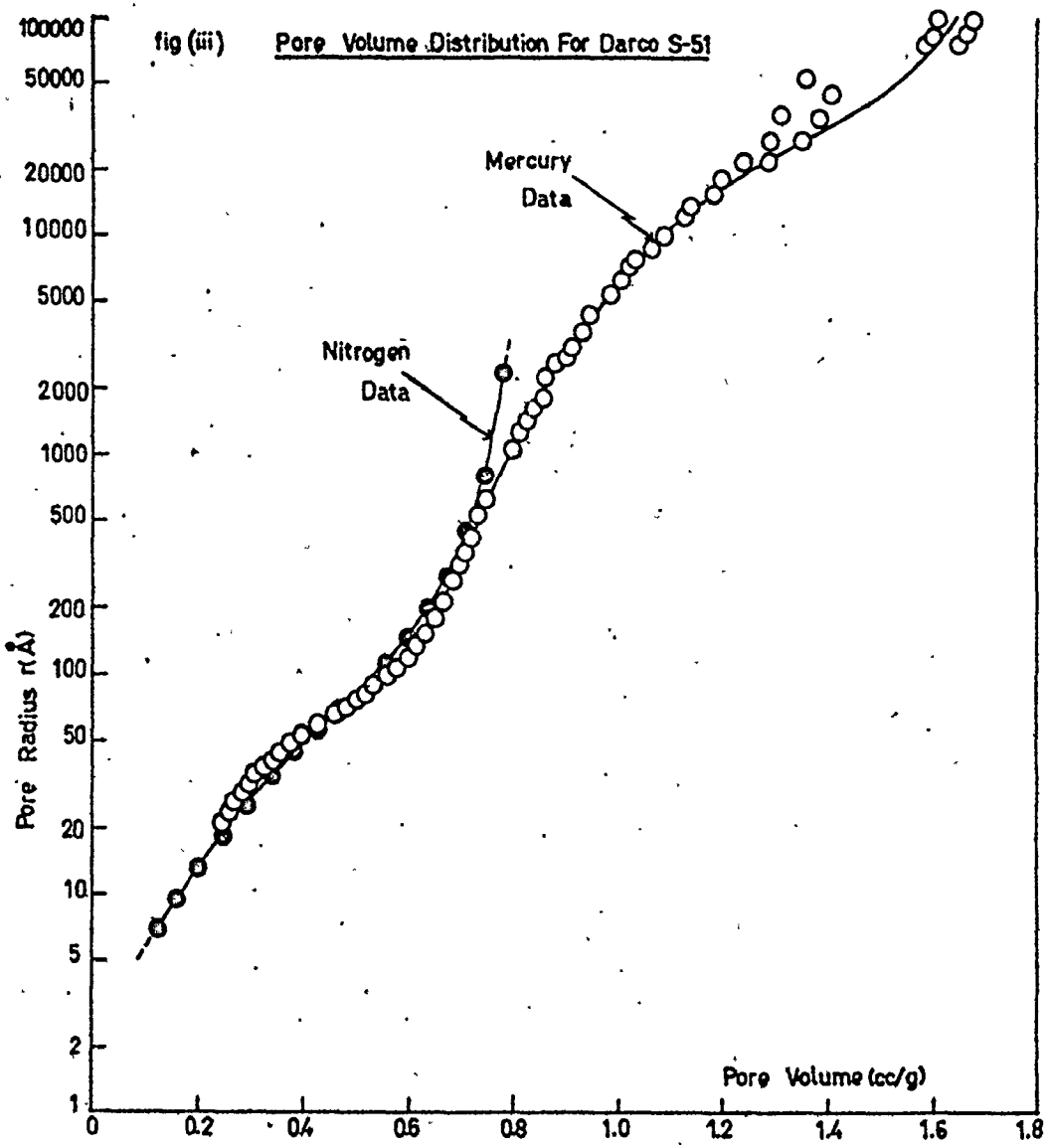
fig (iii) Pore Volume Distribution For Darco S-51
Mercury Data
Nitrogen Data
Pore Radius r(Å)
Pore Volume (cc/g)
100000
50000
20000
10000
5000
2000
1000
500
200
100
50
20
10
5
2
1
0
0.2
0.4
0.6
0.8
1.0
1.2
1.4
1.6
1.8

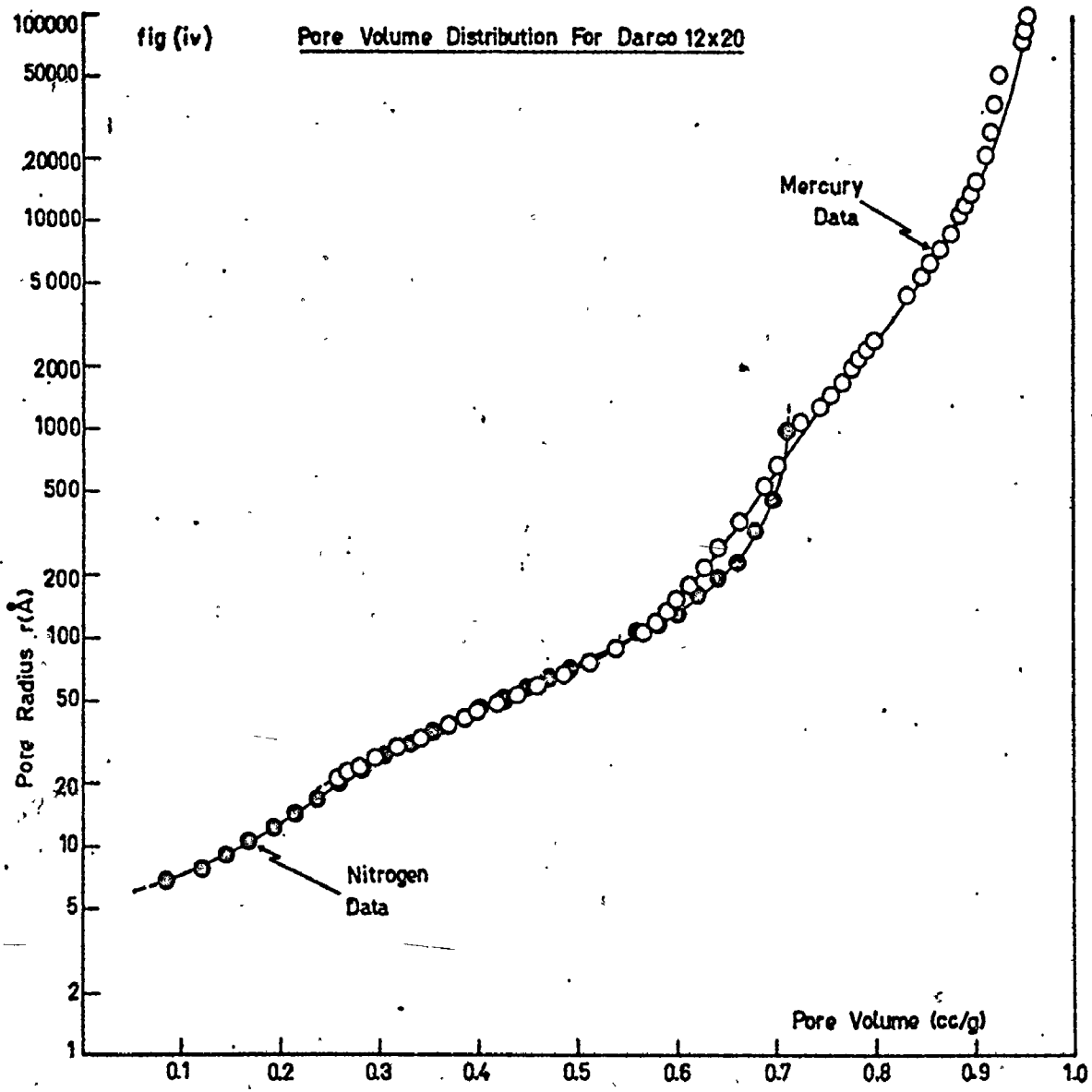
fig (iv)
Pore Volume Distribution For Darco 12x20
Pore Radius r(Å)
100000
50000
20000
10000
5000
2000
1000
500
200
100
50
20
10
5
2
1
Mercury Data
Nitrogen Data
Pore Volume (cc/g)
0.1
0.2
0.3
0.4
0.5
0.6
0.7
0.8
0.9
1.0

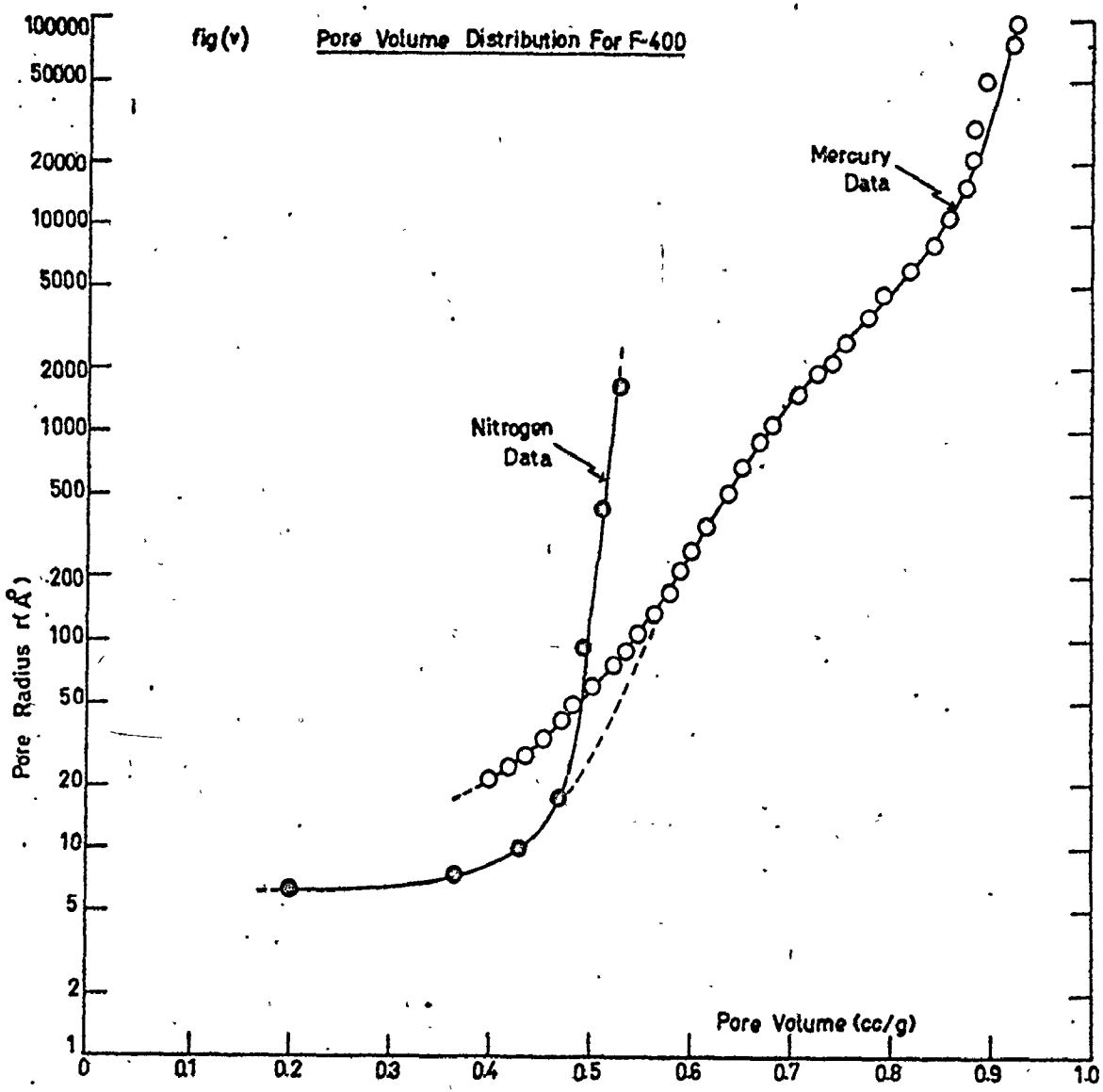
fig (v)
Pore Volume Distribution For F-400
Mercury Data
Nitrogen Data
Pore Radius r(Å)
Pore Volume (cc/g)
100000
50000
20000
10000
5000
2000
1000
500
200
100
50
20
10
5
2
1
0
0.1
0.2
0.3
0.4
0.5
0.6
0.7
0.8
0.9
1.0

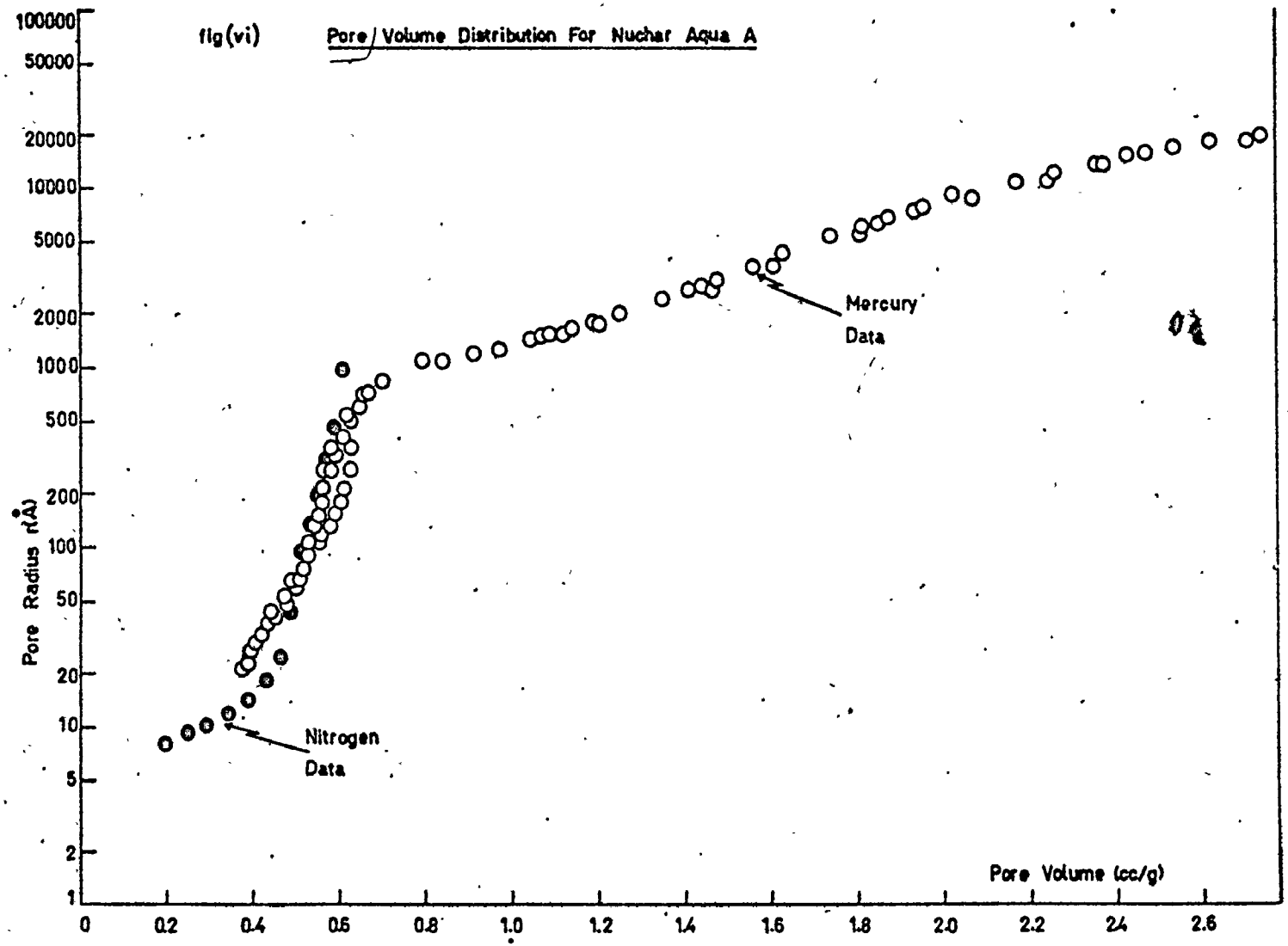
fig(vi)
Pore Volume Distribution For Nuchar Aqua A
Pore Radius r(Å)
100000
50000
20000
10000
5000
2000
1000
500
200
100
50
20
10
5
2
1
Mercury
Data
Nitrogen
Data
Pore Volume (cc/g)
0
0.2
0.4
0.6
0.8
1.0
1.2
1.4
1.6
1.8
2.0
2.2
2.4
2.6

fig (vii) Pore Volume Distribution For Nuchar Granular 12x40

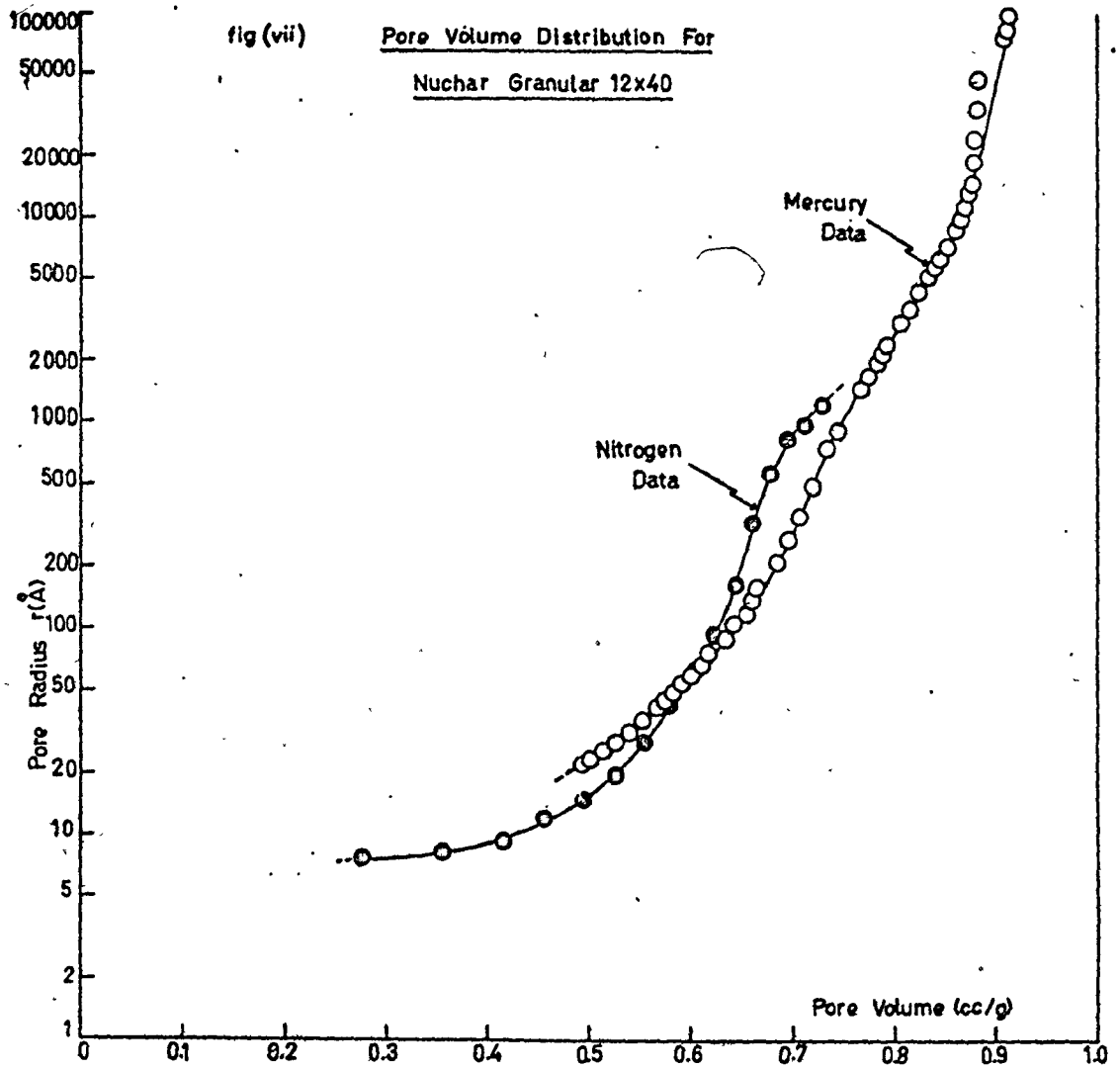

fig (viii) Pore Volume Distribution For Special 'A'

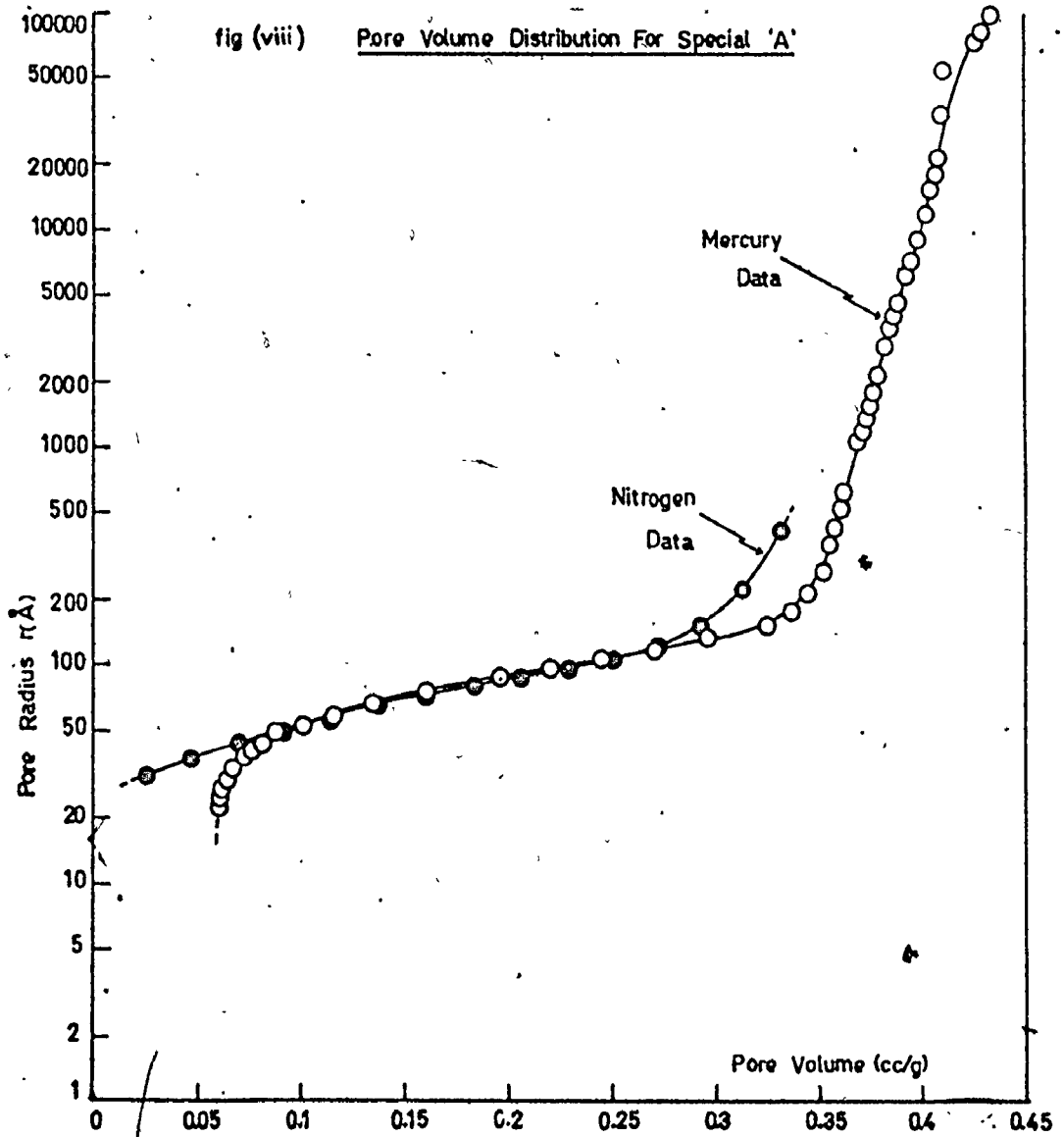

# APPENDIX II.6

## Mercury Compressibility Calibration

Fig. Mercury Compressibility Calibration

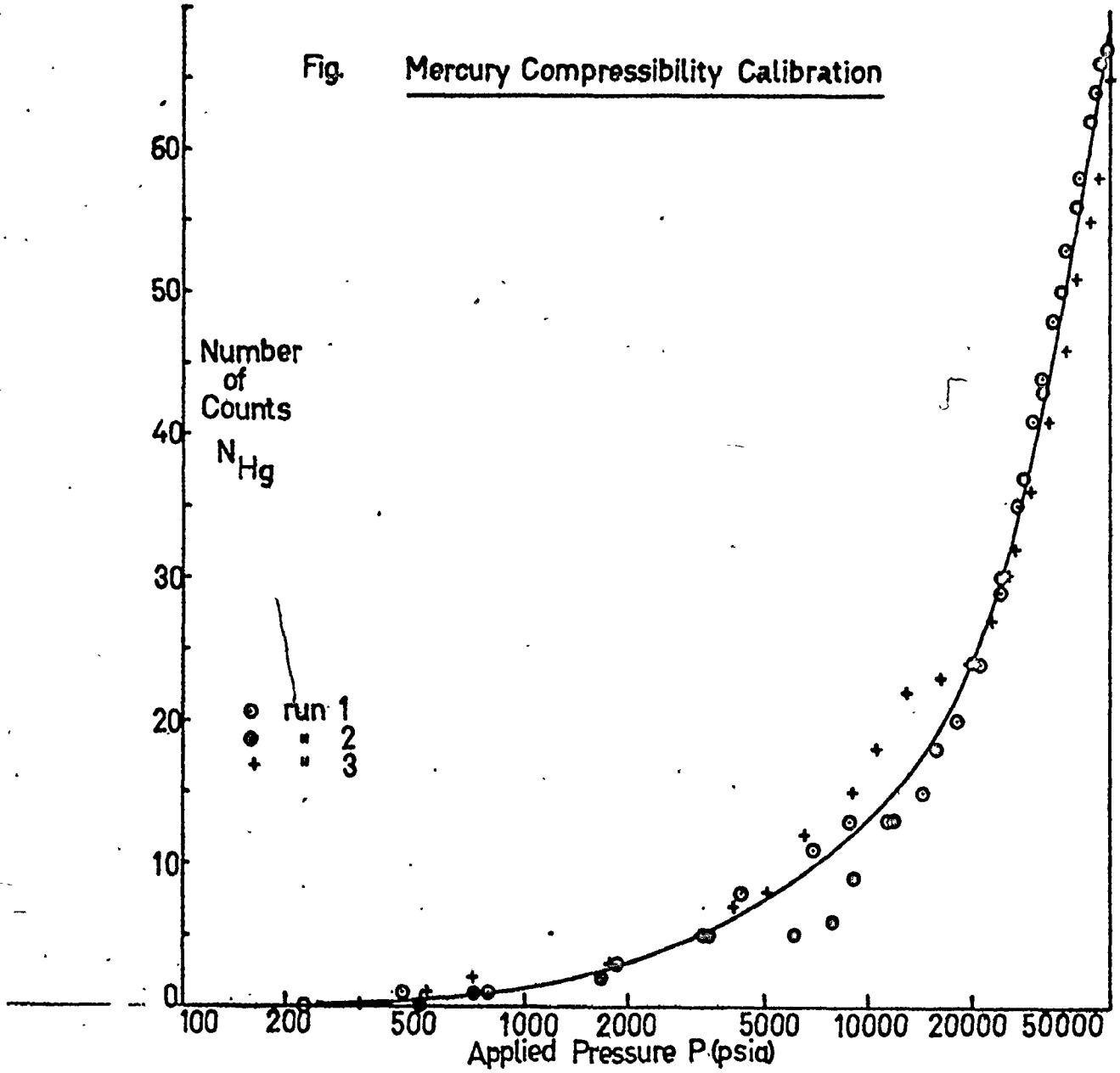

# APPENDIX II.7

## Mercury Penetration Data For the Carbons Studied

FIG.(1). MERCURY PENETRATION DATA FOR COLUMBIA LCK 12/28

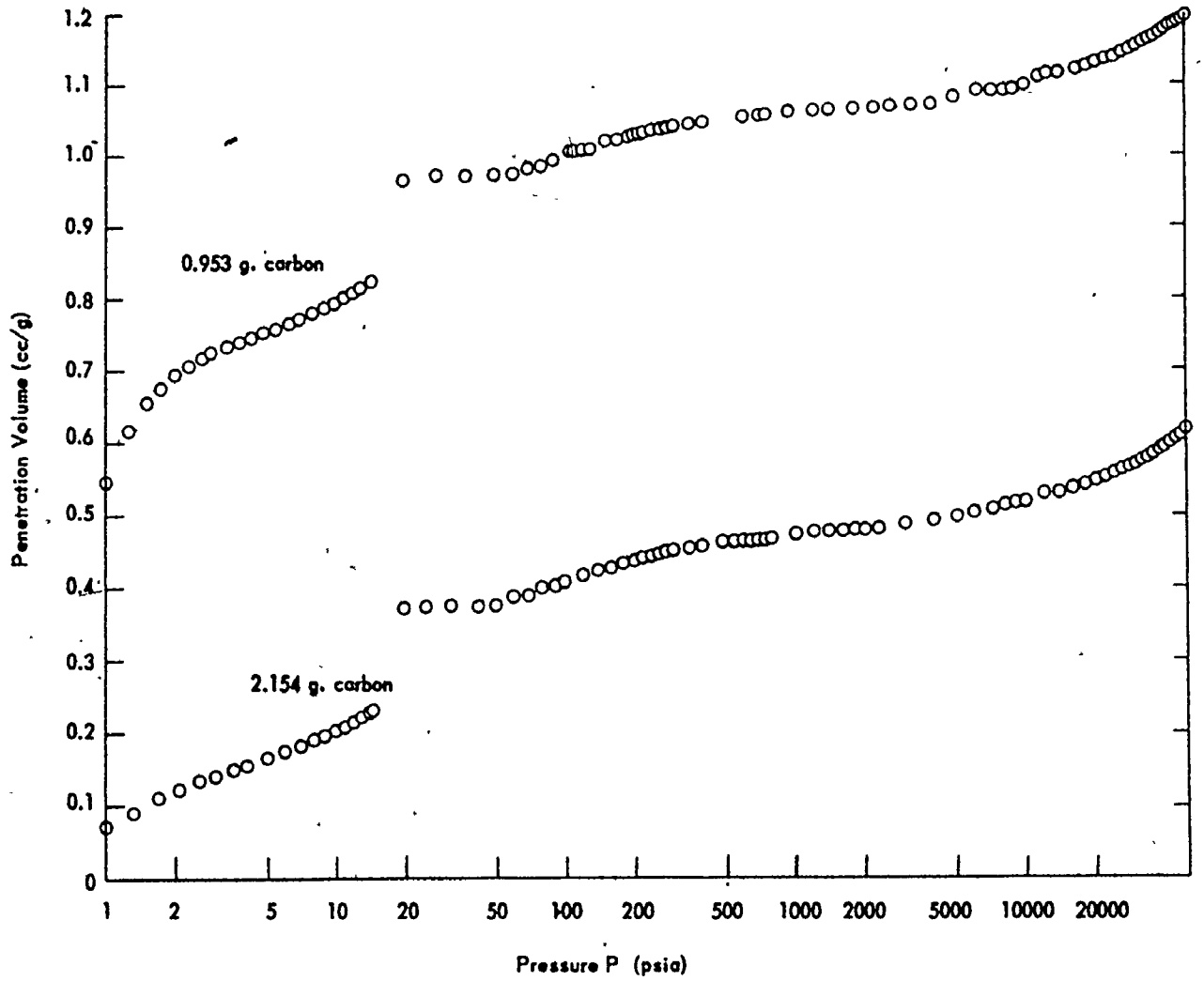

fig. (ii) Mercury Penetration Data For Darco KB

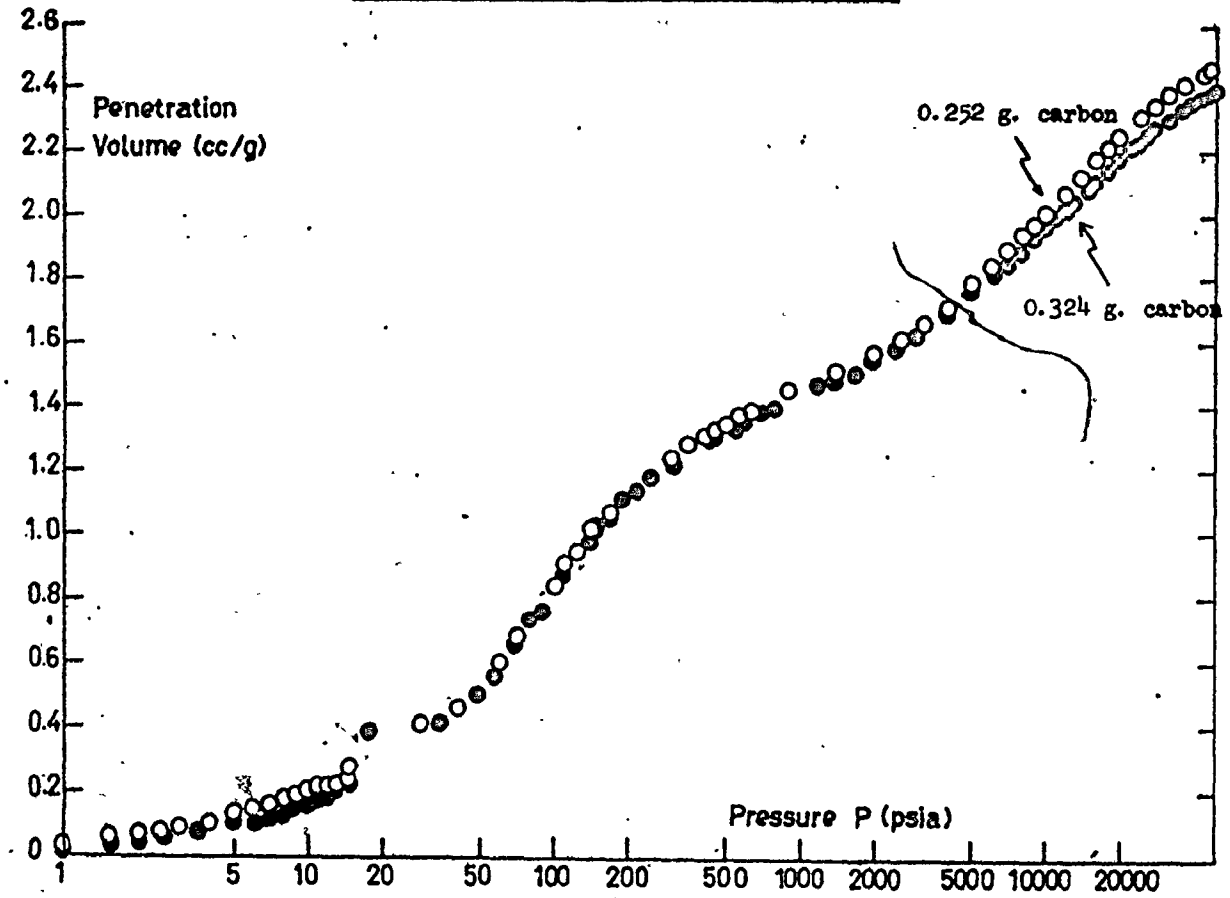

fig.(iii) Mercury Penetration Data For Darco S-51

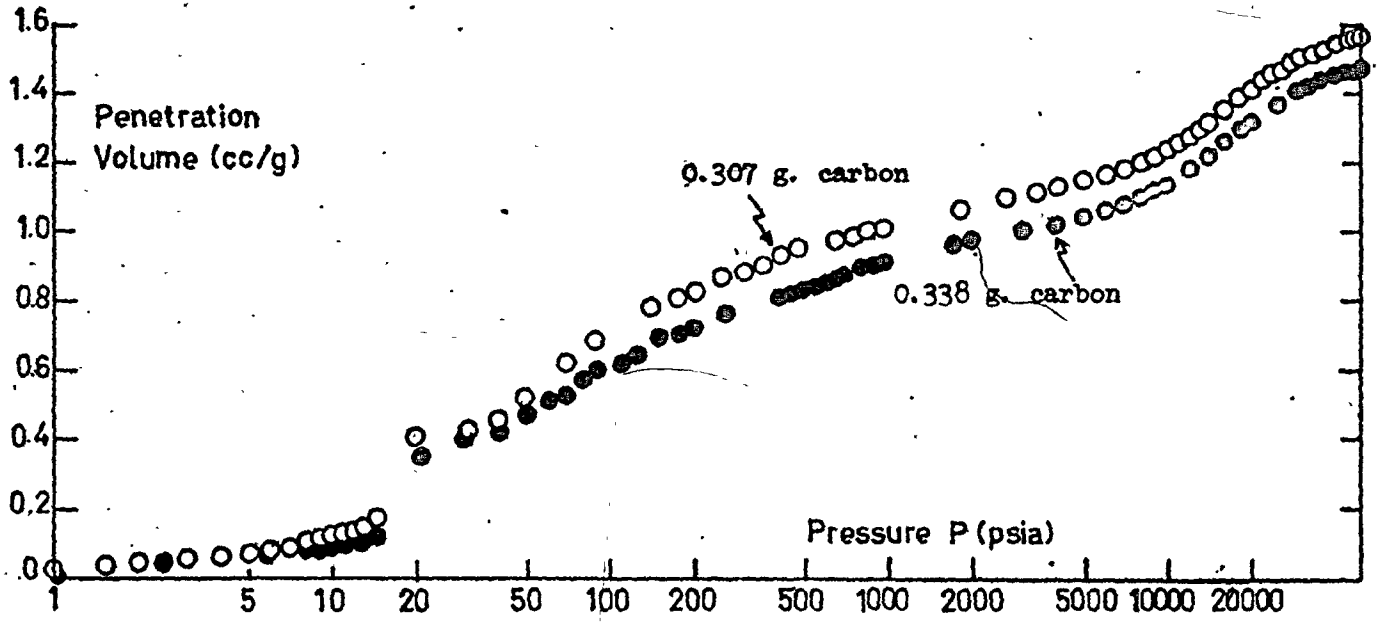

FIG.(iv) MERCURY PENETRATION DATA FOR DARCO 12 x 20

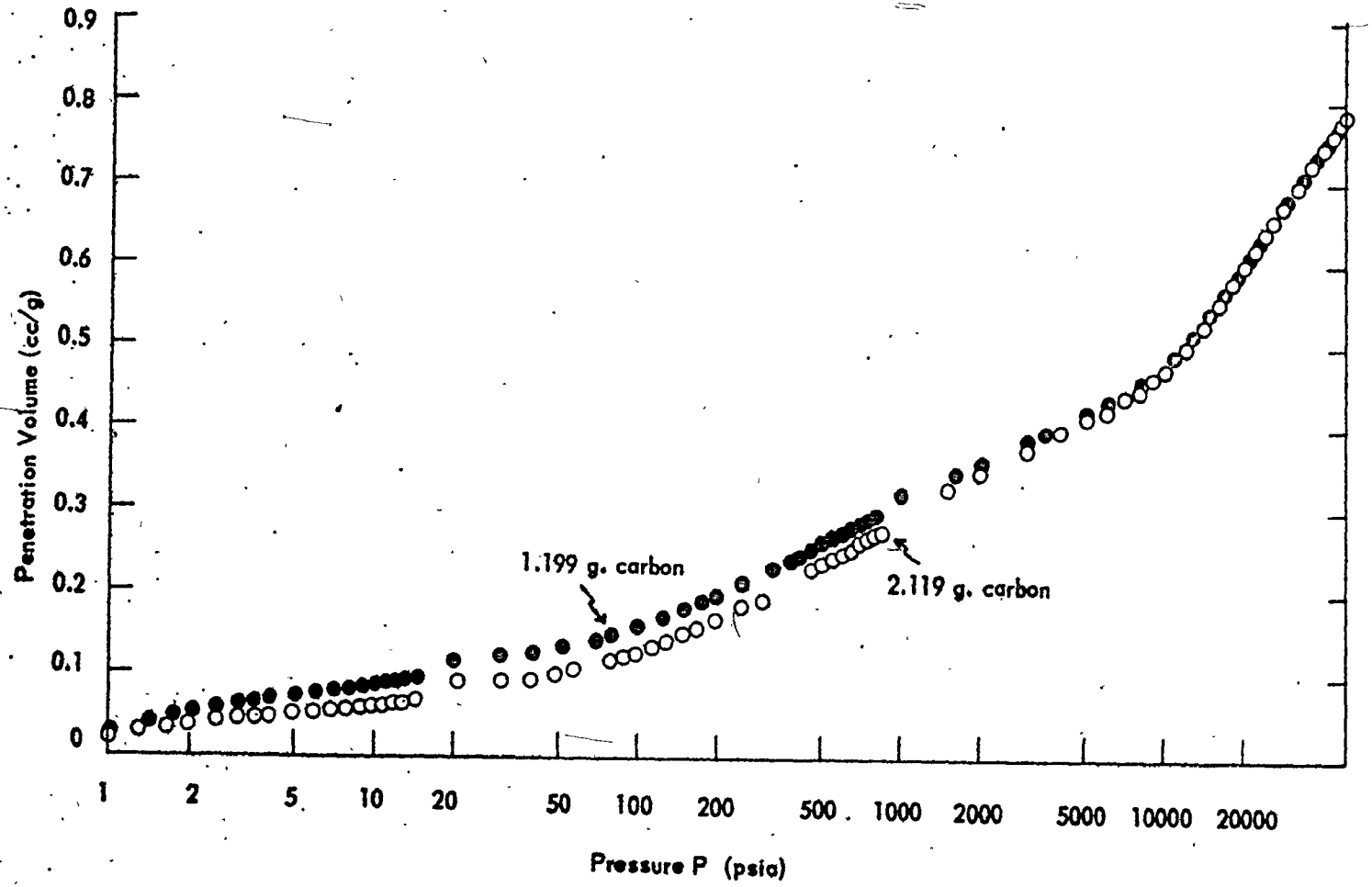

fig.(v) Mercury Penetration Data For F-400

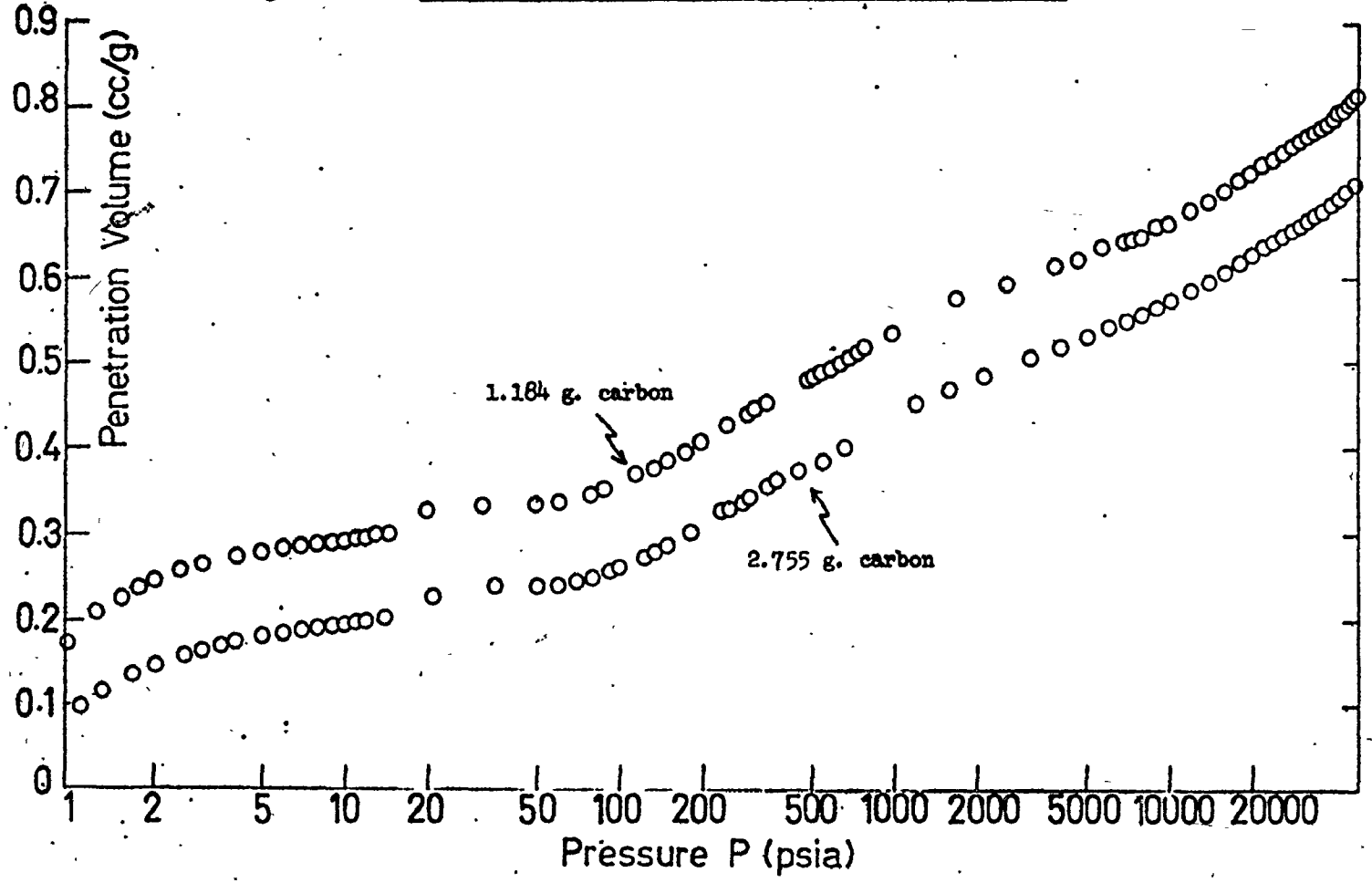

fig.(vi). Mercury Penetration Data For Nuchar Aqua A

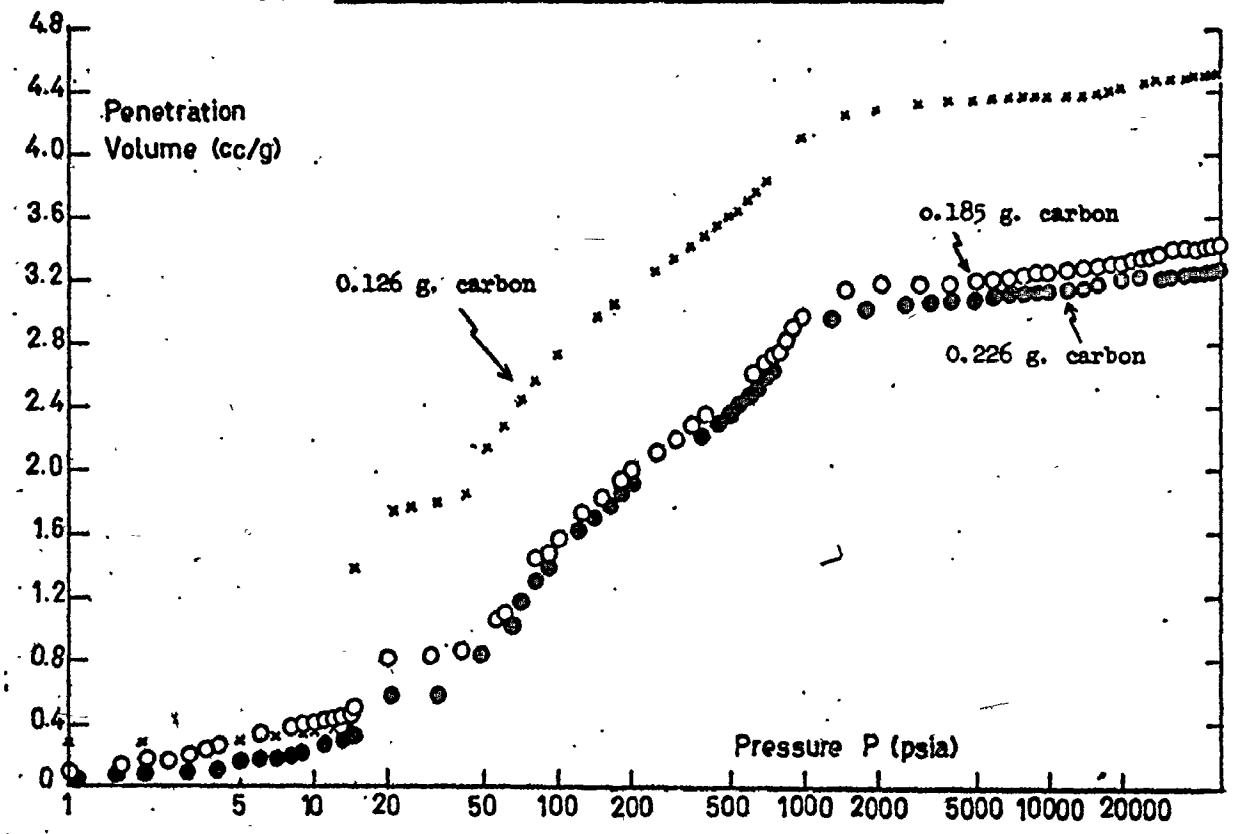

FIG. (vii) MERCURY PENETRATION DATA FOR NUCHAR WV-G 12 x 40

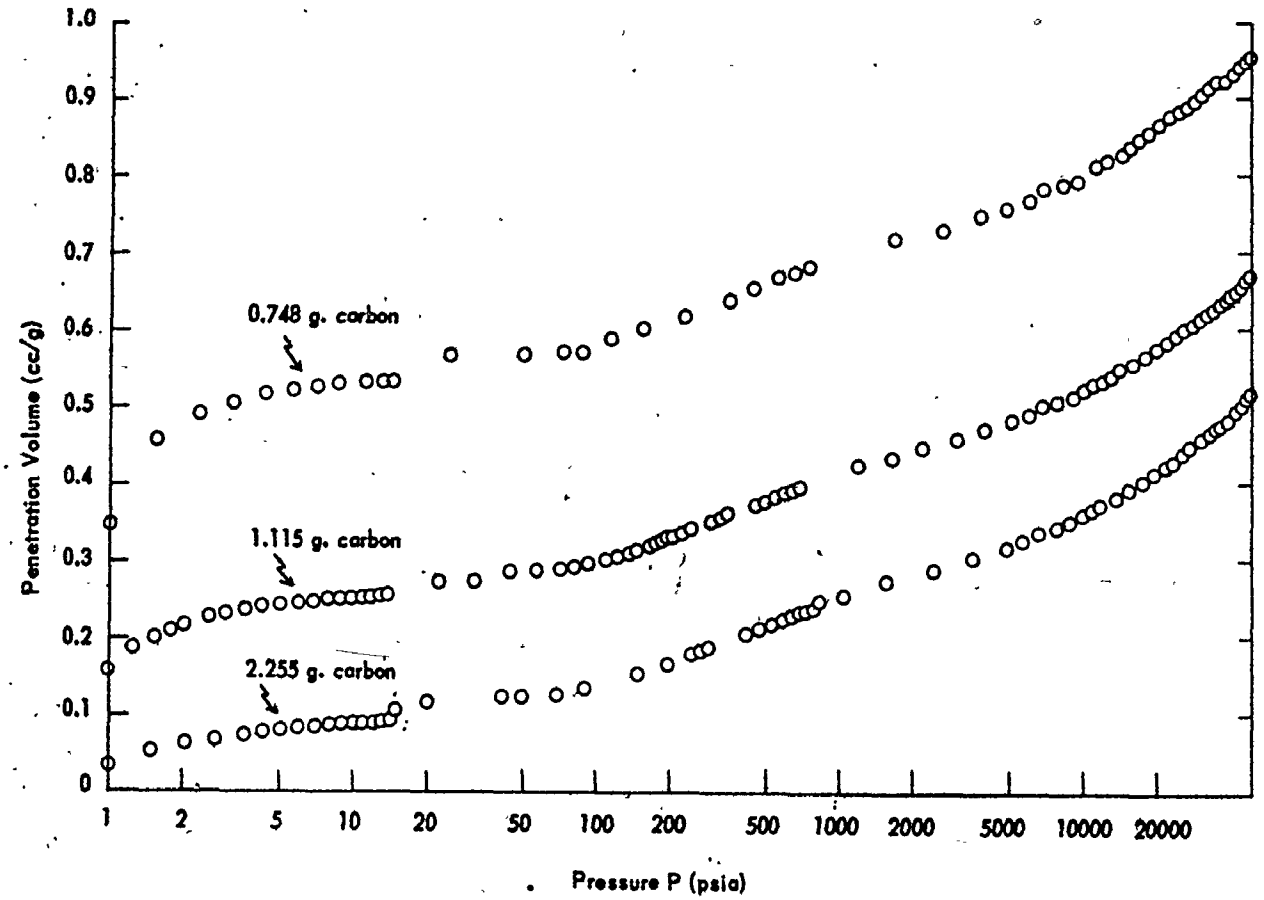

FIG. (viii) MERCURY PENETRATION DATA FOR SPECIAL 'A'

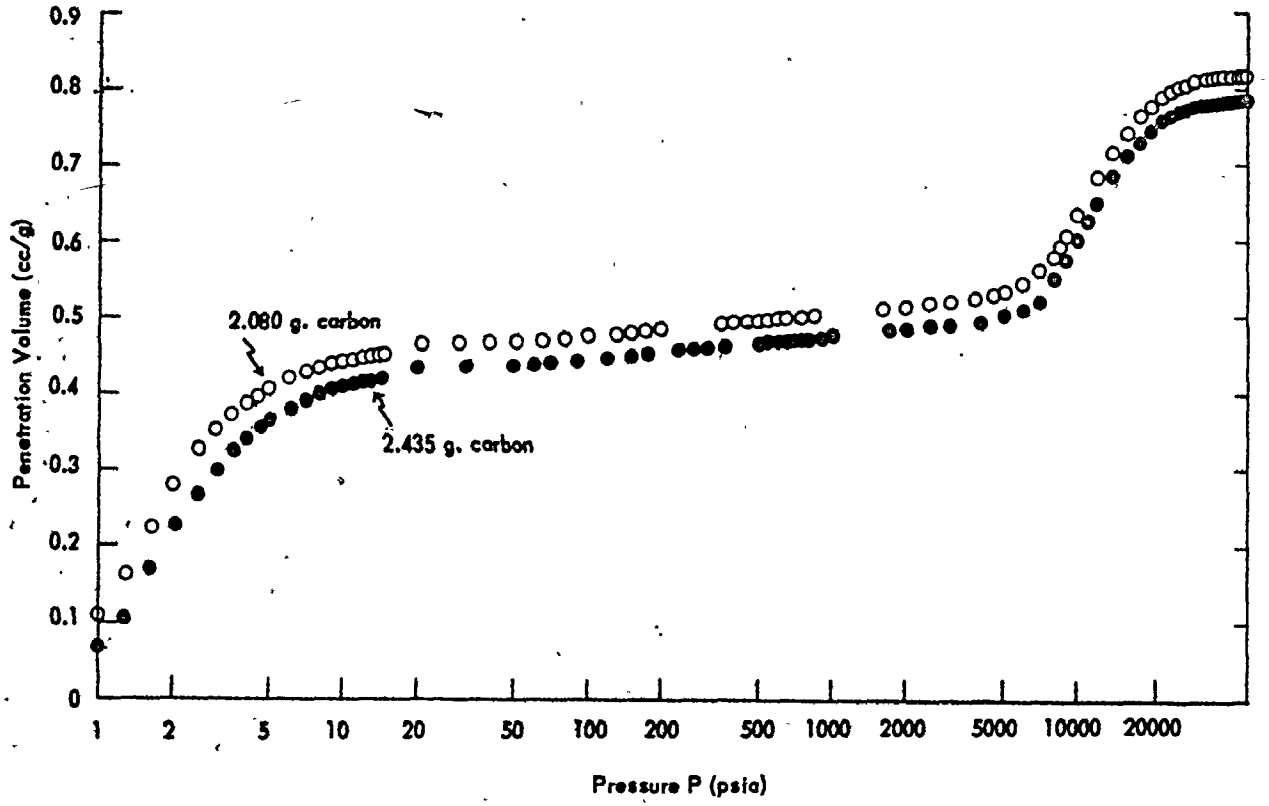

# APPENDIX II.8

## Calculation of Surface Area From Porosimeter Data

Appendix II.8. Calculation of Surface Area from Porosimeter Data

Step 1. Starting at $V_1 = V_{max}$ (i.e. Pore Volume at 50,000 psia), construct horizontal line to a slightly lower suitable pressure $P_1$ (see fig (i))

Step 2. Construct vertical line from point $(P_1, V_1)$ down to a slightly lower penetration volume $V_2$ (see fig (i)).

Step 3. From point $P_1V_2$, construct horizontal line to a new pressure $P_2$ such that this line is bisected by its intercept with the data curve (see fig. (i)).

Step 4. From point $P_2V_2$, construct vertical line down to a lower penetration volume $V_3$.

Step 5. From point $P_2V_3$, construct horizontal line to a new pressure $P_4$ such that this line is bisected by its intercept with the data curve.

Step 6. Continue in this stepwise manner down the P-V data curve, by repeating steps 4 and 5. Stop when a value of P less than 10 psia has been reached (see fig. (i)).

Step 7. Read of the values $P_1, P_2 \ldots\ldots Pn$

$V_1, V_2 \ldots\ldots Vn$

$\Delta V_1, \Delta V_2 \ldots\ldots \Delta Vn$

as indicated in fig. (i). Tabulate these values as shown in Table (i).

Step 8. For each value of P, calculate the corresponding value of r from equation (3.50). (see Table (i)).

Step 9. For each n, calculate the term $P_n \Delta V_n$ (see table (i)).

Step 10. For each n, calculate the value of the incremental surface area $\Delta S_n$ from equation (2.37). (see Table (i)).

Step 11. Calculate the cumulative surface area $\Delta S_{cum}$ for each n by successively adding the various increments $\Delta S$, commencing at the lowest value of Pn. (see Table (i)). For any Pn corresponding to a given $r_n$, the term $\Delta S_{cum}$ represents the cumulative surface area contained in pores greater than or equal to $r_n$. The subsequent plot of $r_n$ versus $\Delta S_{cum}$ represents the surface area distribution in pores as a function of pore radius. (This distribution, for the case of the values derived in table (i) for Nuchar 12 X 40, is depicted in Appendix II.5, fig. (vii)).

Step 12. Calculate the total surface area S by adding $\Delta S$ values for all increments. The value S represents the total surface area contained in pores greater than or equal to 21.5 Å radius.

Table (i) Example of Surface Area Calculations from Porosimeter Data

Carbon: Nuchar Granular WV-G 12 X 40

Sample Weight: 1.1145 g

P-V Curve: See Appendix II.5 fig. (vii)

| n | Pn psia | Vn cc/g | Vn+1 cc/g | Vn cc/g | rn Å | Pn ΔVn | ΔS $m^2/g$ | ΔScum $m^2/g$ |
|---|---|---|---|---|---|---|---|---|
| 1 | 46000 | 0.680 | 0.6535 | 0.0265 | 23.4 | 1219.0 | 23.04 | 90.17 |
| 2 | 37000 | 0.6535 | 0.627 | 0.0265 | 29.1 | 980.5 | 18.53 | 67.13 |
| 3 | 29000 | 0.627 | 0.603 | 0.024 | 37.1 | 696.0 | 13.15 | 48.60 |
| 4 | 23000 | 0.603 | 0.5775 | 0.0255 | 46.7 | 586.5 | 11.08 | 35.45 |
| 5 | 18000 | 0.5775 | 0.562 | 0.0155 | 59.7 | 279.0 | 5.27 | 24.37 |
| 6 | 13000 | 0.562 | 0.5225 | 0.0395 | 82.7 | 514.0 | 9.71 | 19.10 |
| 7 | 7000 | 0.5225 | 0.4810 | 0.0405 | 153 | 290.5 | 5.49 | 9.39 |
| 8 | 3500 | 0.4810 | 0.4525 | 0.0285 | 307 | 99.8 | 1.89 | 3.90 |
| 9 | 1600 | 0.4525 | 0.4170 | 0.0355 | 671 | 56.8 | 1.08 | 2.01 |
| 10 | 800 | 0.4170 | 0.390 | 0.027 | 1343 | 21.6 | 0.41 | 0.93 |
| 11 | 420 | 0.390 | 0.350 | 0.040 | 2560 | 16.8 | 0.32 | 0.52 |
| 12 | 160 | 0.350 | 0.290 | 0.060 | 6710 | 9.6 | 0.18 | 0.20 |
| 13 | 25 | 0.290 | 0.250 | 0.040 | 43000 | 1.0 | 0.02 | 0.02 |
| | | | | | | | 90.17 | |

fig.(i) Graphical Integration Of Porosimeter Data For Surface Area Estimation

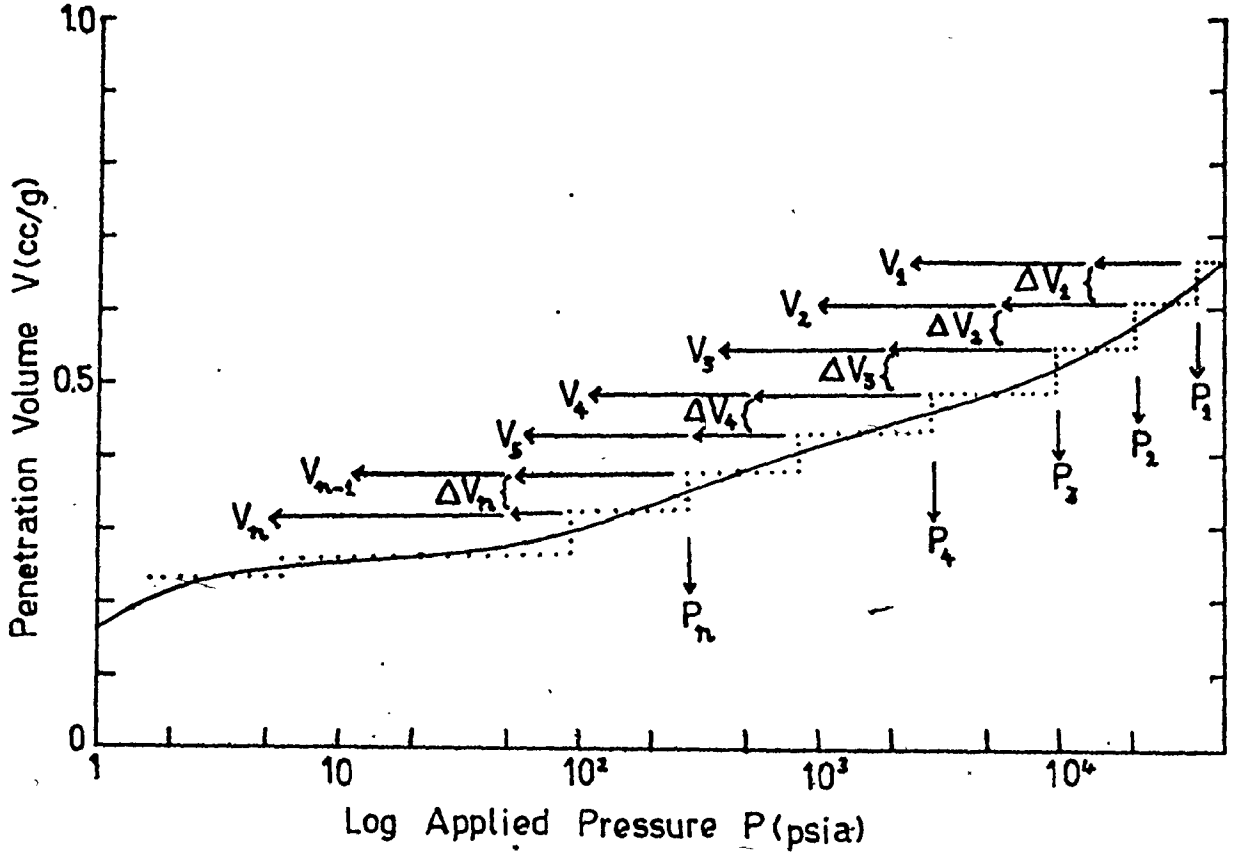

# APPENDIX II.9

## Sieving Analyses of Granular Carbons

fig.(i) Sieving Analysis on Colombia LCK 12/28

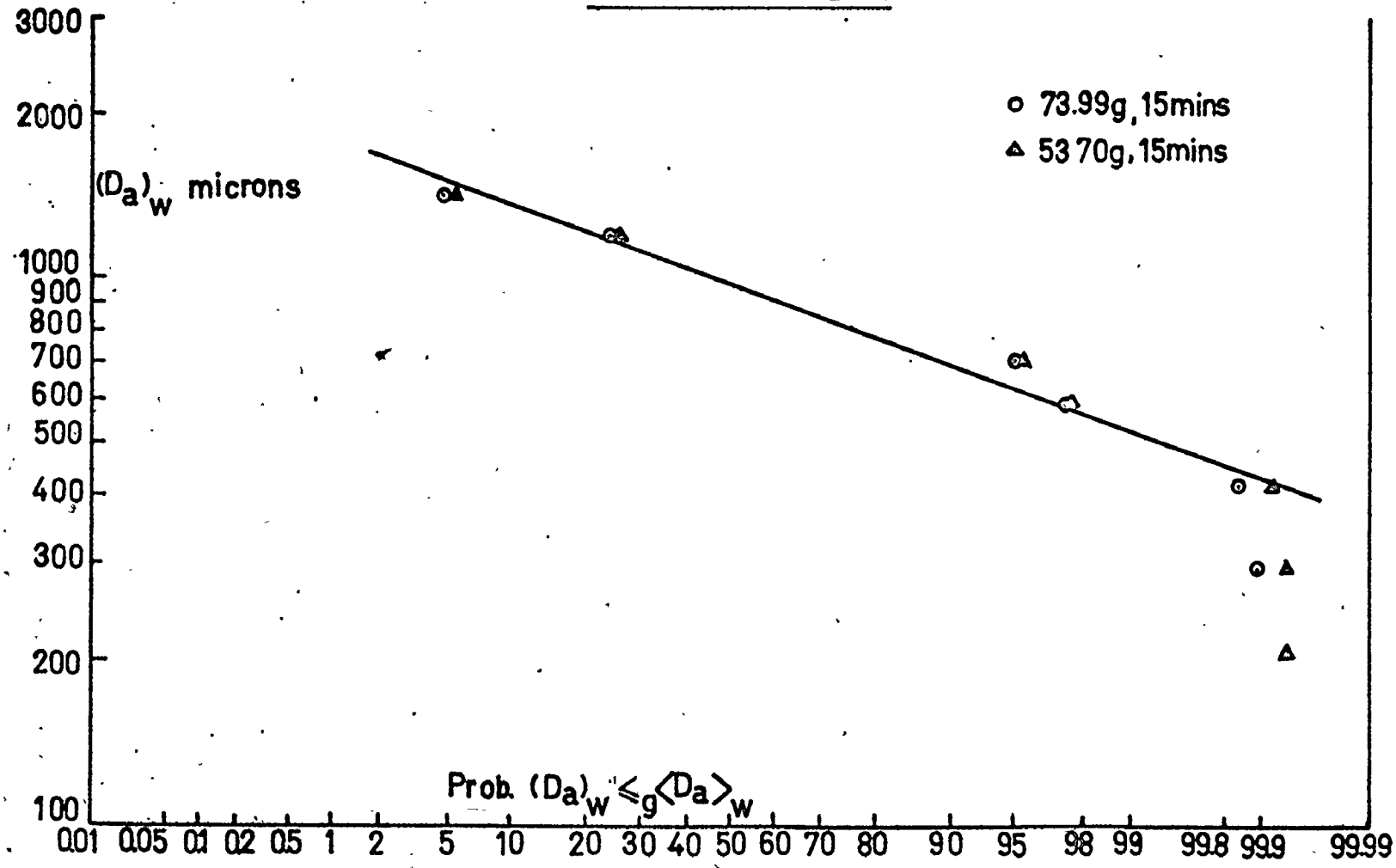

fig.(ii) Sieving Analysis on Darco 12x20

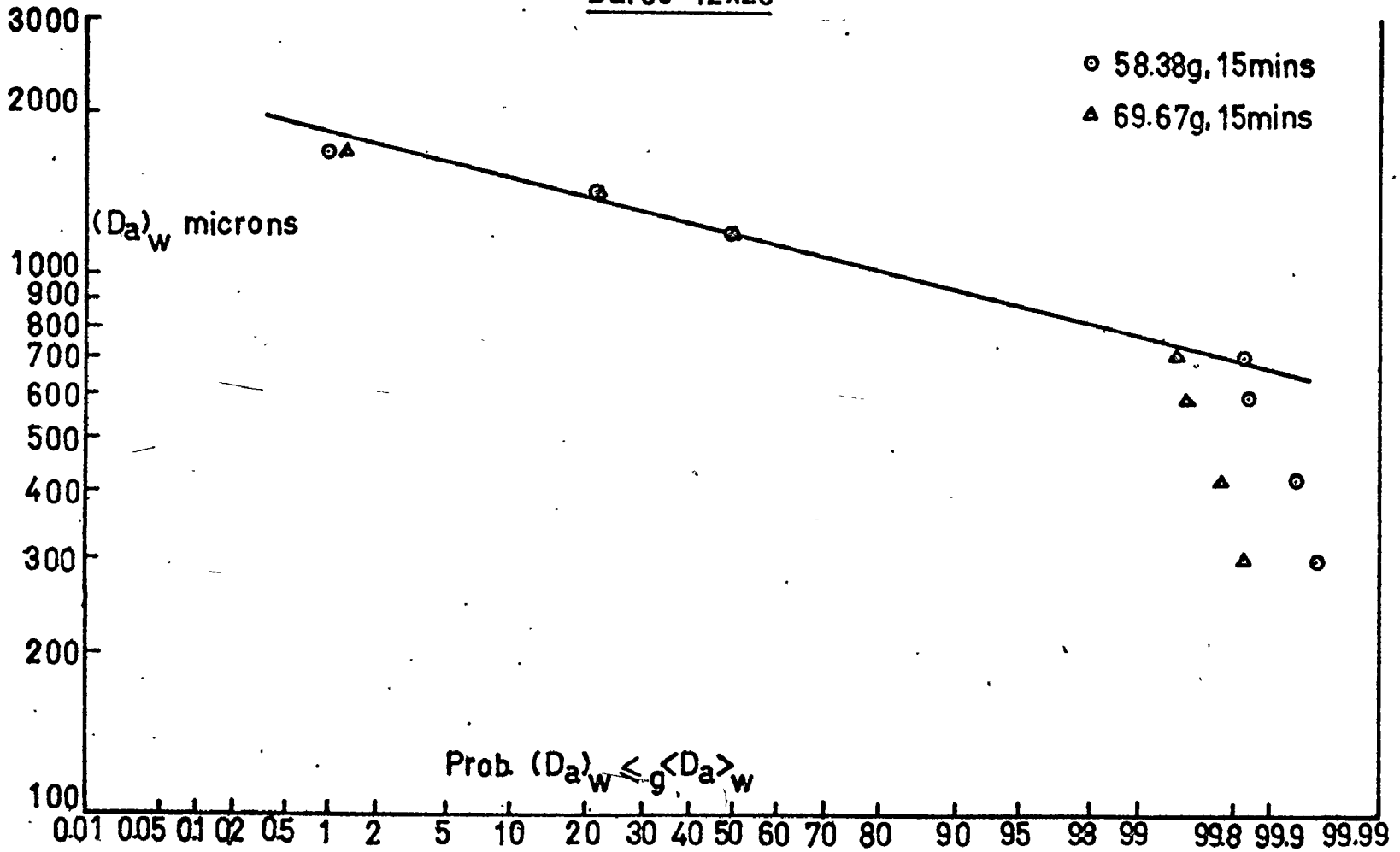

fig (iii) Sieving Analysis on Filtrasorb 400

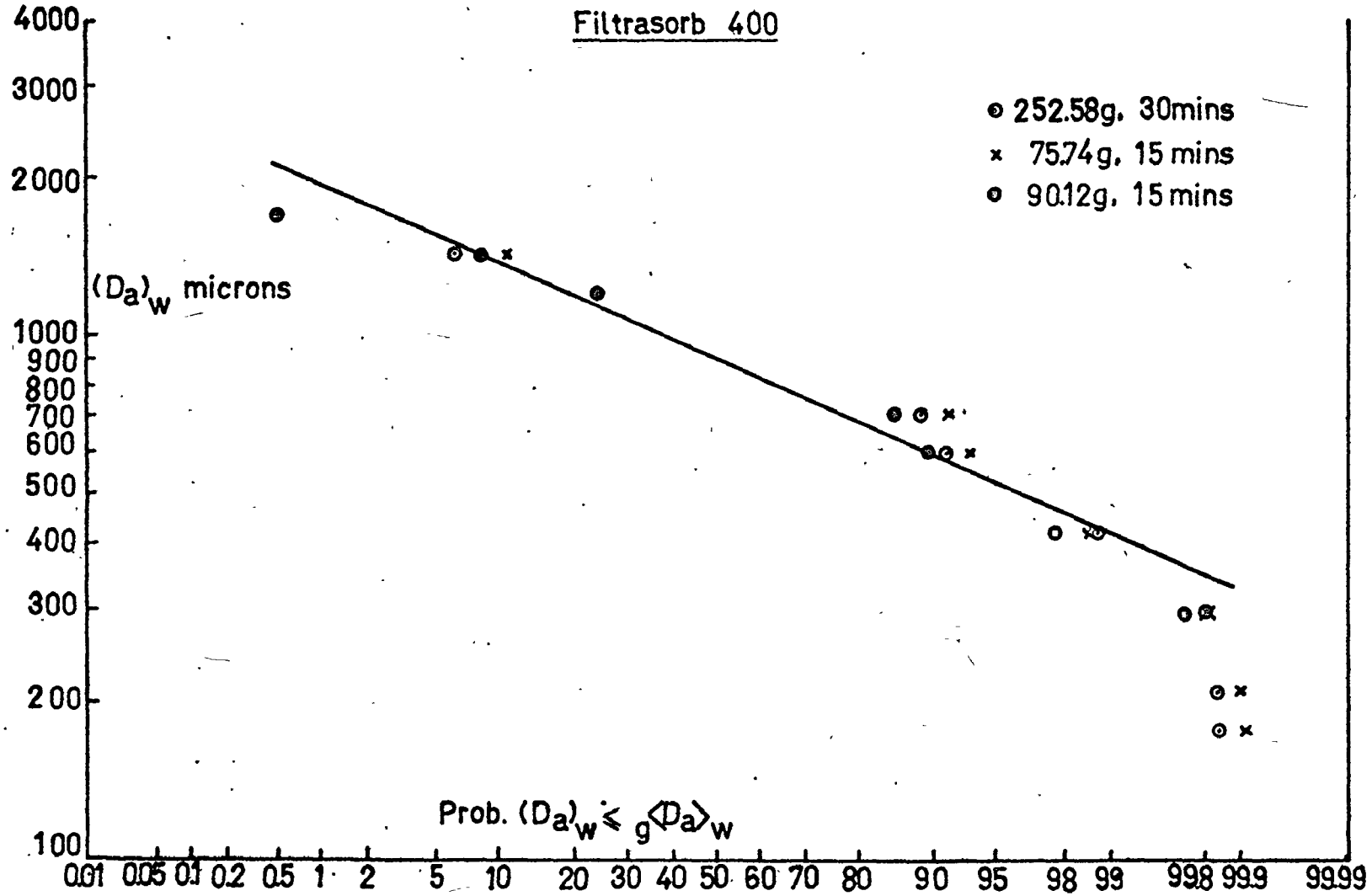

fig (iv) Sieving Analysis on

Nuchar Granular WV-G 12x40

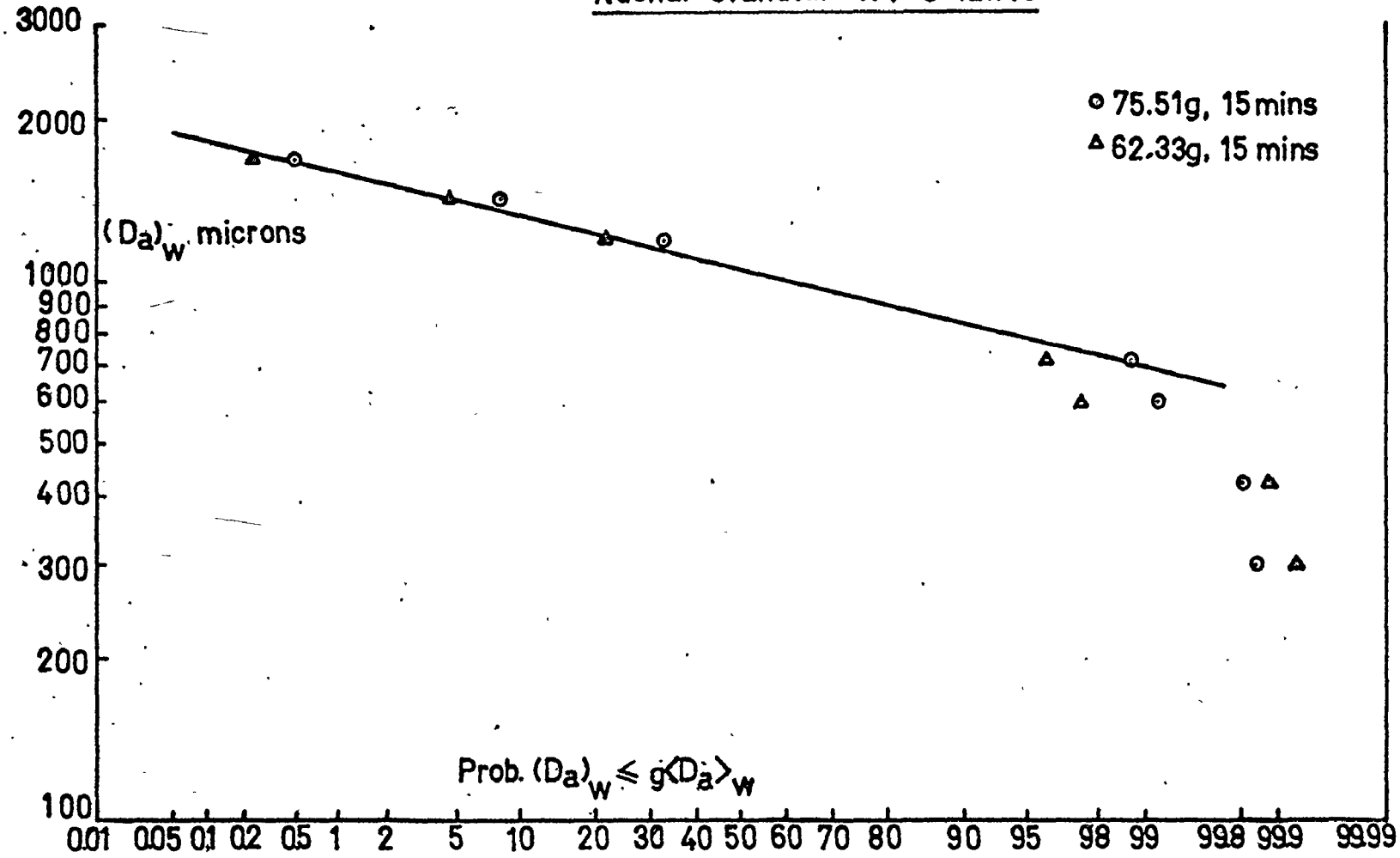

fig.(v) Sieving Analysis on Special 'A' Carbon

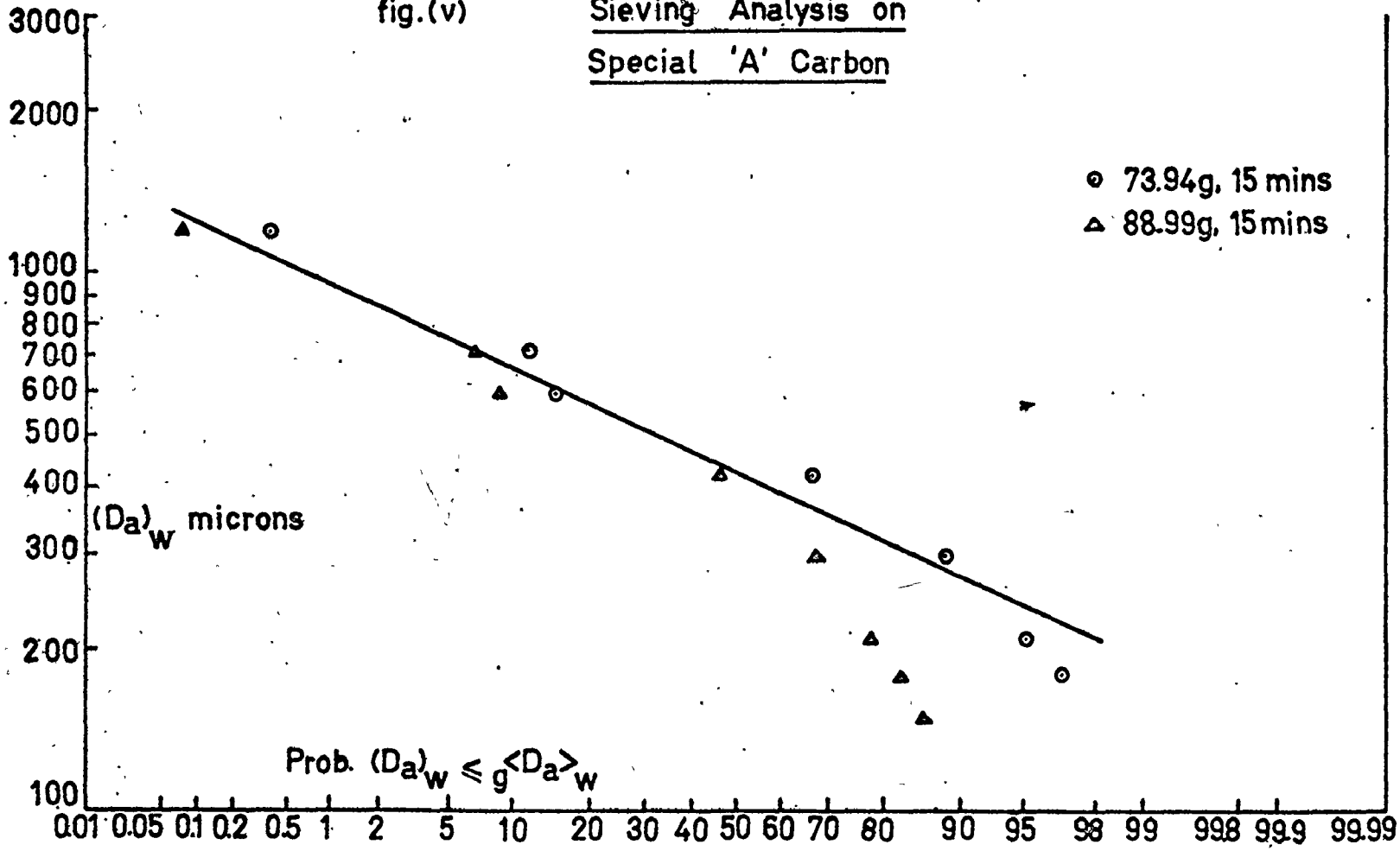

# APPENDIX II.10

## Particle Size Analyses of Powdered Carbons

FIG.(i) PARTICLE SIZE DISTRIBUTIONS - DARCO KB

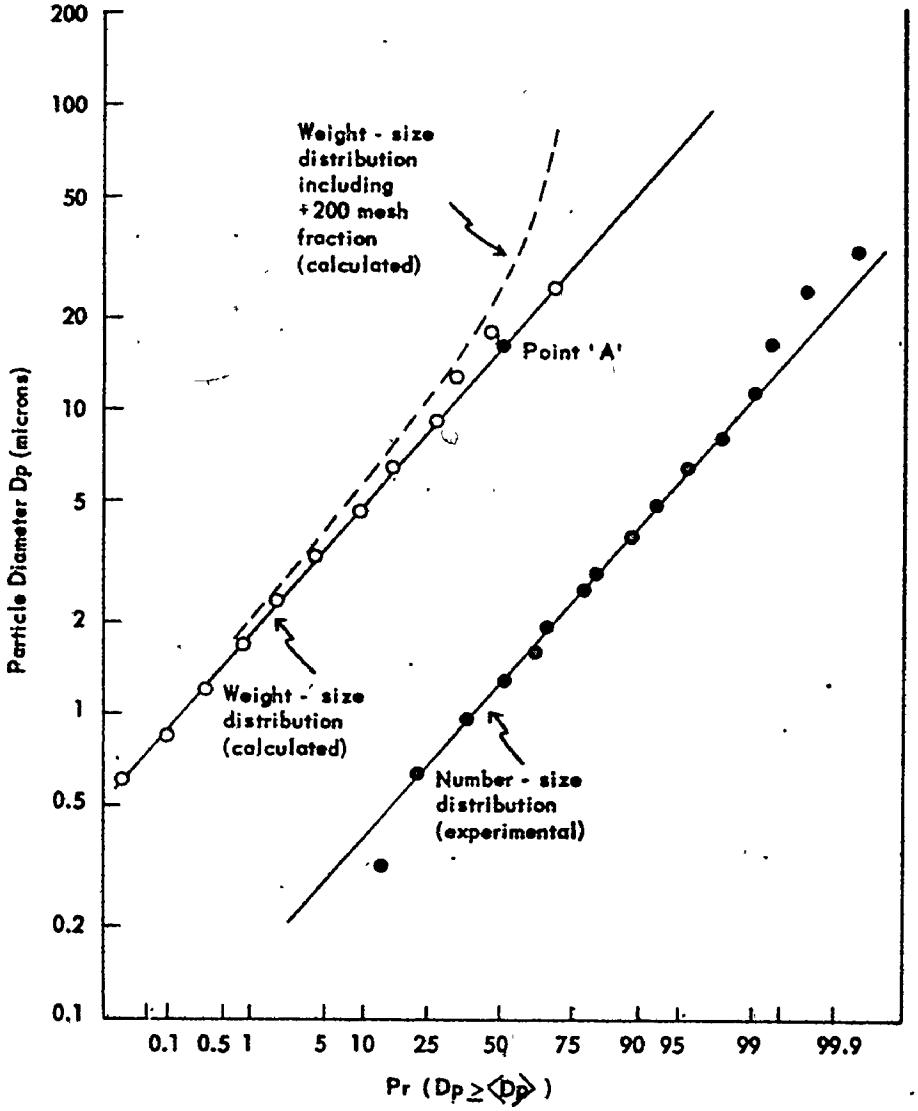

FIG.(ii) PARTICLE SIZE DISTRIBUTION - DARCO S-51

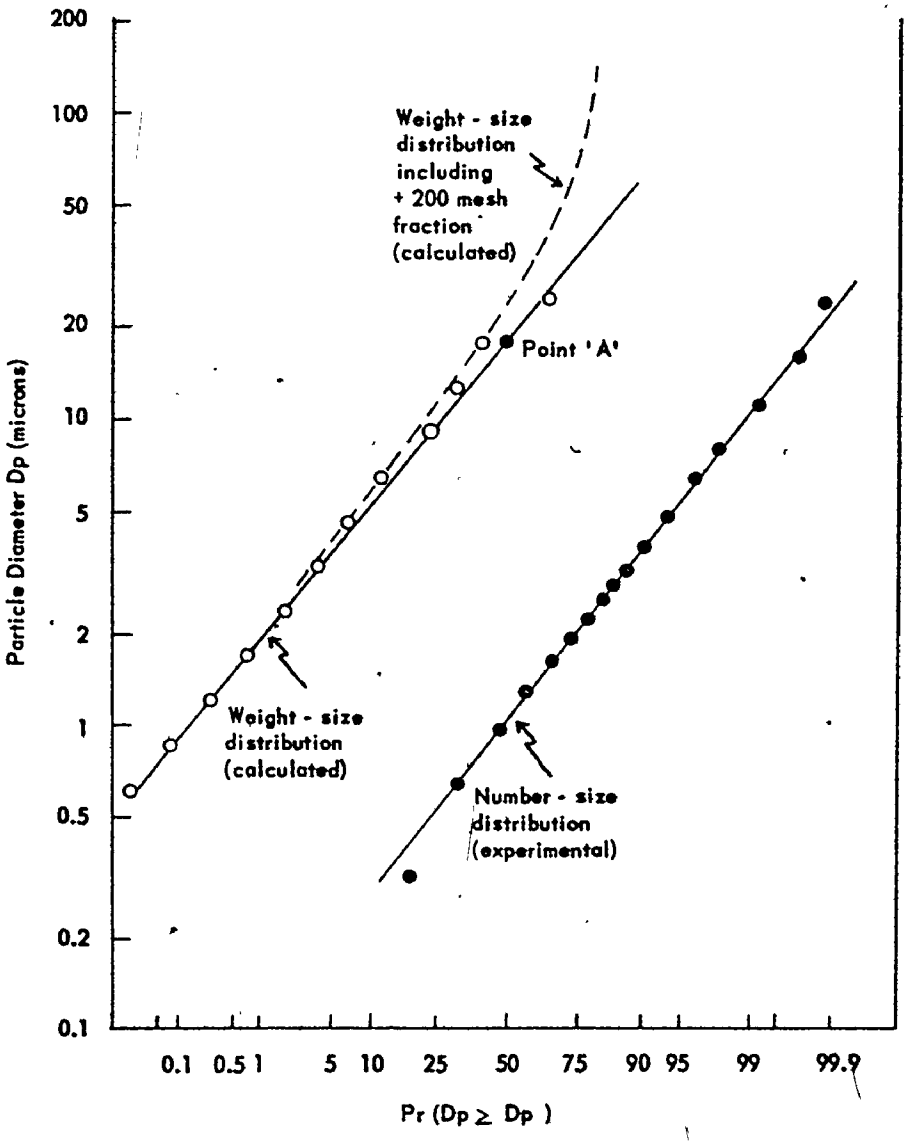

FIG.(iii) PARTICLE SIZE DISTRIBUTION - NUCHAR AQUA A

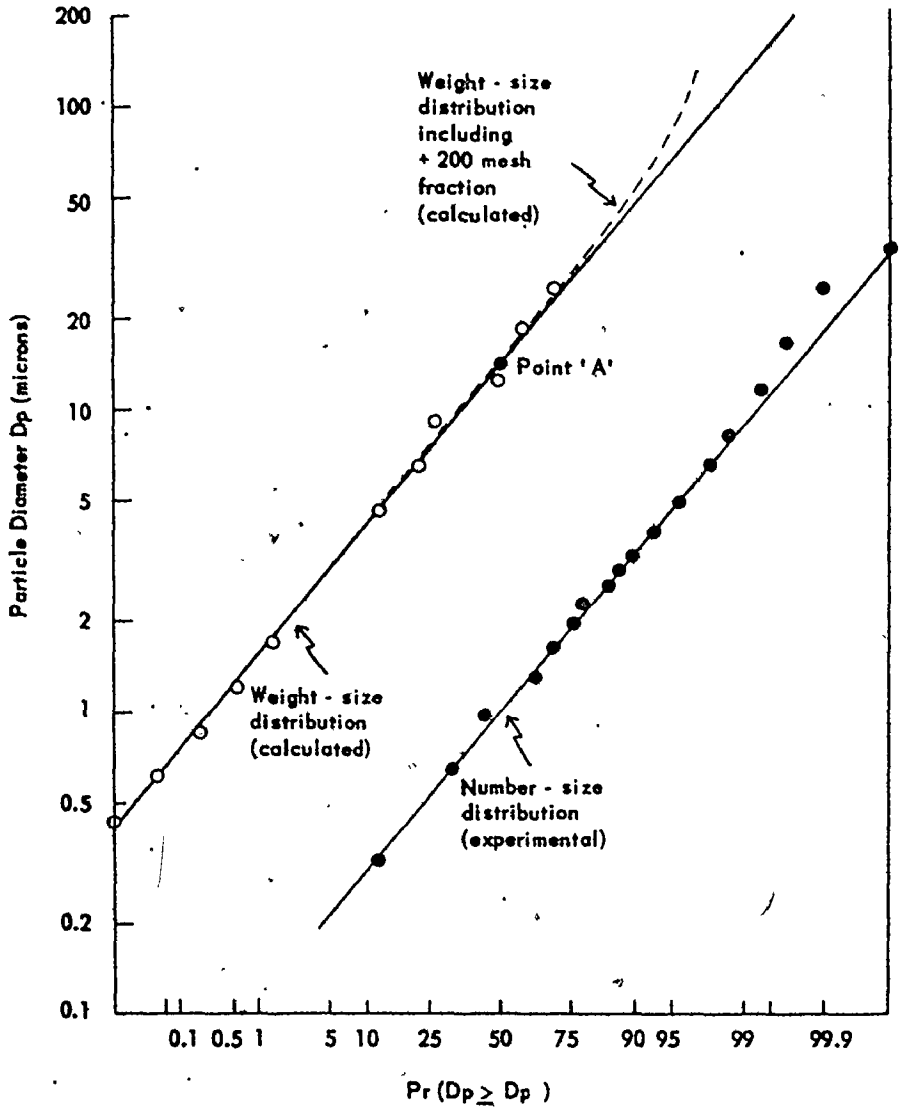

# PART III

# LIGNIN STUDIES

## III.1. INTRODUCTION

Lignins, as they exist in nature, are poly-phenolic plant constituents that form an essential part of the woody stems of both softwoods and hardwoods, and are also found as integral cell wall constituents in most plant forms. Within the cell wall, lignins are always associated with hemicelluloses, not only in an intimate physical mixture but also chemically anchored to the hemicelluloses by covalent bonds. The exact definition and differentiation of lignins from other poly-phenolic plant constituents has only recently emerged. Sarkanen (1971) defines lignins as "those polymeric natural products arising from an enzyme-initiated dehydrogenative polymenisation of one or more of three primary precursors, trans-coniferyl alcohol, trans-sinapyl alcohol and trans-p-coumaryl alcohol" (see Fig. III.1).

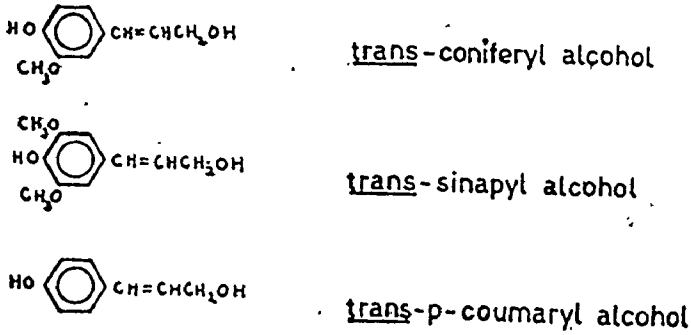


Fig. III.1 Primary Precursors of Lignin

In the production of chemical pulps, wood is subjected to a delignification process aimed at disintegration of wood into its fibrous components. Here the lignin constituents are chemically degraded by breaking carbohydrate-lignin bonds and intro-molecular bondings in the lignin macromolecule. The fragmented lignin is solubilised and physically separated from the wood fibres. The kraft alkaline delignification process is one of the most common procedures for manufacturing chemical pulps. Here an aqueous solution of sodium hydroxide NaOH and sodium sulphide $Na_2S$ - the chemicals being in the correct ratio - is cooked with wood chips for approximately 4 - 6 hours at 165-175°C. During the cooking process, natural lignins are converted to alkali lignins, which then dissolve in the cooking liquor. After cooking, the fibrous material is separated from the kraft "black" liquor which, for a typical kraft fibre yield of about 47%, contains about 70 - 90% of the original wood liquor content. The dissolved lignin, in the form of its sodium salt, constitutes approximately half the organic matter in the black liquor. Additional components include other organic substances arising from carbohydrate and resin dissolution during

cooking, such as carboxylic acids, lactones, rosin acids and alchohols, together with inorganic constituents of the wood substance.

Alkali lignins may be precipitated from kraft black liquor using acid precipitation procedures outlined by Merewether (1962), Nikitin (1960) and Marton (1971). The acid precipitated lignin fraction so isolated contains approximately two thirds of the aromatic components in the black liquor. The non-precipitable aromatic material is comprised of lower lignin oligomers, and pheholic monomers and dimers. In this latter category guaiacol, vanillin, vanillic acid and acetoguaiacone have been identified (Enkvist 1962).

Marton (1964) has summarised the structural information on acid-precipitated softwood kraft lignin in the form of an idealised structural scheme depicted in Fig. III.2. Comparison of this structure with Frendenberg's (1964) proposed natural softwood lignin structure - Fig. III.3. - reveals that the average molecular weight of extracted kraft lignin is much lower than that of natural wood lignin. Furthermore, due to pulping reactions, the nature and extent of the functional groups in the lignin

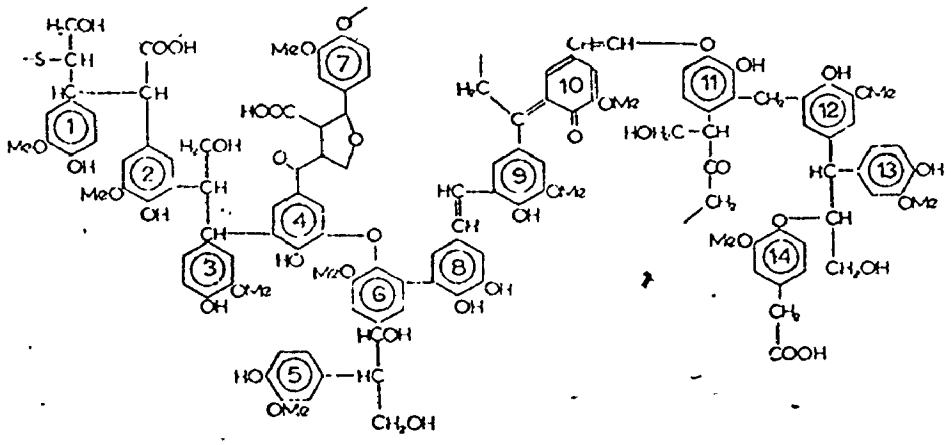

Fig.III.2 Tentative Structural Formula of pine kraft Lignin (Marton)

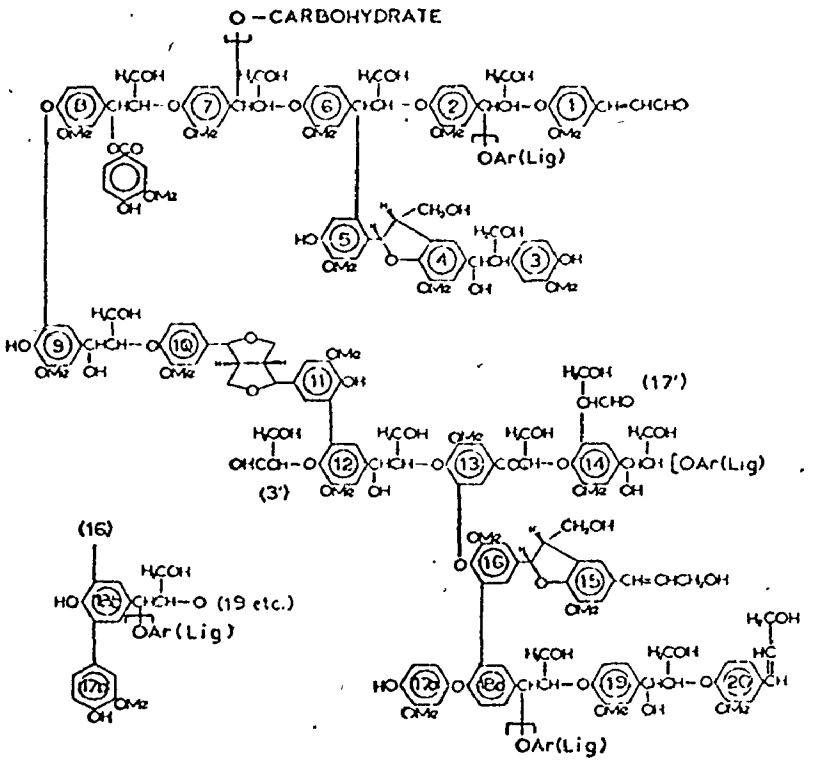


Fig.III.3 Tentative Structural Formula of conifer wood Lignin (Freudenberg)

molecule has changed. Condensation reactions have produced new linkages.

Kraft lignin, as an amorphous powder or in alkaline solution, exhibits a characteristic deep brown color. The observed high absorptivity of kraft lignin above 300 mu wavelength is due to chromophoric groups in the lignin molecule such as vinyl ethers, $\alpha$-carbonyls, stilbenes, quinonoid groups and their conjugated combinations, such as in units 6, 8, 9 and 10 of Fig. III.2. (Marton, 1971). The quinoniod structures may also serve as oxidative species for other functional groups, creating further chromophoric groups (Ganczarczyk, 1972).

Kraft lignin displays properties typical of a polyphenolic polymer. The solid exhibits thermoplastic behaviour (Marton, 1971). Like other polyphenolic materials, kraft lignin is also very susceptible to air oxidation in alkaline solutions, resulting in considerable increase in molecular weight. (Marton and Marton, 1968). Studies of the molecular weight distribution of lignin in alkali lignin extracts have revealed that molecular weights are generally high, as indicated in Table III.1. Further, the lignin molecular weight characteristics appear to be highly

Table III.1 Molecular Weight of Extracted Alkali Lignins

| Wood Species | Pulping Process | Method of Analysis | Lignin Average Molecular Weight | $\bar{M}w/\bar{M}n$ Ratio | Reference |
|---|---|---|---|---|---|
| Pine | Kraft (4) | Ultracentrifugal Sedimentation | 3000-4300 (2) | - | Marton & Marton (1964) |
| Pine | Kraft | Ultracentrifugal Sedimentation | 3500 (1) | 2.2 | Marton & Marton (1964) |
| Hardwood | Kraft | Ultracentrifugal Sedimentation | 2900 (1) | 2.8 | Marton & Marton (1964) |
| Spruce | Sulphate | Light Scattering | 5600 (1) | - | Lindberg et al (1964) |
| Spruce | Sulphate | Gel Filtration | 10,000 (1) | - | Lindberg et al (1965) |
| Spruce | Soda | Light Scattering | 82,000 (1) | - | Lindberg et al (1964) |
| Spruce | Soda | Gel Filtration | 20,000 (1) | - | Lindberg et al (1965) |
| Spruce | Kraft | Continuous Extraction | 1800-51,000 (3) | 3 | McNaughton et al (1967) |
| Spruce | Periodate | Precipitation with Baruim Salt | 35,000-1,700,000 (3) | 5.7 | Gupta & Goring (1960) |

(1) Weight average molecular weight $\bar{M}w$
(2) Number average molecular weight $\bar{M}n$
(3) Molecular weight range
(4) Mildly oxidised in solution

dependent on the wood species, the extraction procedure and the analytical tool used for determination of molecular weight characteristics. The high values of the $\overline{Mw}/\overline{Mn}$ ratio in Table III.1 indicate the wide polydisperisty of alkali lignins, such values being characteristic of non-linear polymers (Adler, 1957). Lindberg (1964) and Goring (1971) have also indicated that in solution, alkali lignin molecular constituents closely approximate Einstein spheres in their molecular configuration.

Kraft lignin in solution thus consists of a variety of different molecular weight-and-size-components which behave as compact spherical macrosolutes. Such constituents exist as cross-linked microgel entities which are swollen by the solvent due to solvation and hydrogen bonding (Schuerch, 1965).

Kraft lignin inevitably finds its way into pulp mill effluent streams as a result of pulp washing, screening and bleaching operations and kraft black liquor spills. Although kraft lignin displays negligible $BOD_5$, it can impart considerable color, COD and TOC to the effluent or receiving stream. The removal of kraft lignin from pulp mill effluents is thus a prerequisite for attainment of a non-polluting pulp mill.

III.1.1. Lignin Used in the Study

A softwood alkali lignin, Indulin A.T. *, was used as the lignin source in this study. It is an acid precipitated pine kraft lignin isolated from black liquor by the two-stage precipitation procedure outlined by Marton (1971). The approximate formula quoted by Bailey (1972) for a basic lignin structural unit is

$$C_9 H_{7.92} O_{2.08} S_{0.09} (OCH_3)_{0.82}$$

having a molecular weight of 178. Its structure may be represented tentatively by Fig. III.2, although the formula of a basic lignin structural unit in Marton's formulation, i.e. $C_{8.35} H_{6.4} O_{2.1} (OCH_3)_{0.78}$, contains slightly less carbon, hydrogen, sulphur and methoxy content than that of Indulin A.T. The Indulin A.T. sample was stated to be of high purity, containing only 0.17 wt.% ash, consisting mainly of sodium carbonate.

---

* supplied as an amorphous brown powder in 5 kg. drums by Westvaco, Charleston Research Centre, Box 5207, North Charleston, S.C., 29406, U.S.A.

## III.2. CHEMISTRY OF LIGNIN IN AQUEOUS SOLUTION

In order to understand the mechanisms involved in lignin adsorption, as color and TOC, from solution into activated carbon, an understanding of lignin behaviour in solution is essential. In this respect, the following questions need to be answered:

a) How does the color and TOC of lignin solutions vary with lignin concentration?

b) How does the color and TOC of lignin solutions vary with solution pH?

c) What is the effect of solution age on the color and TOC of indulin solutions?

d) Does filtration through 0.45 μ membrane filters reduce the color and TOC of lignin solutions?

### III.2.1. Experimental

#### III.2.1. (i) Preparation of Indulin A.T. Solutions

Indulin A.T. is completely soluble in 0.1 M NaOH (Bailey, 1972). The required amount of Indulin was weighed and dissolved in approximately 500 ml of 0.1 M NaOH. Solution pH was then recorded (usually 12.2-12.5).

In cases where a lower solution pH was desired, the Indulin was first dissolved in 0.1 M NaOH and then aliquots

of 0.1 M HCl were added carefully to the agitated solution until the required pH value was attained. Fifty millilitres of buffer solution was then added, the buffers for a particular pH being made up in accordance with specifications outlined in "The Handbook of Chemistry and Physics" (1968). Care was taken to avoid the use of buffers containing carbon in their constituent chemicals. Prepared Indulin solutions were used in experiments as soon as possible since, as will be seen later, the nature of lignin in solution changes as the solution ages.

III.2.1. (ii) Color Measurements

Chloroplatinate color standard solutions containing from 25 to 500 color units (cu) were first prepared according to the procedure outlined in "Standard Methods For The Examination of Water and Wastewater" (1971). Absorbance * of the individual color standards was measured at 465 mμ (Carpenter and Berger, 1971) with a Coleman Model 14 Spectrophometer using a sample cell of 4 cm light path length.

---

* The absorbance A of a sample solution at wavelength $\lambda$ is given by $A = \log \left[\frac{Io}{I}\right]$ where Io, I are the intensities of light of wavelength $\lambda$ incident on, and transmitted by the sample solution respectively.

An identical cell filled with distilled water was used as a reference. A minimum sample size of 20 ml. was used. The subsequent plot of absorbance versus color units depicted in Fig. III.4 indicates that the Beer-Lambert relationship * is valid for solutions of 500 cu or less.

The absorbance of dilute Indulin solutions was similarily measured and the values converted to equivalent color units via Fig. III.4. For concentrated Indulin solutions, the sample required dilution prior to adsorbance measurements. Here dilution was facilitated by adding an appropriate amount of 0.1 M NaOH/0.1 M HCl buffer mixture at the appropriate pH, so as to maintain the diluted sample pH the same as the concentrated sample pH. Absorbance values were again converted to color units via Fig. III.4, and the color content of the concentrated sample was obtained by multiplication of the measured value by the appropriate dilution factor.

---

* The Beer-Lambert Law expresses the relationship between solution concentration c - in g/l - and its absorbance A at a given wavelength by the equation $A = c\ a\ l$ where a = absorptivity ($l.cm.^{-1}\ g^{-1}$)
l = light path length (cm)
Provided that l is constant, and the solution is sufficiently dilute, then the term al in the equation is constant, and hence absorbance varies linearly with concentration.

Fig. III.4 Color - absorbance Calibration
(cell length = 4cm)

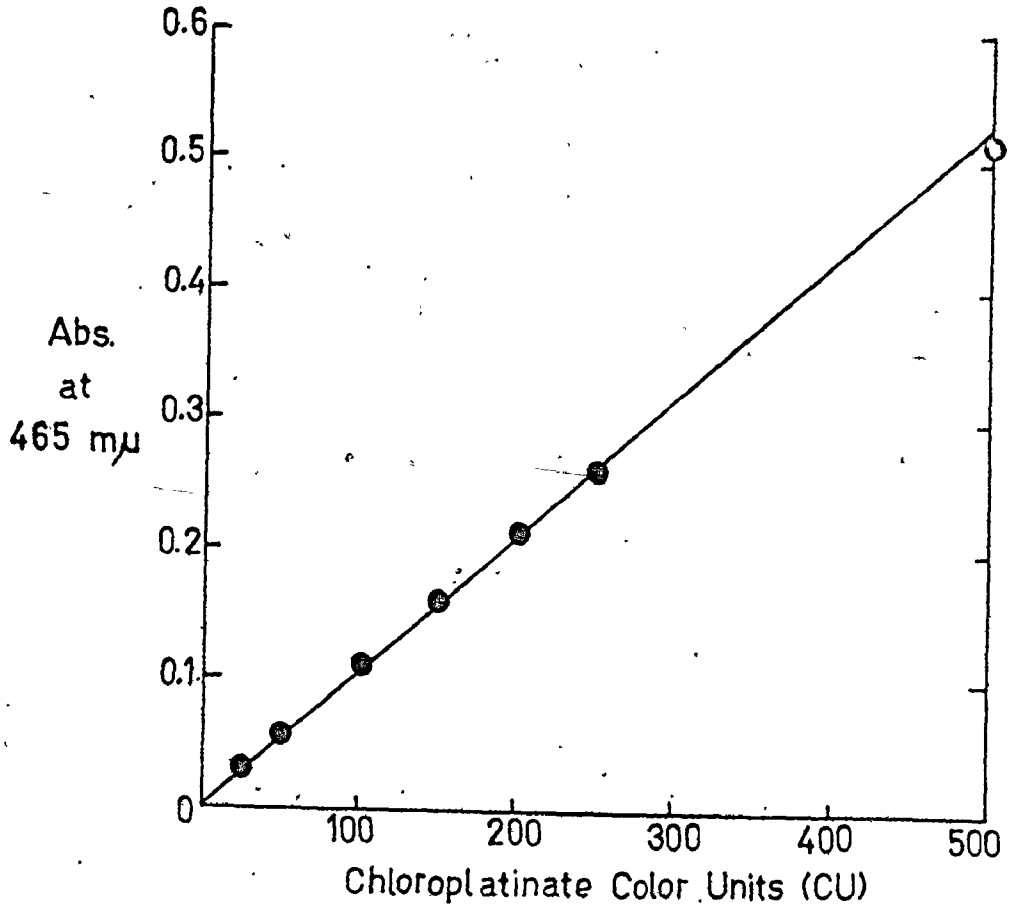

III.2.1. (iii) Total Organic Carbon Measurements

The Total Organic Carbon content (TOC) of a solution is given by its total carbon content (TC) minus its inorganic carbon content (IC). In order to calibrate the TOC analyzer it was necessary to prepare standards of known total carbon and inorganic carbon content.

Potassium hydrogen phthalate ($C_8 H_5 O_4 K$) was used in the preparation of TC standards. Here 2.125 g of this compound was dissolved in distilled water in a litre volumetric flask to give a stock solution of 1000 mg/l TC. From this stock solution several standards ranging from 10 mg/l to 600 mg/l were prepared by dilution. A similar procedure was employed for the IC standards, using a stock solution of 883 mg/l anhydrons sodium carbonate $Na_2CO_3$, corresponding to a IC content of 100 mg/l.

Measurements were carried out in a Beckman Model 915 Total Carbon Analyser. The Analyser was first calibrated with respect to its IC and TC channels by injecting 20 µl samples of the appropriate standards and noting the height of the peaks obtained on the output recorder. Generally an instrument gain of 5 was used, except when considering TC standards of greater than 100 mg/l TC

content, where a gain of 1.2 was used. Typical TC and IC calibration curves obtained fro the instrument are shown in Appendix III.1, figs. (i) to (iii). The instrument was frequently recalibrated. When not in use, TC and IC standards were stored in a 4 °C refrigerator.

The total organic carbon content of Indulin solutions was obtained by injecting 20 µl of the solution into both the TC and IC channels of the instrument. The peaks obtained were then converted to an equivalent TC and IC content - in mg/l - via the appropriate calibration curve. The sample TOC was then recorded as the difference between the obtained TC and IC values.

III.2.2. Results and Discussion

III.2.2. (i) Factors Influencing Indulin Solution Color

a) Indulin Concentration

The effect of Indulin concentration on the color of Indulin solutions is shown in ig. III.5. As expected Indulin solution color increases linearly with concentration at constant pH within the 7 - 12.5 pH range. This is associated with the addition of more color bodies to solution as Indulin concentration is increased.

Fig. III.5

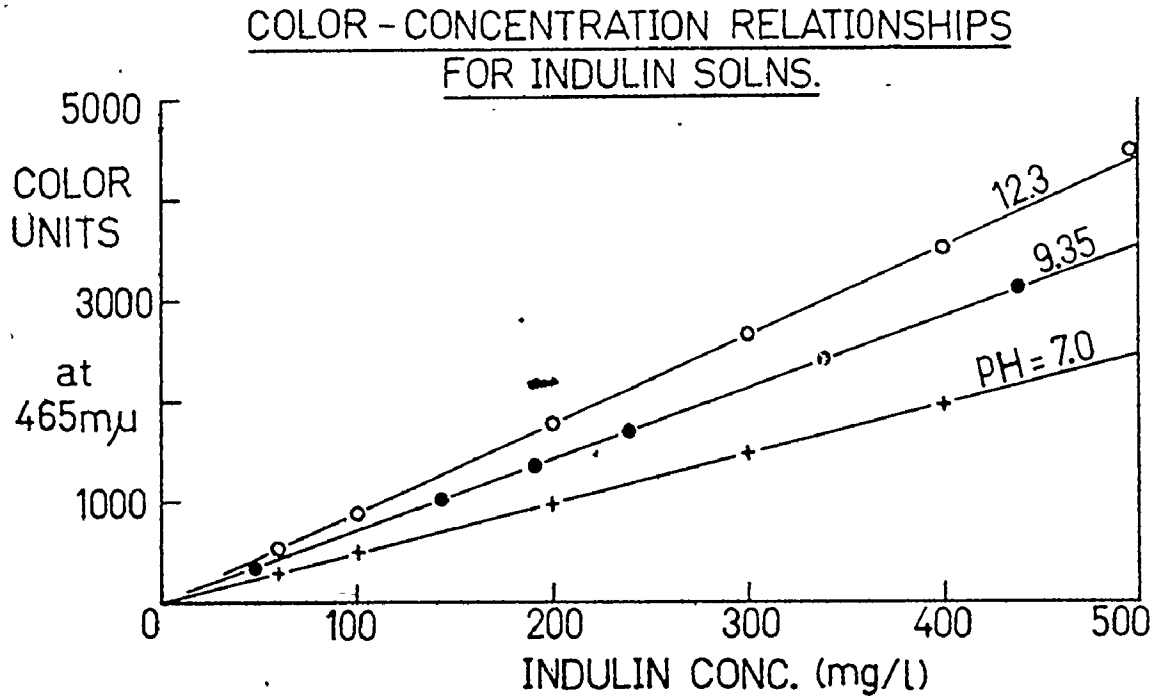
COLOR - CONCENTRATION RELATIONSHIPS
FOR INDULIN SOLNS.
5000
COLOR
UNITS
3000
at
465mμ
1000
0
100
200
300
400
500
INDULIN CONC. (mg/l)
12.3
9.35
PH = 7.0

Fig. III. 6

EFFECT OF SOLN. pH ON INDULIN COLOR

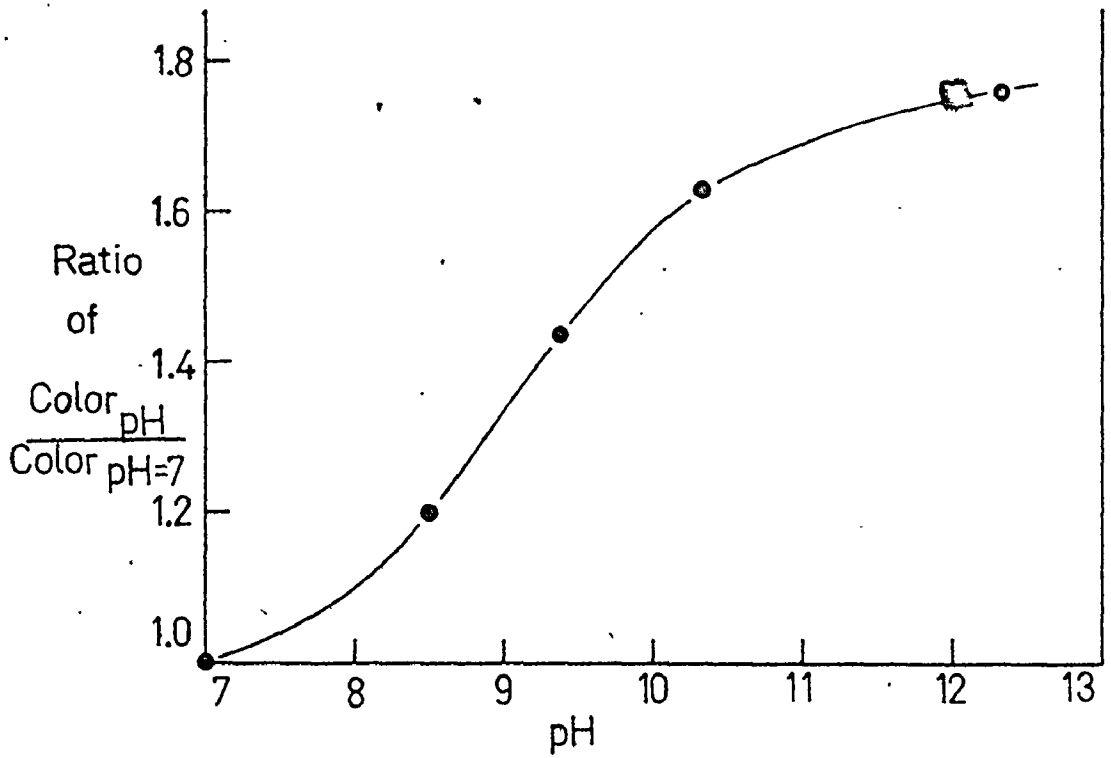

b) Solution pH

The effect of pH on the color of Indulin solutions can also be seen from Fig. III.5, although this effect is more clearly demonstrated in Fig. III.6. Here, for a given Indulin concentration, solution color increases with solution pH, the color change being most sensitive in the 8 - 10 pH range. This effect is probably associated with more complete dissolution of the lignin macromolecular constituents in solution with increased alkalimity, resulting in an increase of true solution color as pH is increased. However, it is also feasible that the pH effect may be associated with a significant change in the chemical nature of the lignin chromophores (see section III.1) rather than a solubility effect. In order to test the latter hypothesis, 50 mg/l Indulin solutions at various pH's were characterised in terms of the fundamental color properties as defined by the tristimulus method of color measurement (Standard Methods for the Examination of Water and Wastewater, 1971). The results are shown in Table III.2. Here pH variation does not produce any significant change in the dominant wavelength, or hue, exhibited by the solution. This suggests that no radical

Table III.2. Color Characteristics of 50 mg/l Indulin Solutions at Various pH's

| Indulin Solution pH | Color Characteristics | | | |
|---|---|---|---|---|
| | Dominant Wavelength mμ | Purity % | Luminence % | Hue |
| 7 | 576.2 | 27.8 | 78.9 | Yellow |
| 8.5 | 576.4 | 30.5 | 71.7 | Yellow |
| 10 | 576.8 | 36.8 | 63.3 | Yellow |
| 12.5 | 577.4 | 48.5 | 59.8 | Yellow |

structural alteration in the nature of lignin chromophones occurs with pH change. Conversely the increase of color purity and decrease of color luminence with pH increase is coincident with the theory that the chromophones simply become more active due to increased solubility at the higher pH values.

From the results in Table III.2 the question arises, "why not measure the color of Indulin solutions at their dominant wavelength - 576 → 577 mμ - instead of at 465 mμ?" The use of 465 mμ as a characteristic wavelength for lignin color measurement was proposed by Berger and Carpenter (1971), who stated that "the spectral transmission characteristics of a pulping waste ..... indentically matched the adsorption of the chloroplatimate standard at 450 - 480 mμ ..... and selection of a wavelength in this range of the adsorption spectrum for color measurement of pulping waste would permit continued use of most present-day instrumentation. In addition, Fig. III.7 shows that the absolute value of absorbance at 465 mμ is greater than the corresponding value at 576 mμ, so that absorbance measurement at 465 mμ would tend to produce

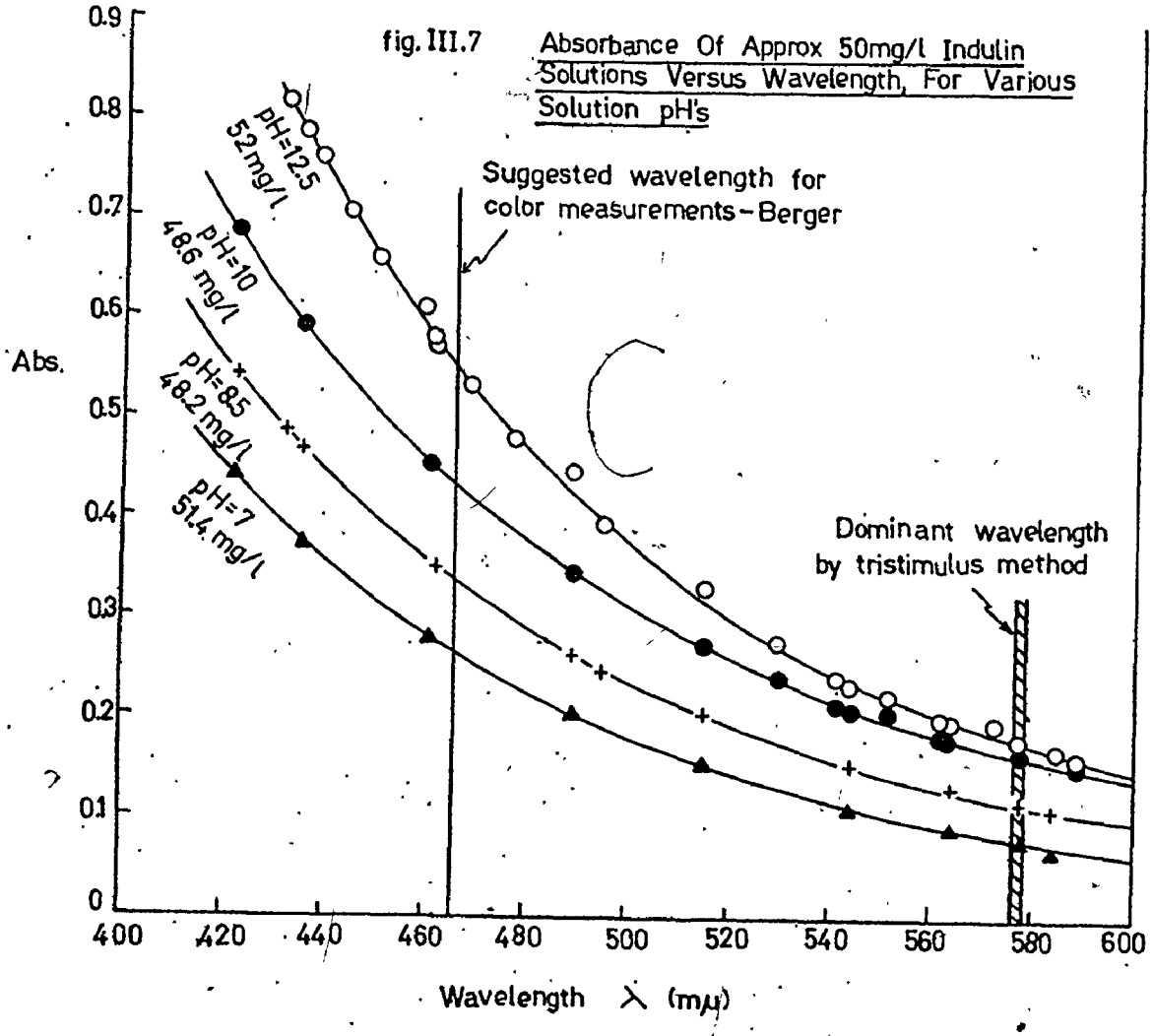
fig. III.7 Absorbance Of Approx 50mg/l Indulin Solutions Versus Wavelength, For Various Solution pH's
Suggested wavelength for color measurements - Berger
Dominant wavelength by tristimulus method
pH=12.5 52mg/l
pH=10 48.6 mg/l
pH=8.5 48.2 mg/l
pH=7 51.4 mg/l
Abs.
0.9
0.8
0.7
0.6
0.5
0.4
0.3
0.2
0.1
0
400
420
440
460
480
500
520
540
560
580
600
Wavelength λ (mμ)

a higher absorbance reading which would aid in determination of activate absorbance values for dilute solutions.

[It should be noted here that comparison of color absorbance measurements at 465 mμ is describing the relative color of Indulin solutions at various pH and concentration conditions is only meaningful and justified if the dominant wavelength is independent of pH and concentration, which is the case for the solutions studied here.]

c) Filtration Through 0.45μ Membrane Filters

Filtration of Indulin solutions through pre-washed 0.45μ membrane filters produces a slight color decrease in the filtrate. The magnitude of this color reduction is dependent on solution pH, ranging from about 3 - 4% at pH 12.3 to about 7 - 8% at pH 7. Below pH 7, Indulin precipitates from solution, producing a drastic reduction in solution color. For example, a 250 mg/l Indulin solution at pH 5.5, after filtration and removal of precipitate, had a color of approximately 100 CU compared to the color in corresponding filtered solutions at pH 7 and 12.3, which amounted to approx-

imately 1000 Cu and 2200 Cu respectively. Color - reduction upon filtration is associated with removal of the high molecular weight lignin species from solution. At high pH, such species only make a small contribution to overall solution color but as pH is lowered their contribution increases until at pH below 7, nearly all solution color is exerted by high molecular weight lignin constituents.

d) Solution Age

The effect of solution age on the color of Indulin solutions is shown in Fig. III.8. Here the bottom graph indicates that the color of a 500 mg/l Indulin solution at pH 12.3 decays with time in an exponential-type fashion, with only 77% of the original color remaining after 15 days incubation at room temperature. The middle graph also shows that a time-dependent color degradation process also occurs in pH 10 Indulin solutions maintained at 35°C. In this case, color degradation is accompanied by a drop in solution pH. Also, as the white circle on the graph indicates, precipitation of lignin as a buff-colored turbidity

Fig. III.8

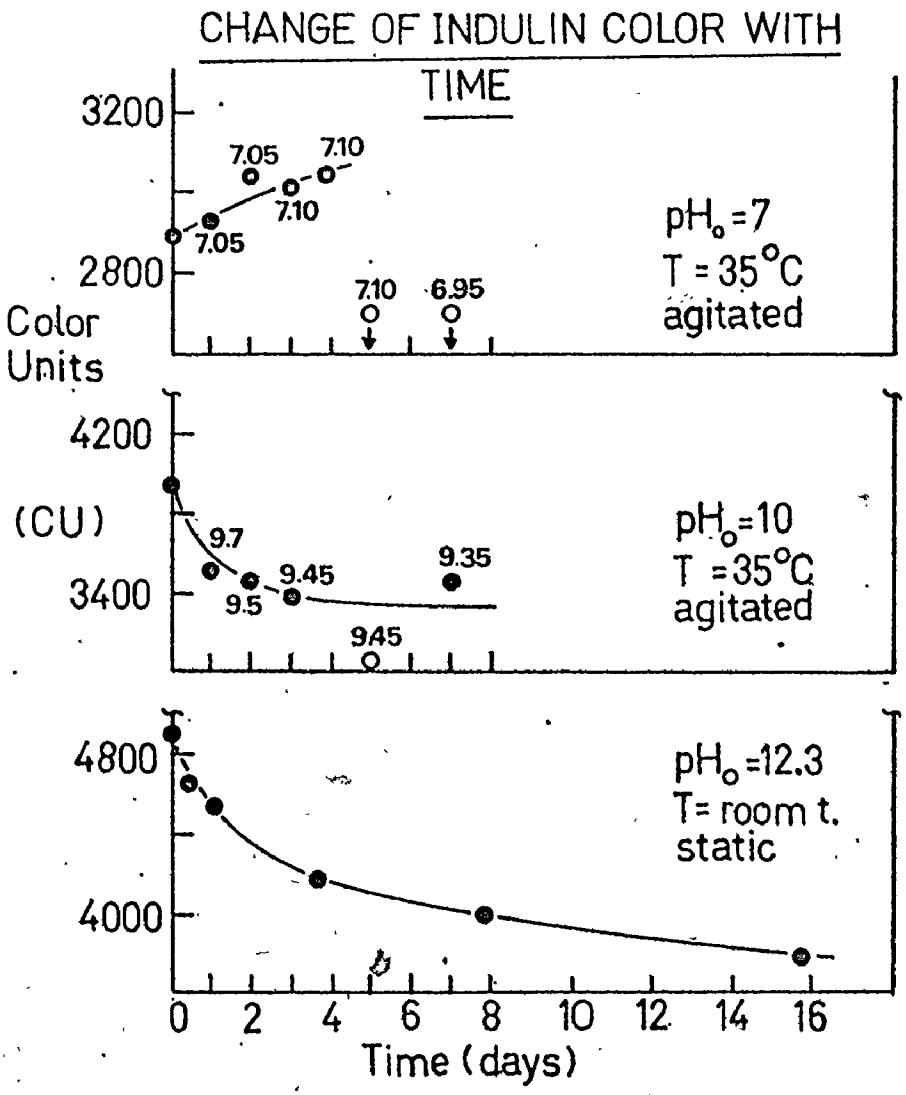
CHANGE OF INDULIN COLOR WITH TIME
3200
2800
Color Units
7.05
7.10
7.10
7.05
7.10
6.95
pH$_o$=7
T = 35°C
agitated
4200
3400
(CU)
9.7
9.5
9.45
9.35
9.45
pH$_o$=10
T =35°C
agitated
4800
4000
pH$_o$=12.3
T= room t.
static
0 2 4 6 8 10 12 14 16
Time (days)

occured in some solutions after approximately 4 days incubation. In contrast, the color of 500 mg/l Indulin solutions at pH 7 and 35°C appears to increase slightly with time, together with a slight pH rise, although lignin precipitation after 4 days incubation is very pronounced.

It is evident from these results that the color of Indulin solutions degrades with time in a manner dictated by initial solution pH and standing conditions. Obviously, the molecular constituents of the Indulin macromolecule undergo some transformation. However there is no noticeable "loss" of Indulin components as solution TOC is unaffected. The noted effect of initial solution pH on the degradation mechanism suggests possible involvement of hydronium $[H_3O^+]$ or hydroxyl $[OH^-]$ ions in a molecular reorientation, whereby condensation of low molecular weight species occurs to form higher molecular weight derivatives of reduced color. In view of Marton's (1971) statement - see section III.1 - it is also feasible that air oxidation of low molecular weight lignin species to higher molecular/ weight forms may also account for the observations.

III.3.2. (ii) Factors Influencing Indulin Solution TOC

a) Indulin Concentration

Based on the formula for Indulin A.T. given by Bailey (1972) - see section III.2.1. (i) - it can be shown that the theoretical TOC of an Indulin solution is given by

$$TOC = 0.664\ c \qquad (3.1)$$

where c is the Indulin concentration in solution. Actual TOC measurments on Indulin solutions at different concentrations and pH's can be seen from Fig. III.9 to be very close to the theoretically predicted TOC value, indicating the validity of Bailey's formula. The results in Fig. III.9 also illustrate that the Indulin TOC - concentration is linear and unaffected by solution pH above Indulin concentrations of about 30 mg/l. Below this concentration the measured TOC generally deviates upwards from the theoretical value, the magnitude of this deviation being higher at increased pH. This phenomena likely occurs as a result of dissolution of $CO_2$ from the surroundings into the sample solution.

b) Other Factors

Indulin solution TOC is unaffected by change in

Fig.III.9

CONCN.-TOC RELATIONSHIP FOR INDULIN SOLNS.

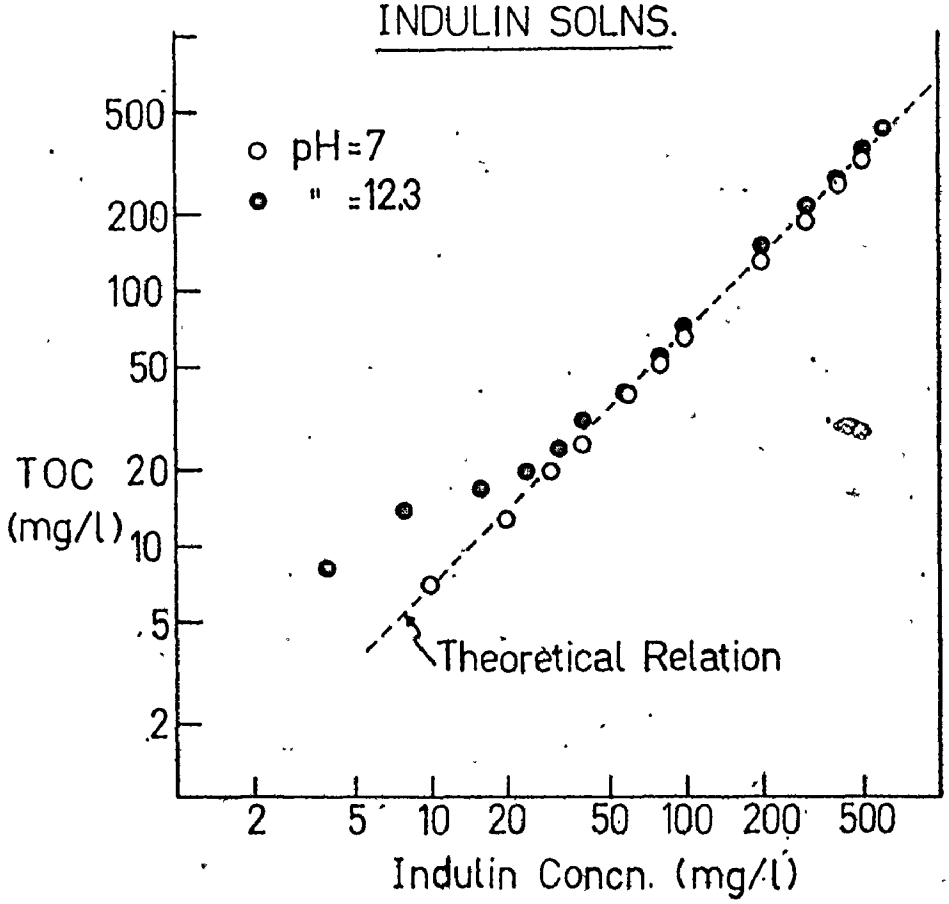

solution pH, except in dilute solutions as outlined previously. Overall Indulin solution TOC is also unaltered by solution age. However, the relative contributions to the overall solution TOC by the various Indulin molecular species present in solution is influenced by solution age. Filtration of Indulin solutions through pre-washed 0.45μ filters produces an effect similar to that observed for color (see section III.2.2.(i).(c)), viz. that slight solution TOC removal occurs upon filtration, the magnitude of this removal increasing with decrease in solution pH.

## III.3 ULTRAFILTRATION OF LIGNIN SOLUTIONS

Ultrafiltration of Indulin solutions through a series of ultrafiltration membranes of decreasing membrane pore diameters can provide valuable information regarding the molecular weights and sizes of the various molecular constituents present in such solutions. Furthermore, fractional color and TOC analysis affords the opportunity to gain insight into the specific color and TOC contributions of the various molecular weight species to the overall color and TOC exerted by the Indulin solution.

III.3.1. Theory

In ultrafiltration, solvent flows through a membrane under the action of a hydraulic pressure gradient. The amount of solute retained by the membrane is dependent primarily on the apparant membrane pore diameter - solutes which are smaller than the membrane pore diameter pass through the membrane by convection with the solvent whereas solutes larger than the membrane pore diameter are retained in solution above the membrane. Ultrafiltration can thus be used as a polymer fractionation procedure by using appropriately sized membranes in series. Until recently, ultrafiltration membranes suffered from two major drawbacks, i.e. their tendency to plug rapidly, resulting in a rapid drop in flux, and their inability to discriminate between species of similar molecular weights.

Recently a range of ultrafiltration membranes has been developed which overcome the problems encountered with earlier types. These new membranes, described by Baker (1969), are unlike the previous isotropic structures in that they consist of a dense membrane layer, 1 - 2μ

thick, supported on a 50 - 100μ thick porous substructure. The "skin" side, which faces the solution to be filtered, contains a network of microporous capillaries which are capable of retaining molecules with radii from 5 - 100 Å, depending on the membrane used (Amicon Corp. 1971).

III.3.2. Experimental

III.3.2. (i) Selection and Operation of the Ultrafiltration Cell

A Diaflo model 10PA propellent-pressurised 15 $cm^3$ unstirred ultrafiltration cell * was used to obtain molecular weight fractionation with various pore size ultrafiltration membranes as it is compact, easy to use and relatively inexpensive. The unit is depicted schematically in Fig. III.10. In order to perform ultrafiltration of a given solution the base section was first removed. The piston was returned to the "Zero" position and the unit internals washed with distilled water. The cell was then inverted and filled with distilled water. The appropriate membrane was then inserted, together with the porous plastic support plate,

* Amicon Corp., Lexington, Mass., U.S.A.

Fig. III.10 Schematic Diagram Of Amicon Model 10PA Unstirred 15 $cm^3$ Ultrafiltration Cell

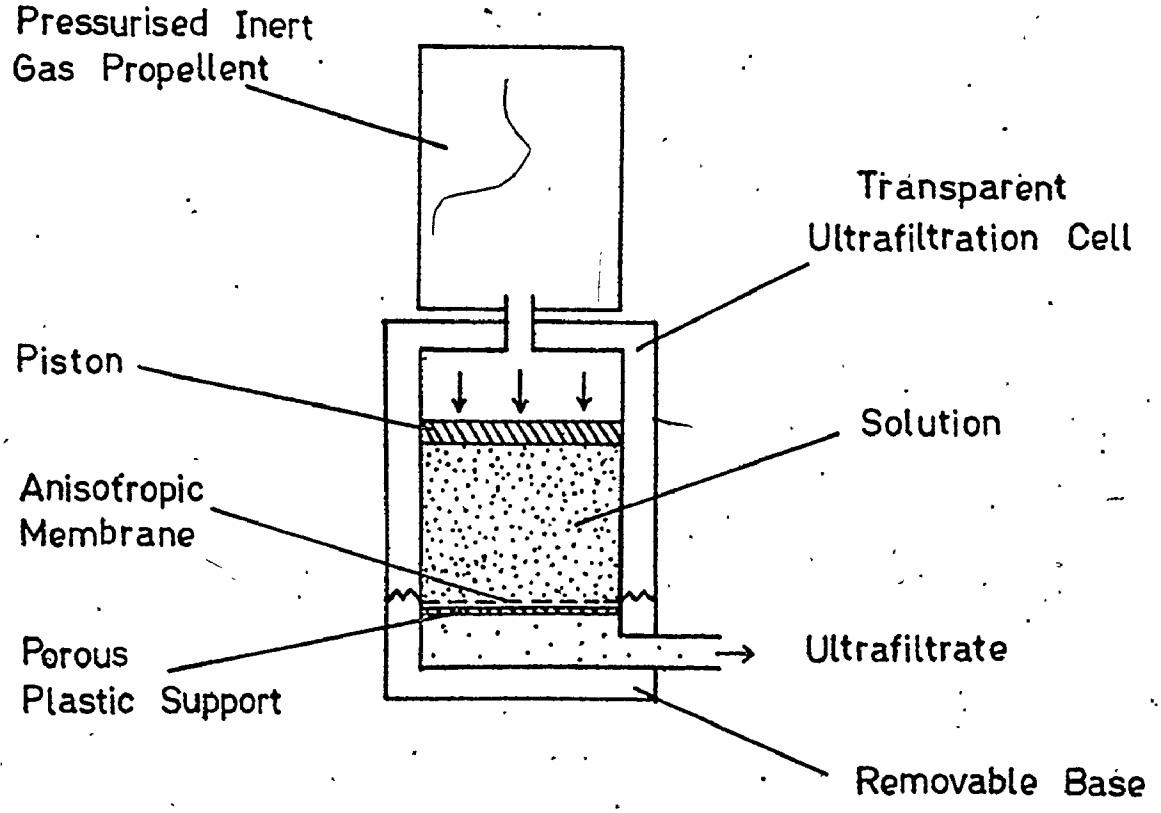

and the base section then screwed back on. The unit was then uprighted and a small graduated cylinder placed at the ultrfiltrate outlet for collection of the filtrate solution. A propellent container was then clipped onto the top of the unit, and ultrafiltration of the solution allowed to commence. Initially the flux was relatively high, but decreased sharply during the first 15 minutes due to compression of the membrane. Soon after, however, the flux stabilized. When nearly all the water had been collected as filtrate (about 15 ml), the propellent was removed, the unit disassembled, washed, and the procedure repeated using the test solution. After use the membrane was washed and stored in distilled water in a 4°C refrigerator until required again.

III.3.2. (ii) Selection and Calibration of Membranes

Due to the expected extensive molecular weight range of molecular constituents in Indulin solutions, and lack of previous research on lignin ultrafiltration, it was decided to use the whole range of Diaflo 25 mm diameter membranes* i.e. the XM, PM and UM series, (Amicon Corp. 1971).

* Amicon Corp., Lexington, Mass. U.S.A.

These membranes have already been calibrated by other researchers using a variety of organic solutes in water solution (Amicon Corp. 1971). Their calibrations were performed with both globular molecules (proteins, enzymes and peptides) and linear and flexible molecules (polysaccharides, glycols and nucleic acids.) Since lignin in dilute aqueous solution exists as a variety of approximately spherical molecular species (see section III.1), only the membrane calibrations based on globular molecules was considered relevant to this study. Fig. III.11 displays Amicon's calibration of their anisotropic membranes with globular proteins. Although Fig. III.11 is based on data obtained from a stirred ultrafiltration cell, it was felt justified to apply this calibration to the unstirred cell studies in this work. Stirring does not radically alter membrane separation characteristics; it merely enhances the rate of ultrafiltration and establishment of ultrafiltration equilibrium conditions by dispersing the solute concentration gradient in the retained solution above the membrane.

Fig.III.11 Calibration Of Ultrafiltration Membranes

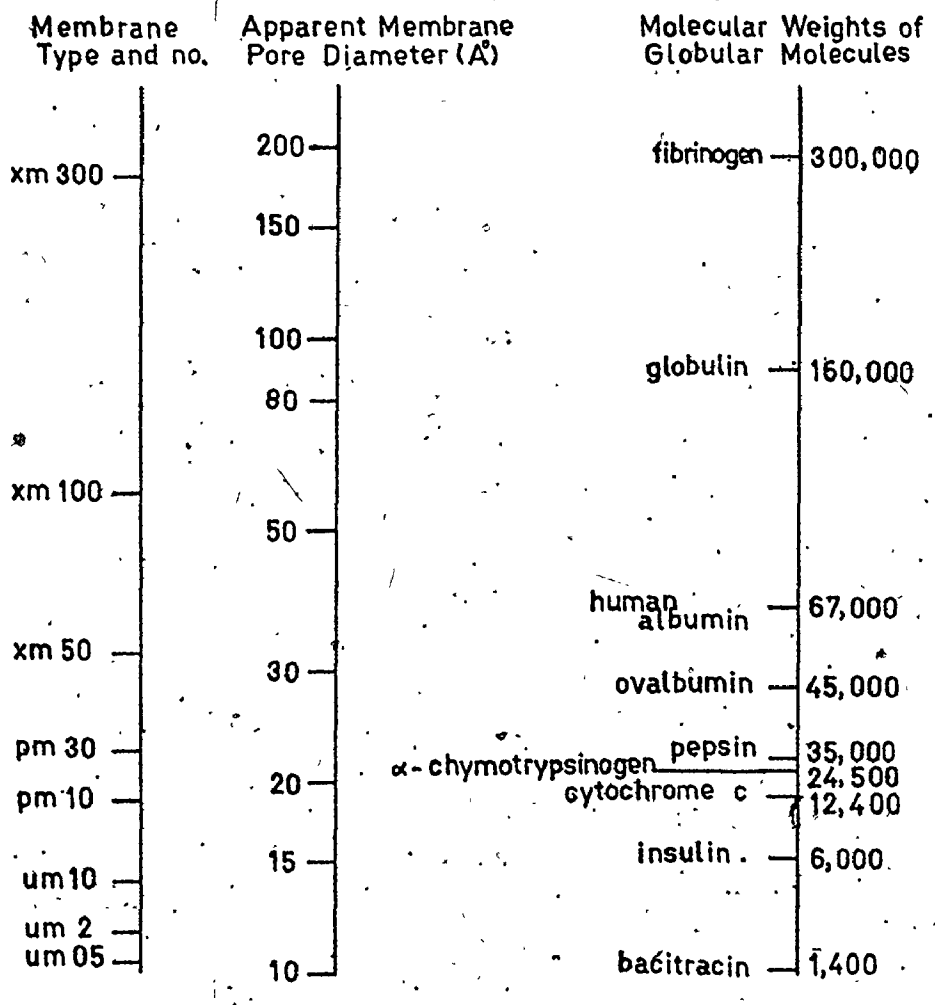

III.3.2 (iii) Contribution of Membrane Water Soluble Extractives to Ultrafiltrate TOC

Ultrafiltration membranes usually contain organic wetting agents which will dissolve in aqueous solvents and appear in the ultrafiltrate. If ultrafiltrate TOC measurements are used as indicators of membrane separation characteristics - such as is the case in ultrafiltration of Indulin solutions - then the measured ultrafiltrate TOC will necessarily include a contribution from membrane organic extractives. Experiments were thus performed to evaluate the TOC contribution of membrane organic extractives in the ultrafiltrate. Here, for each membrane used, five successive 15 $cm^3$ distilled water aliquots were subjected to ultrafiltration, and the ultrafiltrates analyzed for TOC content. The results are shown in Table III.3. Here all membranes impart some TOC to the ultrafiltrate, particularly the XM50 and UM 05 membranes. Furthermore, it appears that all the membrane extractives are not removed in the first one or two filtrations - as is usually the case with millipore filters (Hals, 1974) - but continue to produce a significant effect on ultrafiltrate TOC even in the fifth ultrafiltrate. For each membrane, the average

Table III.3 Contribution of Membrane Extractives to Ultrafiltrate TOC

Feed solution: distilled $H_2O$ (TOC = 0 mg/l)
Ultrafiltrate Volume: 15 $cm^3$

| Membrane | Ultrafiltrate TOC (mg/l) | | | | | Average Ultrafiltrate TOC (mg/l) of 5 filtrations |
|---|---|---|---|---|---|---|
| | 1st Filtration | 2nd | 3rd | 4th | 5th | |
| XM 300 | 3 | 3 | 3 | 4 | 4.5 | 3.5 |
| XM 100 | 4.5 | 3 | 3 | 2 | 3 | 3 |
| XM 50 | 3 | 8 | 7 | 7.5 | 7.5 | 6.5 |
| PM 30 | 2 | 4.5 | 3 | 4 | 5 | 3.5 |
| PM 10 | 1.5 | 1.5 | 4 | 2 | 2 | 2 |
| UM 10 | 3 | 2.5 | 2 | 2.5 | 1.5 | 2.5 |
| UM 2 | 4.5 | 7 | 2 | 4 | 4.5 | 4.5 |
| UM 05 | 6.5 | 5 | 11.5 | 7.5 | 9.5 | 8 |

value of ultrafiltrate TOC over five filtrations was used as a correction factor in estimation of Indulin ultrafiltrate TOC. It should be noted that membrane extractives contributed no color to the ultrafiltrate.

III.3.2. (iv) Ultrafiltration of Aqueous Indulin Solutions

A 500 mg/l Indulin solution was prepared at given pH, and its color and TOC content measured. Using the appropriate membrane, pre-washed five times, ultrafiltration of a 15 $cm^3$ aliquot of the original solution was performed, and halted when approximately 14 $cm^3$ of ultrafiltrate had been collected. For each membrane, three separate ulstrafiltrations were performed, with the ultrafiltration cell and membrane being washed with distilled water after each ultrafiltration. This procedure was repeated using different membranes. The color and TOC of the ultrafiltrate samples from each membrane were measured, the latter being corrected for membrane extractive TOC contribution by subtraction of the appropriate value given in Table III.3. Color measurements were performed at the pH of the original solution; pH adjustment where necessary being achieved

by the addition of a few drops of 0.1 M NaOH or 0.1M HCl solution. After completion of all necessary ultrafiltrations, original solution color and TOC were again measured.

The above procedure was performed for both pH 7 and pH 10 Indulin solutions.

III.3.3. Results and Discussion

The results of the ultrafiltration experiments outlined in the previous section are depicted in Figs. III. 12 and III. 13. The data is expressed as percent of original solution color or TOC remaining in the ultrafiltrate after filtration through a membrane of given pore diameter.

Here it can be seen that Indulin, as it exists in the solution studied, is comprised of various molecular weight species. A significant portion of overall solution color and TOC is seen to be exerted by molecular constituents of greater than about 300,000 molecular weight (MW), corresponding to a hydrodynamic diameter of greater than approximately 200 Å. At the other end of the scale, a small but significant fraction of the overall Indulin solution color and TOC is also contributed by

Fig. III.12 Ultrafiltration of Indulin Solutions

Color Analysis

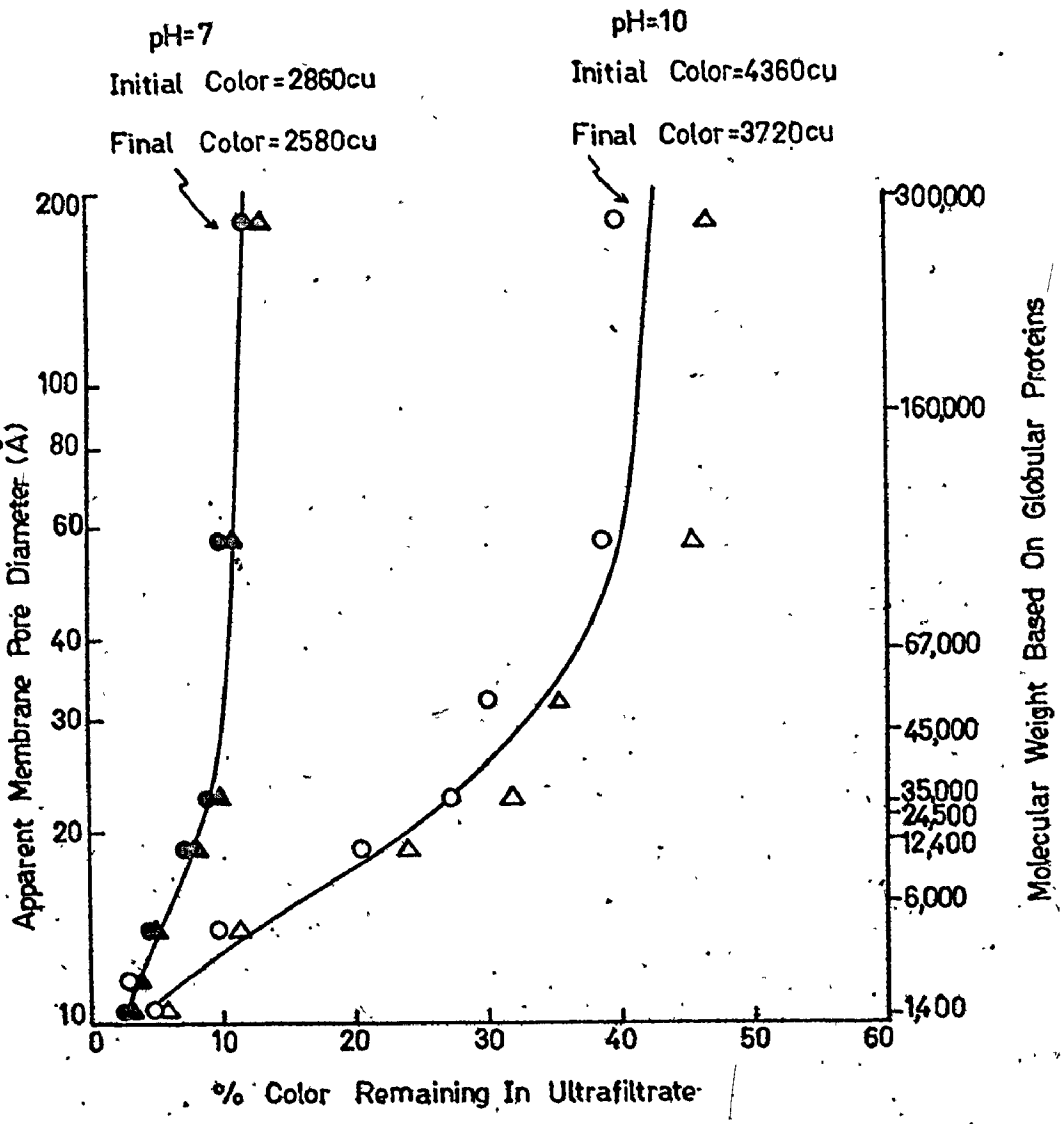

Fig. III.13 Ultrafiltration of Indulin Solutions

TOC Analysis

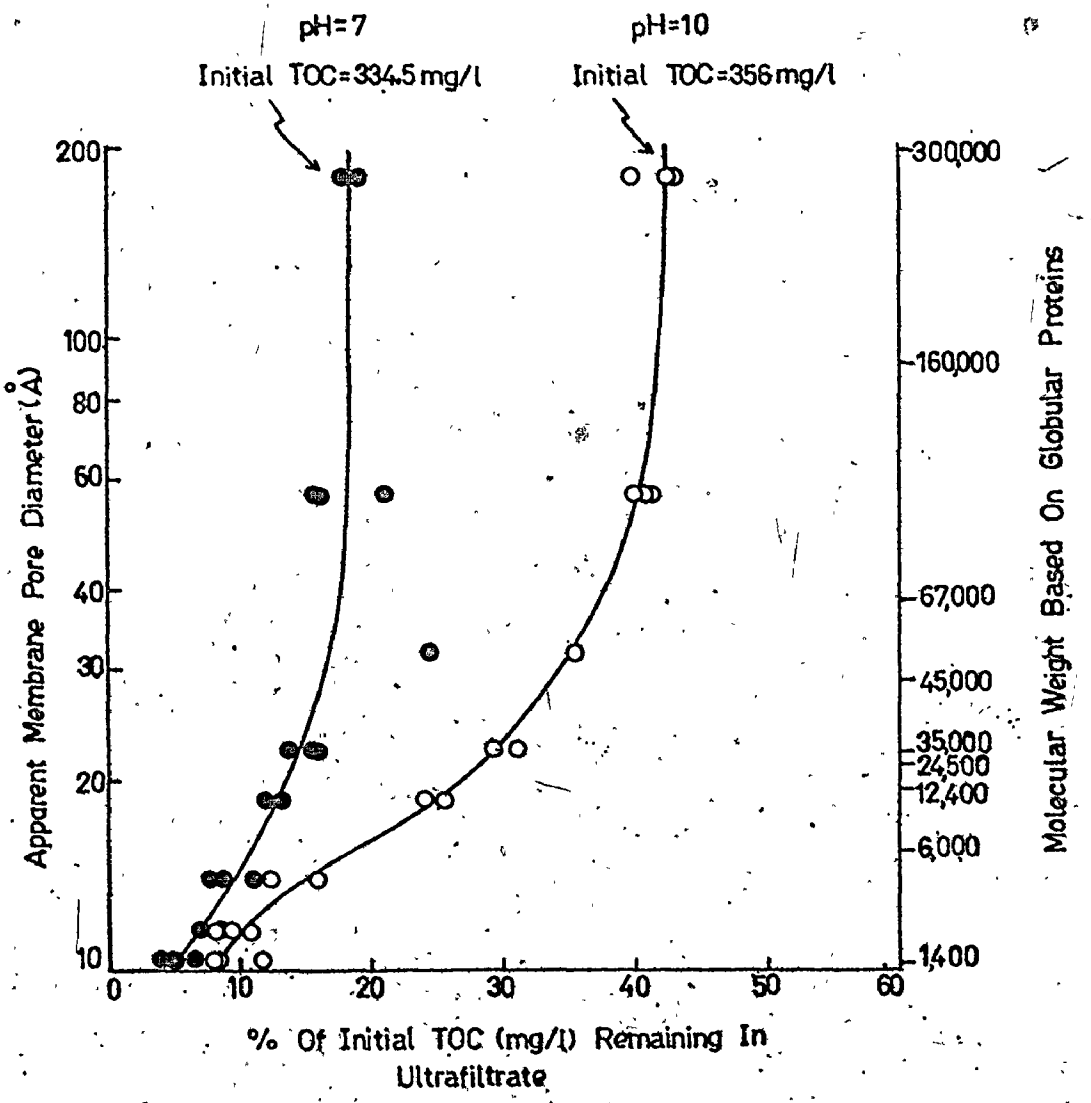

molecular species of less than about 1400 MW, corresponding to hydrodynamic diameters of less than 10 Å.

The effect of solution pH on the distribution of Indulin components in solution is interesting. As Figs. III.12 and III.13 show, decrease in solution pH from 10 to 7 produces a higher percentage of the larger molecular constituents (i.e. those of greater than 300,000 MW) at the expense of the smaller molecular species. This pH decrease is also associated with a decrease in overall solution color, although overall solution TOC remains unchanged. This finding supports the deductions regarding the pH effect made earlier (see section III.2.2. (i).b); it appears that the 'amount of color per molecule' increases as molecular weight decreases, due probably to solubility considerations. As pH is reduced the average molecular weight of components is seen to decrease, thereby reducing overall solution color.

Molecular weight fractionation using ultrafiltration membranes has an advantage over Gel Filtration (see section III.4) in that any pH solution

may be characterised. However, it suffers from the fact that it is slow, requires relatively large samples (approximately 500 ml for a complete characterisation), and that ultrafiltrates are always associated with solubilised membrane extractives, even after extensive pre-washing. A further disadvantage of ultrafiltration as a method of characterising lignin solutions is that during filtration, the larger molecular weight lignin fractions can tend to plug up the membrane pores and thus reduce the effective molecular size resolution of the membrane. This effect would be more pronounced in an unstirred ultrafiltration cell, as used in this work. However, by proper operation of the ultrafiltration cell and good treatment of membranes this tendency can be minimised.

## III.4 GEL FILTRATION OF LIGNIN SOLUTIONS

Gel Filtration can be used to determine the nature and extent of the distribution of the various molecular weight species present in lignin solutions. Furthermore, this technique can be used to isolate various molecular weight fractions; by performing color and TOC measurements on these fractions it is possible to obtain information on the contribution of different molecular species to overall lignin solution color and TOC.

### III.4.1. Theory

In Gel Filtration, the various molecular weight species present in a polymer solution can be separated by passing the solution through a gel bed. Polymeric materials such as dextran, agar, starch, polyacrylamide and polyvinyl alcohol have been used as gels (Laurent and Killander, 1964). In this study a bead-formed dextran, Sephadex G-100 * was used. In water or electrolyte solutions the Sephadex beads swell, due to the strongly bydrophilic nature of the hydroxyl groups present in the polsaccharide chains of the dextran beads, forming a gel.

---

* supplied by Pharmacia AB, Uppsala, Sweden

Upon filtration of a polymer solution through the swollen gel bed, molecular weight species of hydrodynamic radii greater than the diameter of the largest pores in the swollen gel cannot penetrate the gel particles and hence pass through the bed in the liquid phase outside the gel beads. They are eluted first, appearing in the eluant at a collected colume $V_o$. This volume corresponds to void volume of the gel bed. Lower molecular weight species having smaller hydrodynamic radii, however, will penetrate the gel pores. Such species will thus be 'side-tracked' in their passage through the bed, appearing in the eluant at a higher collected volume $V_e$. The amount of gel pore penetration depends on solute molecular size; smaller molecules being able to penetrate a greater number of gel pores. Hence elution of solutes from the gel bed will occur in order of decreasing molecular size, each species appearing in the collected eluant at a unique collected volume $V_e$. Finally, at a species of sufficiently low molecular weight and hydrodynamic radius, the gel is no longer able to effect molecular separation. All species of this molecular weight and less will be able

to penetrate the total pore structure of the gel bed, all being eluted at the same collected eluant volume $V_t$, where $V_t$ represents the total volume of the swollen gel bed.

The extent of separation occurring in Gel Filtration is primarily dictated by gel and polymer characteristics. Laurent and Killander (1964) have shown that a gel column can be characterised in terms of a separation parameter $K_{AV}$, where $K_{AV}$ is related to gel column elution characteristics by the equation

$$K_{AV} = \frac{V_e - V_o}{V_t - V_o} \qquad (3.2)$$

where $V_e$ = the elution volume corresponding to appearance of a given molecular weight or size constituent in the eluant

$V_o$ = the void volume of the gel bed

$V_t$ = the total volume of the gel bed

Here solutes completely excluded from the gel matrix will have $K_{AV} = 0$, whereas solutes passing through all the gel pores will have $K_{AV} = 1$. The solutes effectively separated by the gel will have $K_{AV}$ values between 0 and 1, with each resolved species being characterised by a unique $K_{AV}$ value.

Assuming that the chain molecules which constitute the skeleton of the swollen gel are straight rigid rods, which are infinitely long and randomly distributed throughout the gel, Ogston and Phelphs (1961) have shown that $K_{AV}$ may be related to the hydrodynamic radius r of a spherical solute molecule by the equation

$$K_{AV} = \exp\left[-\pi L (r + r_r)^2\right] \qquad (3.3)$$

where L = the concentration of rods in solution

$r_r$ = the rod radius

For Sephadex G-100 gel swollen in water at neutral pH, Laurent and Killander (1964) have determined values of L ($2.9 \times 10^{12}$ cm rod / $cm^3$) and $r_r$ ($7 \times 10^{-8}$ cm) experimentally. From Gel Filtration data it is thus possible, using equations (3.2) and (3.3) coupled with a knowledge of L and $r_r$, to calculate the hydrodynamic radii of the various molecular constituents present in the original polymer solution. Generally, however, L and $r_r$ are not known for the gel system used. For this reason, separation characteristics are based on molecular weight, rather than molecular size, although it must be remembered that Gel Filtration is based on steric hindrance principles and is thus

dependent on solute molecular size.

For Gel Filtration through a Sephadex G-100 gel bed, Squire (1964) has shown that the relationship between eluant volume and species molecular weight is given by

$$M^{1/3} = \frac{C^{1/3}}{g}\left[1 + g - (V_e/V_o)^{1/3}\right] \qquad (3.4)$$

where C = molecular weight of the smallest molecule that is completely excluded from the gel pores, i.e. at $V_o$

M = molecular weight of the largest molecule that is able to penetrate all the gel pores, i.e. at $V_t$

g = a constant (0.45 - 0.48 in aqueous solutions)

An alternative procedure for expression of separation based on molecular weight is simply to run monodisperse standards of known molecular weight through the gel bed. Their corresponding elution volumes are converted to the appropriate $K_{AV}$ values via equation (3.2). Usually calculated $K_{AV}$ values are found to vary linearly with respect to the logarithm of molecular weight (Pharmacia AB, 1970).

Generally the models of Gel Filtration behaviour summarised have assumed negligible solute-gel interactions. However, ion exclusion, adsorption and Donnan equilibrium effects arising from solute-gel interactions

can result in molecules either not being eluted at all, or being eluted later or earlier than predicted by the model used. Coss (1973) has adequately summarised the present information available in this context.

III.4.2. Experimental

III.4.2. (i) Selection and Preparation of the Gel

Sephadex G-100 was used as the gel media in this study. The gel is stated (Pharmacia AB, 1970) to be able to separate solutes having molecular weights in the range 4,000 - 150,000, assuming spherical molecules. This gel was used by Bailey (1972) and Obiaga and Ganczarczyk (1973) in molecular weight characterisation of Indulin A.T. solutions.

The gel beads were swollen in distilled water by boiling for 8 hours with frequent gentle agitation. * After swelling was complete, the slurry was sterilised in a steam antoclave at 20 psi for 20 mins. The sterilised swollen gel was stored in a 4°C incubator prior to use.

---

* too severe agitation may cause bead rupture and subsequent destruction of gel separation efficiency.

III.4.2. (ii) Packing the Gel Column

Good even packing of the gel bed is a pre-requisite of efficient gel separation characteristics. Uneven packing gives rise to formation of column dead spots, resulting in an uneven radial flow profile through the column and its associated poor separation effect.

Here the swollen sterilised gel was separated from supernatant water by decantation, the resultant thick slurry being then poured carefully down a vertical 1.6 cm diameter, 100 cm high Pharmacia model K16/40 glass column containing a small amount of distilled water. Care was taken not to entrap air bubbles in the bed during pouring. After addition of the gel, the remaining space at the top of the bed was filled with distilled water. Simultaneously the outlet was opened to drain water from the bed at a rate of approximately 6 - 8 ml/hr. As the bed drained, more water was allowed to enter the column via a Mariotte bottle (see Fig. III.14.) Flow was then allowed to continue for 48 hours in order to facilitate gel bed stabilization.

fig. III.14 Gel Filtration Experimental Unit

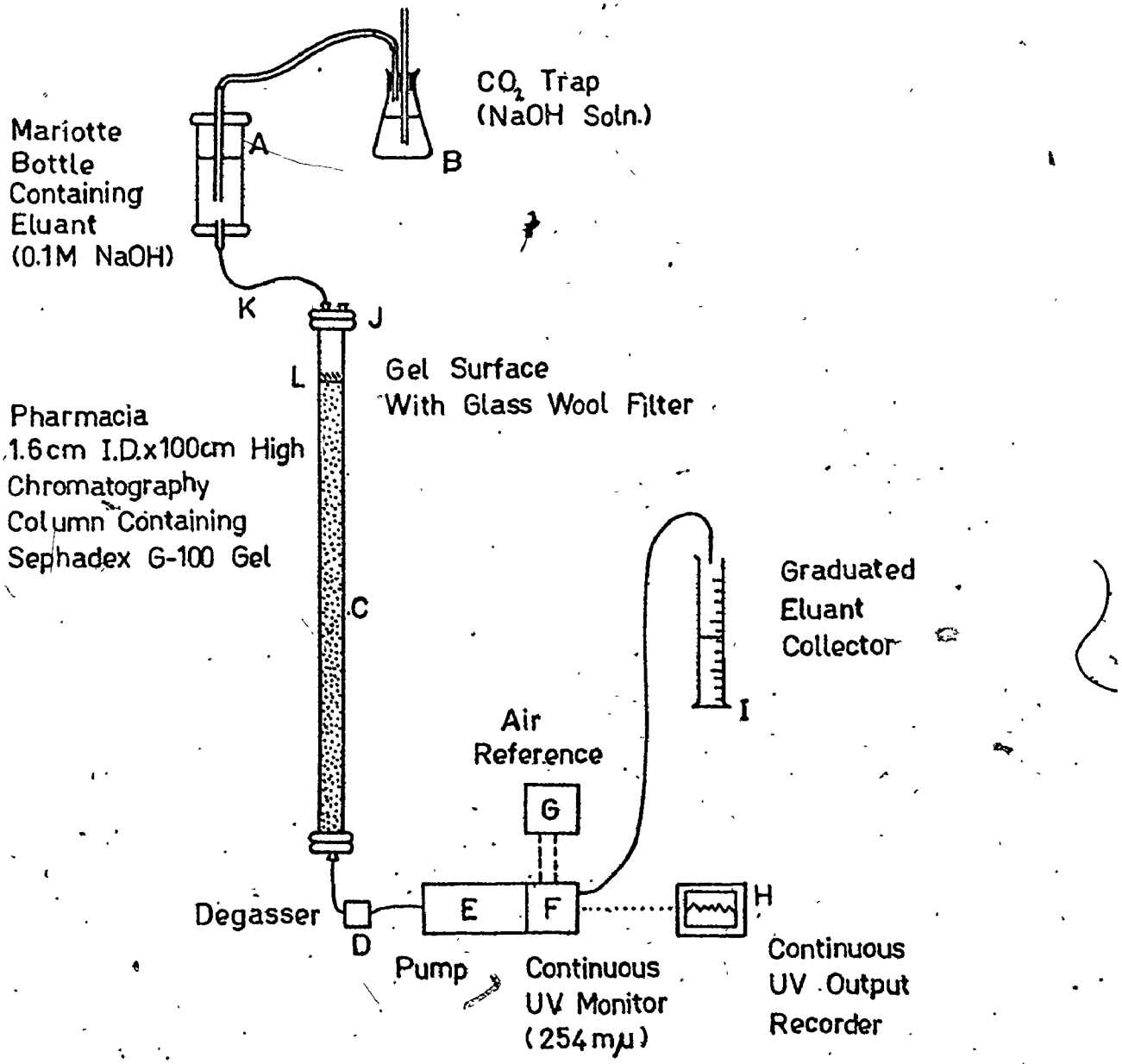

After stabilisation, the carrier in the Mariotte bottle was changed to 0.1 M NaOH solution and drainage allowed to proceed for a further 72 hours. Thereafter, the flow was halted by sealing the eluant outlet tube.

III.4.2. (iii) Description and Operation of the Gel Filtration Unit

A schematic diagram of the Gel Filtration unit used in this work is shown in Fig. III.14. The 0.1 M NaOH carrier solution at pH 12.5 was stored in a Mariotte reservoir (A).* The caustic trap (B) was required to strip $CO_2$ from the air entering the reservoir, thus preventing any change in carrier solution pH due to $CO_2$ adsorption, as this would have effected column operation. The eluant from the gel bed was subjected to continuous measurement of its 254 mμ absorbance, utilising a continuous UV detector (E) incorporating an air reference cell (G). A continuous trace of eluant absorbance was obtained on a chart recorder (H). The eluant was finally collected in a graduated cylinder (I).

In Gel Filtration experiments, the sample to be characterised was first adjusted to column operating

* a device capable of allowing liquid to flow into the gel column at a constant rate.

pH of 12.5 by addition of a few drops of conc. NaOH solution. A 1.5 $cm^3$ aliquot of the pH - adjusted sample was taken up in a small graduated bent tip pipette. The aliquot was then introduced to the top of the bed by holding the pipette top just above the gel surface (L) and allowing the sample to drain slowly onto the bed surface, at the same time slowly rotating the pipette to ensure even distribution of sample over the gel surface. A thin layer of glass wool on the bed surface (L) helped minimize bed disturbance during sample introduction, as did the use of bent-tip pipette. After sample intorduction, the column top (J) was screwed on, care being taken to exclude entrainment of air bubbles in the carrier liquid. The carrier solution feed clamp (K) was opened and the sample bank above the gel bed visually checked for uniformity. * The eluant outlet plug (I) was then removed and filtration allowed to proceed at a constant flow rate of about 6 - 10 ml/hr, this having been predetermined by the adjustment of the

---

* This was only possible with the colored samples such as Indulin solutions. It is not possible to do this for the colorless samples of globular protein molecular weight standards used in column calibration.

operating head of the column (i.e. the vertical distance between the eluant outlet (I) and the base of the Mariotte reservoir air inlet tube). Flow rates in excess of 10 ml/hr were found to cause bed compression. The column eluant 254 mμ absorbance was monitored continuously via the UV detector and output recorder. The carrier solution, 0.1 M NaOH, exhibits no 254 mμ absorbance. However, solutions of alkali lignins such as Indulin display considerable 254 mμ absorbance (Kleinert and Joyce, 1958). Thus a positive recorder trace will indicate the appearance of separated Indulin molecular weight constituents in the eluant. After all sample species had been eluted from the gel bed - as indicated by a return of the recorder UV trace to its initial base-line position - filtration was complete. The filtration unit was then either injected with another sample or shut off by clamping off inlet and outlet tubes until required again.

III.4.2. (iv) Calibration of the Gel Bed

The gel bed was first calibrated in order to determine molecular weight separation characteristics of the gel column under the operating conditions used in

this study. Since the polymeric lignin molecule in solution is comprised of approximately spherical macro- and micro-solutes (see section III.1), calibrations were performed using mainly globular protein standards of known molecular weight, although some linear-type molecule standards were also included for comparison. The standards used in this study are listed in Table III.4. All standards were found to exhibit significant absorbance at 254 mμ; their presence in the collected eluant could thus be readily detected. The column was standardised using samples of the standards dissolved in 0.1 M NaOH solution to give a concentration of approximately 2 mg/cm$^3$. The standards were either run through the column singly or combined with other standards.

III.4.3 Results and Discussion

III.4.3. (i) Molecular Weight Calibration of the Gel Bed

An example of the 254 mμ UV absorbance trace on the collected eluant from gel filtration of an alkaline standard solution containing Blue Dextran, Cytochrome C, Insulin and Phenylalanine is shown in Fig. III.15. Here

Table III.4. Standards Used in Calibration of the Gel Filtration Unit

| Standard | Type of Molecule (1) | Molecular Weight | Stokes Radius (2) (Å) |
|---|---|---|---|
| Aldolase | G | 158,000 | 46.0 |
| Blue Dextran | L | 2,000,000 | -- |
| Dnase | L | 65,000 | -- |
| Ovalbumin | G | 45,000 | 27.3 |
| Pepsin | G | 32,700 | 22.9 |
| Chymotrypsinogen a | G | 25,000 | 22.4 |
| Ribonuclease a | G | 13,700 | 19.2 |
| Cytochrome c | G | 12,400 | 16.4 |
| Insulin | G | 5,800 | -- |
| Glucagon | G | 3,900 | -- |
| Phenylalanine | L | 165 | -- |

G = Globular Molecule

L = Linear or Flexible Molecule

(1) from Noller (1965)

(2) from Laurent and Killander (1964)

fig. III.15 Separation Of Molecular Weight Standards By Sephadex G-100

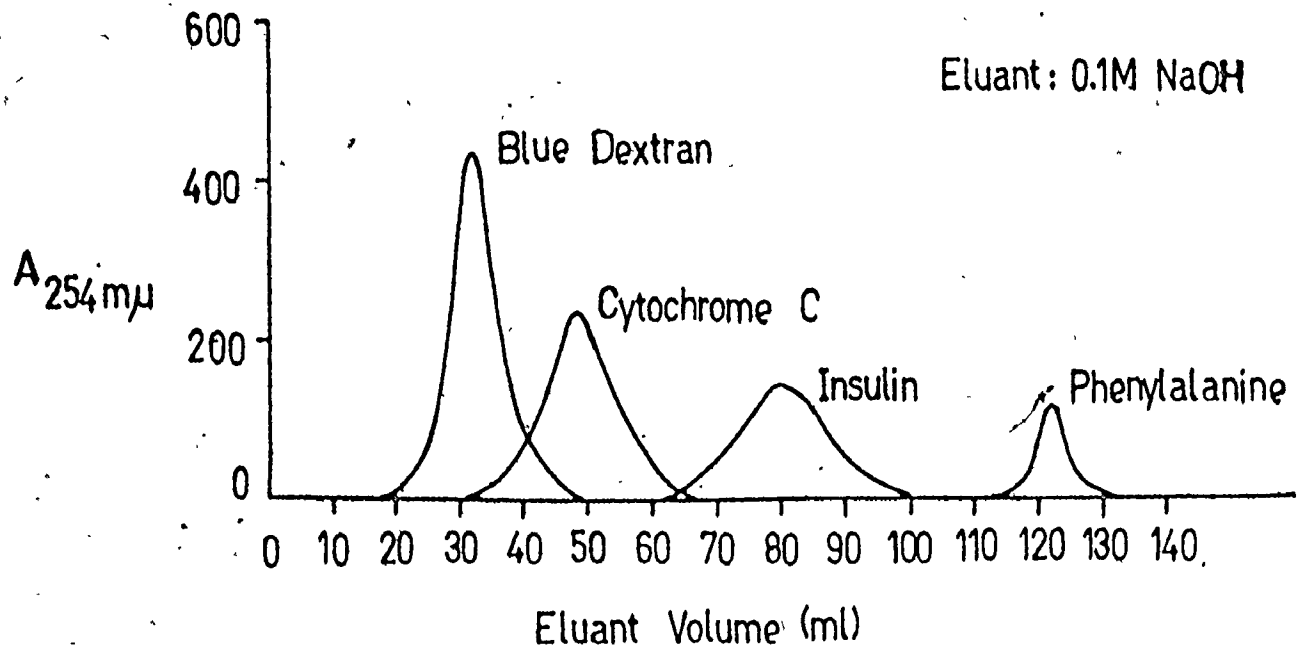

the eluant volume corresponding to elution of blue dextran from the gel bed is representative of the bed void volume $V_o$, since the blue dextran molecules are sterically excluded from all the gel pore volume. Hence, for blue dextran from equation (3.2), $V_e = V_o = 32$ ml * and so $K_{AV} = 0$. In contrast, the collected eluant volume at which phenylalanine is eluted from the bed is indicative of the total bed volume $V_t$, as all the gel pore volume is available to penetration by phenylalanine molecules in view of their very small molecular weights and size. Thus for phenylalanine, from equation (3.2) $V_e = V_t = 122$ ml * and so $K_{AV} = 1$. Substituting the obtained values of $V_t$, $V_o$ into equation (3.2), one obtains

$$K_{AV} = \frac{V_e - 32}{90} \qquad (3.5)$$

* during passage of sample through the gel bed, the original 'band' of sample solution is subject to a certain amount of axial diffusion within the carrier solution. This tends to broaden the sample 'band' as it passes through the bed, giving rise to a eluant UV trace that, if tailing is negligible, is evenly distributed about a peak mean value. (See Fig. III.15) The elution volume corresponding to this mean or maximum value was used as being most representative of the true elution volume $V_e$ in this study.

From equation (3.5) the value of $K_{AV}$ for all solutes separated by the gel can be calculated from a knowledge of their elution volumes. Thus for cytochrome c and Insulin, having $V_e$ equal to 48 ml and 80 ml respectively, the values of $K_{AV}$ are 0.18 and 0.53 respectively.

Using equation (3.5), $K_{AV}$ values for all standards were calculated using the appropriate values of $V_e$ obtained from Gel Filtration runs. The calculated $K_{AV}$ values were then plotted against the logarithmn of the standards molecular weight. The resultant curve, shown in Fig. III.16, represents the separation characteristics of the gel, based on globular solutes. The nature of this curve differs somewhat from expectations. Firstly, the molecular weight range of solutes effectively seaparated by the gel filtration unit used here, i.e. approximately 4000 - 70,000 MW, is less than that stated by the gel manufacturers, viz. 4,000 - 150,000 MW, based on globular protein standards. Secondly, the relationship between $K_{AV}$ and log MW over the separation range is not linear. These phenomena are no doubt associated with the high operating pH of the

Fig. III. 16

SEPHADEX G-100 COLUMN CALIBRATION

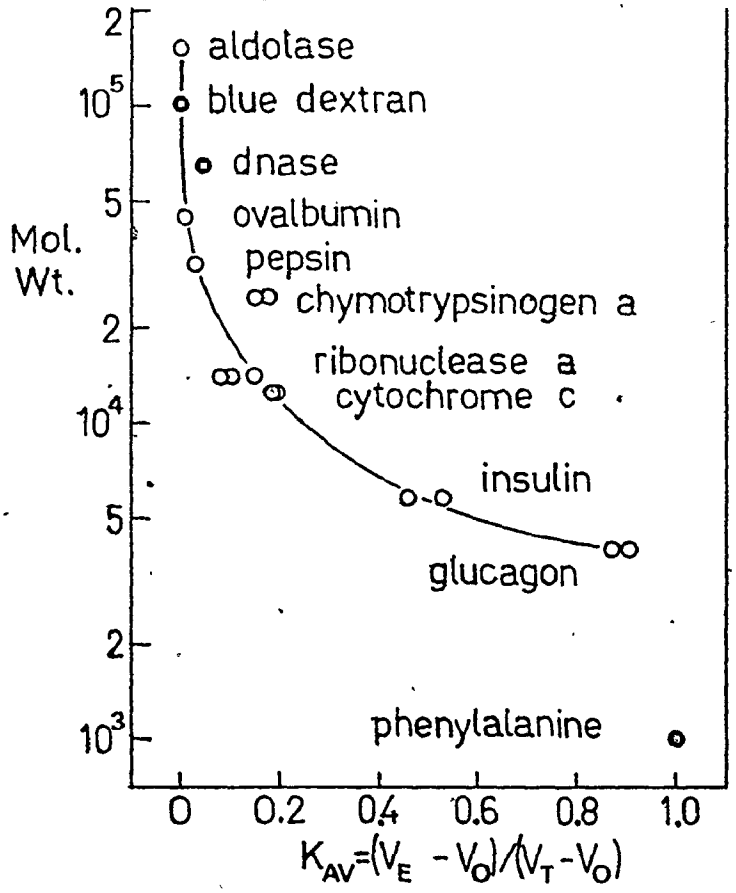

unit used here. Comparison of $K_{AV}$ values of some globular protein standards obtained for a sephadex G-100 gel bed under two operating pH's are shown in Table III.5 , where it can be seen that increase in column operating pH decreased the $K_{AV}$ value of all the standards used. This increase in column pH tends to produce earlier elution of solutes.

Consultation with equation (3.3) - see section III.4.1 - indicates that in order for the $K_{AV}$ value of a given solute to decrease, either the solute hydrodynamic radius r, the radius of the gel rods $r_r$, or the concentration of gel rods in solution L, must necessarily increase. Since L is necessarily independent of pH, providing no gel washout occurs *, it thus appears that either an increase in the size of the gel rods due to alkaline hydrolysis of the polysaccharide chains, or alkaline hydrolysis of the solute molecules themselves, resulting in an increase in their hydrodynamic radii, would be responsible for the nature of the calibration

---

* It is feasible that some of the gel material could be solubilised in a high pH solution and hence be eluted, thus decreasing L. However, TOC analyses of collected eluant samples indicated that this did not occur.

Table III.5 Effect of Column Operating pH on Sephadex G-100 Gel Resolution of Globular Proteins

| Globular Protein | $K_{AV}$ | |
|---|---|---|
| | pH 7 (1) | pH 12.5 (2) |
| Ovalbumin | 0.22 - 0.29 | 0.01 |
| Chymotrypsinogen a | 0.45 | 0.15 - 0.18 |
| Ribonuclease a | 0.58 | 0.08 - 0.15 |
| Cytochrome c | 0.59 - 0.66 | 0.18 - 0.2 |

(1) Laurent and Killander (1964)

(2) from Fig. III.16

curve in Fig. III.16. The data collected in this work does not, however, provide sufficient information to decide which of the two aforementioned effects is primarily responsible for the nature of the calibration curve obtained here.

In view of the aforementioned, one may pose the valid question "why operate the gel column at such a high pH?" The reason for this is that gel filtration of Indulin solutions at lower operating pH were found to result in excessive precipitation and/or adsorption of lignin components in the gel matrix. This was especially evident in the upper part of the bed, as noted by a brown discoloration of the gel. Here the carboxylate and phenolate anions in the Indulin macro molecule certainly have the ability to chemically associate with functional groups in the gel polysaccharide chains to an extent governed by column operating pH and ionic strength in the carrier solution (Bailey, 1972).

The adsorbed species were not desorbed and subsequently eluted until column pH was increased to approximately 12. Then observations contradict those

of Ganczarczyk and Obiaga (1973), who indicate negligible precipitation of indulin components on sephadex G-100 gel during gel filtration at pH 10, this operating pH being achieved using a carrier solution of 0.1 M NaOH buffered with $NaHCO_3$.

III.4.3. (ii) Molecular Weight Distributions in Aqueous Indulin Solutions

The following Indulin solutions were subjected to gel filtration analysis by the procedure outlined in section III.4.2 (iii).

a) A freshly prepared 500 mg/l Indulin solution at pH 12.5.

b) A 500 mg/l Indulin solution agitated for 5 days at pH 10 and 35 C.

c) A 500 mg/l Indulin solution agitated for 5 days at pH 7 and 35 C.

The subsequent plots of absorbance $A_{254\ mu}$ versus eluant volume obtained from experiments were first converted to $A_{254\ mu}$ versus $K_{AV}$ plots via equation (3.5), and then to $A_{254\ mu}$ versus MW plots via the gel calibration curve, Fig. III.16. The

resultant molecular weight distributions in the indulin solutions studied are shown in Fig. III.17.

Here Indulin, as it exists in a freshly prepared 500 mg/l alkaline solution, is seen to be comprised of at least 3 distinct molecular weight solutes. The first peak in the distribution, corresponding to $K_{AV} = 0$, is indicative of the presence of high molecular weight solutes of 70,000 MW and greater. The intermediate peak occurring at $K_{AV} - 0.5$ indicates the existance of species of approximately 5600 MW. The peak at $K_{AV} - 0.87$ relates to the presence of low molecular weight lignin fragments of approximately 4000 MW and less. *

Gel filtration of a 500 mg/l Indulin solution aged for 5 days at neutral pH yields a molecular weight distribution curve that is not noticeably different to that of the original distribution, but similar aging at

---

* There is also a UV peak at $K_{AV} = 1$. This peak probably reflects the presence of very low molecular weight lignin solutes which assume a more linear molecular configuration in solution, rather than the spherical configuration of their larger cousins. However, since this peak is small in relation to the other observed peaks, the proportion of such species, compared to the total number of all species in solution, is small.

Fig.III.17

GPC ANALYSIS OF 500 mg/l INDULIN SOLUTIONS

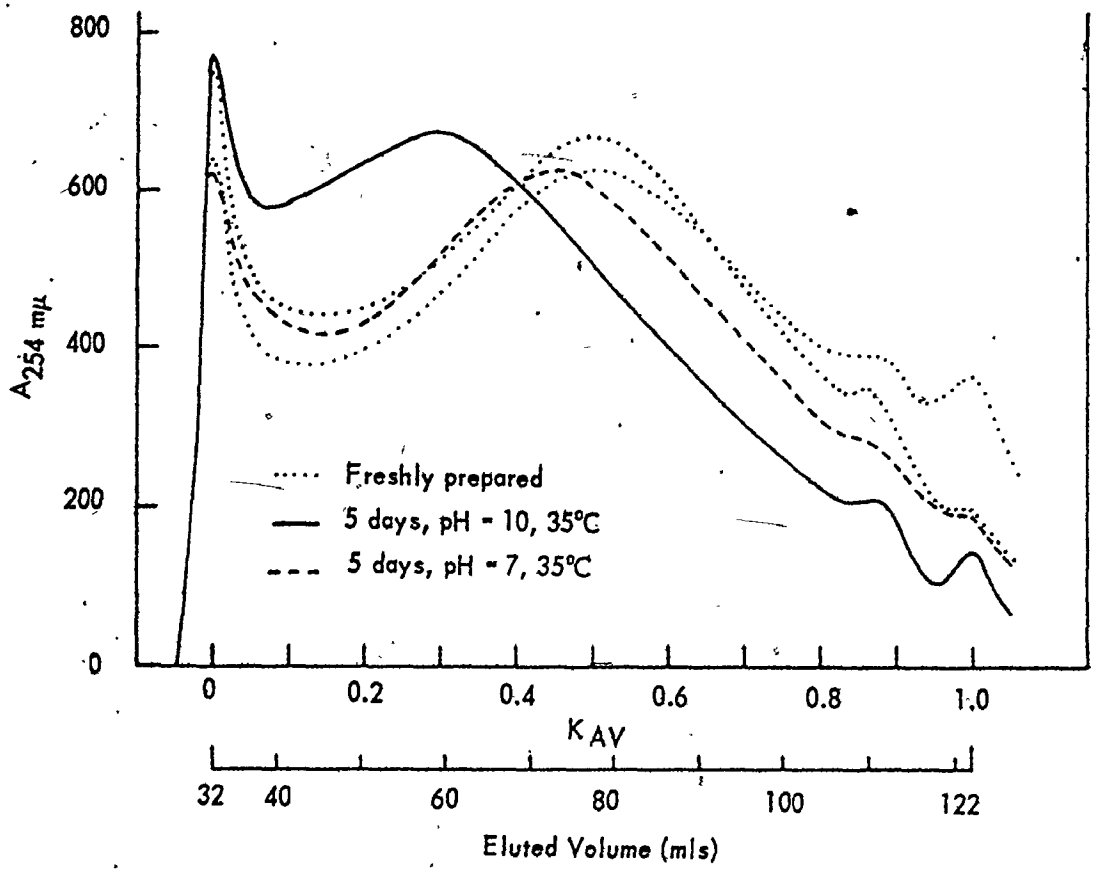

pH 10 results in a different molecular weight distribution. Here there is a decrease in absorbance values for $K_{AV}$ values less than approximately 0.4, coupled with an increase in absorbance values for $K_{AV}$ values in excess of 0.4. Provided that the following assumptions are valid, * i.e.

a) the 254 mu UV absorbance at each $K_{AV}$ value is directly proportional to the concentration - or number - of that particular molecular weight species in solution.

b) the 254 mu UV absorbance - concentration relationship is similar at all $K_{AV}$ values, and hence for all molecular weight species in solution.

---

* The validity of assumption (a) is supported by the extensive dilution of the lignin sample during gel filtration, and assumption (b) is validated by Goring's (1971) statement that " in softwood lignins .... UV adsorption .... has been found to vary only slightly, if at all, with molecular weight".

then aging of alkaline indulin solutions is associated with redistribution of the relative numbers of the various molecular weight constituents present in the original solution: more of the higher molecular weight species are formed at the expense of lower molecular weight constituents. This observation confirms what has been said earlier with respect to Indulin solution aging (see section III.2.2.(i) d).

The number average molecular weights $\overline{M}_n$ * of Indulin in the solutions studied, as calculated from the distributions in Fig. III.17, are shown in Table III.6.

These values are of the same order of magnitude as those obtained by other researchers and summarised earlier (see Table III.1). More recently, both Bailey (1972) and Ganczarczyk and Obiaga (1973) have evaluated molecular weight distributions in Indulin solutions by sephadex gel filtration. Bailey determined $\overline{M}_n$ to be

---

* the value of $\overline{M}_n$ is the value of molecular weight corresponding to the $K_{AV}$ value at which the total area under the molecular weight distribution curve is divided into two portions of equal area.

Table III.6 Average Molecular Weight of Indulin Species in Solution (as determined by gel filtration at pH 12.5)

| Indulin Solution | | | $\bar{M}_n$ |
|---|---|---|---|
| concn. (mg/l) | pH | age (days) | |
| 500 | 12.5 | fresh | 5,900 - 6,100 |
| 500 | 10 | 5 | 7,600 |
| 500 | 7 | 5 | 6,200 |

10,800 from sephadex G-100 gel filtration experiments conducted at pH 12.5, using a 280 mu UV absorbance detector. However, Bailey did not calibrate the gel bed separately with molecular weight standards, but rather used equations (3.2) and (3.3), in conjunction with a knowledge of the hydrodynamic radius/molecular weight relationship of globular proteins, in his calculations. For reasons discussed in section III.4.3. (i), this approach is not valid at highly alkaline column operating pH. Ganczarczyk and Obiaga determined values of $\overline{M}_n$ to be 2,800 and 10,000 respectively in the case of fresh and 7 day-aged indulin solutions, by G-100 and G-50 gel filtration experiments conducted at pH 10. Their gel was calibrated with both globular protein and narrow molecular weight fraction lignosulphonate standards. Our observations confirm their findings regarding an increase in $\overline{M}_n$ in alkaline Indulin solutions with age.

In order to obtain information on the contribution of the various molecular weight constituents to the overall Indulin solution color and TOC, a fractional color and TOC analysis was performed on discrete

eluant fractions collected in Gel Filtration of a freshly prepared 500 mg/l Indulin solution. The resultant TOC and color distributions so obtained are shown in Figs. III.18 and III.19.

From Fig. III.18, it appears that all the molecular species contribute TOC in approximate proportion to their relative concentrations in solution (cf. Fig. III.17). However, as Fig. III.19 shows, the overall solution color is predominately supplied by intermediate molecular weight species of about 5,500 - 6,500 MW, as characterised by $K_{AV}$ values in the 0.42 - 0.53 range. In contrast, the high molecular weight species of molecular weights in excess of 70,000 (i.e. where $K_{AV} = 0$) exert very little visible color in proportion to their concentration. * Although the low molecular weight constituents, characterised by $K_{AV}$ values in excess of 0.8 do not appear to exert much color, their concentration in solution is also small. Hence, per molecule, the color exerted by these

---

* this finding was also confirmed by visual observation of the gel filtration unit while in operation; no significant coloration of the collected eluant occurred until at least 40 - 50 ml had been collected.

Fig. III.18

**GPC ANALYSIS OF INDULIN SOLUTION - TOC FRACTIONATION**

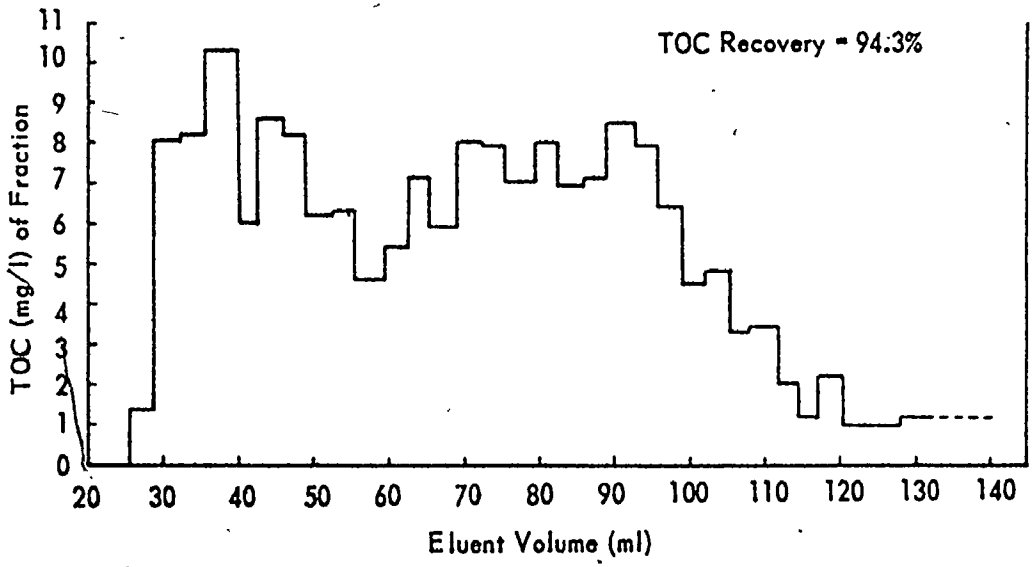

Fig. III.19

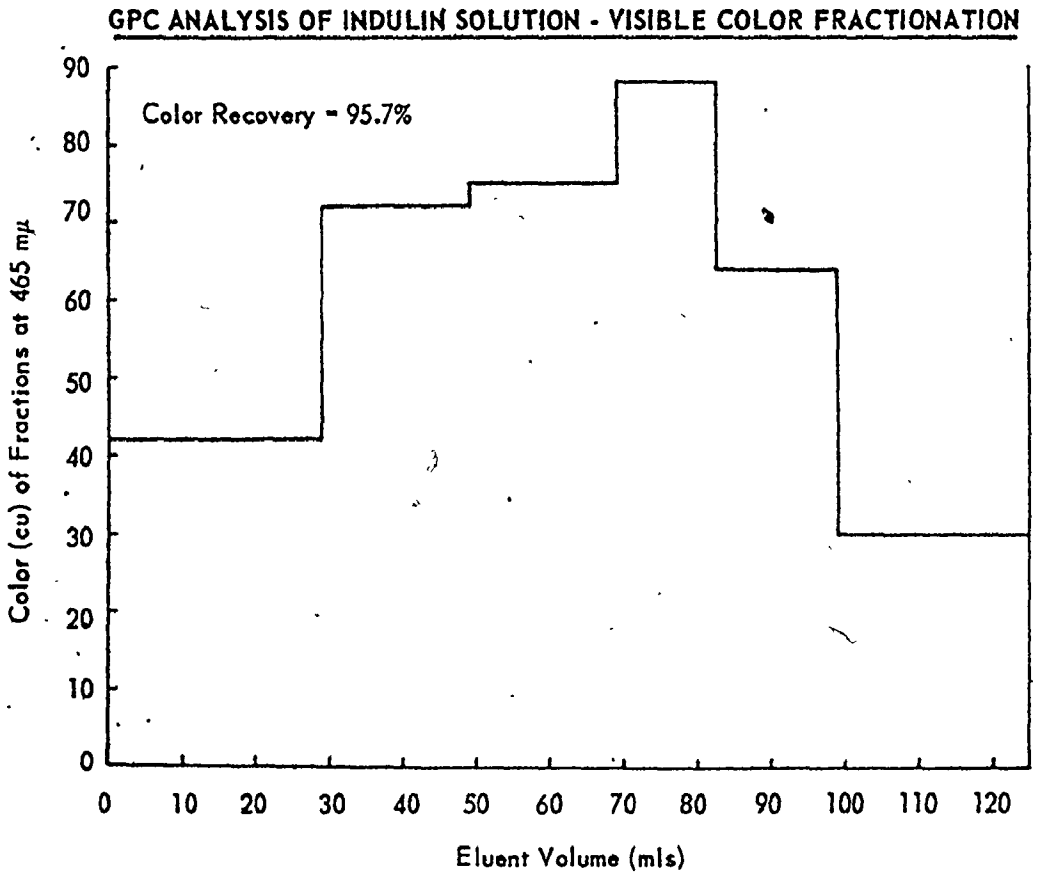
GPC ANALYSIS OF INDULIN SOLUTION - VISIBLE COLOR FRACTIONATION
Color Recovery = 95.7%
Color (cu) of Fractions at 465 mμ
0
10
20
30
40
50
60
70
80
90
100
110
120
Eluent Volume (mls)

species may be significant.

The percent recovery of original sample TOC and color in the collected eluant after completion of gel filtration, amounting to 94.3% and 95.7% respectively, supports the fact that minimal irrevisible adsorption or precipitation of lignin components takes place on the gel bed under the high operating pH used in this work.

Compared to Ultrafiltration, the use of Gel Filtration techniques provides a more rapid means of determining molecular weight distributions in Indulin solutions. In addition, Gel Filtration permits the use of smaller sample amounts, and will still give representative distributions even in dilute Indulin solutions, such as residual Indulin solutions from carbon adsorption. Unlike Ultrafiltration, however, Gel Filtration of lignin solutions has one major disadvantage, namely that the solution to be analysed must be adjusted to pH 12.5 before its introduction into the gel column. It has been shown from ultra-filtration experiments in Figs. III.12 and III.13 that

solution pH alters the molecular weight distribution of Indulin components in solution. Thus the molecular weight distribution in a pH 10 Indulin solution as determined by Gel Filtration experiments may not accurately reflect the distribution of components present in the original solution, the latter having a higher value of $\overline{M}_n$ than that derived from Gel Filtration analysis. This disadvantage will tend to complicate interpretation of Indulin adsorption data in subsequent activated carbon adsorption studies.

## III.5 SUMMARY

Studies conducted using an acid-precipatated pine kraft lignin, Indulin A.T., have shown that in aqueous solution, lignin exhibits behavior characteristic of a polydisperse polymer. The polydispersivity is due to the presence of various molecular weight solutes, arising from varying degrees of crosslinking of the monomeric lignin unit.

The number and distribution of the various molecular species in an Indulin solution ultimately dictate the magnitude of those bulk solution properties that are directly dependent on Indulin content

such as overall solution color and TOC. The observed linearity of both solution color (1) and TOC (2)* with Indulin concentration (up to 0.5 g/l) in fixed-pH alkaline solutions is thus explained in terms of the molecular distribution: increase in Indulin content merely serves to increase, in direct proporation, the number of each molecular weight species in solution without changing the overall molecular weight distribution.

Conversely, this study has also shown that "externally controlled" solution properties that are independent of Indulin content such as pH and solution age in term influence the nature of the molecular weight distribution. Here the observed color decrease with decrease in solution pH is attributed to an $H_3O^+$ initiated condensation reaction, wherein lower molecular weight solutes of relatively

---

* (1) expressed as equivalent chloroplatinate color units at 465 my absorbance

(2) the TOC - indulin concentration relationship deviates from linearity at indulin concentrations less than about 25 mg/l, notably at high pH. This effect is caused by dissolution of $CO_2$ from the surroundings.

high solubility and color content associate to form higher molecular weight derivatives of lower solubility and reduced chromophoric activity. Since Indulin solution dominant wavelength (576 - 577 mu) has been found to be independent of solution pH, it is concluded that the activity of the lignin chromophores in exhibiting color is directly related to the solubility of theor parent molecular weight fragment. Ultrafiltation and Gel Filtration experiments have indicated that at high pH, most of the color exerted by indulin solutions is contributed by solutes of less than approximately 10,000 MW, whereas at close to neutral pH, solutes of greater than 300,000 MW are responsible for the bulk of solution color. Overall solution TOC is unaffected by pH as it is not altered by solute solubility. However, like color, the distribution of TOC in solution is altered by pH, a greater proporation of overall TOC being contributed by the increased numbers of higher molecular weight solutes formed as pH is lowered.

Increase of solution age also gives rise to a decrease in overall Indulin solution color, notably at high pH. Gel Filtration experiments have indicated that this degradation is due to continuous formation of higher molecular weight solutes at the expense of the lower molecular weight forms. Although this effect is attributed to air oxidation of the lignin fragments (Marton and Marton, 1971), the associated pH drop with degradation and gel filtration molecular weight distribution data suggest that a $H_3O^+$ initiated condensation reaction may also be involved. Overall solution TOC is unaffected by solution age.

Filtration of Indulin solutions through a 0.45 membrane filter can result in significant removal of color and TOC from Indulin solutions, notably at pH's approaching neutral. This effect is due to retention of high molecular weight colloidal and suspended lignin fragments on the membrane by steric exclusion from the membrane pores.

Both Gel Filtration (using a Sephadex G-100

gel bed run at pH 12.5 with a 0.1M NaOH solvent) and Ultrafiltration (using a series of Diaflo membranes) experiments have proved useful for molecular weight characterisation of Indulin solutions. The average molecular weight $\overline{M}_n$ of species in a pH 12.5 Indulin solution as determined by Gel Filtration is approximately 6,000 - 7,500, this value being comparable to those found by other researchers. However, ultrafiltration experiments indicate that $\overline{M}_n$ rapidly increases with increase in solution pH.

# APPENDIX III.1

## Calibration Curves For The TOC Analyzer

fig.(i) Typical Calibration Curve For Total Carbon On Beckman 915 Carbon Analyser Using Standard Potassium Hydrogen Phthalate Solutions

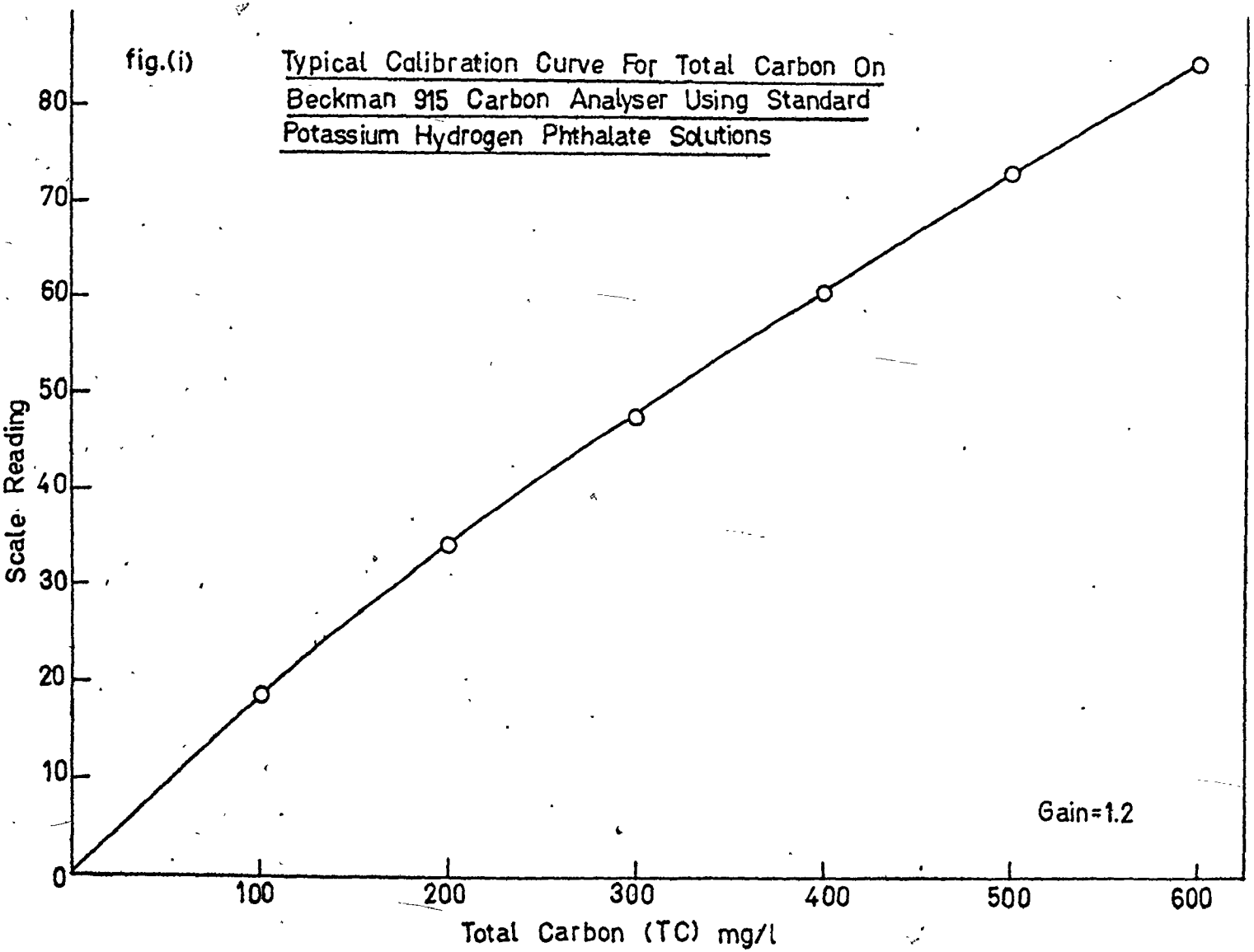

fig (ii) Typical Calibration Curve For Total Carbon On Beckman 915 Carbon Analyer Using Standard Potassium Hydrogen Phthalate Solutions

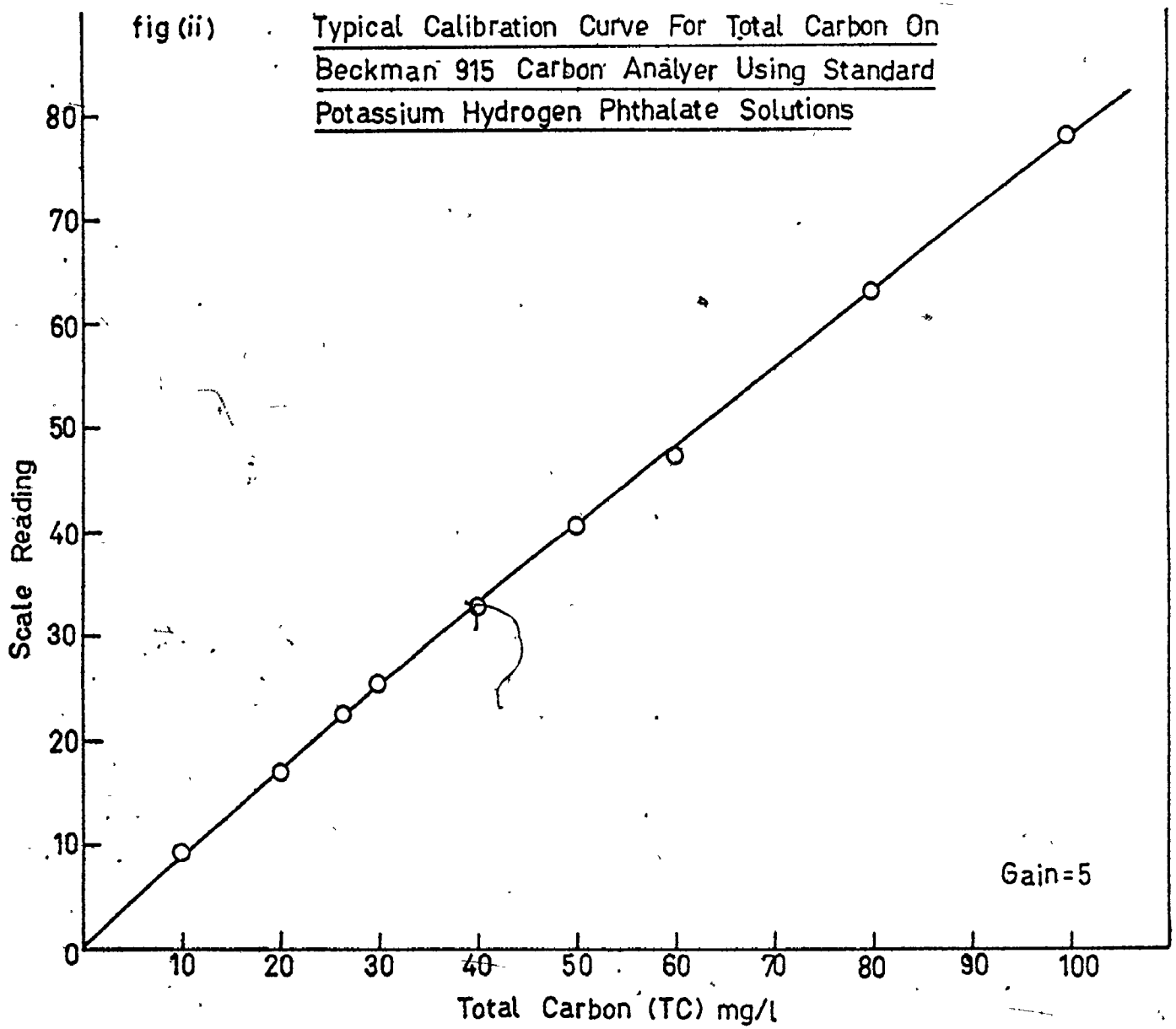

fig.(iii) Typical Calibration Curve For Inorganic Carbon On Beckman 915 Carbon Analyser Using Standard Sodium Carbonate Solutions

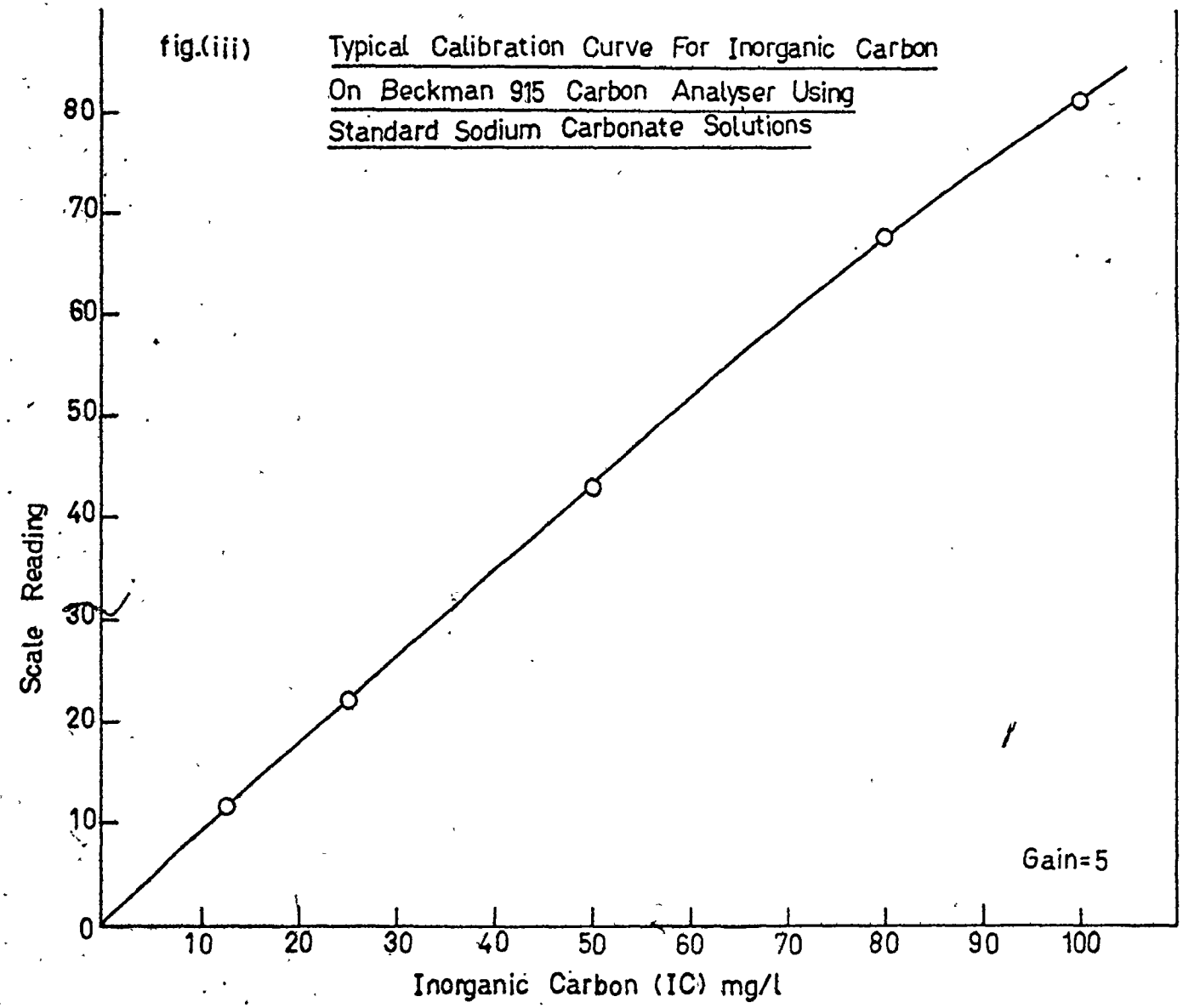

## REFERENCES


Adamson: A.W.; Physical Chemistry of Surfaces; 2nd Ed., Interscience, N.Y. (1967)

Adler: E., Pepper: J.M., Erikson: E.; Ind. Chem. Eng. 49 1391 (1957)

Amborski: L.E., Black: C.E., Goldfinger: G.; Rubber Chem. Tech. 23 417 (1950)

Amicon Corporation; Ultrafiltration for Laboratory and Clinical Uses; Publication #403A, (1971)

Anderson: R.B.; An Annotated Outline of a Course in Heterogeneous Catalysis; McMaster Iniv. Publications, (1970)

APHA/AWWA/WPCF Joint Publication; Standard Methods for the Examination of Water and Wastewater; 13th Ed., (1971)

Atlas Chemical Industries; Properties to Consider in Selecting Powdered Activated Carbons; Publication #D96, (1968)

Atlas Chemical Industries; A Symposium on Activated Carbon; Publication #D114, (1968)

Baker: R.W.; J. Appl. Polymer Sci. 13 369 (1969)

Bailey: C.W.; Westvaco, Charleston Research Centre, Charleston, N.C., Private Communication (1972)

Barrett: E.P., Joyner: L.G., Hallenda: P.P.; J.Am. Chem. Soc. 73 373 (1951)

Benedek: A., Ho: A.; McMaster University, Hamilton, Ontario, Unpublished Data (1973)

Berger: H.F.; Pulp and Paper Mag. Canada, 11, 48 (1969)

Berry: D,; Ontario Research Foundn., Mississauga, Ont., Private Communication (1971)

Blopdgood: D.E., Sami El-Naggar: A.; "Decolorisation of Semichemical Bleaching Wastes"; Paper Presented at the 16th Ind. Waste Conf., Purdue University, Ind. (1962)

Boehm: H.P.; Adv. Catalysis 16 179 (1964)

Boyd: G.E., Schubert: J., Adamson: A.W.; J.Am. Chem. Soc. 69 2818 (1947)

Brunauer: S.; The Adsorption of Gases and Vapours; Univ. Press, Princeton (1943)

Brunauer: S., Emmett: P.H., Teller: E.: J. Am. Chem. Soc. 60 309 (1938)

Butler: J.A., Ockrent: C.; J. Phys. Che. 34 2841 (1930)

Calgon Corporation; Basic Concepts in Adsorption on Activated Carbon; (1971)

Carpenter: W.L. and Berger: H.F.; NCASI Tech. Bull. #253 (1971)

Chaney: N.K.; Trans. Am. Electrochem. Soc. 39 91 (1919)

Chen: W.; "The Effect of Surface Curvature on the Adsorption Capability of Porous Adsorbents"; Ph.D. Thesis, Univ. South Carolina, (1970)

Claesson: I., Claesson: S.; Arkiv. Kemi. 19 5 (1945)

Clarke: J.; Ph.D. Thesis, Univ. of South Carolina (1969)

Cohan: L.H.; J. Am. Chem. Soc., 60 433 (1938)

Copeland: G.G., Sithson: G.R.; ' The Clarification of Paper Mill Effluents by Activated Carbon Produced from Waste Sulphite Liquor and Other Refuse.' Paper Presented at the 25th Ind. Waste. Conf., Purdue Univ., Ind. (1971)

Coss: J.; ' The effect of Lime Treatment on the 'Soluble' Organics in Domestic Wastewater'; M. Eng. Project, McMaster Univ. (1973)

Crank: J.; Phil. Mag. 39 140 (1948)

Cranston: R.W., Inkley: F.A., Adv. Catalysis 9 143 (1957)

Daniel: S.G.; Trans Faraday Soc. 47 1345 (1951)

Davis: J.T., Rideal: E.K.; Interfacial Phenomena; Academic Press, N.Y. (1961)

Day: J.; Abitibi Research Centre, Mississauga, Ont., Private Communication (1972)

DeBoer: J.H.; J. Catalysis 3 32 (1964)

Dedrick: R.L., Beckman: R.B.; Chem. Eng. Progr. Synp. Ser. 75 63,68 (1967)

Dintenfass: L.; Kolloid Z. 161 70 (1958)

Dugal: H.S., Swanson: J.W., Buchanan: M.A., Dickey: E.E.; 'Chemical and Physical Nature of Color Bodies in Kraft Mill Effluents before and after Lime Treatment' Paper presented at 64th AICHE meeting, San Francisco, Calif. (1971)

Eberman: N.F., Patrick: W.A.; J. Phys. Chem. 29 220 (1925)

Eduskuty: F.J., Amundson: N.R.; Ind. Eng. Chem. 44 1698 (1952)

Eirich: F.R., Lopatin: G.; Paper Presented at the 3rd Int. Congress of Surface Activity, Mainz Univ., 1960

Enkvist: T., Ashom: T., Hästbacka: K.; Paperi Puu 44 395 (1962)

Fava: A., Eyring: H.; J. Phys Chem. 60 890 (1956)

Faxon: H.; Ann. Physik. 68 89 (1922)

Felicetta: V.F., McCarthy: J.L.; Tappi 46 347 (1963)

Freudenberg: K.; Holzforschung, 18 3 (1964)

Freundlich, H.; Colloid and Capillary Chemistry, Methuen, London (1926)

Frisch: H.L., Hellman: M.Y., Lundberg: J.L.; J. Polymer Sci, 38 441 (1959)

Fuchs: R.E.; NCASI Tech. Bull. #181 (1965)

Ganczarczyk: J.; 'Fate of Lignin In Activated Sludge Treatment of Kraft Effluents'; Univ. Toronto Publ. #72-02 (1972)

Garten: V.A., Weiss: D.E.; Aust. J. Pure & Appl. Chem. 7 69 (1957)

Gibbs: J.W.; The Scientific Papers of J. Willard Gibbs; Vol. I, Dover Publ'ns, N.Y. (1961)

Gilliland: E.R,, Guthoff: E.B.; J. Phys. Chem., 64 407 (1960)

Goring: D.A.I.; in Lignins, Ch. 17 (1971)

Graham: D; Chem. Eng. Prog. Symp. Ser. 55 17 (1959)

Grant: R.J.; Basic Concepts of Adsorption on Activated Carbon, Pittsburgh Chem. Co., Pittsburgh, Penn. (1960)

Gregg: S.J., Sing: K.S.W.; Adsorption Surface Area and Porosity; Academic Press, London (1967)

Gupta: P.R., Goring: D.A.I.; Can. J. Chem. 38 270 (1960)

Hals: O.; M. Eng. Thesis, McMaster University, (1974)

Hansen: R.S., Hansen: R.D., Craig: R.P.; J. Phys. Chem. 57 215 (1953)

Hansen: R.S., Craig: R.P.; J. Phys. Chem. 58 211 (1954)

Hassler: J.W.; Activated Carbon; Chem. Publ. Co., N.Y., (1962)

Haydon: D.A.; Kolloid Z. 179 72 (1961)

Herdan: G.; Small Particle Statistics; Butterworths, London (1960)

Heywood: H.; Paper Presented at Symposium on Particle Size Analysis, London (1947)

Hobden: J.F., Jellinek; H.H.; J. Polymer Sci, 11 365 (1953)

Huppenthal: L.; Roczniki Chem. 37 1001 (1963)

Jackson: R.D., Nielsen: D.R., Nakayama: F.S.; Diffusion Laws Applied to Porous Materials; U.S. Dept. Agr. ARS Rep. 41-86, (1963)

Jäger: L., Erdös: E.; Coll. Czech. Chem. Comm. 24 2851, 3019 (1959)

Jain: J.S., Snoeyink: V.L.; JWPCF 45 2425 (1973)

Jenkel: E., Rumback: B.; Z. Electrochem. 55 612 (1951)

Jowett: A., Frangiskos: N.Z., Harris: C.C.; in 'Proceedings of the 3rd Int. Congress of Surface Activity'; Mainz Univ. (1961)

Juhola: K.A., Wiig: L.; J. Amer. Chem. Soc. 71 2069 (1949)

Kawecka: J., Lason: A.K.; Chem. Stosowana 7 441 (1963)

Kabeya: H., Fujii: T., Jubo: T., Kimura: Y.; ' A study of Renovation of Pulp Mill Waste Water Adsorption Characteristics of Kraft Pulp Lignin on Activated Carbon'; Shikoku (Japan) Gov. Ind. Res. Inst. Publ. #P.762.3.025.2 (1971)

Kipling: J.J., Wright: E.H.; J. Chem. Soc. 855 (1962)

Kipling: J.J.; Adsorption from Solutions of Non-Electrolytes; Academic Press, London (1965)

Kisilev: A.V., Novikova: V.N.; Proc. Acad. Sci (U.S.S.R.) 149 210 (1963)

Kleinert: T.N., Joyce: C.S.; Tappi 41 372 (1958)

Kolthoff: I.M., Kahn: A.; J. Phys. Chem. 54 251 (1950)

Kolthoff: I.M., Gutmacher: R.G.; J. Phys. Chem. 56 740 (1952)

Koral: J., Ullman: R., Eirich: F.R.; J. Phys. Chem. 62 541 (1958)

Kraus: G., Dugone: J.; Ind. Eng. Chem. 47 1809 (1955)

Kruyt: H.R., DeKadt: G.S.; Kolloid Z. 47 44 (1929)

Laurent: T.C., Killander: J., J. Chromatog. 14 317 (1964)

Lindberg: J.J., Tylli: H., Majani: C.; Paperi Puu 46 521 (1964)

Lindberg: J.J., Penttinen: K., Majani: C.; Paperi Puu 47 95 (1965)

Lundelius: E.F.; Kolloid Z. 26 145 (1920)

Mantell: C.H.; Carbon and Graphite Handbook, Wiley Interscience N.Y. (1968)

Marton: J., Marton: T.; Tappi 47 713 (1964)

Marton: J., Marton: T.; unpublished data (1968)

Marton: J.; in Lignins; Ch. 16 (1971)

Mayer: R.P., Stowe: R.A.; J. Colloid Sci. 20 893 (1965)

McBain: J.W.; J. Amer. Che. Soc. 57 699 (1935)

McBain: J.W., Humphreys: C.W.; J. Phys. Chem. 36 300 (1962)

McGlasson: W.G.; NCASI Tech. Bull. #199 (1967)

McKelvey: J.B. Holmes: H.N.; J. Phys. Chem. 32 1522 (1958)

McNaughton: J.G., Yean: W.Q., Goring: D.A.I.; Tappi 50 548 (1967)

Merewether: J.W.T.; Tappi 45 159 (1962)

Michaelis: L., Roma: P.; Biochem. Z. 15 196 (1908)

Micromeritics Corporation; Mercury Penetration Porosimeter Instruction Manual; Norcross, Ga. (1970)

Nikitin: U.M., Obolenskaya: O.V.; Tr. Leningr. Leso Tekhn. Akad. 85 13 (1960)

Noller: C.R.; Chemistry of Organic Compounds; 3rd Ed. W.B. Sanders & Co., London (1965)

Obiaga: T., Ganczarczyk: J.; 'Removal of Lignin from Kraft Mill Effluents: II. Changes In Molecular Size Distribution' Toronto Univ. Publ. #72-08 (1973)

Ogston: A.G., Phelps: C.F.; Biochem J. 78 827 (1961)

Orr: C., KallaValle: J.M.; Fine Particle Measurement; MacMillan Co., N.Y. (1959)

Pharmacia AB; Gel Filtration In Theory and Practice, Pharmacia Publ. #6-1970, Uppsala, Sweden (1970)

Phelphs: H.J.; Prod. Royal Soc. London, A131 17 (1931)

Pierce: C.; J. Phys. Chem. 63 1076 (1959)

Piret: E.L., Ebel: R.A., Kiang: C.T., Armstrong: W.P.; Chem. Eng. Progr. 47 405, 628 (1951)

Patat: F., Schliebener: C.; Makromol. Che. 44 643 (1961)

Perkel: R., Ullman: R; J. Polymer Sci, 54 127 (1961)

Peterson: C., Kwei: T.K.; J. Phys. Chem. 65 1330 (1961)

Roberts: B.F.; J. Colloid Interf. Sci., 23 266 (1967)

Rootare: H.M., Prenzlow: C.F.; J. Phys. Chem. 71 2733 (1967)

Sarkanen: K.V., Ludwig: C.W.; Lignins; Wiley Interscience, N.Y. (1971) Ch. 1.

Schuerch: C.; Ind. Eng. Chem. Prod. R & D. 4 61 (1965)

Shilov: N.; Kolloid Z. 52 107 (1930)

Simha: R., Frisch: H.L., Eirich: F.R.; J. Physc. Chem. 57 584 (1953)

Smith: D.R., Berger: H.F.; Tappi 51 37A (1968)

Smith: R.N., Geiger: C.F., Pierce: C.; J. Physc. Chem. 57 584 (1953)

Snoeyink: V.L.; 'Adsorption of Strong Acids, Phenol and 4-Nitrophenol from Aqueous Solution by Activated Carbon In Agitated Non-Flow Systems'; Ph.D. Thesis, Univ. Michigan (1968)

Sonntag: F., Jenkel: E.; Kolloid Z. 135 1,81 (1954)

Squire: P.G.; Archiv. Biochem. Bio Phys. 107 471 (1964)

Steenberg: B.; Svensk Kem. Tid. 53 774 (1941)

Studebaker: M.L., Huffman: E.W.; Ind. Eng. Chem. 48 162 (1956)

Swain: R.C., McBain: J.W.; Proc. Royal Soc. London A154 608 (1930)

Thibodeaux: L.J., Berger: H.; Tappi 49 521 (1966)

Thomas: J.M., Thomas: W.J.; Introduction to the Principles of Heterogeneous Catalysis; Academic Press, London (1967)

Tien: C.; Can. J. Chem. Eng. p28 (Feb. 1960)

Timpe: W.G., Lang: B.W., Haynie: R.B., Garrett: M.R.; Proc. 7th TAPPI Water and Air Conf., Minneapolis. (1970)

Timpe: W.G.; 'Removal of Color From Kraft Mill Effluents by Activated Carbons and Combined Treatment'; Paper presented at NCASI South-South Central Reg. Meeting, Atlanta (1970)

Timpe: W.G., Lang: E.W.; 'Removal of Color from Kraft Mill Effluents by Activated Carbon and Combined Treatment' Paper presented at TAPPI Gulf Coast Section Annual Meeting, Biloxi, Miss. (1971)

Timpe: W.G.; 'A Chemical Engineering Approach to a Closed Water Cycle in the Kraft Industry' Paper Presented at the 9th API-TAPPI Res. Conf., Seattle (1971)

Timpe: W.G.; St. Regis Paper Co., Pensacola, Fla.; Private Communication

Traube: I.; Ann. 265 27 (1891)

Treiber: E., Porod: G.; Makromol. Chem. 9 241 (1953)

Union Carbide Corpn., New York, N.Y. 10017, Tech. Bulletin #591-20581, (1972)

Weber: W.J., Levy: E.M.; Can. J. Chem.; 37 1235 (1959)

Weber: W.J., Morris: J.C.; J. Sanit. Eng. Div. Amer. Soc. Civ. Eng. 89 SA2 31 (1963)

Weber: W.J., Morris: J.C.; J. Sanit. Eng. Div. Amer. Soc. Civ. Eng. 90 SA3 79 (1964)

Weber: W.J., Rumer: R.R.; Water Resources Res. 1 361 (1965)

Weber: W.J.; Physico Chemical Process for Water Quality Control, Wiley Interscience, N.Y. (1972) Ch.5

West Virginia Pulp and Paper Co.; A Study of Powdered Carbons For Wastewater Treatment and Methods for Their Application U.S. Water Poll. Cont. Res. Ser. #17020DNQ 09/69 (1969)

Wheeler: A.; in Catalysis; edited by P.H. Emmett, Vol. II, Reinhold, N.Y. (1955)

Young: D.M., Crowell: A.D.; Physical Adsorption of Gases; Butterworths, London (1962)

Zeichmeister: L.; Progress in Chromatography; J. Wiley & Sons, N.Y. (1950)

Zsigmondy: R.; Z. Anorg. Chem. 71 356 (1911)